REACTIVE POLYMER ENHANCED MISCIBLE DISPLACEMENT IN POROUS MEDIA

By

DEBNATH DE, M. TECH

A Thesis

Submitted to the School of Graduate Studies

in Partial Fulfillment of the Requirements

for the Degree

Doctor of Philosophy

McMaster University

REACTIVE POLYMER ENHANCED MISCIBLE DISPLACEMENT IN POROUS MEDIA

DOCTOR OF PHILOSOPHY (1996) McMASTER UNIVERSITY

(Chemical Engineering) Hamilton, Ontario

TITLE: Reactive Polymer Enhanced Miscible Displacement in Porous Media

AUTHOR: Debnath De, B. Tech (University of Calcutta)

M. Tech (IIT, Kanpur)

SUPERVISOR: Dr. R. H. Pelton

NUMBER OF PAGES: xviii, 280

ABSTRACT

The displacement of aqueous Kraft model black liquor (MBL) from a porous bed with cationic polymer solution (polyDADMAC) was investigated to determine the mechanisms by which polyDADMAC influenced the miscible displacement. The porous bed consisted of a 1.7 cm diameter central channel of 638 μm glass beads surrounded by an annulus of 121 μm glass beads contained in a 5.2 cm internal diameter cylindrical glass column. Flow visualization experiments and displacement washing experiments were performed. Conductivity probes were installed at twelve locations inside the beds to monitor the velocity and locations of displacement fronts.

Flow visualization experiments in a transparent cell gave direct evidence of the presence of cross flow of fluid elements from annulus to the channel in a model channel bed during water displacement. After selective plugging of the channel with precipitate formed from reaction of lignin and polyDADMAC, fluid elements in annulus were observed to move straight down the model channel bed.

Results of the displacement experiments in the model beds confirmed that washing efficiency, a measure of the miscible displacement performance,

increased by 1.7 to 2 times and permeability of channel decreased by 34% to 18% when the bed was displaced with polymer solution instead of water. The improvement in the displacement performance with polymer solution resulted due to the reduction in channeling of polymer solution in the model channel bed.

Results of data obtained by the probes gave direct evidence of the reduction in velocity and mixing length of front in the channel confirming reduction in the channeling in a model channel bed during displacement with polymer solution. Increased velocity of front in the annulus during displacement with polymer solution confirmed better miscible displacement in a channel bed with polymer solution than that with water.

A communicating channel bed model was developed based on a technique called network of zones. The model predicts the breakthrough curves and the profiles of interstitial velocities inside the model beds during different displacement washing conditions. The model successfully predicts pressure drop profiles across homogeneous beds during displacement with either water or polymer solution and channel bed during washing with water. However, the pressure drop predicted by the model was higher than that obtained experimentally during washing with polymer solution in a model channel bed.

ACKNOWLEDGMENTS

With the deepest gratitude and respect, I would like to thank my supervisor, Professor Robert H. Pelton for his relentless support, kindness, and inspiration that benefited me immensely in my Ph.D. program. I would like to appreciate Prof. Andrew Hrymak for his advice and suggestion that was very helpful during my Ph.D. program. Thanks are due to Prof. J. R. Kramer for his critical evaluation of this work.

I would like to thank Dr. Ray Lappan and Mike Kempe for their constructive criticism of this dissertation. Thanks are due to every member in MCPPR who had created a congenial atmosphere in JHE-139. Special thank goes to Dr. Ian McLennan for his special friendship. I also thank Mr. Paul Gatt for fabricating the equipments. I like to appreciate S.E.E.S for building the Multichannel conductivity apparatus. Thanks are due to Department of Chemical Engineering, Mechanical and Chemimechanical Wood-pulp network, Networks of Centres of Excellence, and Dorset Industrial Chemicals for their financial support.

I like to thank everybody in the Department of Chemical Engineering for their helping attitude and friendship that made my stay in McMaster memorable.

Finally, I will never forget the support and sacrifice of my parents and family that has brought me here today.

TABLE OF CONTENTS

LIST OF FIGURES

LIST OF TABLES

Chapter 1

Introduction and Organization of Thesis

1.1 Introduction

Miscible displacement in a porous medium involves displacement of a fluid from the porous medium by another fluid that is miscible with the first fluid. Miscible displacement in porous media is of paramount interest in many branches of engineering including the recovery of oil from underground reservoirs, the contamination of fresh ground water supplies by landfill seepage, and the encroachment of saline water in hydrology. The work in this thesis is aimed at the role of miscible displacement of black liquors from a pad of pulp fibers with water in the brownstock washing stage in a Kraft pulping process. Brownstock washing is an important unit operation; high production rates and low environmental loading require effective brownstock washing in a modern Kraft pulp mill.

The performance of miscible displacement in a heterogeneous porous medium that contains higher permeable channels surrounded by lower permeable regions is severely affected by channeling (Lake, 1989). Bypassing

of resident phase by the displacing phase that preferentially passes through these channels in a heterogeneous porous medium is referred as channeling (Lake, 1989; Tang et al., 1989, Blackwell et al., 1959; Crotogino, 1987, Lee, 1984). In the oil industry, channeling has been reduced by the use of polymer solutions (Lake, 1989), gels (McCool et al., 1991), emulsions (Lake, 1989), and foams (Miller et al., 1995). In these approaches, channeling of the displacing phase is suppressed by the reduction of mobility of the displacing phase in channels during miscible displacement in a heterogeneous porous medium.

Recently, Li and Pelton (1992) have described a similar approach to improving displacement in brownstock washing. They used an aqueous solution of a cationic polymer, polyDADMAC, as the displacing phase instead of water to suppress channeling. They simulated the pulp pad by model channel beds that consisted of a central core of bigger glass beads surrounded by an annulus of smaller glass beads. They speculated that the permeability of the channel in their model bed of glass beads was reduced by the selective plugging of channel by a macroscopic precipitate formed from reaction of lignin and polyDADMAC during the displacement process. Pelton and Grosse (1994) have experimentally shown that the selective deposition of macroscopic precipitate occurs only in the central channel during displacement of spent liquors with aqueous solution of polyDADMAC in a model channel bed similar to that used by Li and Pelton (1992). They hypothesized that the selective formation of the precipitate only in

the central channel was due to the mixing of polyDADMAC in the channel with lignin that was driven from the annulus to the channel by a transverse pressure gradient which, in turn, was due to the difference in velocity of fluid in the channel and annulus during the displacement process. However, none of these studies nor any published research has provided experimental verification of the hypothesis of Pelton and Grosse (1994).

1.2 Objectives

The overall objective of this research is to develop an understanding of the effects of using an aqueous solution of polyDADMAC as displacing phase on the miscible displacement of model black liquor (MBL) from a model heterogeneous porous bed. The specific objectives described in this thesis are:

Objective 1: To provide experimental evidence for the hypothesis of Pelton and Grosse (1994) concerning selective plugging of channel by precipitates formed from reaction of polyDADMAC and lignin during miscible displacement in a heterogeneous porous bed by performing flow visualization experiments.

Objective 2: To measure directly the effects of variables including the concentration of lignin in MBL, the polyDADMAC concentration in water, the flow rate of displacing phase, and the permeability of channel on miscible displacement of MBL in a heterogeneous porous bed.

Objective 3: To provide direct experimental evidence of the modification of flow profile inside the heterogeneous porous bed by using conductivity probes at various axial and radial locations inside the bed during miscible displacement of MBL by an aqueous solution of polyDADMAC.

Objective 4: To develop a mechanistic model to predict the improvement in the performance of miscible displacement of MBL by aqueous solution of polyDADMAC in a heterogeneous porous bed.

1.3 Plan of Experiments

Flow visualization experiments were performed in a flat transparent cell to observe the process of selective precipitate formation in a model channel bed during displacement washing of MBL with an aqueous solution of polyDADMAC. Diagnostic tests of streamlines of fluid elements in model channel beds washed with either water or the polymer solution were performed. Chapter 3 reports in detail the materials, procedures, and results of flow visualization experiments in model beds of glass beads.

A computer automated displacement washing apparatus was built to evaluate the improvement in the displacement washing performance of the MBL from model beds using the aqueous solution of polyDADMAC as a displacing phase instead of water. The effects of four variables, i.e., the concentration of lignin in MBL, flow rate of displacing phase, concentration of polyDADMAC in

water, and permeability of the channel in a heterogeneous model bed on miscible displacement of MBL were studied through a statistically designed set of displacement washing experiments. Chapter 4 reports the details of the displacement washing apparatus and the procedure and results of displacement washing experiments.

Conductivity probes were placed at various axial and radial locations in the model beds to monitor the flow profiles during displacement washing experiments, which is reported in Chapter 4. Locations of the probes in the model beds and the results of analysis of the breakthrough curves obtained by probes are given in Chapter 5.

1.4 Organization of Thesis

Chapter 3 through Chapter 6 of this thesis have been written for intended publications in refereed journals.

Chapter 2 of the thesis describes the relevant properties of lignin.

Chapter 3 presents the results of flow visualization experiments conducted in the model channel beds.

Chapter 4 reports the procedure and results of a statistically designed set of washing experiments conducted in model channel beds. Washing efficiencies and steady state permeabilities of the model channel beds were computed from the breakthrough curves and pressure drop profiles respectively. A detailed

description of the computer automated displacement washing apparatus used in this work is also included in this chapter.

Chapter 5 describes the analysis of the breakthrough curves obtained by conductivity probes inserted into the model channel beds during displacement washing experiments. The implications of the results towards modification of flow profile inside model channel beds and the conclusions are discussed.

Chapter 6 describes a mechanistic model that predicts the exit breakthrough curves, the velocity profiles inside the model channel beds, and the profiles of pressure drop across the model channel beds obtained during displacement washing experiments.

Abbreviation

MBL Model black liquor

References:

Blackwell, R. J., J. R. Rayne, and W. M. Terry, Trans AIME, **216**, 1 (1959).

Crotogino, R. H., N. A. Poirier, and D. T. Trinh, "The Principles of Pulp Washing," Tappi, **70**, 95(1987).

Lake, L.W., Enhanced Oil Recovery, Prentice Hall, New Jersey (1989).

Lee, P. F., "Channeling and Displacement Washing of Wood Pulp Fiber Pads," Tappi, **67(11)**, 100 (1984).

Li, P., and R. H. Pelton, "Wood Pulp Washing: 2. Displacement Washing of Aqueous Lignin from Model Beds with Cationic Polymer Solutions," Colloids and Surfaces, **64**, 223 (1992).

McCool, C. S., D. W. Green, and G. P. Willhite, "Permeability Reduction Mechanisms involved in *in-situ* Gelation of a Polyacrylamide/Chromium (VI)/ Thiourea system," SPERE, 77-83, Trans AIME, **291**, February (1991).

Miller, M. J., and H. S. Fogler., "A Mechanistic Investigation of Waterflood Diversion using Foamed Gels," SPE Production & Facilities, **63**, February (1995).

Pelton, R. H., and B. Grosse, "Polymer Enhanced Displacement of Lignin Solution from Model Packed Beds," JPPS, **20(3)**, March (1994).

Tang, R. W., Behrens, R. A., and Emanuel, A. S.,"Reservoir Studies using Geostatistics to Forecast Performance," SPE 18432, SPE symposium on Reservoir Simulation, Houston, 321 (1989).

Chapter 2

Relevant Properties of Lignin

Lignin, the second most abundant component in wood, is removed from wood in the Kraft pulping process. No definite chemical structure of lignin is available in the literature. However, some structural details of lignin have been elucidated from the degradative studies based on oxidation, reduction or hydrolysis as a function of pH (Nyman et al., 1986). Lignin is not optically active and the structure of the lignin molecule has been simulated mathematically by several researchers (Sarkanen and Ludwig, 1971). According to these simulations, lignins are polymers of phenyl propane units. Depending on the type of pulping process, different functional groups are inserted into the lignin structure (Nyman et al., 1986). In a pulping process, the wood chips are chemically treated with either acidic or basic reagents to separate lignin from the cellulosic fibers in wood. In a Kraft pulping process, wood chips are cooked with a mixture of sodium hydroxide and sodium sulfite in a digester at an elevated temperature and pressure. As a result, phenolic hydroxyl groups and carboxyl groups are inserted into the lignin structure (Nyman et al., 1986). The carboxyl

groups in a lignin macromolecule are dissociated at a pH above 8, making lignin water soluble (Nyman et al., 1986). Current research indicates that solubilized lignin, derived from the pulping process, behaves as an essentially spherical, negatively charged, and amorphous macromolecule with a polydisperse molecular weight distribution (Nyman et al., 1986). Researchers (Lindström et al., 1980; Benko, 1964) have suggested that strong intermolecular association of the lignin macromolecules occur through secondary forces, such as Van der Waals forces, acid-base interactions, and hydrogen bonding.

The swelling behavior of Kraft lignin gel in an aqueous solution of sodium hydroxide was studied by Lindström et al., 1980. They found that the degree of swelling of lignin network reached a maximum and then decreased with addition of more NaOH. They also studied the absorbed amount of alkali (the number of charged groups in the lignin network) versus added amount of alkaline hydroxide and found that absorption was complete up to a level of addition that was approximately equal to the carboxyl content of the Kraft lignin. They inferred that the degree of maximum swelling of the network corresponded to a full degree of dissociation of the carboxylic groups present in the network. An increase in the degree of dissociation of the carboxylic groups in the network increased the electrostatic repulsion between the chain segments and thus led to greater swelling (Lindström et al., 1980). Addition of sodium hydroxide beyond the maximum degree of swelling, however, increased the ionic strength that shielded

the charged groups in the network and reduced the electrostatic repulsion between the charged groups, resulting in the lowering of swelling (Lindström et al., 1980). The effect of the higher ionic strength was found to be more important towards the lowering of swelling of Kraft lignin gels than the increased ion exchange capacity of the network at higher pH (Lindström et al., 1980). The swelling behavior and ion exchange capacity were nonspecific towards the type of alkaline solution added (Lindström et al., 1980).

Lindström et al. (1980) also found that the mechanical properties of the Kraft lignin gels were strongly dependent on the ability of carboxyl groups to form intermolecular hydrogen bonds. In addition, they reported that the effective number of cross links in the network was dependent on the state of dissociation of the carboxylic groups.

The coagulation effects of simple cations on negatively charged Kraft lignin sol at various conditions of pH has been studied by Lindström (1980). He found that the critical coagulation concentration (CCC) of lignin sol increased with increasing pH due to an increase in the number of ionized groups on the lignin sol particles. At low pH (pH < 9), when the charge on the particles was low, partial flocculation of lignin sol particles resulted due to intermolecular hydrogen bonding among the particles, even before the addition of electrolytes (Lindström, 1980). Lindström (1980) argued that this intermolecular hydrogen bonding among the lignin sol particles became more prominent at low pH and could be

expected to lower the critical coagulation concentration (CCC) of sol particles at low pH. At low pH, mobility of the macromolecular chain segments in the surface region of the microgel lignin sol particles decreased due to increased intramolecular association of the chain segments (Lindström, 1980). Consequently, at low pH when the electrostatic repulsive forces among the chain segments also decreased, the loose layer of chain segments on the surface of particles was compressed; thus the particles lost their protective action of steric stabilization against coagulation (Lindström, 1980). As a result, the protective action of chain segments on the surface of particles against coagulation or steric stabilization became significant at high pH (pH > 9) when the sensitivity against electrolyte such as NaCl was lost. This resulted in a stable colloidal solution of sol particles (Lindström,1980).

Knowledge of the kinetics of complexation between lignin and cationic polymer is important for understanding the formation of precipitates during displacement of black liquor with an aqueous solution of a cationic polymer in a porous bed. Kraft lignin is an anionic polyelectrolyte. The formation of a complex between two oppositely charged polyelectrolytes is well known. The different types of forces that interplay in the complex formation process are electrostatic forces, hydrogen bonding, acid-base interactions and Van der Waals forces. However, the major driving force for complexation is the electrostatic attraction between oppositely charged polyelectrolytes. Several researchers (Lindström et

al., 1980; Ström et al., 1981; Michaels, 1965) have reported that the electrostatic interaction between the polyelectrolytes depends on charge density, charge equivalence, chain length, flexibility, and conformation of the two polyelectrolytes. The ionic strength of the solution also has profound effect on the electrostatic interaction. It has been suggested (Michaels, 1965) that due to complexation there might be phase separation where both stoichiometric and non-stoichiometric relationships between the polyelectrolytes may be observed. Deviation from stoichiometry occurs with tightly coiled polymers, particularly in presence of salt (Michaels, 1965). Phase separation has been observed to give flocculated precipitate or complex coacervate (Ström et al., 1986).

Li and Pelton (1992) have carried out a systematic study of the complexation between lignin and different cationic polymers. They reported that 80-90% of lignin could be precipitated from an aqueous solution using cationic polymers and the yield of the precipitate was not sensitive to the molecular weight of added polymers. However, they reported that the charge density of the cationic polymers was found to be an important parameter for the yield. They observed that polyDADMAC, having a higher charge density than poly(DADMAC-co-acrylamide), was a more efficient precipitant. Li and Pelton (1992) also found that the yield was not sensitive to salt concentration and observed a stoichiometric relationship between the polyelectrolytes in the macroscopic complex. The colloidal phase was stable when one of the

polyelectrolytes was in excess because the excess polyelectrolyte was on the particle surfaces providing electrostatic stabilization (Li and Pelton, 1992).

References:

Benko, J., Tappi, **47**, 508(1964).

Li, Pei., and R. Pelton., "Wood Pulp Washing 1. Complex Formation Between Kraft Lignin and Cationic Polymers," Colloids and Surfaces, **64**, 217 (1992).

Lindström, T., "The Colloidal Behavior of Kraft Lignin II. Coagulation of Kraft lignin sols in the presence of simple and complex metal ions," Colloids and Polymer Science, **258**, 168 (1980).

Lindström, T., and L. Westman., "The Colloidal Behavior of Kraft Lignin III. Swelling behavior and mechanical properties of Kraft Lignin gels," Colloids and Polymer Science, **258**, 390 (1980).

Michaels, A. S., "Polyelectrolyte Complexes," Ind. Eng. Chem., **57(10)**, 32 (1965).

Nyman, V., G. Rose, and J. Ralston, "The Colloidal Behavior of Kraft Lignin and Lignosulfonates," Colloids and Surfaces, **21**, 125 (1986).

Sarkanen, K. V., and H. Ludwig (Ed.), Lignins: Occurrence, Formulation, Structure, and Reactions, Wiley-Interscience, New York, 1971.

Ström, G., and P. Stenius, "Formation of Complexes, Colloids, and Precipitates in aqueous mixtures of Lignin Sulfonate and some Cationic Polymers," Colloids and Surfaces, **21**, 125 (1986).

Chapter 3

Flow Visualization of *in situ* Precipitate Formation during Displacement Washing of Model Black Liquor from Model Beds of Glass Beads

Abstract

Flow visualization experiments in a flat transparent cell were performed to investigate the modification of streamlines of fluid elements in a model black liquor (MBL) saturated model channel bed of glass beads that was washed with an aqueous solution of polyDADMAC (29.4 g/L, MW = 10^5). During displacement washing with a polymer solution in a MBL-saturated model channel bed of glass beads, precipitates of lignin and the polymer were observed to form selectively only in the center channel of the model bed. The *in situ* selective precipitation in the model channel bed during displacement washing with the polymer solution was ascribed to two mechanisms: higher longitudinal dispersion in the center channel of the model channel bed; and interfacial mixing of MBL and the polymer at the edges of the center channel due to a cross flow of the MBL, caused by a screen-bead interaction reported by Lappan et al. (1996). In a model channel bed that was modified by selective precipitation in its center channel, channeling was reduced due to the modification of streamlines of fluid

elements towards those in a homogeneous bed. No selective precipitation was observed when the ratio of the particle Reynolds numbers in the channel to that in the annulus part of a channel bed was 3.5.

3.1 Introduction

The study of miscible displacement of a fluid from a porous medium by another fluid occurs in many areas of chemical engineering such as in brownstock washing in pulp and paper industry, in tertiary oil recovery in petroleum engineering, in hydrology, etc. In miscible displacement in porous media, the displacing phase is forced to flow through a porous bed to displace the resident fluid from the bed. The major objective of miscible displacement is to displace the maximum volume of the resident fluid using the minimum volume of the displacing phase. Ideally, in a plug flow where interfacial mixing is absent, one volume of displacing phase is required to displace one volume of resident fluid from the bed. However, in reality, more than one volume of displacing phase is required due to the presence of appreciable amount of interfacial mixing during a miscible displacement process.

In tertiary oil recovery, the performance of miscible displacement floods is affected by fingering and channeling of the displacing phase (Lake, 1989). Fingering refers to bypassing of a resident fluid by a displacing fluid in a

homogeneous medium. In a strict sense, the definition of fingering encompasses instabilities caused by unfavorable differences in viscosity and density of the resident and displacing phases (Lake, 1989). Channeling refers to bypassing of the resident phase by the displacing phase due to heterogeneities in permeability across the bed (Lake, 1989; Tang et al., 1989; Mathews et al., 1988 and Blackwell et al., 1959). Though fingering in miscible displacements can be prevented by proper choice of viscosity and density differences of the two phases, channeling caused by heterogeneities in permeability cannot. Channeling can only be suppressed by reducing the mobility of the displacing phase that preferentially passes through the channels (Lake, 1989).

In brownstock washing in pulp and paper industry, spent chemicals and lignin are displaced from a pad of pulp fibers by water. The performance of displacement washing of pulp pad by water is limited by channels of higher permeability through which wash water passes preferentially bypassing spent liquor and lignin in the pulp pad (Crotogino et al., 1987; Lee, 1984). As a result, the displacement washing process becomes inefficient causing a large volume of wash water in the effluent and an increase in load on the evaporators. Also, it creates an environmental problem as unwashed spent liquors are carried over to the downstream operations. Lee (1984) demonstrated that the use of nonionic polymer in wash water improved the displacement washing performance considerably by reducing the mobility of displacing phase through the channels.

However, the technology proposed by Lee (1984) was not used on a large scale due to reduction in production capacity. Recently, Li and Pelton (1992) have reported that the displacement washing performance can be enhanced substantially by the use of cationic water soluble polymers in the wash water. They simulated pulp pad with a model channel bed consisting of a central core of glass beads as channel surrounded by an annulus of smaller beads. They hypothesized that improved washing had a fluid mechanical origin and was due to a "clotting effect". "Clotting" refers to selective plugging of the more permeable central channel of the model bed by macroscopic precipitates formed from lignin and the cationic polymer. "Clotting" changed the properties of the model channel bed towards those of a bed without any channel. Furthermore, washing performance was improved by suppressing the channeling effect in the model channel bed. They also reported that the pH and ionic strength of the solution and the structure and molecular weight of the polymers had no significant effect on displacement washing performance in the model channel bed.

Pelton and Grosse (1994) have carried out flow visualization experiments of displacement washing process in a flat transparent cell using model channel beds analogous to that used by Li and Pelton (1992). They observed selective plugging of central channel in the model channel bed by precipitate formed from lignin and cationic polymer when a model bed was washed with a polymer solution. They also observed that a model bed consisting of only smaller beads

did not retain any precipitate at the end of washing with polymer solution. Furthermore, no selective precipitation was possible in the central channel of a model channel bed when the permeability ratio of central channel to annulus went below 1.4. On the basis of flow visualization, they postulated a mechanism of selective plugging of the central channel by precipitates in a model channel bed. They hypothesized that during displacement washing with a polymer solution, lignin from the annulus region of the model bed would mix with the polymer solution flowing in the channel due to a transverse pressure gradient that was a result of an inertial effect caused by higher velocity of fluid in the channel than that in the annulus part of the bed. They ascribed the absence of precipitate deposition in a bed of smaller beads to the retardation of the mixing of lignin with the polymer solution by a thin, soluble polymer-lignin complex formed at the interface between lignin and polymer solution in the bed. However, there is no direct experimental verification of the speculated mechanism of Pelton and Grosse (1994).

The major objectives of this work were to visualize the displacement processes in detail; to examine the streamlines of fluid elements in the bed in the presence and absence of selective plugging of central channel in a model channel bed; to visualize the process of precipitate formation and retention at the particle level inside the bed during a displacement washing process; and to investigate the mechanism speculated by Pelton and Grosse (1994).

3.2 Experimental

3.2.1 Materials

3.2.1.1 Preparation of Model Black Liquor (MBL) Solution

Indulin C, a mixture of sodium salt of lignin (80-90%) and sodium carbonate (10-15%), was supplied by Westvaco, South Carolina, USA. Three types of model black liquor (MBL) solutions were prepared by mixing either 25, 13.75 or 2.5 g of Indulin C in 900 mL of distilled de-ionized water and 100 mL of 1 (N) NaOH solution. The resultant mixtures were stirred at 1000 r.p.m by a RZR 50 mechanical stirrer supplied by Caframo, Canada, for 30 minutes to ensure complete dissolution of solids into the solutions.

3.2.1.2 Preparation of Polymer Solution

Percol 1697, an aqueous solution (40% by volume) of cationic polyelectrolyte, polydiallyldimethyl ammonium chloride or polyDADMAC, was supplied by Allied Colloids (Canada) Inc., Ontario, Canada. Two types of polymer solutions were prepared by mixing either 29.4 or 14.7 g of Percol 1697 in distilled de-ionized water and the total volumes of the resultant mixtures were made up to 1000 mL.

Viscosities and densities were measured by a Cannon Fenske viscometer and specific gravity bottles at 25°C. pH was measured by a Corning pH/ion meter 150. Table 3.1 shows the physical properties of various MBL and polymer solutions.

Table 3.1 Physical properties of various MBL and polymer solutions at 25°C. Margin of error is ± 5% based on three replicate measurements.

Solutions	pH	Density (g/mL)	Relative Viscosity
MBL (25 g/L)	$12.35 \pm 4.5 \times 10^{-3}$	$1.007 \pm 2.17 \times 10^{-4}$	$1.17 \pm 2.4 \times 10^{-2}$
MBL (13.75 g/L)	$12.5 \pm 3.34 \times 10^{-3}$	$1.003 \pm 2.4 \times 10^{-4}$	$1.06 \pm 5.7 \times 10^{-3}$
MBL (2.5 g/L)	$12.56 \pm 6.2 \times 10^{-3}$	$0.999 \pm 3.26 \times 10^{-5}$	$1.05 \pm 1.2 \times 10^{-2}$
Polymer (29.4 g/L)	$5.27 \pm 2.1 \times 10^{-2}$	$0.996 \pm 7.87 \times 10^{-5}$	$3.2 \pm 4.7 \times 10^{-2}$
Polymer (14.7 g/L)	$5.21 \pm 4.6 \times 10^{-3}$	$0.995 \pm 5.8 \times 10^{-4}$	$2.24 \pm 4.5 \times 10^{-2}$

3.2.1.3 Glass Beads

Three types of glass beads were used in this work. All of these glass beads were supplied by Orlick Industries, Hamilton, Ontario, Canada. A summary of their size distributions which were measured by a RX-29 Rotap sieve analyzer, W. S. Tyler Incorporated, Ohio, USA, is given in Figure 3.1 through 3.3

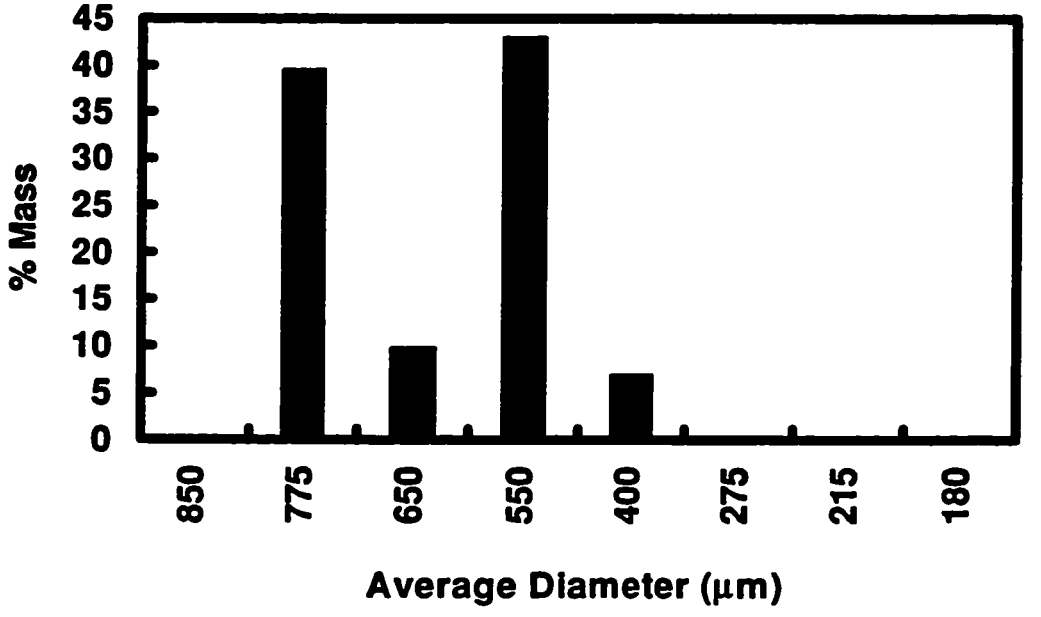

Figure 3.1 Size distribution of particles of no: 3 glass beads.

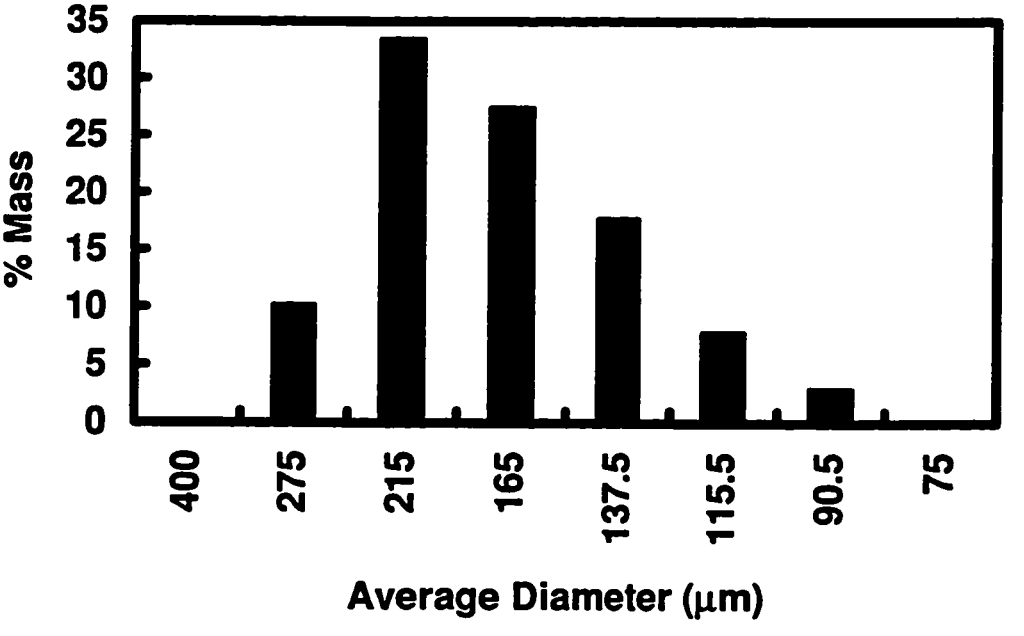

Figure 3.2 Size distribution of particles of no: 7 glass beads

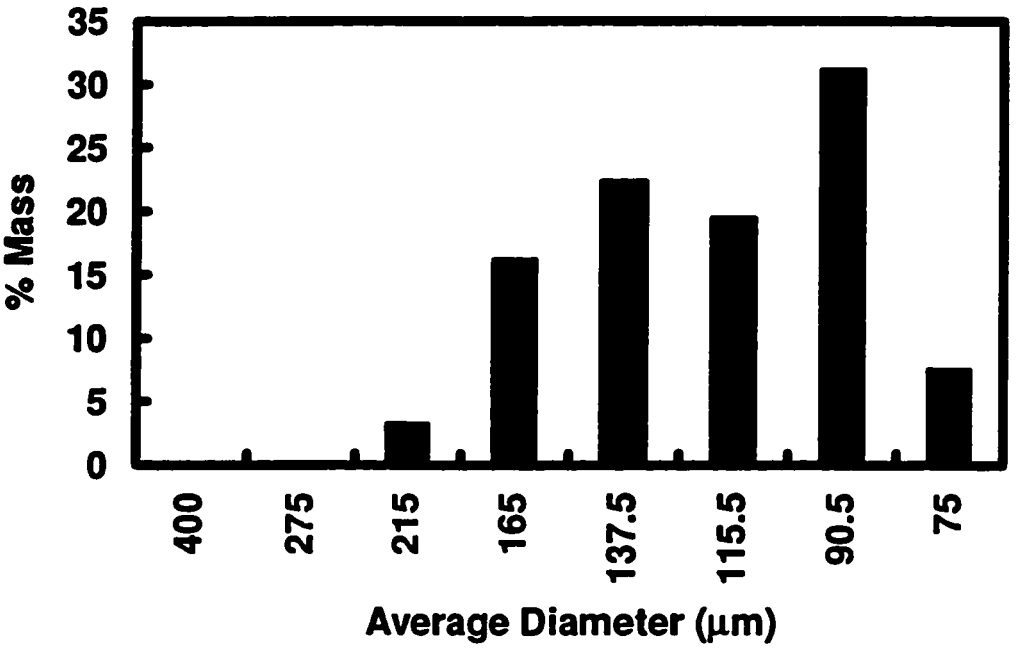

Figure 3.3 Size distribution of particles of no: 10 glass beads.

and in Table 3.2 on the next page. The density of the glass beads was reported by Orlick Industries to be 2.5 g/mL. The mass average particle diameter of each type of glass bead was calculated by the relation

$$\text{mass average diameter} = \Sigma\ (\%\ \text{mass} \times \text{nominal diameter})/100 \qquad \textbf{3. 1}$$

The average diameters for No: 3, No: 7 and No: 10 glass beads were calculated as 638, 182 and 121 μm respectively.

Table 3.2 Summary of size distributions of glass beads used in this work.

US Sieve Range	Size of Sieve (μm)	Nominal Diameter (μm)	Glass Bead No:3 (mass%)	Glass Bead No:7 (mass%)	Glass Bead No:10 (mass%)
20	850	>850	0.146	0	0
20 - 25	850 - 700	775	39.57	0	0
25 - 30	700 - 600	650	9.87	0	0
30 - 35	600 - 500	550	43.02	0	0
35 - 50	500 - 300	400	6.95	0.22	0
50 - 60	300 - 250	275	0.256	10.22	0
60 - 80	250 - 180	215	0.11	33.45	3.24
80 - 100	180 - 150	165	0.073 (<180)	27.46	16.25
100 - 120	150 - 125	137.5	0	17.71	22.37
120 - 140	125 - 106	115.5	0	7.86	19.52
140 - 200	106 - 75	90.5	0	2.97	31.15
>200	<75	<75	0	0.11	7.47

Ballotini glass beads of size range 0.4 to 0.455 mm and 3 mm diameter glass beads were also used. Ballotini beads and 3 mm diameter glass beads were supplied by Perrytech Educational Products, Ontario, Canada and Fisher Scientific, Canada respectively.

Model black liquor (25 g/L) (MBL) and the polymer solution (aqueous solution (29.4 g/L) of polyDADMAC, MW: 10^5) were used in flow visualization experiments. No: 3 (mean diameter 638 mm), no: 7 (mean diameter 182 mm) and no: 10 (mean diameter 121 mm) glass beads are denoted as coarse (subscript "c"), medium (subscript "m"), and fine (subscript "f") beads respectively in the rest of this chapter.

3.2.1.4 Flat Transparent Cell

The schematic of the rectangular flat Plexiglass® cell used for flow visualization experiments is shown in Figure 3.4. The cell had an open channel of length 25 cm, breadth 17.7 cm and width 1 cm. A perforated stainless steel screen (Type no: 80 P) was placed at the bottom of the cell to support a bed above it. The screen was supplied by Paper Research Material, Camas, USA. The diameter of the holes in the screen was 120 μm with a US mesh equivalence of 80. The percentage of open area on the screen was 14.5. Two vents were provided below the screen to ensure maintenance of atmospheric pressure below the screen during the draining of fluids from the bed.

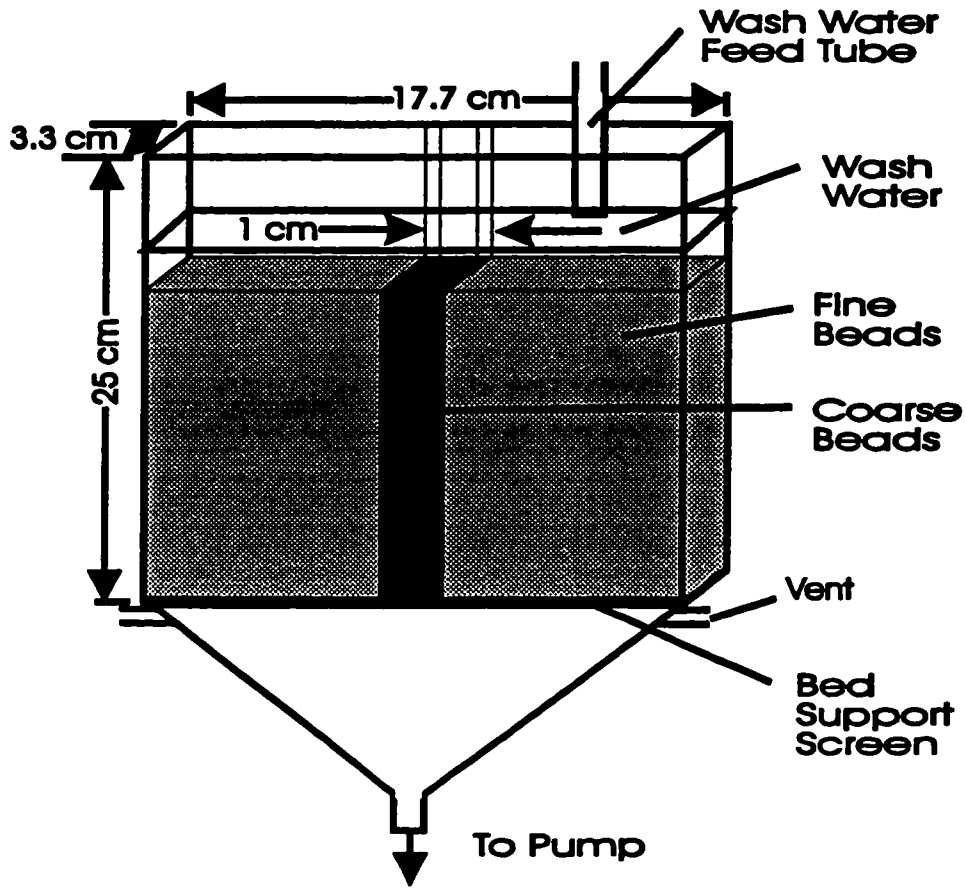

Figure 3.4 Schematic of the flat cell employed in flow visualization experiments (Adapted from Pelton and Grosse, 1994).

3.2.2 Experiment in a Homogeneous Bed

Dry fine glass beads were poured slowly inside the cell until the height of the bed reached 8.5 cm. The cell was tapped frequently during pouring of beads to ensure a uniform packing of beads. The bed was saturated with MBL (25 g/L) by pumping the MBL from the bottom of the cell at a rate of 7 mL/min by a

peristaltic pump. A Whatman® no:1 filter paper was placed on the top of the saturated bed to minimize any mixing of the MBL and the wash liquor during the filling of the top of the bed with wash liquor. The polymer solution (29.4 g/L) was then poured carefully on top of the bed using a funnel as shown in Figure 3.5. A displacement experiment was started by opening the vents and the outlet of the cell simultaneously. Pressure at the entrance of the bed remained constant since the height of the polymer solution above the bed was maintained at 4.5 cm by adjusting the flow rate in the funnel. During the constant pressure head displacement, sequential pictures of the displacement flow profile were taken by a Cannon AF 100 camera.

3.2.3 Experiment in a Channel Bed

A channel bed consisted of a central core of coarse glass beads sandwiched between outer cores of fine glass beads. A rectangular top panel and two rectangular Plexiglass® bars as shown in Figure 3.6 were employed to form a channel bed. Figure 3.7 depicts the top panel that had a height of 5.1 cm, breadth of 17.7 cm, and thickness of 1.3 cm. Rectangular grooves with width 0.3 cm and depth 0.5 cm were indented in one of its faces along its height. Grooves were indented on both sides of the center of that face at a distance of 0.5, 1.5, 2.4, and 3.4 cm. The top panel was fitted to the top of the flat cell and its face containing the grooves faced the inside of the cell. Two rectangular

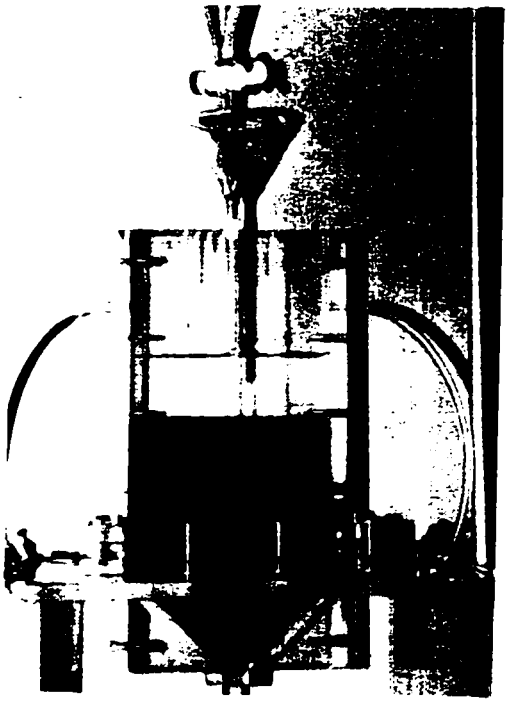

Figure 3.5 Photograph of the set up for displacement washing in the flat cell.

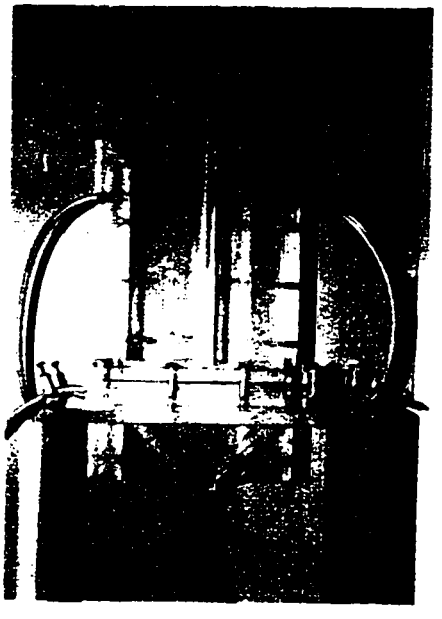

Figure 3.6 Photograph of the set up for preparation of a channel bed.

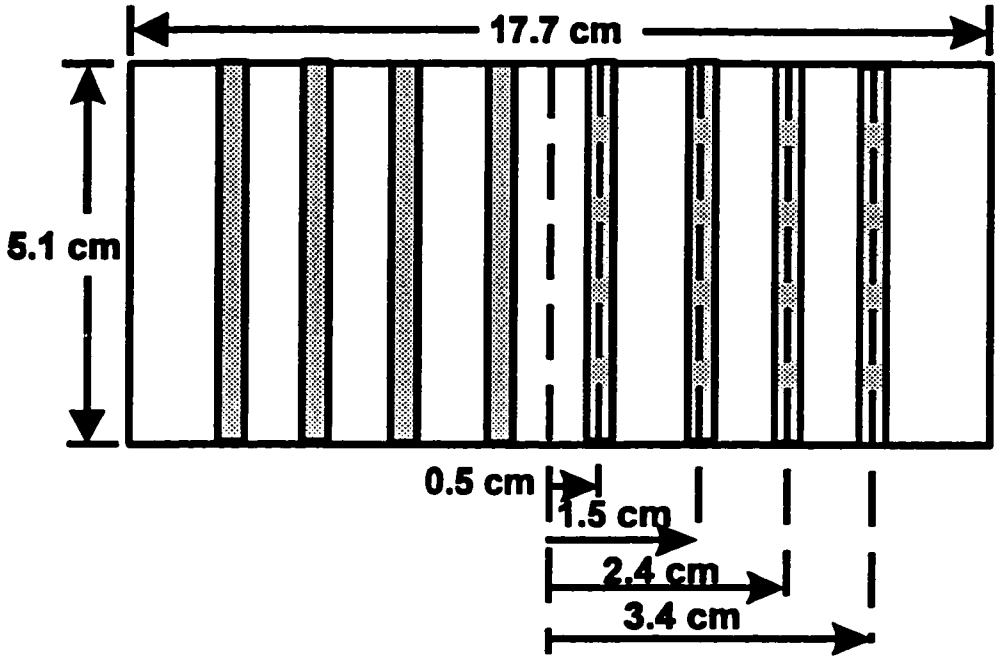

Figure 3.7 Schematic of the top panel employed to prepare a channel bed.

Plexiglass® bars, each of length 28.5 cm, breadth 0.9 cm, and thickness 0.3 cm, were inserted into the cell through two grooves that were equidistant from the center of the face of the panel. The bars were placed firmly on the screen and were held vertical and equidistant from each other all along the height of the flat cell. As a result, the flat cell was divided into three separate chambers.

Coarse and fine glass beads were poured in the central and outer chambers respectively until the height of the bed reached 8.5 cm. The cell was tapped frequently during filling of the cell ensuring a uniform bead packing. At

the end of filling, the bars were pulled very slowly and vertically out of the cell ensuring a minimal mixing of beads at the interface of two types of beads. This resulted into a channel bed with a 1.3 cm wide central channel of coarse glass beads. The procedures for saturating a channel bed with MBL and displacement experiments either with water or the polymer solution were similar to those described for the case of a homogeneous bed.

At the end of a displacement run, a diagnostic test was performed to trace the streamlines of fluid elements in different sections of the bed. About 0.2 mL of food color solution was introduced into different sections of the bed. The subsequent movement of tracer with either water or polymer solution flow under a constant pressure head condition was photographed.

3.2.4 Experiment in a Mixed Bed

A mixed bed consisted of two adjacent central channels packed with coarse and medium glass beads separately. These channels remained sandwiched between two outer cores of fine glass beads. The procedure for preparing a mixed bed was similar to that of a channel bed except that the cell was divided into four chambers with the help of three Plexiglass® bars inserted into three grooves in the top panel.

A 8.5 cm long mixed bed consisting of two adjacent channels each of width 3.3 cm was formed. The methods for the saturation of a mixed bed with

MBL, the displacement experiment with polymer solution, and the diagnostic test of the movement of a tracer element inside the bed after a displacement run were similar to those described for the case of a channel bed.

3.2.5 Experiments using a Macroscope

A Wild Heerbrugg Makroscope with Wild Stereo 40/14, Model: M420 was used to observe a magnified view of a section of bed during washing with polymer solution. Magnified views of sections of beds were videotaped with a Panasonic video cassette recorder, Model: AG-6750A.

3.3 Results

3.3.1 Sequential Profiles of Displacement Front during Washing

Figures 3.8 and 3.9 show the sequential profiles of displacement front in homogeneous beds of fine and coarse glass beads respectively during washing with polymer solution. The homogeneous bed of fine glass beads did not retain any visible precipitate at the end of the experiment, as shown in Figure 3.8. On the other hand, precipitates that could not be washed out with the polymer solution at the end of the experiment, were retained in the homogeneous bed of coarse glass beads, as shown in Figure 3.9.

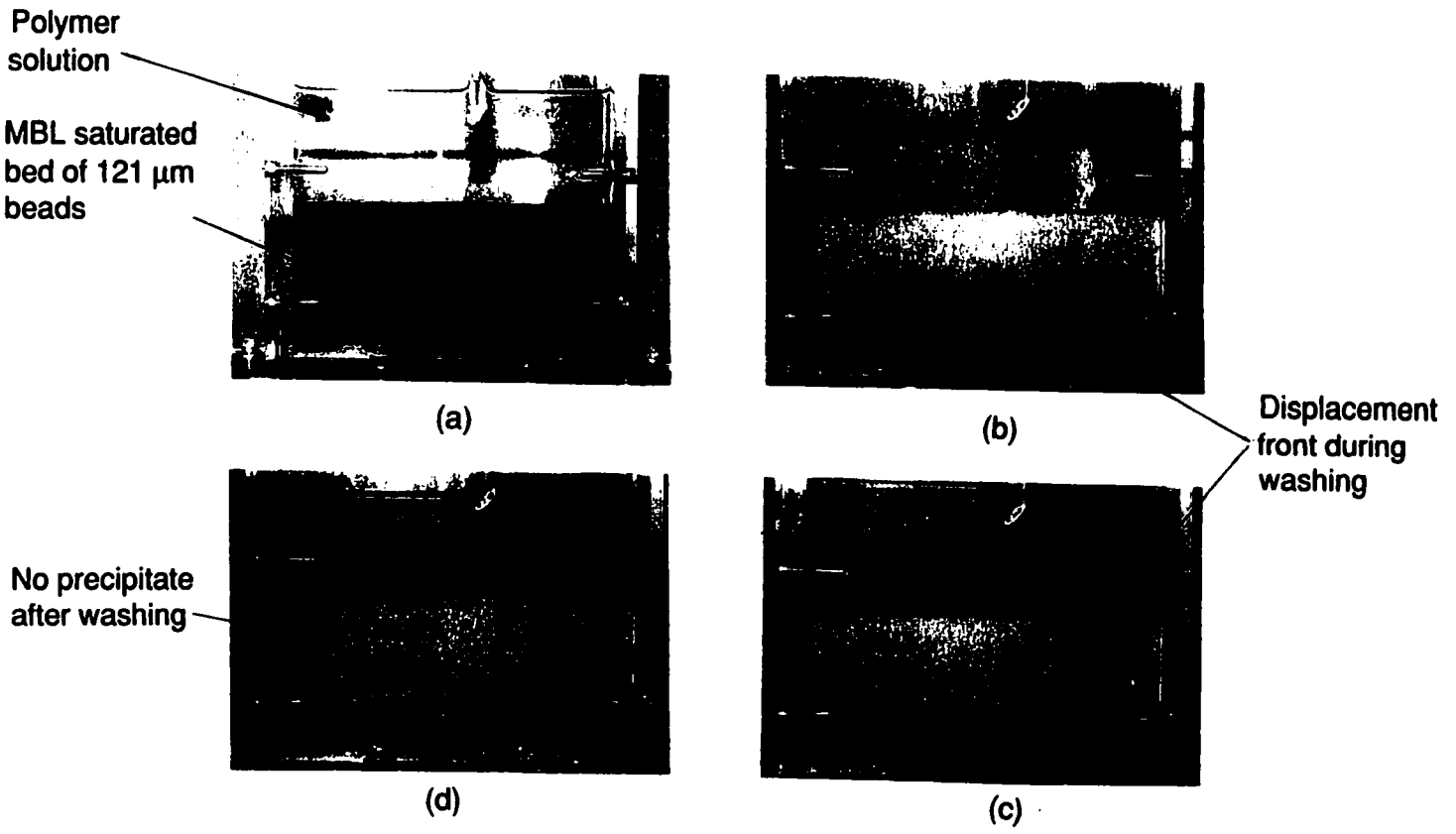

Figure 3.8 Sequential profiles of displacement front in a homogeneous bed of fine beads (121 μm) during displacement of MBL with polymer solution. No precipitate was observed in the bed after washing. Displacement proceeded from (a) through (d).

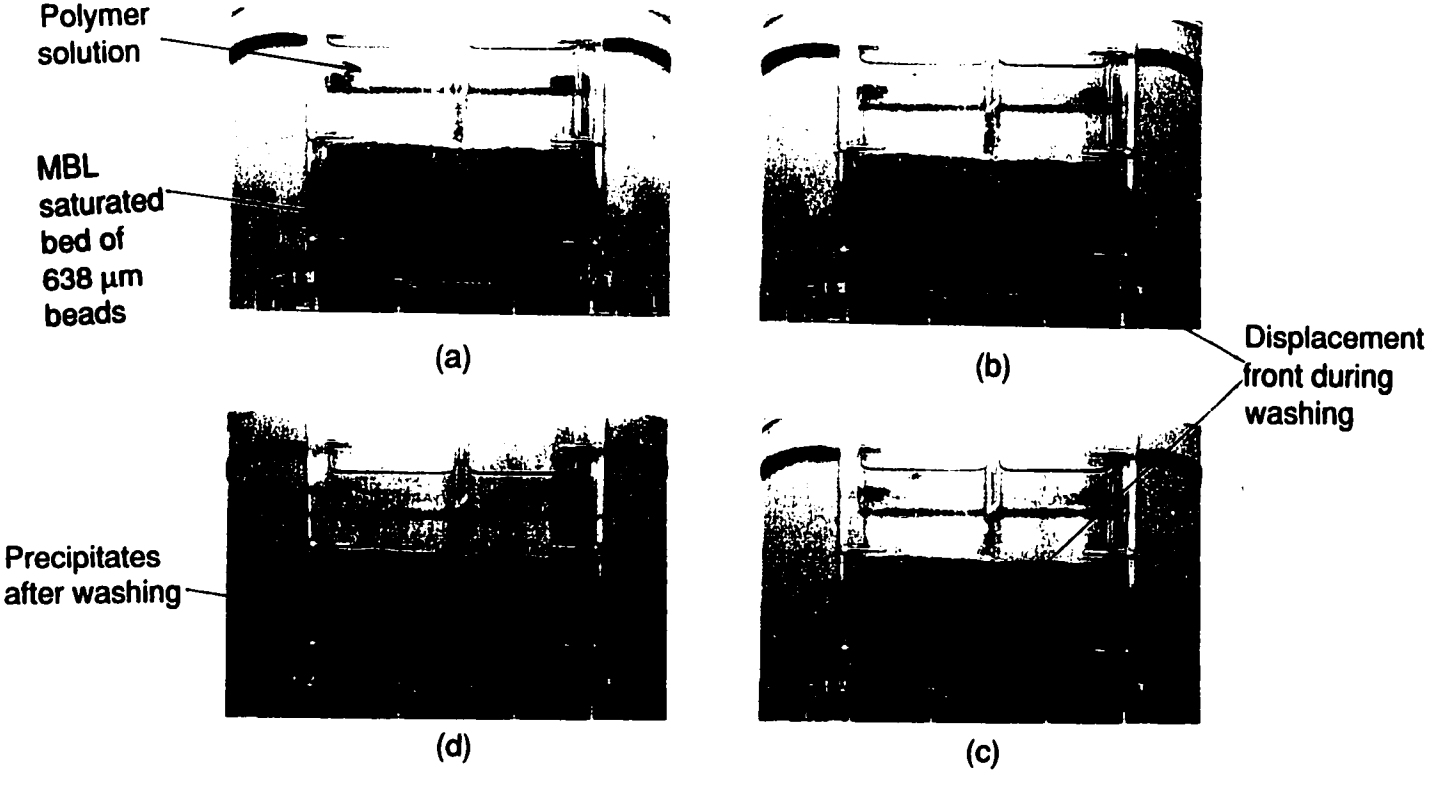

Figure 3.9 Sequential profiles of displacement front in a homogeneous bed of coarse beads (638 μm) during displacement of MBL with polymer solution. Precipitate was observed in the bed after washing. Displacement proceeded from (a) through (d).

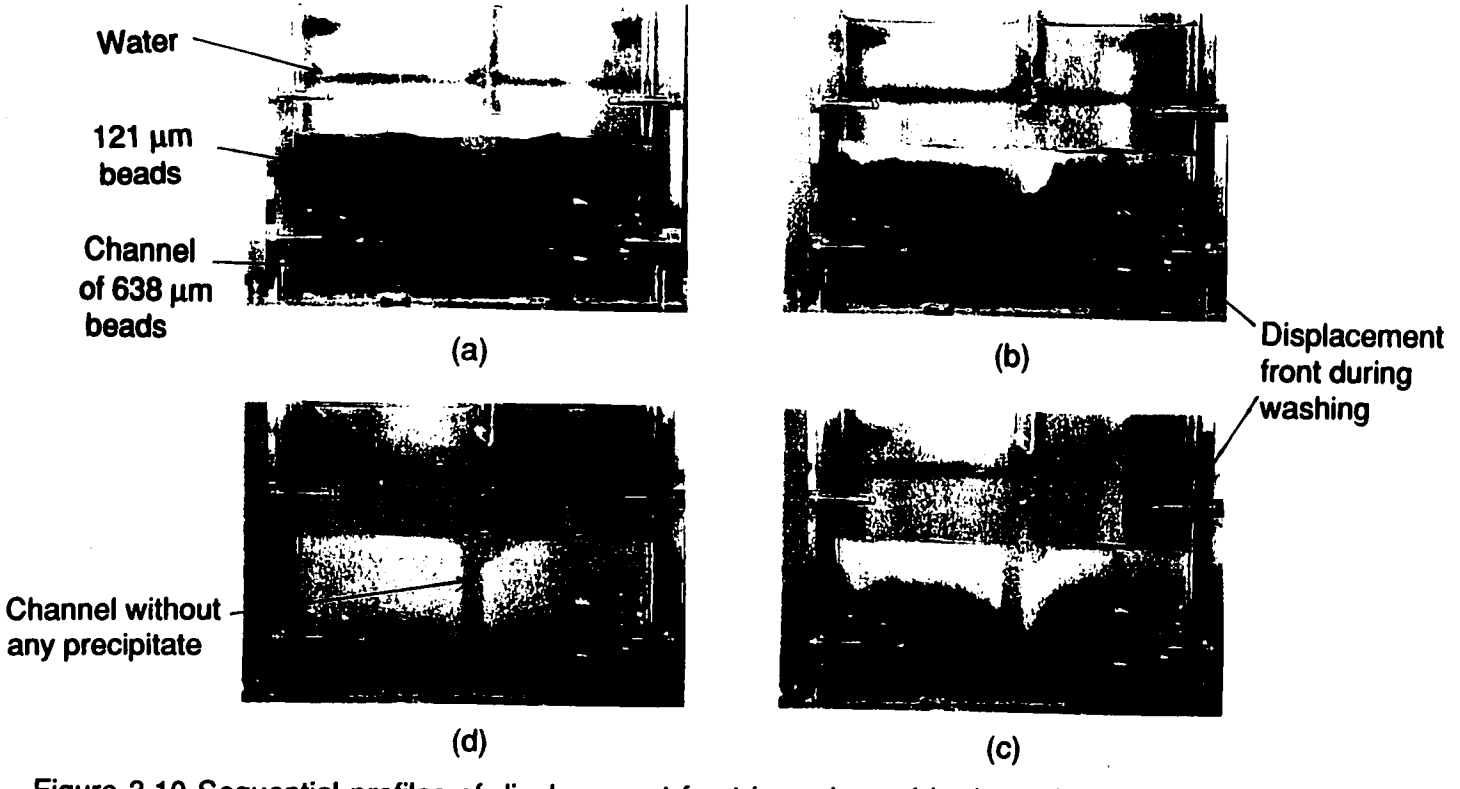

Figure 3.10 Sequential profiles of displacement front in a channel bed consisting of coarse beads (638 μm) and fine beads (121 μm) during displacement of MBL with water. Displacement proceeded from (a) through (d).

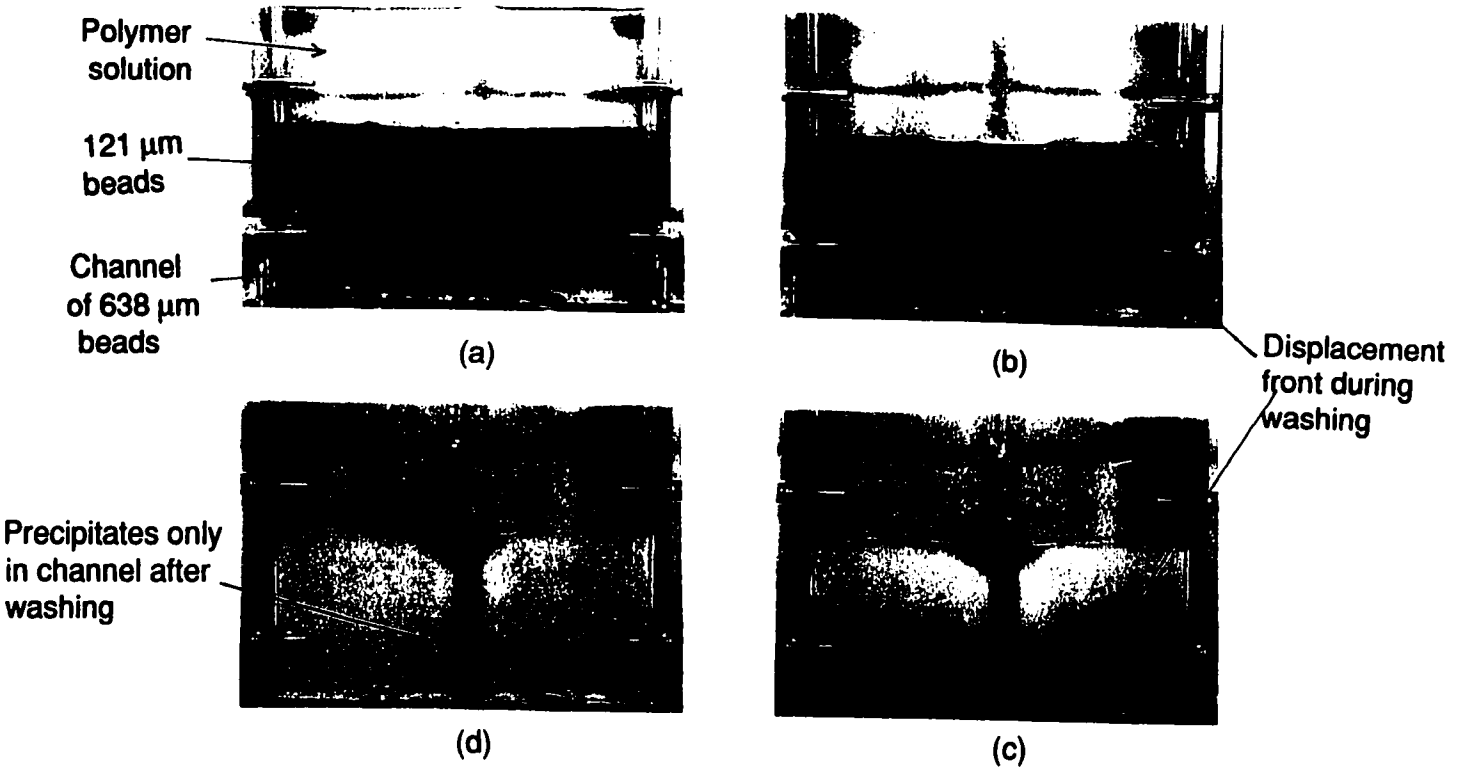

Figure 3.11 Sequential profiles of displacement front in a channel bed consisting of coarse beads (638 μm) and fine beads (121 μm) during displacement of MBL with polymer solution. Precipitates were selectively retained only in the center channel of coarse beads after washing. Displacement proceeded from (a) through (d).

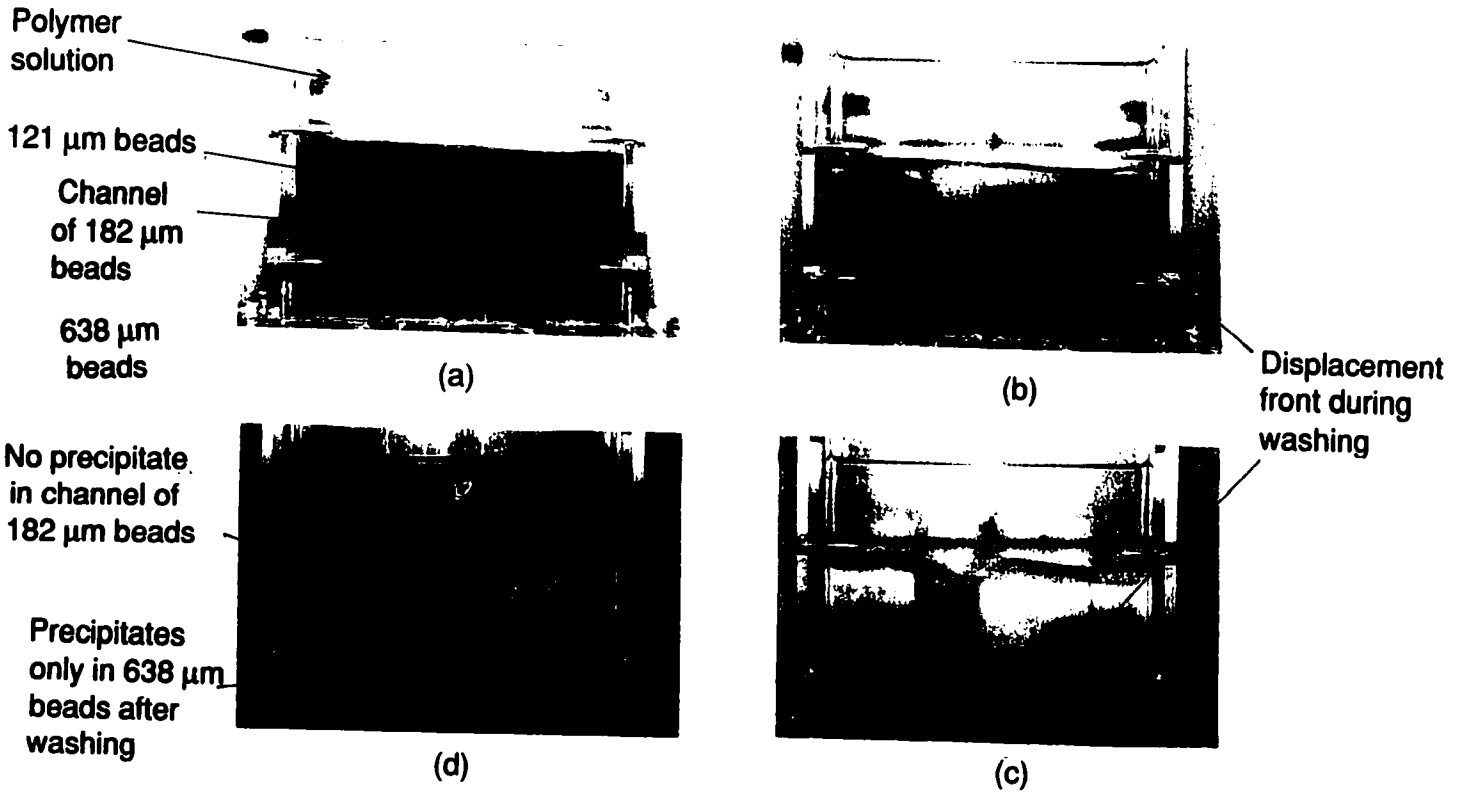

Figure 3.12 Sequential profiles of displacement front in a mixed bed consisting of coarse beads (638 μm), medium beads (182 μm), and fine beads (121 μm) during displacement of MBL with polymer solution. Precipitates were selectively retained only in the channel of coarse beads. No precipitate was observed in the channel of medium beads and in fine beads after washing. Displacement proceeded from (a) through (d).

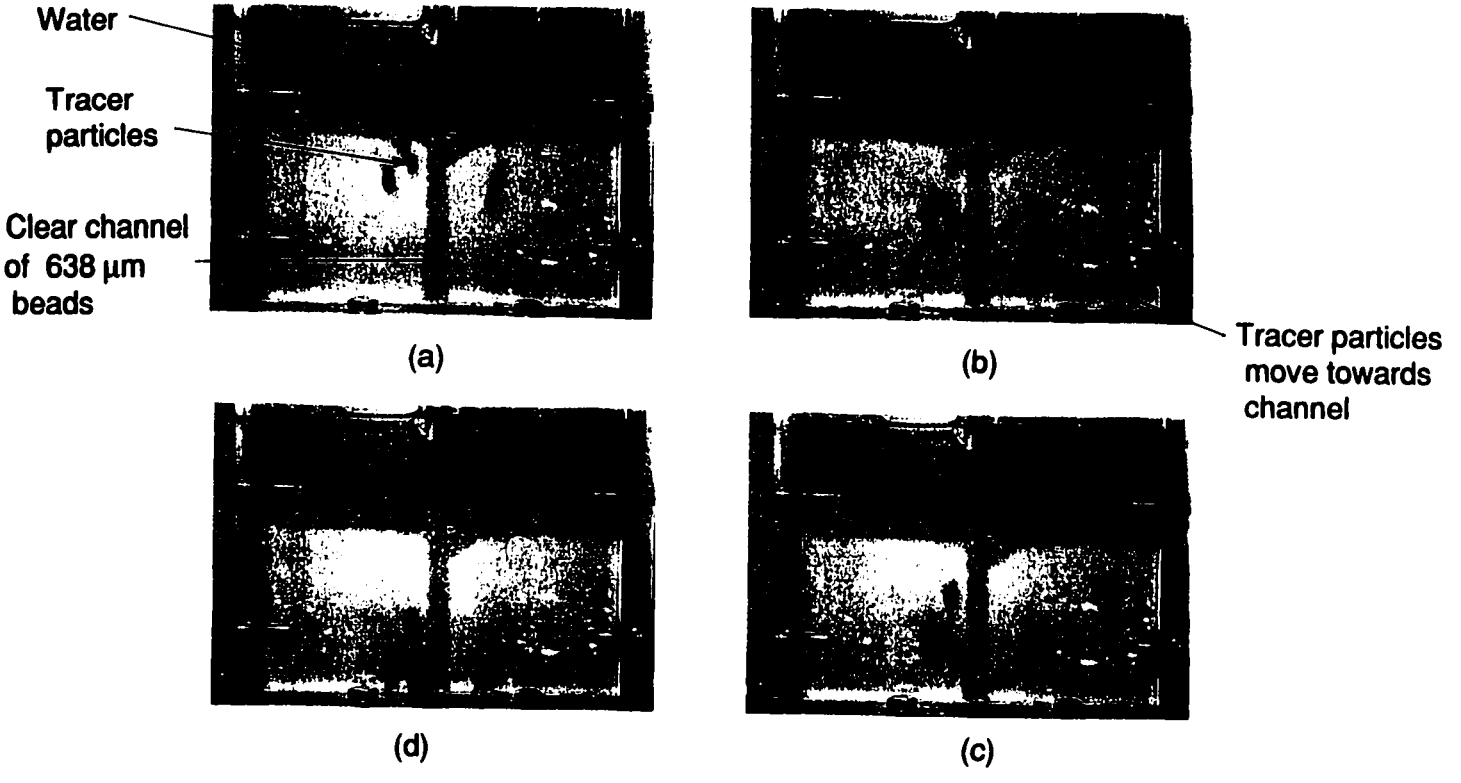

Figure 3.13 Sequential movement of tracer particles from fine beads (121 µm) towards the channel of coarse beads (638 µm) in a channel bed after displacement washing of MBL with water. Movement of tracer particles from fine to coarse beads indicated the presence of cross flow. Sequential positions of tracer particles are in the order, (a) through (d).

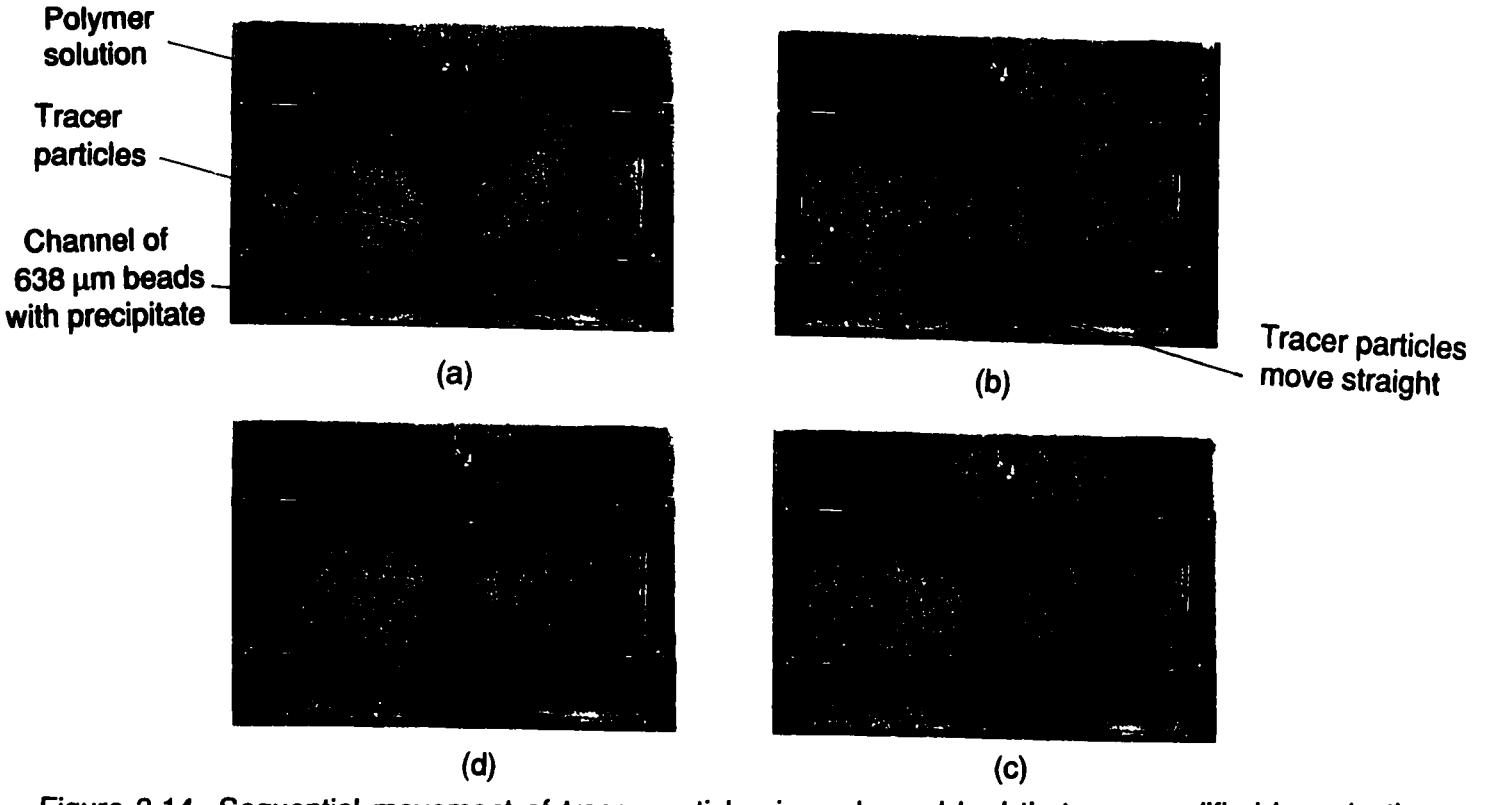

Figure 3.14 Sequential movement of tracer particles in a channel bed that was modified by selective precipitation in the channel of coarse beads (638 μm) during displacement washing of MBL with polymer solution. Straight movement of tracer particles indicated absence of cross flow and modification of bed properties towards a homogeneous bed after washing. Sequential positions of tracer particles are in the order, (a) through (d).

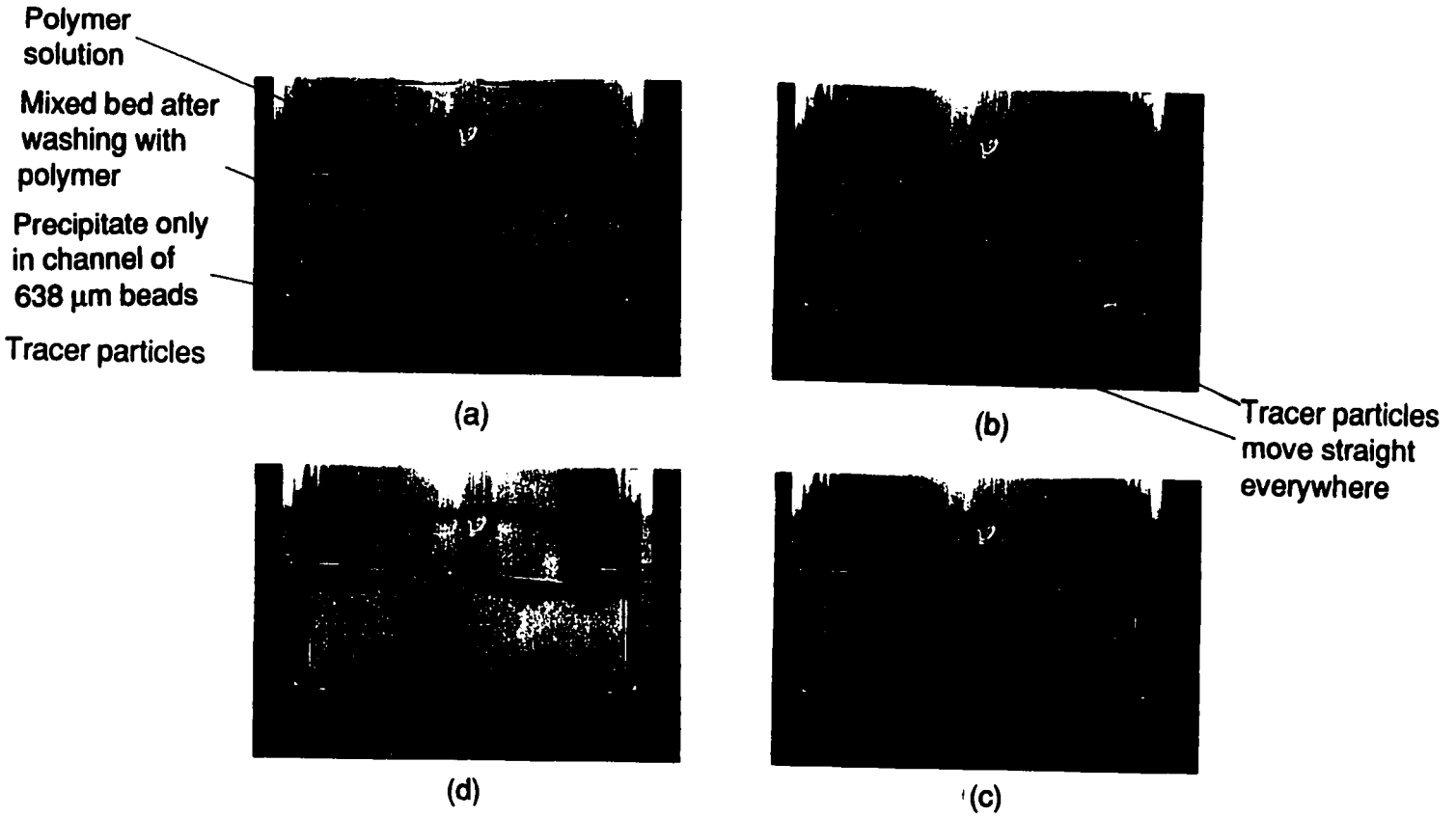

Figure 3.15 Sequential movement of tracer particles in a mixed bed that was modified by selective precipitation only in the channel of coarse beads (638 μm) during displacement washing of MBL with polymer solution. Straight movement of tracer particles indicated the absence of cross flow in every section of the bed after washing Sequential positions of tracer particles are in the order, (a) through (d).

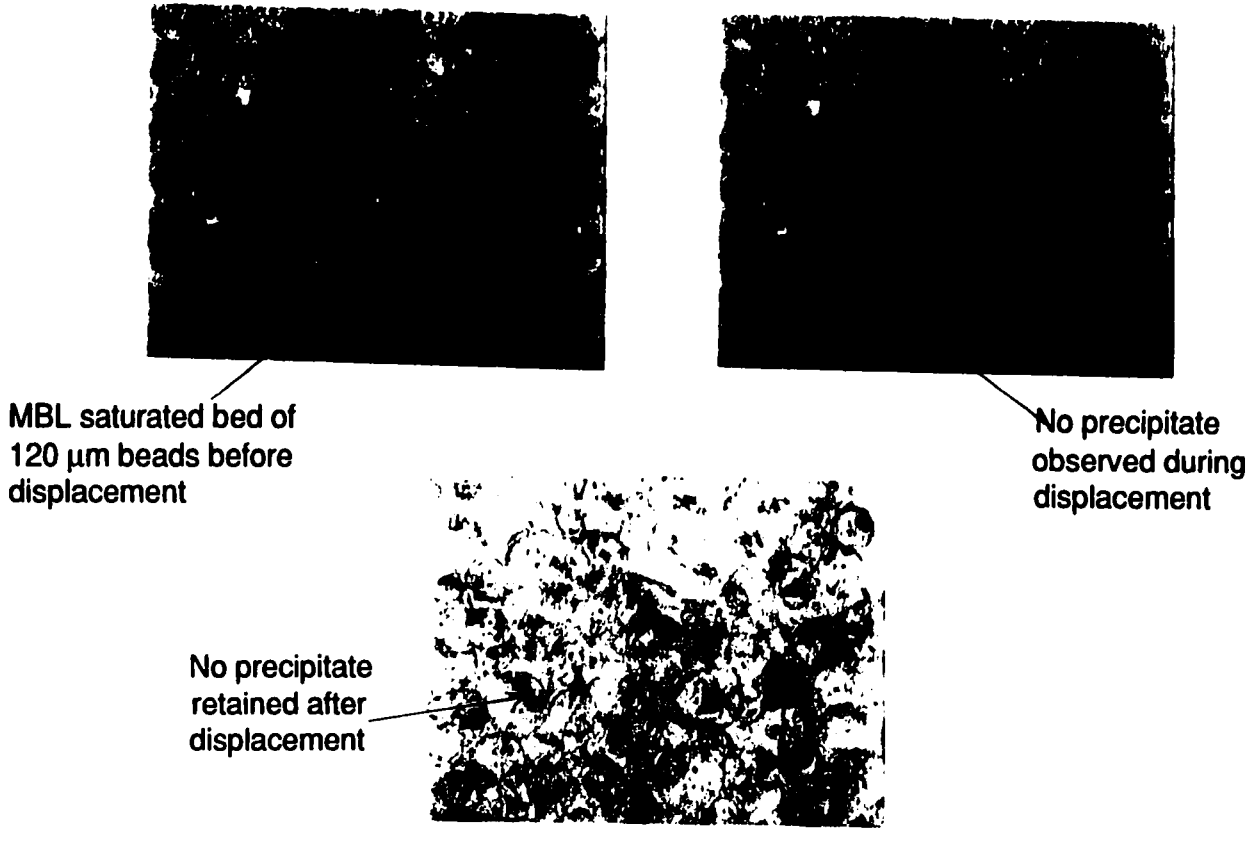

Figure 3.16 Sequential pictures of the magnified (50x) views of a section of homogeneous bed of fine beads (121 μm) during displacement of MBL with polymer solution. No precipitate was located in the bed during and after washing. Displacement proceeded from (a) through (d).

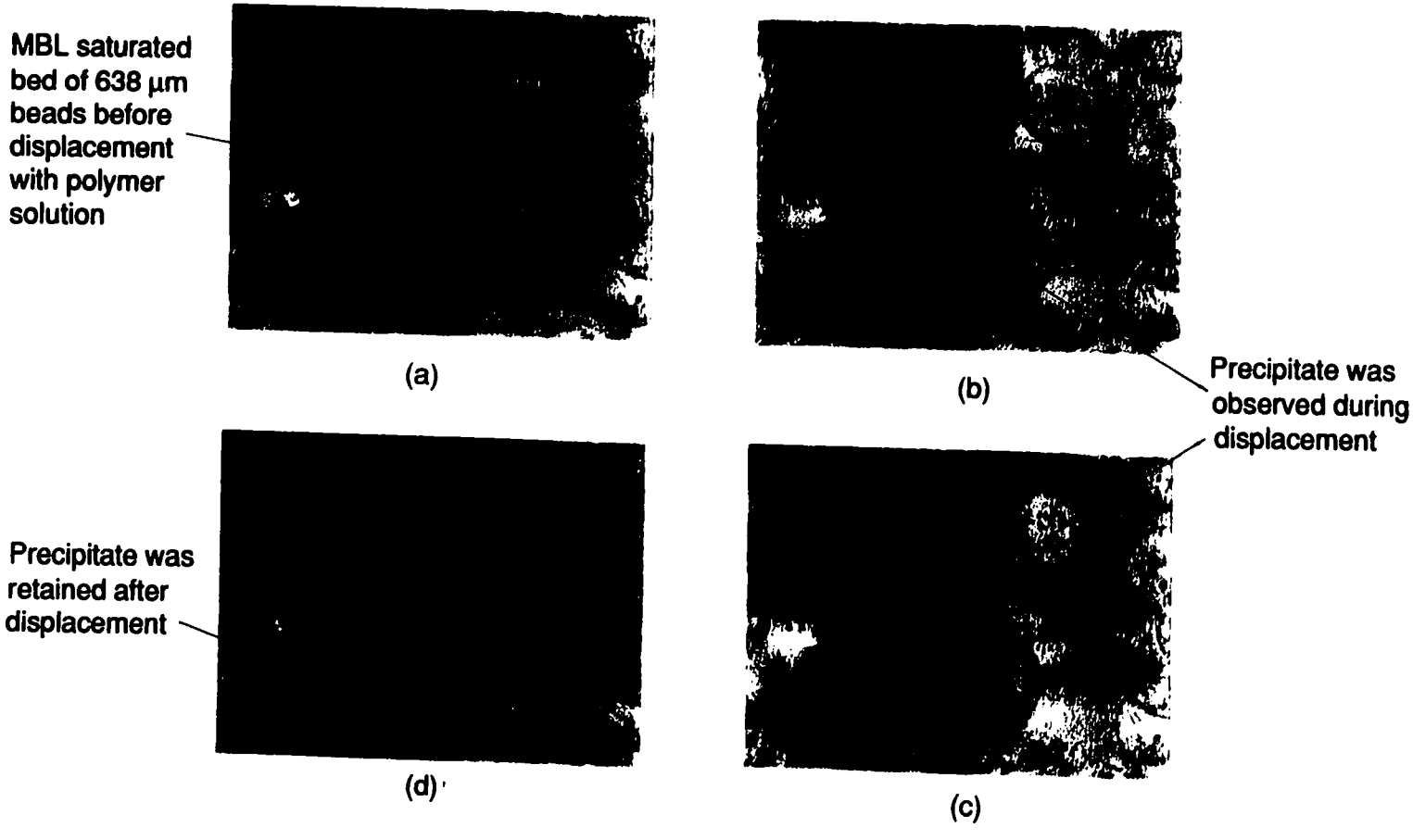

Figure 3.17 Sequential pictures of the magnified (18x) views of a section of homogeneous bed of coarse beads (638 μm) during displacement of MBL with polymer solution. Precipitates were observed in the bed during and after washing. Displacement proceeded from (a) through (d).

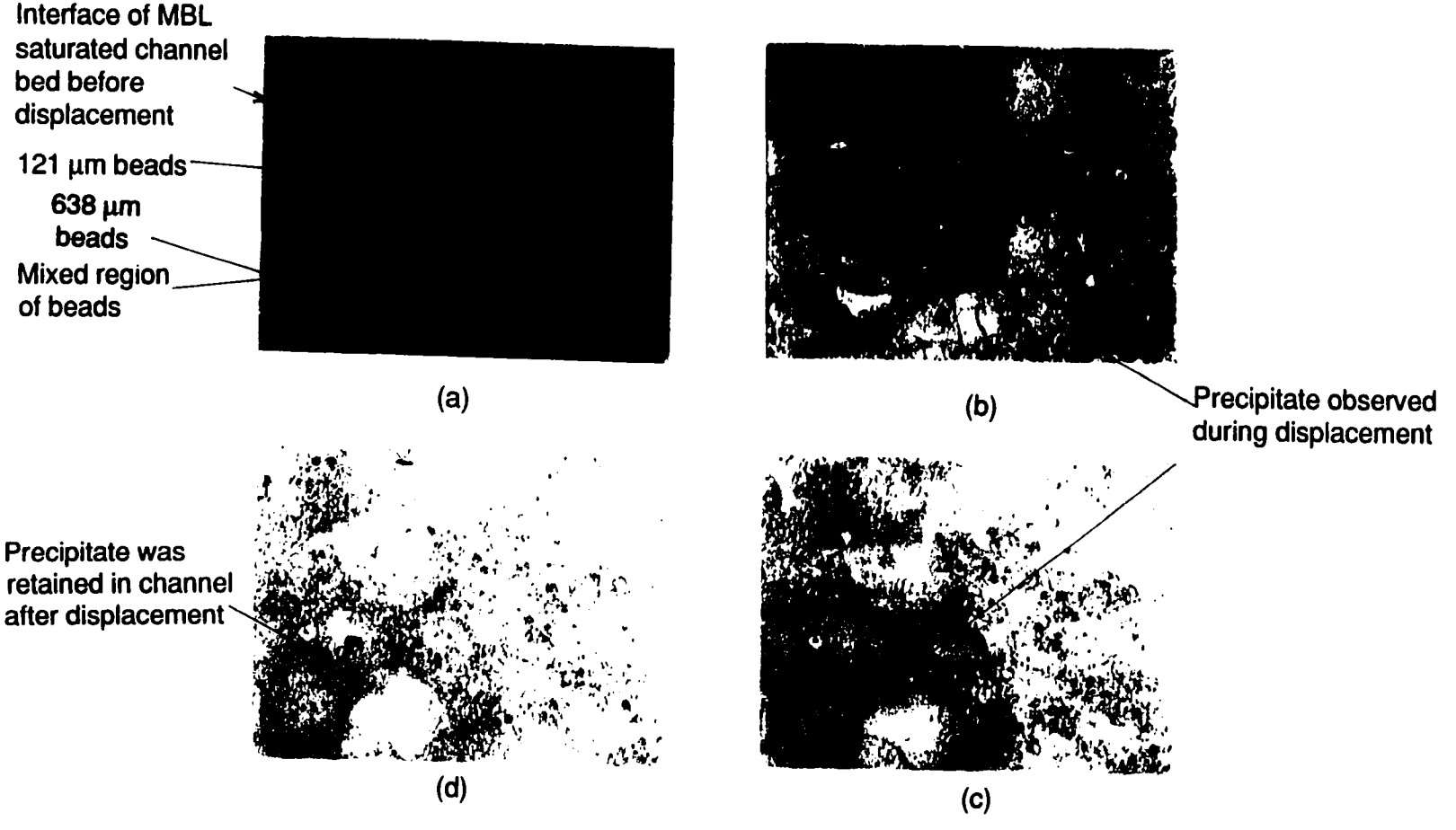

Figure 3.18 Sequential pictures of the magnified (18x) views of a section of the interface of coarse beads (638 μm) and fine beads (121 μm) in a channel bed during displacement of MBL with polymer solution. Precipitates were observed only in the channel of coarse beads during and after washing. Displacement proceeded from (a) through (d).

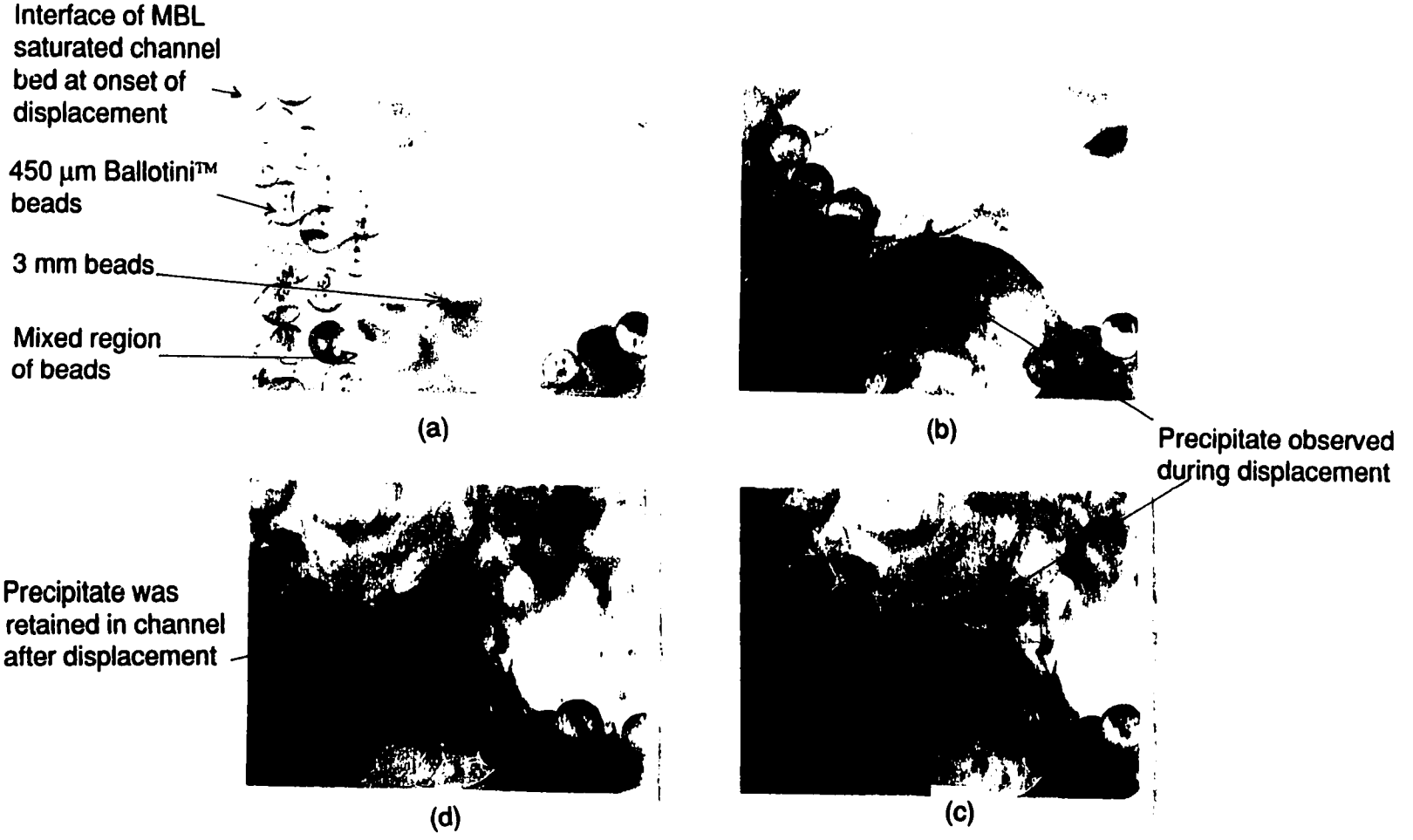

Figure 3.19 Sequential pictures of the magnified (16x) views of a section of the interface of Ballotini® beads (450 μm) and 3 mm glass beads in a channel bed during displacement of MBL with polymer solution. Precipitates were located only inside the channel of 3 mm beads during and after washing. Displacement proceeded from (a) through (d).

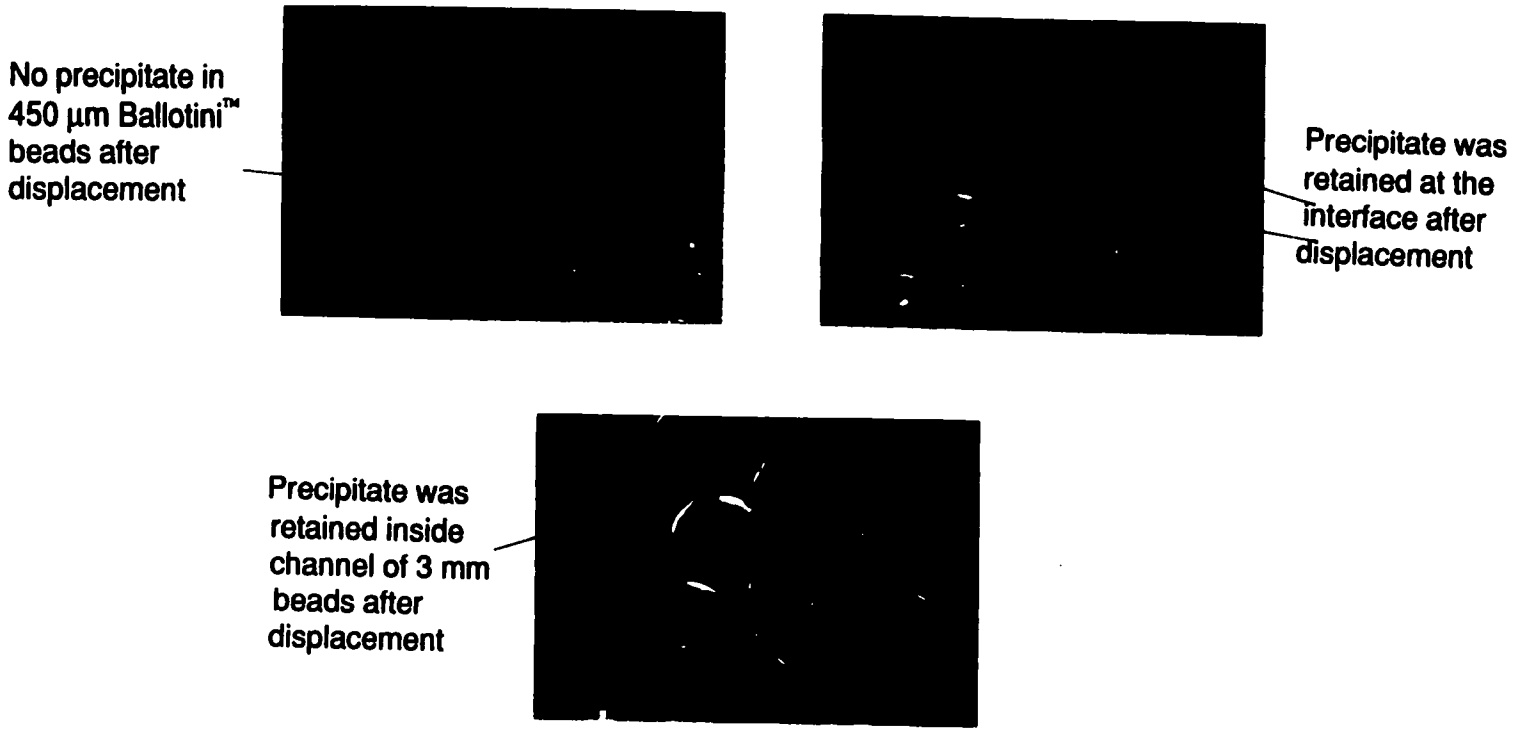

Figure 3.20 Magnified (4x) views of different parts of a channel bed consisting of 3 mm glass beads in channel and 450 µm Ballotini® beads in annulus after displacement of MBL with polymer solution. Precipitates were located only in the channel of 3 mm beads, and at the interface where 450 µm Ballotini® beads and 3 mm glass beads were mixed. No precipitate was located in 450 µm Ballotini® beads.

Figures 3.10 and 3.11 depict the sequential profiles of displacement fronts in a channel bed during washing with water and the polymer solution respectively. After washing, it was observed that precipitates were only retained in the center channel in a channel bed within 0.3 cm of both sides of the channel.

Figure 3.12 shows the sequential profiles of displacement fronts in a mixed bed during washing with the polymer solution. It was observed that precipitates were only retained in the channel of coarse glass beads after washing. The profile of precipitate retention was similar to that observed in a channel bed washed with the polymer solution.

3.3.2 Streamlines of Fluid Elements in a Channel Bed

Sequential pictures of the movement of tracer particles with time in a channel bed after the completion of displacement experiments are shown in Figure 3.13 and Figure 3.14. After washing a channel bed with water, the tracer particles were observed to move in transverse direction from the fine part of the bed towards the central channel, shown in Figure 3.13. However, Figure 3.14 shows that in a channel bed that was washed with the polymer solution, tracer particles went straight through the fine part of the bed instead of moving towards the central channel.

Figure 3.15 shows the movement of tracer particles with time in different regions of the mixed bed after it was washed with the polymer solution. Tracer elements in every section of the bed went straight through the bed with time.

3.3.3 Results of Experiments using Makroscope

Figures 3.16 and 3.17 show sequential pictures of the magnified views of sections of homogeneous beds made of fine and coarse beads separately when the displacement front passed through them. In a homogeneous bed of fine beads, no precipitate was observed during displacement of MBL with the polymer solution. However, during the displacement of MBL with the polymer solution in a homogeneous bed of coarse glass beads, precipitates were observed to form and deposit on particle surfaces and in pore throats. At the end of washing, precipitates were retained as a film on the surface of particle or near the pore mouths, plugging the pores.

Figure 3.18 shows sequential pictures of magnified views of a section of the interface between fine (121 mm) and coarse (638 mm) beads during displacement of MBL with polymer solution in a channel bed. Sequential pictures of the magnified views of the interface between 450 μm diameter Ballotini beads and 3 mm diameter glass beads is shown in Figure 3.19 during displacement with the polymer solution. Arrays of smaller beads from fine part of the channel bed intruded into the channel. Beads at the interface of the two kinds of beads

were seen to move during displacement. This resulted in mixed areas in the interface where the sizes of pore throats decreased from that in channel to that in fine part of the bed. Precipitates were located inside the channel during displacement. In the mixed areas at the interface (within about 0.3 cm of both sides of channel) of two kinds of beads, both deposition and filtration of precipitates were observed. Figure 3.20 shows magnified views of the fine and channel parts of the channel bed after washing with the polymer solution. About 0.3 cm away from both sides of channel, precipitates were retained in the channel either as a film on the surface of beads, as pendular rings between the beads, and in the pore throats appearing to plug them. There was no evidence of precipitate retention inside the fine part of the channel bed.

3.4 Discussion

3.4.1 Interpretation of Results of Displacement Experiments

Mixing of lignin and the polymer was required in order to form a precipitate inside a bed during a displacement experiment. Figures 3.9 and 3.17 demonstrate that precipitates were formed and retained in homogeneous beds of coarse beads during a displacement experiment with the polymer solution. On the other hand, no precipitates were observed in homogeneous beds of fine

beads during a displacement experiment, shown in Figures 3.8 and 3.16. Figures 3.11, 3.18, 3.19, and 3.20 show that precipitates were selectively formed and retained in the channel in a channel bed. Figure 3.13 shows that in the absence of selective precipitation in the channel of a channel bed that was washed with water, tracer particles moved laterally with flow from the fine part to the channel of the channel bed.

In the absence of any channelling in a homogeneous bed, better mixing of lignin and the polymer, potentially caused by higher longitudinal dispersion of them across the interface between MBL and the polymer solution in a homogeneous bed of coarse beads than that in a homogeneous bed of fine beads, resulted in the formation of precipitates only in a homogeneous bed of coarse beads. Potential reasons for selective precipitation in the channel of a channel bed during washing with the polymer solution were: (a) higher longitudinal dispersion and hence better mixing of lignin and polymer in the channel of a channel bed than that in the fine part of the channel bed (similar to that observed for homogeneous beds); and (b) at the interface of two kinds of beads, mixing of the laterally moving lignin from the fine part of a channel bed with the polymer flowing down in the channel.

3.4.1.1 Mixing of Lignin and Polymer due to Hydrodynamic Dispersion

One of the possible reasons of mixing of lignin and the polymer during displacement washing in porous beds was hydrodynamic dispersion of each component across the interface between phases, MBL and the polymer solution. Bear (1972) reviewed hydrodynamic dispersion as "the macroscopic outcome of (a) external forces acting on the liquid, (b) the microscopic intricate geometry of the pore system, (c) molecular diffusion caused by species concentration gradients, (d) variation in liquid properties, such as density and viscosity, that affect the flow pattern, (e) changes of the species concentration due to chemical and physical processes within the liquid phase, and (f) interactions between the liquid and the solid phases. Two basic elements in this kind of mixing are flow (convective mixing) and presence of the pore system (mechanical dispersion) through which flow takes place". In addition to the local inhomogeneity in pore structures on a microscopic scale, inhomogeneity on a macroscopic scale due to variation in permeability across the flow domain also contributes to mechanical mixing of the species (Bear, 1972).

For one-dimensional flow, E_L, the longitudinal dispersion coefficient, which is a measure of longitudinal mixing of a species between the displaced and displacing phases, can be expressed as (Lake, 1989)

$$E_L = C_1 D_0 + C_2 \left(\frac{|v| d_p}{D_0}\right)^{\beta} D_0 \qquad 3.2$$

where C_1, C_2, and b are properties of the medium and flow regime, D_0 is the effective binary molecular diffusion coefficient of the species between miscible displacing and displaced fluids, d_p is the average particle diameter, and $|v|$ is the absolute value of the interstitial velocity of the fluid flowing in the bed. The first term in Equation (3.2) accounts for the contribution of molecular diffusion to longitudinal dispersion and the second term accounts for the contribution of mechanical and convective dispersion to the overall longitudinal dispersion of any species. The relative contribution of these two mechanisms of mixing on the overall longitudinal dispersion process depends on particle Peclet number (Lake, 1989) defined in Equation (3.3).

$$Pe_p = \frac{vd_p}{D_0} \qquad 3.3$$

When particle Peclet number based on the molecular diffusion coefficient is greater than 10, convective dispersion controls the mechanism of mass transport and the first term in Equation (3.2) can be neglected, resulting in Equation (3.4) (Lake, 1989).

$$E_L = C_2(\frac{|v|d_p}{D_0})^{\beta} D_0 \qquad 3.4$$

Based on experimental results, Perkins and Johnston (1963) found the value of b that ranged between 1 and 1.25 in the flow regime where convective

dispersion was the controlling mechanism of mass transport. Taking the minimum value β as 1, Equation (3.4) can be written as

$$E_L = C_2 |v| d_p \qquad 3.5$$

Correlation among E_L, v, and d_p similar to that in Equation (3.5) has also been proposed by Harleman et al., (1963). Interstitial velocity (v) in Equation (3.5) can be calculated using Darcy's law of fluid permeation in a porous medium to be

$$\frac{Q}{\varepsilon A} = v = \frac{K\Delta P}{\varepsilon \mu L} \qquad 3.6$$

where Q is the flow rate of the fluid, A is the area normal to flow, ε is the porosity of the medium, K is the permeability of the porous medium, μ is the viscosity of flowing fluid, L is the length of the bed, and ΔP is the pressure drop across the bed. Bear (1972) proposed that when particle Reynolds number based on average particle diameter as defined in Equation (3.7) is below 10, Darcy's law of fluid permeation is valid and inertial effects could be neglected since the flow remains predominantly in the laminar regime:

$$Re_p = \frac{\rho u d_p}{\mu} \qquad 3.7$$

where ρ is the density of fluid flowing through the bed and u is the superficial velocity.

3.4.1.2 Mixing of Lignin and Polymer in Homogeneous Beds

Particle Reynolds number and particle Peclet number based on the molecular diffusion coefficient can be calculated using Equations (3.3) and (3.7) respectively to characterize the flow regime and controlling mechanism of mass transport in longitudinal dispersion of a species in both beds of coarse and of fine particles. The difference in the extent of mixing of lignin and the polymer during displacement with the polymer solution in homogeneous beds of fine and coarse beads can be estimated from a comparison of longitudinal dispersion coefficients of a component in the two beds using Equation (3.2).

For constant pressure head displacement experiments in homogeneous beds, Equation (3.6) can be written for homogeneous beds of fine and coarse beads, resulting in

$$\frac{Q_c}{A_c} = u_c = \varepsilon_c v_c = \frac{K_c \Delta P_c}{\mu_c L_c} \qquad 3.8$$

$$\frac{Q_f}{A_f} = u_f = \varepsilon_f v_f = \frac{K_f \Delta P_f}{\mu_f L_f} \qquad 3.9$$

where v_c and v_f are the interstitial velocities and u_c and u_f are the superficial velocities of fluid in homogeneous beds of coarse and fine glass beads

respectively. The permeability (K) of a porous bed comprising of beads of average diameter, d_p, and voidage, ε can be expressed from Ergun equation as

$$K = \frac{d_p^2 \varepsilon^3}{150(1-\varepsilon)^2} \qquad \textbf{3. 10}$$

(McCabe et al., 1976). Since ε for both beds of fine and of coarse beads were measured to be 0.4, the ratio of permeabilities of beds of coarse and fine beads can be computed using Equation (3.10) as

$$\frac{K_c}{K_f} = \frac{d_{p,c}^2}{d_{p,f}^2} \approx 28 \qquad \textbf{3. 11}$$

The flow area A, viscosity μ, and ΔP over the length L were the same for both beds of fine and coarse glass beads under constant pressure head displacement washing in homogeneous beds. Dividing Equation (3.8) by Equation (3.9), and using Equation (3.11) one gets,

$$\frac{\frac{Q_c}{A_c}}{\frac{Q_f}{A_f}} = \frac{u_c}{u_f} = \frac{v_c \varepsilon_c}{v_f \varepsilon_f} = \frac{K_c}{K_f} \approx 28 \qquad \textbf{3. 12}$$

For the constant pressure head displacement experiments in 8.5 cm long beds, the available net pressure head for driving the flow was 4.5 cm of water. Using Equation (3.7), it can be written that

$$Re_{p,f} = \frac{\rho u_f d_{p,f}}{\mu} = 0.004 \qquad \textbf{3. 13}$$

$$Re_{p,c} = \frac{\rho u_c d_{p,c}}{\mu} = 0.641 \qquad \textbf{3. 14}$$

Equations (3.13) and (3.14) suggest that Darcy's law was valid and laminar flow prevailed during constant pressure head displacement in homogeneous beds of fine and of coarse beads since particle Reynolds numbers in both beds were less than 10.

Equation (3.3) can be used to calculate the particle Peclet numbers based on the molecular diffusion coefficient of lignin (assumed 10^{-8} cm^2/s) as

$$Pe_{p,f} = \frac{v_f d_{p,f}}{D_0} = 1.08 \times 10^4 \qquad \textbf{3. 15}$$

$$Pe_{p,c} = \frac{v_c d_{p,c}}{D_0} = 1.6 \times 10^6 \qquad \textbf{3. 16}$$

(Lake, 1989). Since the particle Peclet numbers in both beds of fine and of coarse beads were much greater than 10, the contribution from molecular diffusion to the overall dispersion process was negligible compared to that from convective and mechanical dispersion (Lake, 1989). As a result, a comparison of longitudinal dispersion coefficients for two beds using Equations (3.5) and (3.12) results in

$$\frac{(E_L)_c}{(E_L)_f} = \frac{v_c d_{p,c}}{v_f d_{p,f}} = 148 \qquad 3.17$$

Equation (3.17) describes that the longitudinal dispersion coefficient E_L, the measure of longitudinal mixing of lignin and polymer during constant pressure head displacement washing, was 148 times higher in a bed of coarse glass beads than that in a bed of fine glass beads. When convective mixing is the dominant mechanism of mass transport and particle Peclet number based on molecular diffusion coefficient is greater than 10, the longitudinal dispersion coefficient, E_L, will increase with increase in particle Peclet number based on the molecular diffusion coefficient, as has been reported by several authors (Perkins and Johnston, 1963; Bues and Aachib, 1991, and Blackwell, 1962, Han et al., 1985). Due to higher mixing of lignin and the polymer in beds of coarse glass beads than that in beds of fine glass beads, chances of formation of precipitates were higher in the beds of coarse beads than in the beds of fine beads.

3.4.1.3 Mechanism of Precipitate Retention during Displacement

Figure 3.21 delineates the plausible mechanism of precipitate retention in the porous bed during the process of displacement washing with polymer solution. Le Goff et al.(1970) have reviewed the process of colmatage (clogging)

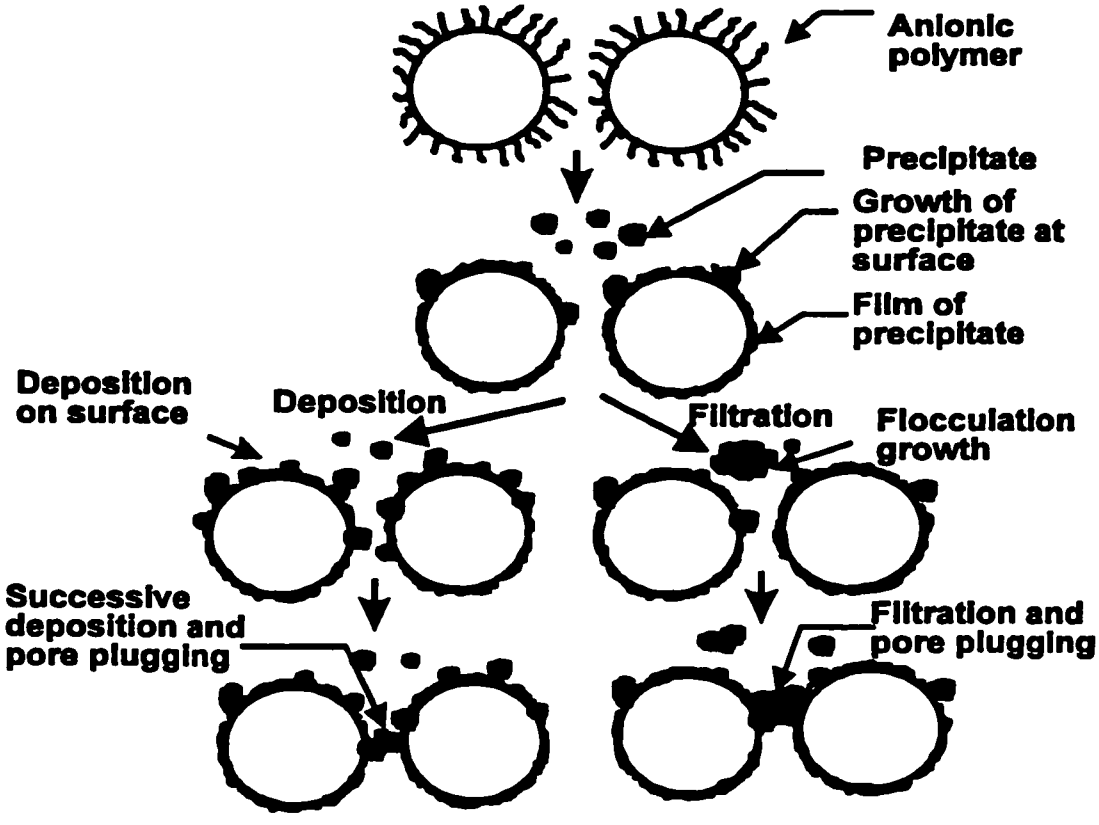

Figure 3.21 Probable mechanisms of precipitate retention in the porous bed during displacement of MBL with polymer solution.

and decolmatage of a porous bed when a suspension flows through a porous bed. Two major mechanisms of colmatage or clogging reported by them are mechanical filtration of large particles and physiochemical filtration or deposition of small particles. For intermediate particles, both mechanical and physiochemical phenomena intervene. Particles of colloidal range (diameter < 1 μm) are retained by Van der Waals and electrokinetic forces. Large particles are retained in crevice sites (particle becomes wedged between convex surfaces of

two grains), constriction sites (particle cannot penetrate into a pore of a smaller size that its own), and in cavern sites (particle is retained in a small pocket formed by several grains). Large particles are retained by fluid friction and fluid pressure and capture mechanisms are sedimentation forces and direct interception with a retention site. Small particles are deposited on surface sites by direct interception and the retention forces are Van der Waals forces and electrokinetic forces.

During the displacement washing process, small particles of precipitates were observed to deposit on the surfaces of glass beads, forming a film. Due to successive deposition on the same site, pores were observed to be plugged. In the majority of cases, bigger particles were observed to be mechanically filtered in the pore throats, plugging the throats. It is postulated that higher mixing in a bed of coarse beads might have caused orthokinetic flocculation growth of precipitates into larger particles and subsequently mechanical filtration in pore mouths in a homogeneous bed of coarse beads. Small particles of precipitates deposited on the surface of glass beads were seen to migrate from one surface retention site to another.

3.4.1.4 Mixing of Lignin and Polymer due to Dispersion in Channel Bed

One potential reason for selective formation and retention of precipitates in the channel of a channel bed was higher longitudinal dispersion, which

caused better mixing of lignin and the polymer in the channel than that in the fine part of a channel bed. An analysis similar to that for homogeneous beds could be performed to compare the longitudinal dispersion coefficients in the channel and in the fine part of a channel bed.

For constant pressure head displacement experiments in a channel bed, Equations (3.8) through (3.17) are still valid. Equations (3.13) and (3.14) show that the particle Reynolds numbers in the channel and in the fine part of the channel bed were both less than 10. As a result, the flow regime in both the channel and the fine part of the channel bed were in the laminar region. Equations (3.15) and (3.16) show that particle Peclet numbers in the channel and in the fine part of a channel bed were much greater than 10. Consequently, the controlling mechanism of mass transport in the channel and in the fine part of a channel bed was mechanical and convective dispersion. Equation (3.17) suggests that longitudinal dispersion coefficient E_L, in the channel was 148 times higher than that in fine part of the channel bed. Because of a greater amount of mixing of lignin and the polymer, precipitates were selectively formed in the channel. As the precipitates moved towards the bottom of bed with the flow, they appeared to be filtered and deposited in the mixed areas in the interface of the two kinds of beads where size of pore throat decreased from that in the channel to that in the fine part of the bed. Since the mixed areas were limited to about 0.3 cm from both sides of the channel, more precipitates were retained near the

interface at the end of washing, as shown in Figure 3.20. Precipitates moving in the center of channel were deposited on surface of coarse particles and sometimes bigger ones were mechanically filtered at the pore throats, plugging the throats, as depicted in Figure 3.21. As a result, the characteristic of a channel bed was changed towards that of a homogeneous bed.

3.4.1.5 Mixing of Lignin and Polymer caused by Lateral Flow of Lignin

Figure 3.13 shows that in a channel bed that was not modified by selective plugging of channel by precipitates, tracer elements were driven by flow from fine part of the bed towards the center channel. This indicated the presence of a cross flow of lignin from the fine part of a channel bed towards the center channel during a displacement experiment with the polymer solution. One of the potential reasons for selective precipitation in the center channel of a channel bed was cross flow driven mixing of lignin at the interface of the two kinds of beads with the polymer that was flowing down the center channel. As a result, precipitates were selectively formed and retained near the interface of the center channel.

Pelton et al. (1994) hypothesized that the cross flow was due to a transverse inward pressure gradient that was a result of an inertial effect caused by higher superficial velocity of fluid in the channel than that in the fine part of the channel bed. The magnitude of the transverse pressure gradient resulting

from the inertial effect can be computed by making an energy balance at any cross section of the channel bed using Bernoulli's equation. A mechanical energy balance along a streamline between point 1 and point 2 in the fine part of the bed as depicted in Figure 3.22 results in

$$\frac{P_{1f}}{\rho g}+\frac{(u_{1f})^2}{2g}=\frac{P_{2f}}{\rho g}+\frac{(u_{2f})^2}{2g}-Z+h_f \qquad 3.18$$

where g is acceleration due to gravity, Z is the vertical distance between point 1 and point 2 in fine part of bed, and h_f is the frictional head loss.

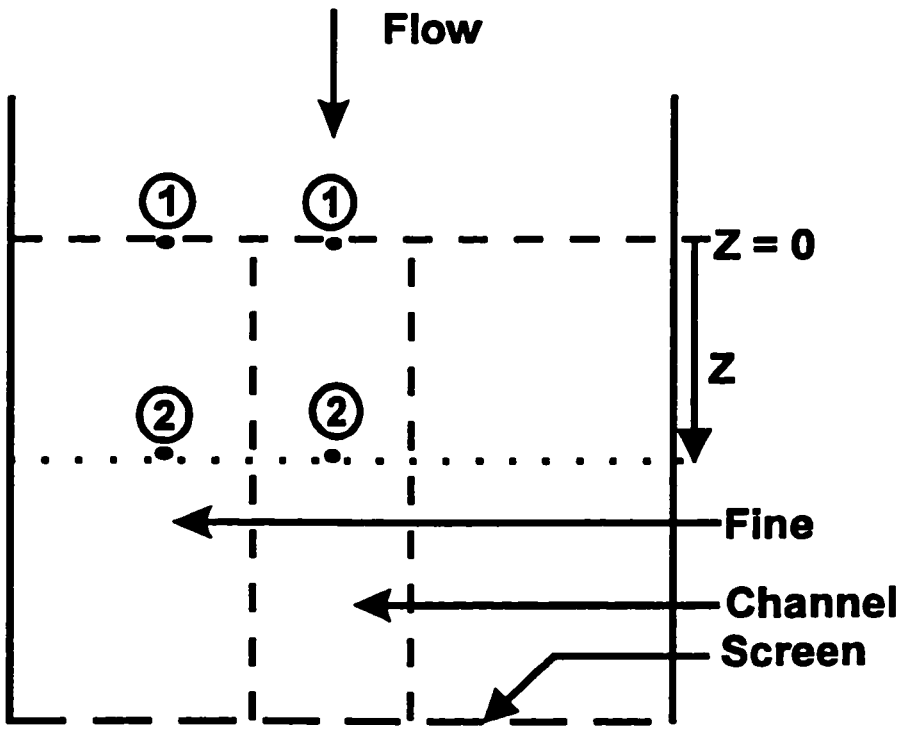

Figure 3.22 Schematic of a channel bed used for making an energy balance using Bernoulli's Equation

An energy balance between the reference points at the same elevation inside the channel results in

$$\frac{P_{1c}}{\rho g}+\frac{(u_{1c})^2}{2g}=\frac{P_{2c}}{\rho g}+\frac{(u_{2c})^2}{2g}-Z+h_c \qquad \textbf{3. 19}$$

Under steady state flow of water through either channel or annulus where each has a constant cross sectional area, the superficial velocity of water remains the same between point 1 and point 2 along the streamlines either in channel or in annulus to satisfy the conservation of mass. As a result, $u_{1f} = u_{2f}$ and $u_{1c} = u_{2c}$. Subtracting Equation (3.19) from Equation (3.18), rearranging, and assuming $P_{1f} = P_{1c}$ at the entrance of the bed for a constant pressure head displacement results in

$$\frac{P_{2f}-P_{2c}}{\rho g}=(h_c-h_f) \qquad \textbf{3. 20}$$

From Equation (3.6), which describes Darcy's law of fluid permeation under steady incompressible flow of fluid through a porous medium of permeability K, it can be written that

$$\frac{\Delta P_z}{Z}=\frac{\mu u}{K} \qquad \textbf{3. 21}$$

where ΔP_Z is the pressure drop along the vertical distance Z in either channel or in annulus in Figure 3.22. Equation (3.21) dictates that for constant viscosity of

fluid (μ), superficial velocity (u), and permeability of porous medium (K), frictional pressure drop per unit vertical distance either in channel or in annulus in Figure 3.22 is constant. Since the inlet and outlet pressures in both regions were the same under constant pressure head displacement, the irrecoverable frictional head losses across the two regions were the same. Hence Equation (3.20) can be rewritten as

$$\frac{P_{2f} - P_{2c}}{\rho g} = 0 \qquad 3.22$$

Equation (3.22) indicates that under a constant pressure head displacement in a model channel bed, the inertial effect resulting from the difference in superficial velocities of fluid in the fine part and in the channel did not cause any transverse pressure difference. Therefore, transverse pressure difference was not the reason for the cross flow of tracer particles, as observed in Figure 3.13.

Recently, based on Computational Fluid Mechanics modeling, Lappan et al. (1996) have confirmed that no cross flow was possible under the conditions of constant pressure head displacement experiments where the flow regimes in both the fine part and channel in a channel bed remained in the laminar region. Based on experimental results, they have proposed that if the ratio of particle diameter to diameter of screen holes goes below a critical ratio of 2.5, the interfacial resistance developed due to bead-screen interaction becomes

significant, resulting in a back pressure on the flowing fluids. In the fine part of a channel bed, the ratio of bead diameter to the diameter of holes in the screen was close to 1, whereas in the channel, it was close to 5.3. The resultant back pressure that offered additional resistance to the flow of fluid in the fine part of the channel bed caused the transverse movement of tracer particles towards the center channel shown in Figure 3.13. Due to the cross flow, MBL was driven from the fine part of the channel bed towards the channel and at the interface of fine and coarse beads, it mixed with the polymer solution which was flowing in the channel. As a result, precipitates were formed at the interface. In a channel bed washed with the polymer solution, pore throats in the center channel and in the interface were plugged by deposition of precipitates. As a result, the bed's characteristic had changed towards that of a homogeneous bed and the channel and fine part of the channel bed became non-communicating to each other, explaining the straight movements of tracer particles along the bed shown in Figure 3.14.

The relative effects of transverse cross flow and longitudinal dispersion on precipitate formation in a channel bed would be dictated by the flow regime, diameters of beads in channel and in the fine part of the bed, relative sizes of the channels and properties of the displaced and displacing phases.

At the inception of washing, the presence of a sharp change from the concentration of lignin in MBL in the annulus to that in the lignin-free polymer

solution in the channel at the interface might have also caused the transfer of lignin from the MBL in the annulus to the polymer in the center channel. As the washing proceeded, lignin transferred from the annulus reacted with the polymer in the channel to form precipitate. Subsequently, deposition and filtration of the precipitate in the center channel changed the center channel's permeability, resulting in a time-dependent rate of transfer of lignin from the annulus to the center channel.

3.4.5 Interpretation of Displacement Results in a Mixed Bed

Figure 3.12 shows that in a mixed bed that was washed with the polymer solution, precipitates were only retained in the channel of coarse beads. No precipitates were retained in the channel of medium beads. Potential reasons for selective precipitate formation and retention in the channel of coarse beads in a mixed bed were higher longitudinal dispersion in the channel of coarse beads and presence of cross flow of lignin from the fine part of the channel bed towards the channel of coarse beads.

An analysis similar to that performed for channel beds can be extended for mixed beds. For the constant pressure head displacements experiment in a mixed bed, Equations (3.8) through (3.17) are still valid. Equations (3.3), (3.7) and (3.12) can be extended to

$$\frac{\Delta P}{\mu L} = \frac{u_c}{K_c} = \frac{u_f}{K_f} = \frac{u_m}{K_m} \qquad 3.23$$

$$Pe_{p,m} = \frac{v_m d_{p,m}}{D_o} = 1.42 \times 10^4 \qquad \textbf{3. 24}$$

$$Re_{p,m} = \frac{\rho u_m d_{p,m}}{\mu} = 0.014 \qquad \textbf{3. 25}$$

$$Re_{p,f} = \frac{\rho u_f d_{p,f}}{\mu} = 0.004 \qquad \textbf{3. 26}$$

$$Re_{p,c} = \frac{\rho u_c d_{p,c}}{\mu} = 0.641 \qquad \textbf{3. 27}$$

$$\frac{Re_{p,c}}{Re_{p,f}} = 160 \qquad \textbf{3. 28}$$

$$\frac{Re_{p,m}}{Re_{p,f}} = 3.5 \qquad \textbf{3. 29}$$

Since the particle Reynolds number as predicted by Equations (3.25) through (3.27) in every part of the mixed bed was less than 10, flow in every section of a mixed bed was within laminar regime during the constant pressure head displacement experiment. In every part of the mixed bed, particle Peclet numbers as predicted by Equation (3.15), (3.16), and (3.24) were much greater than 10 and convective dispersion was the controlling mechanism of mass transport. Equation (3.17) can be extended to

$$\frac{(E_L)_m}{(E_L)_f} = \frac{v_m d_{p,m}}{v_f d_{p,f}} = 3.3 \qquad \textbf{3. 30}$$

Since longitudinal dispersion in the channel of medium glass beads was only 3.3 times higher than that in fine part of the bed, it was probably not sufficient to induce tangible amount of precipitation. However, the longitudinal dispersion coefficient in the channel of coarse beads was 148 times higher than that in fine beads and 45 times higher than that in the channel of medium beads resulting in precipitate formation only in the channel of coarse beads, as shown in Figure 3.12.

In a mixed bed, tracer particles introduced in fine beads adjacent to the channel of medium beads moved straight through the bed as shown in Figure 3.15. This was due to the fact that the ratio of particle diameter to diameter of the holes in the screen was below the critical ratio of 2.5 in both the regions of fine beads and the channel of medium beads in the mixed bed. As a result, the back pressures developed in those regions due to bead-screen interaction were not significantly different from each other. Consequently, there was not sufficient driving force to cause the transverse inward flow of tracer particles from the fine part towards the channel of medium beads. As a result, formation and retention of precipitates were not observed in the channel of medium glass beads in a mixed bed after washing with polymer solution as shown in Figure 3.12.

3.5 Conclusions

(a) Formation and retention of precipitates in a homogeneous bed of coarse beads were attributed to higher longitudinal mixing of lignin and polymer during constant pressure head displacement with the polymer solution.

(b) Presence of transverse flow of tracer particles towards the center channel in a channel bed after it was washed with water was explained by the presence of a back pressure caused by bead-screen interaction in the fine part of a channel bed (Lappan et al., 1996). In a channel bed that was washed with the polymer solution, bed properties changed due to selective precipitate retention in the channel and cross flow of tracer particles was absent.

(c) An analysis using Bernoulli's equation demonstrated that the cross flow of tracer particles in a channel bed during constant pressure head displacement washing experiments was not caused by the transverse pressure difference caused by inertial effect, which was speculated on by Pelton and Grosse (1994).

(d) Higher longitudinal dispersion of lignin and polymer in the channel and back pressure due to bead-screen interaction in the fine part of the channel bed were the reasons for selective precipitation in the channel in a channel bed during washing with polymer solution.

(e) Results from mixed bed experiments suggested that when the ratio of particle Reynolds number was 3.5, no selective precipitation was possible in a channel bed during washing with the polymer solution.

List of Variables

A	Cross sectional area of bed, m^2.
C_1	Constant in Equation (3.2), dimensionless.
C_2	Constant in Equation (3.2), dimensionless.
D_0	Effective binary molecular diffusion coefficient, m^2/s.
d_p	Diameter of particle, m.
E_L	Coefficient of longitudinal dispersion, m^2/s.
g	Acceleration due to gravity, m/s^2.
h	Frictional head loss in Figure 3.22, m.
K	Permeability of bed, m^2.
L	Length of the bed, m.
P_1	Pressure at position 1 in Figure 3.22, Pa.
P_2	Pressure at position 2 in Figure 3.22, Pa.
ΔP	Pressure drop across the bed, Pa.
ΔP_z	Pressure drop along the distance Z in Figure 3.22, Pa.
Pe_p	Particle Peclet number, dimensionless.
Q	Superficial flow rate, m^3/s.
Re_p	Particle Reynolds number, dimensionless.
u	Superficial velocity, m/s.
u_1	Superficial velocity at position 1 in Figure 3.22, m/s.
u_2	Superficial velocity at position 2 in Figure 3.22, m/s.
v	Interstitial velocity, m/s.
Z	Distance from top of the bed in Figure 3.22, m.

Subscripts

c	Coarse beads.
f	Fine beads.
m	Medium beads.

Greek Letters

β	Constant in Equation (3.2), dimensionless.
ε	Porosity of bed, dimensionless.
μ	Viscosity of fluid, Pa.s.
ρ	Density of fluid, Kg/m^3.

Abbreviations

MBL	Model black liquor.
MW	Molecular weight.

References

Bear, J., Dynamics of Fluids in Porous Media, Elsevier, New York (1972).

Blackwell, R. J., "Laboratory Studies of Microscopic Dispersion Phenomena," Soc. Petrol. Eng. J., **2**, 1 (1962).

Blackwell, R. J., J. R. Rayne, and W. M. Terry, Trans AIME, **216**, 1 (1959).

Bues, M. A., and M. Aachib, "Influence of the Heterogeneity of the Solutions on the Parameters of Miscible Displacement in Saturated Porous Medium," Experiments in Fluids, **25**, 11 (1991).

Crotogino, R. H., N. A. Poirier, and D. T. Trinh, "The Principles of Pulp Washing," Tappi, **70**, 95(1987).

Han, N. W., J. Bhakta, and R. G. Carbonell, "Longitudinal and Lateral Dispersion in Packed Beds: Effect of column length and particle size distribution," AIChE Journal, **31(2)**, 277 (1985).

Harleman D. R. F., P. F. Mehlhorn, and R. R. Rumer, "Dispersion-Permeability Correlation in Porous Media," Proc. ASCE J. Hydr. Div., **67**, 67 (1963).

Lake, L.W., Enhanced Oil Recovery, Prentice Hall, New Jersey (1989).

Lappan, R., A. N. Hrymak, and R. H. Pelton, unpublished work, McMaster University, 1996.

Lee, P. F., "Channeling and Displacement Washing of Wood Pulp Fiber Pads," Tappi, **67(11)**, 100 (1984).

Le Goff, P., D. M. Leclerc, and J. P. Herzig, "Flow of Suspensions through Porous Media," Ind. & Eng. Chem., **62(5)**, 8 (1970).

Li, P., and R. H. Pelton, "Wood Pulp Washing: 2. Displacement Washing of Aqueous Lignin from Model Beds with Cationic Polymer Solutions," Colloids and Surfaces, **64**, 223 (1992).

Mathews, J. L., Emanuel, A. S., and Edwards, K. A., "A Modeling Study of the Mitsue Stage 1 Miscible Flood using Fractal Geometries," SPE 18327, 63rd Annual Technical Conference of SPE, Houston, 661(1988).

McCabe, W. L., J. C. Smith, and P. Harriot, Unit Operations of Chemical Engineering, 4 th ed., McGraw-Hill, New York (1985).

Pelton, R. H., and B. Grosse, "Polymer Enhanced Displacement of Lignin Solution from Model Packed Beds," JPPS, **20(3)**, March (1994).

Perkins, T. K., and O. C. Johnston, "A Review of Diffusion and Dispersion in Porous media," Society of Petroleum Engineers Journal, **3**, 70 (March 1963).

Tang, R. W., Behrens, R. A., and Emanuel, A. S.,"Reservoir Studies using Geostatistics to Forecast Performance," SPE 18432, SPE symposium on Reservoir Simulation, Houston, 321(1989).

Chapter 4

Reactive Polymer Enhanced Miscible Displacement of Model Black Liquor in Model Beds of Glass Beads -- An Experimental Study

Abstract

Displacement washing experiments in model black liquor (MBL)-saturated model beds of glass beads were performed to evaluate the effects of the concentration of lignin in the MBL solution, the flow rate of water as displacing phase, the presence of a cationic polymer in water, and the presence of a more permeable channel at the center of the model bed on the performance of miscible displacement. Two types of model beds used were (a) a 5.2 cm diameter homogeneous bed that consisted of only 121 μm diameter glass beads, and (b) a 5.2 cm diameter channel bed that consisted of a 1.7 cm diameter central channel of 638 μm diameter glass beads. Channeling of water through the more permeable channel in the channel bed caused washing efficiency (31 to 33%) to be significantly lower than that in a homogeneous bed (84 to 93%). With the addition of cationic polymer, polyDADMAC, in water, washing efficiency in a channel bed improved significantly by 1.7 to 2 times due to selective

plugging of center channel with precipitate formed from reaction of lignin and the cationic polymer. At a flow rate of 30 mL/min, selective plugging rendered 34.5% and 17.3% decreases in permeability of the center channel at lignin concentrations of 25 g/L and 2.5 g/L respectively at the end of displacement with polymer solution. Permeability of the center channel was observed to decrease by 28.1% and 19.8% at lignin concentrations of 25 g/L and 2.5 g/L respectively at a flow rate of 230 mL/min after displacement with polymer solution was completed in the model channel bed. An increase in flow rate from 30 mL/min to 230 mL/min caused 9-12% decrease in washing efficiency in a homogeneous bed due to the increase in interfacial mixing of MBL and displacing phases. Increased flow rate reduced washing efficiency by 6% in a channel bed washed with polymer solution due to probable dislodging and removal of precipitates from the channel. An increase in the concentration of lignin enhanced washing efficiency in a channel bed by 5% due to the formation of a maximum amount of precipitate.

4.1 Introduction

Miscible displacement in a porous medium involves the displacement of one fluid from a porous medium by a second fluid that is miscible with the first fluid. Miscible displacement in a porous medium occurs in many branches of

engineering such as in recovery of oil in petroleum engineering, contamination of fresh water supplies by encroachment of salt water or from the disposal of waste products into underground fresh water reservoirs, recovery of spent liquors from a suspension of pulp fibers in brownstock washing in a Kraft pulping process, and so on.

The performance of miscible displacement floods in tertiary oil recovery is limited by fingering and channeling of the displacing phase (Lake, 1989). Bypassing of a resident fluid by a displacing fluid in a homogeneous medium due to instabilities caused by unfavorable differences in viscosity and density of the resident and displacing phases is called fingering (Lake, 1989). Heterogeneities in permeability across the bed causes bypassing of resident phase by the displacing phase and is called channeling (Lake, 1989; Tang et al., 1989; Mathews et al., 1988 and Blackwell et al., 1959). Poor miscible displacement performance caused by channeling of water through a pulp pad due to the pad's heterogeneous formation in brownstock washing in a Kraft pulping process has also been reported by Crotogino et al., 1987, and Lee, 1984.

In tertiary oil recovery, profile modification techniques have been developed to reduce channeling, resulting in an improved miscible displacement performance. Profile modification techniques involve reduction of permeability of high permeability streaks in a heterogeneous porous bed. Profile modification

can be achieved by injecting polymer floods, gel placement, flow of emulsions, and placement of foamed gels in heterogeneous porous media (Miller et al., 1995; Hofman et al., 1991; Lake, 1989, Todd et al., 1993, McCool et al., 1991). Extending the use of these tertiary oil recovery concepts, Lee (1984) used nonionic polymer additives in water to improve displacement washing of spent liquors from a pad of pulp fibers in brownstock washing in a Kraft pulping process. He argued that presence of swollen microgels of polymer in water increased resistance to flow in channels and thus lowered channeling, increasing displacement performance in the pad of pulp fibers. Li and Pelton (1992) used a cationic polymer in water and observed improved displacement performance in their model bed of glass beads due to selective plugging of channels with precipitate formed from the reaction of cationic polymer with anionic lignin in the spent liquor. However, neither Lee (1984) nor Li and Pelton (1992) had measured quantitatively the effects of variables such as the flow rate of water, the concentration of lignin in the spent liquor in the saturated porous bed, the concentration of polymer in water, and the permeability of channels on displacement performance when polymeric additives were used in water.

The objective of the present work was to measure quantitatively the improvement in displacement performance when an aqueous solution of a cationic polymer was used to displace spent liquor from model beds. In addition, the effects of variables such as the flow rate of the displacing water, the

concentration of lignin in the spent liquor, the concentration of the cationic polymer in water, and the permeability of the channel on both displacement performance and change in the properties of the bed after displacement were investigated.

4.2 Experimental

4.2.1 Materials

Glass beads of kind no: 3, no:7, and no: 10, model black liquor solutions (MBL), and polymer solutions, described in Chapter 3, section 3.2.1, were used in the following experiments. Details of size distributions of no: 3 (mean diameter 638 mm), no: 7 (mean diameter 182 mm), and no: 10 (mean diameter 121 mm) glass beads are given in detail in Figures 3.1 through 3.3 respectively in Chapter 3. Three types of MBL solution were used. The concentrations of Indulin C in the MBL solutions were 2.5 g/L, 13.25 g/L, and 25 g/L respectively. Polymer solutions contained either 29.4 or 14.7 g/L of polyDADMAC ($MW=10^5$) respectively.

No: 3 , no: 7, and no: 10 glass beads are denoted as coarse (subscript "c"), medium (subscript "m"), and fine (subscript "f") beads respectively in the rest of this chapter.

4.2.2 Displacement Washing Apparatus

A computer automated displacement washing apparatus was built to evaluate the performance of displacement washing of MBL solutions from model beds of glass beads. The following section describes the details of the apparatus, testing of the apparatus, and the procedures for preparing model beds in the displacement washing column.

4.2.2.1 Hardware

4.2.2.1.1 Multiport Displacement Washing Cell

4.2.2.1.1.1 Commercial Glass Column

The multiport displacement washing cell was built by modifying a commercial aqueous-compatible glass column supplied by Supelco Canada Ltd. (catalogue no: 5-7809). The commercial column had an inner diameter of 5.2 cm, outer diameter of 6 cm, and length of 30 cm. A photograph of the column is shown in Figure 4.1. Both ends of the column were fitted with internally threaded

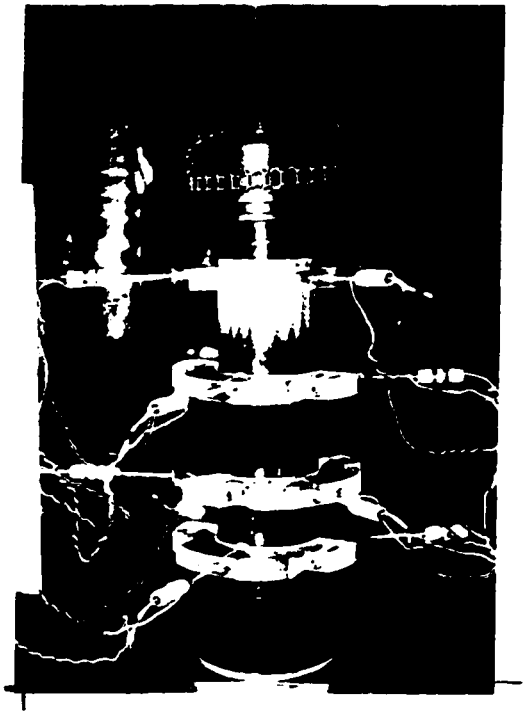

Figure 4.1 Photograph of modified commercial glass column

Figure 4.2 Modification done to the lower end plate of column.

polypropylene collars. Externally threaded polypropylene plates were mounted on the collars at both ends of the column. A collar compression O-ring and a sealing gasket compressed between the collar and the end plate at both ends of the column prevented leakage of fluid from the column during experiments. A mesh cloth support held at the top of the lower end plate by a retainer ring was provided to support the bed inside the column. The upper and lower end plates were connected with Teflon multifit tubing connectors of outer diameter 0.32 cm.

4.2.2.1.1.2 Modification of Commercial Glass Column

Figure 4.1 depicts the modifications to the commercial glass column. The mesh cloth support at the top of the lower end plate was replaced by a perforated stainless steel screen of diameter 5.2 cm. The stainless steel screen (Type no: 80 P) was supplied by Paper Research Material, Camas, USA. The diameter of holes on screen was 120 μm and the US mesh equivalence was 80. The percentage open area on the screen was 14.5.

The top part of the lower end plate was tapered slightly towards its center and three grooves each of width 0.3 cm and depth 0.5 cm were cut along its diameter at 60^0 to each other as shown in Figure 4.2. These grooves promoted free flow of fluid from every part of the screen to the column outlet. The multifit Teflon tubing connector at the lower end plate of the column was replaced by a stainless steel Swagelock®.

Figure 4.3 Photograph of column showing holes drilled in it.

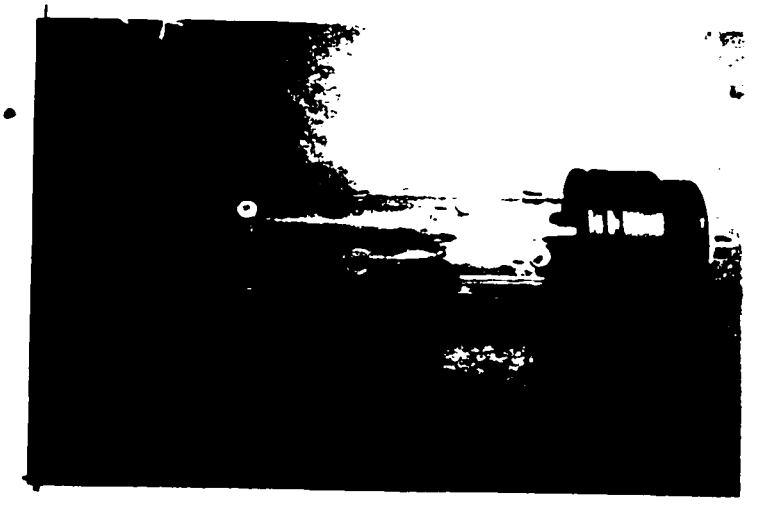

Figure 4.4 Photograph of column showing rubber septums in the holes.

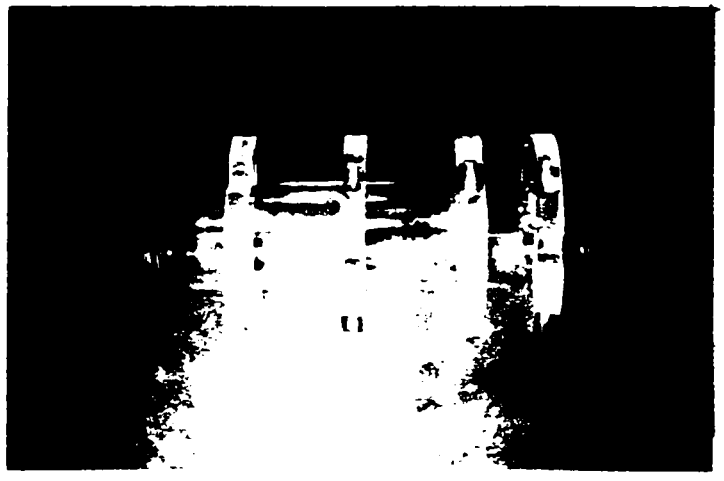

Figure 4.5 Photograph of circular clamps holding rubber septums placed inside the holes in column.

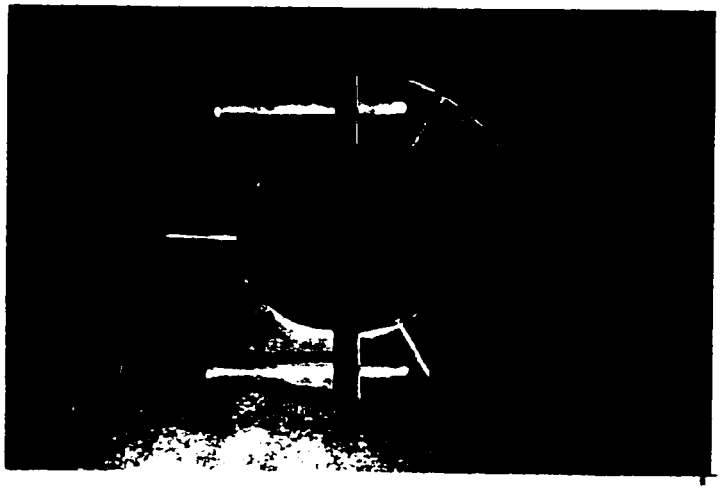

Figure 4.6 Photograph of a circular clamp.

An adjustable polypropylene plunger made for a glass column of internal diameter 5.2 cm replaced the upper end plate of the column. The 32 cm polypropylene plunger was supplied by Supelco Canada Ltd. (catalogue no: 5-7729).

Figure 4.3 shows twelve 0.6 cm diameter holes drilled at four axial positions, i.e., 5.3, 9.4, 15.3, and 21.4 cm from the screen of the column. Three holes at each axial position were drilled at 120^{o} to each other. At consecutive axial positions, the holes nearest to each other were staggered by 60^{o}. Each hole was sealed as shown in Figure 4.4 by a 0.75 cm diameter Wheaton rubber stopper which was held in position by a circular Plexiglass® clamp of internal diameter 6.3 cm, external diameter 11.3 cm, and thickness 1.3 cm shown in Figure 4.5. Each circular clamp consisted of two semi-circular detachable parts, shown in Figure 4.6, allowing independent placement of them at any of the four axial positions of the cell. Three holes, each of diameter 0.2 cm, were drilled diametrically along the center of each stopper in the clamp. Conductivity probes, described in following section, were inserted into the cell through these holes in the clamp.

4.2.2.1.2 Conductivity Probes

Twelve conductivity probes were fabricated for measuring the instantaneous conductivity of fluid flowing through a porous bed. During

displacement washing of the MBL in the model beds, the MBL and the wash liquor, either water or the polymer solution, remained separated from each other by the displacement front or interface between them. The conductivity of fluid across the displacement front changed from that of the MBL (13 mS/cm) to that of either water (0 mS/cm) or the polymer solution (2.5 mS/cm) during displacement washing of the MBL in the model bed. Conductivity probes were placed at various locations inside the porous bed to monitor the location of displacement front in beds during displacement washing. The detail of fabrication of the conductivity probe is given in section A.1 in Appendix A.

4.2.2.1.3 Multichannel Conductivity Apparatus

A multichannel conductivity apparatus built by S.E.E.S (Science and Engineering Electronics Shop), McMaster University, was an assembly of twelve conductivity measurement units each having single ended outputs of 0 to 10 VDC. Two amplifier banks encased six of these units each. The integration time or speed and range of conductivity measured by each unit were selected by external jumpers. Conductivity probes as described in section 4.2.2.1.2 were connected to these units stacked inside the amplifier banks through circular slots called channels. Details of the multichannel conductivity apparatus and the operating principle of a conductivity unit are given in section A.2 in Appendix A.

4.2.2.3 Assembly of the Apparatus

The displacement washing unit was built to evaluate the displacement washing performance of the MBL using various kinds of wash liquors. The schematic and photograph of the apparatus are shown in Figures 4.7 and 4.8

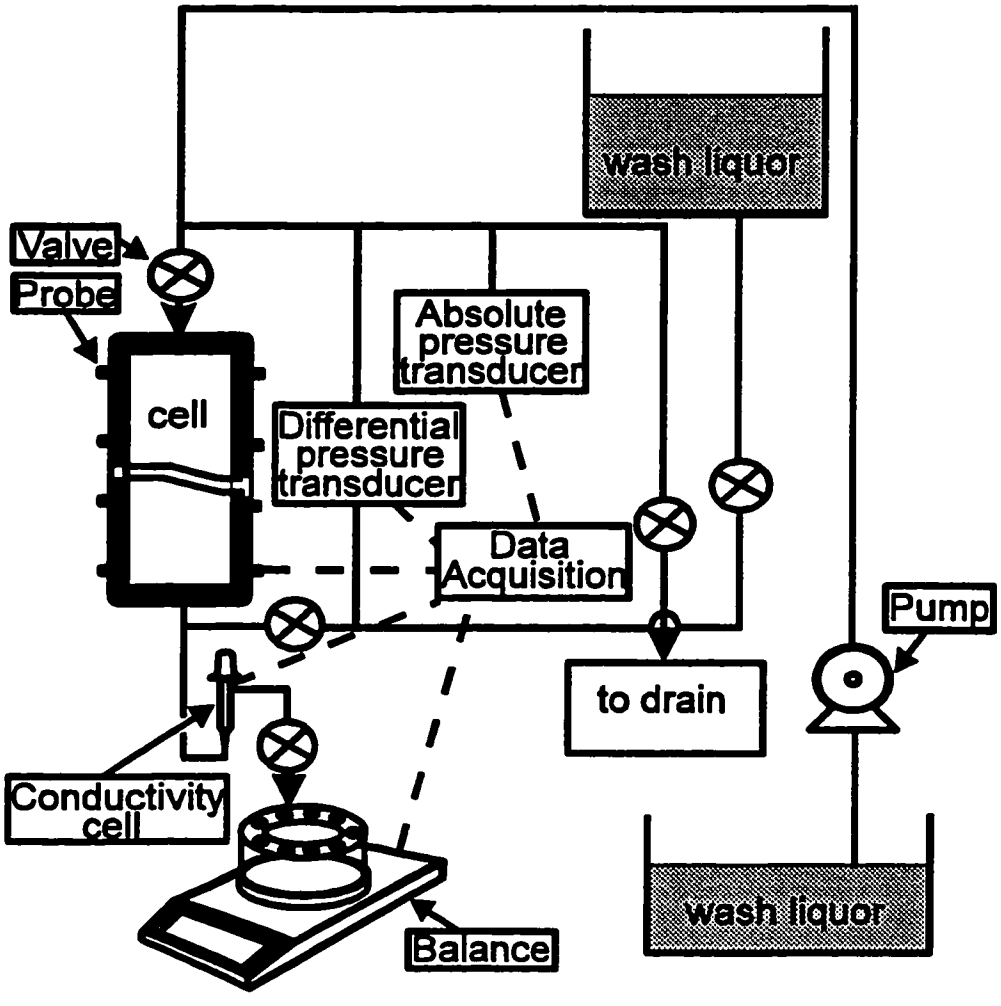

Figure 4.7 Schematic of the displacement washing apparatus.

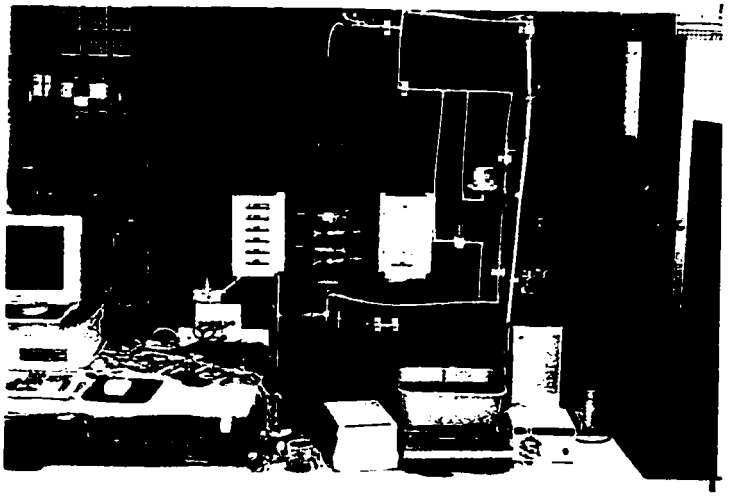

Figure 4.8 Photograph of the displacement washing apparatus.

Figure 4.9 Photograph of placement of amplifier banks around the column.

respectively. The multiport displacement washing cell described in section 4.2.2.1.1 was held vertically on a Plexiglass® base. Two amplifier banks, each containing six conductivity measuring units, were positioned on both sides of the washing cell as shown in Figure 4.9. The polypropylene adjustable plunger was fitted to the top part of the column. A rubber O-ring was compressed between the plunger and the inner surface of the washing cell to prevent leakage of fluid through them. A Masterflex® computerized drive peristaltic pump was used to pump various types of wash liquors into the washing cell. The rotors in two heads used in the pump were staggered to each other to minimize the amplitude of pulses generated by them. The Masterflex® pump had the ability to pump liquid in either a clockwise or anticlockwise direction and at a constant flow rate that was set by a control panel. Eluate coming out of the washing cell went through a conductivity cell, Model No: CDC114, Radiometer, Copenhagen. Subsequently, the eluate was collected in a bucket placed on a Mettler PM16 balance that measured the cumulative mass flow rate of eluate. Another Masterflex® pump connected to a separate line was used to pump the MBL solution into the cell during preparation of model beds in the washing cell. The pressure drop across the washing cell was measured by a Celesco DP30-0001-111 differential pressure transducer. The absolute pressure at the inlet of the column was measured by a Heiss absolute pressure transducer.

4.2.2.4 Hydraulic Connection

The hydraulic line between the exit of the washing cell and the flow through conductivity cell was divided into two parts. One of them was connected to the negative port of the differential pressure transducer and the other led to an overhead fresh wash liquor storage container for flushing residual MBL out of the lines after a displacement run. A line branched from the inlet of the washing cell led to the positive port of differential pressure transducer and then to a drainage line via the absolute Heiss pressure transducer. The location of four ball valves connected in the lines is shown in Figure 4.7. To remove the effect of expansion of a flexible tube on pressure drop, hard Tygon® tube was used for all tubes except at the entrance and exit of the flow through conductivity cell.

4.2.2.5 Sensors and their Calibration

4.2.2.5.1 Pressure Transducers

The differential pressure transducer, which had a range of 0 to 172 kPa (0 to 25 psi), was connected to a Celesco Carrier Demodulator that had an output range of 0 to 10 VDC. The absolute pressure transducer had a range of 0 to 34.4 kPa (0 to 5 psi) and voltage output of 0-10 VDC. Both differential and absolute pressure transducers were calibrated by Series 65-120 Portable

Pneumatic Calibrator manufactured by Wallace and Tieman division of Pennwalt Corporation.

4.2.2.5.2 Flow through Conductivity Cell

The conductivity of eluate coming out of washing cell was measured by a conductivity cell that was connected to the conductivity meter. The cell constant was determined by calibrating it against standard NaCl solutions. Batch and semi-batch experiments were performed, involving dilution of the MBL with either water or the polymer solution. The results of batch and semi-batch experiments demonstrated the linear relationships between conductivity of the MBL solution during dilution to the concentrations of lignin, sodium and hydroxyl ions in the solution. Details of the batch and semi-batch experiments are given in Appendix A, section A.3.

4.2.2.6 Data Acquisition

Output signals from the Carrier Demodulator for the differential pressure transducer, multichannel conductivity apparatus, and CDM83 conductivity meter were connected to fourteen nonreferenced, single-ended, analog input slots of a multifunction input / output (I/O) AT-MIO-16 data acquisition board, purchased from National Instruments, USA. Each of these signals was referenced to a common ground. The AT-MIO-16 board, which was a high performance

multifunction analog, digital, and timing I/O board, consisted of 12-bit analog to digital converters with up to either sixteen either single-ended analog inputs or eight differential inputs and two 12-bit digital to analog converters with voltage outputs. An amplifier of gain 7.5 was used to amplify the signal from the CDM83 to the AT-MIO-16 board.

The board was configured for sixteen referenced single ended unipolar analog inputs by selection of external jumpers. Every analog input and output channel was calibrated according to the instructions given in the manual of AT-MIO-16 board. The board was installed in an Odyssey 386 40 MHz Personal Computer. The board was configured by software to read each of these analog signals as unipolar and in the range of 0 to 10 VDC. A software-triggered digital output line multiplexed among measuring three voltages V_1, V_2, and V_3, as described in section A.2 in Appendix A, for each conductivity unit in multichannel conductivity apparatus. Each reading of these voltages was synchronized with a reading from other analog input channels through software. A BASIC program was written to read and store the digital values from the fourteen analog input channels against time measured by the computer clock. These values were written in "csv" output files for later analysis. The serial RS-232C response of the balance was read by another computer via its communication port. A separate BASIC program was written to read the balance. The codes of the computer programs are given in Appendix B.

4.2.2.7 Preparation of Model Beds

4.2.2.7.1 Homogeneous Bed

A homogeneous bed consisted of only one kind of glass beads. The bed was saturated with either water or MBL. Water or MBL was pumped into the washing cell at a rate of 7 mL/min until the level of water or MBL was 13 cm above the stainless steel screen of the washing cell. Glass beads were then poured slowly into the washing cell and the cell was tapped frequently to remove air bubbles trapped inside the suspension. The glass beads were allowed to settle and the height of the bed and final level of water or MBL in the column were measured. In order to protect the bed from any disturbance, a stainless steel screen identical to that at the bottom of bed was carefully placed at the top of the bed. The adjustable plunger was then fitted at the top of the bed. Tubing inside the plunger was filled with either water or the MBL and connected to the line leading to other peristaltic pump. The bed was conditioned for five minutes by pumping either water or MBL at a rate of 230 mL/min using the peristaltic pump. Afterwards the plunger was removed. Liquid on the top of bed was drained until the liquid level touched the top screen.

4.2.2.7.2 Channel Bed

A channel bed consisted of a central core of glass beads of either no: 3 or 7 surrounded by an annulus of glass beads no: 10. The diameter of the central core was 1.7 cm. Channel beds were formed with the help of a glass tube and a circular top panel made of Plexiglass. The circular panel was made from a circular Plexiglass disc of outer diameter of 8.3 cm and width 1.67 cm, shown in Figure 4.10. A hole of diameter 1.7 cm was drilled at the center of the disc. Three holes each of diameter 1.28 cm were drilled at a radius of 2.31 cm and at 120^0 to each other. A circular region of diameter 6.78 cm and concentric to the disc was cut out from one surface of the disc to a depth of 1.1 cm. The glass tube had a length of 37.5 cm, inner diameter of 1.5 cm, and outer diameter of 1.7 cm.

The washing cell was placed on its Plexiglass base. The circular panel was placed on the top of the cell and inner circular region of the panel encircled the top edge of column, as shown in Figure 4.11. The glass tube was then inserted through the central hole of the panel and placed on the bottom screen concentric to the column. MBL was pumped at a rate 7 mL/min into the cell until level of liquid inside the cell reached 13 cm. The required amount of glass beads, either no: 3 or 7, were poured inside the central tube, with frequent tapping of the tube. No: 10 glass beads were then poured into the annulus region of the cell through the other three holes and the cell was tapped frequently to drive out any

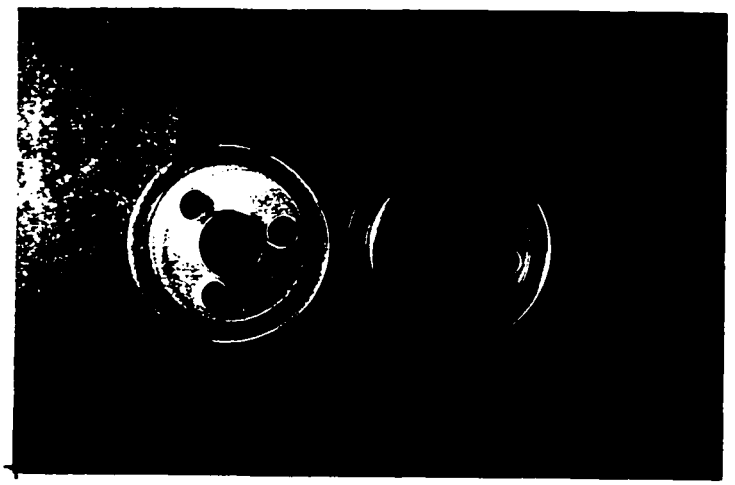

Figure 4.10 Photograph of the top circular panel for making a channel bed.

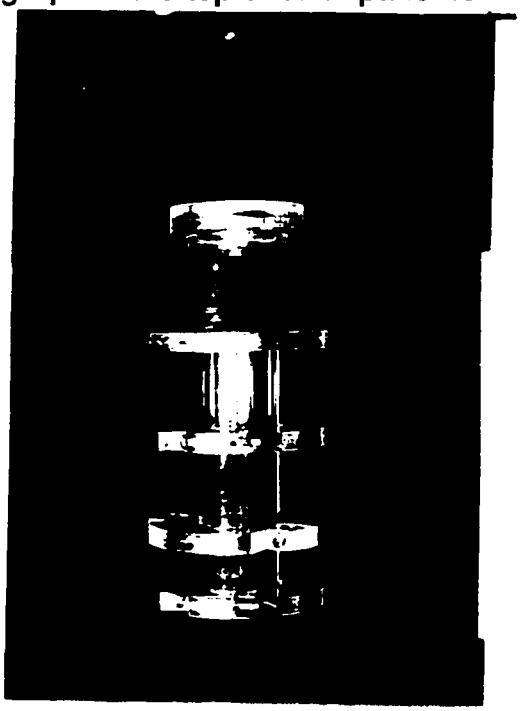

Figure 4.11 Photograph of the setup for preparing a channel bed.

air bubble from the suspension. It was ensured that the central glass tube remained in its position throughout the process of packing the bed. At the end of pouring of beads, the central glass tube was taken out of the cell vertically and very slowly to minimize any mixing of glass beads at the interface of two kinds of beads. A procedure similar to that described for forming homogeneous beds was followed onwards.

4.2.2.7.3 Calculation of Volume Void Fraction

The volume void fraction (ε) of either a homogeneous or channel bed was calculated from the following relation:

$$\varepsilon = \frac{V_{bed} + V_i - V_f}{V_{bed}} \qquad 4.1$$

where V_{bed} was volume of bed, V_i was the initial volume of water or MBL taken in the cell before pouring glass beads, and V_f was the volume up to the final level of liquid in the cell after beads were poured in the cell.

4.2.2.8 Testing of Displacement Washing Apparatus

The accuracy of the washing apparatus was tested by carrying out experiments of permeation of water in porous media. Homogeneous beds of no:10 glass beads saturated with water were formed in the washing cell according to the procedure described in section 4.2.2.7.1. A detailed procedure

and the results of testing of the displacement washing apparatus are given in Appendix A, section A.4. It was verified that experiments conducted in the washing apparatus remained in Darcy flow regime as long as superficial flow rate of water did not exceed 230 mL/min.

4.2.3 Procedure

Miscible displacement of model black liquor (MBL) using either water or polymer solution as displacing phase was studied in 5.2 cm diameter model beds of glass beads. Model beds were of two kinds: (1) homogeneous beds consisting of only fine glass beads (average diameter 121 μm), and (2) channel beds comprising of a 1.7 cm diameter center channel of either coarse beads (638 μm) or medium glass beads (182 μm) surrounded by an annulus consisting of fine glass beads.

The procedure for preparing a model bed in the displacement washing cell is described in section 4.2.2.7. The bed was saturated with the MBL solution. Height of the bed was noted and the porosity or volume void fraction (ε) of the bed was calculated as discussed in section 4.2.2.7.3. Conductivity probes were inserted into the bed through the side ports of the cell and it was ensured that each probe registered the correct conductivity value of the MBL solution inside the bed. The details of probes and results obtained from probes are discussed in Chapter 5. A uniform packing of beads in the bed was achieved by

conditioning the bed with the MBL solution, described in section 4.2.2.7. At the end of conditioning, the plunger was removed and excess MBL at the top of the bed was drained. A screen identical to that placed at the bottom of bed was carefully placed at the top of bed to minimize any mixing of the MBL with the wash liquor. Three layers of 6 mm diameter glass beads were poured on the top of the screen in order to distribute the wash liquor uniformly at the entrance of the bed. Wash liquor was poured slowly on the top of the bed, minimizing any mixing of MBL with wash liquor. The plunger was carefully fitted on the top of the bed, removing any void between the plunger and 6 mm diameter glass beads. The plunger was connected to the inlet line for pumping wash liquor into the displacement washing cell.

A miscible displacement experiment was started by pumping wash liquor into the cell at a constant flow rate that was set in the control panel of the peristaltic pump. During a miscible displacement experiment, pressure drop across the cell, the conductivity of eluate at the exit of bed, conductivity recorded by probes, and the cumulative mass flow rate of eluate were acquired as a function of time by the data acquisition system, described in section 4.2.2.6.

The disturbance in flow pattern caused by the intrusive way of measuring conductivity inside the bed using probes was tested by performing displacement experiments in homogeneous beds with and without the presence of probes

using water as wash liquor. The presence of probes inside model beds had little effect on the performance of displacement, as discussed in detail in section 4.3.

4.2.4 Experimental Design

The effect of four key variables on miscible displacement performance of model black liquor (MBL) from a model bed was studied. These four variables were the concentration of Indulin C in the MBL; the concentration of polyDADMAC in the wash liquor; the flow rate of the wash liquor; and the permeability of the center channel, which was controlled by selection of diameter of glass beads in the center channel of model beds. The variables were tested at two levels. Table 4.1 shows the levels of the variables and their corresponding values used in the experimental design. To examine the non-linear behavior of the response spanning the range of the levels of the variables, an experiment at the center of the levels of the variables was performed.

Table 4.1 Key variables and their levels employed in the experimental design.

Variables	Nomenclature	High (+)	Central (C)	Low (-)
Concentration of Lignin (g/L)	[L]	25	13.75	2.5
Concentration of polymer(g/L)	[P]	29.4	14.7	0
Flow rate (mL/min)	F	230	130	30
Diameter of beads in channel (μm)	D	638	182	121

Table 4.1 implies that a model channel bed consisting of a central channel of fine glass beads is a homogeneous bed of fine glass beads. The levels of the variables were chosen to ensure that all experiments in the experimental design were performed within Darcy's flow domain. This was examined by calculating the particle Reynolds number of the flow in an experiment using the equation,

$$Re_P = \frac{\rho V D_p}{\mu} \qquad 4.2$$

where ρ was the density of the wash liquor, D_p was the particle diameter, V was the superficial velocity based on Darcy's law of fluid permeation, and μ was the viscosity of the wash liquor. In the extreme case of maximum flow rate (230 mL/min), minimum viscosity of wash liquor (1 mPa.S), water, and the largest diameter of glass beads (638 μm), Re_p was calculated to be 1.15. If the particle Reynolds number is low (<10), viscous forces dominate the inertial forces and the flow remains laminar where Darcy's law is valid (Bear, 1972). Since the particle Reynolds number in each experiment in the experimental design was below 10, it was ensured that the experimental design was performed in the domain of Darcy's flow. Concentration of Indulin C in the MBL solution was chosen to simulate MBL solutions closely to black liquor at the inlet of the brownstock washing stage in a Kraft pulping process. Concentration of

polyDADMAC in water was chosen to yield a maximum amount of precipitate between lignin and polyDADMAC as determined by an optimum ratio reported by Lappan et al., 1996.

A two level factorial design on four variables with an experiment at the center of the levels of variables was selected to evaluate the effects of four key variables on displacement washing performance of MBL solutions in the model beds of glass beads. The design matrix and the random order in which all the runs were performed are depicted in Table 4.2 on next page. Each of the seventeen experiments was replicated thrice. Consequently, all fifty-one runs were carried out in a random manner to achieve truly replicated runs in the experimental design.

4.3 Results

4.3.1 Treatment of Data

Conductivity of the eluate measured at the exit of the bed was made dimensionless following the relation

$$\text{Dimensionless exit conductivity } (C) = \frac{C_{measured} - C_w}{C_0 - C_w} \qquad 4.3$$

Table 4.2 Design matrix of 2^4 factorial design with an experiment at center and with three replicates of each experiment. (-), (+), and (c) denote low, high, and central levels of variables.

Experiment. no.	Concentration of lignin	Concentration of polymer	Flow rate of wash liquor	Bead size in channel	Order of runs
1	-	-	-	-	12,3,35
2	+	-	-	-	48,20,27
3	-	+	-	-	43,2,28
4	+	+	-	-	1,4,22
5	-	-	+	-	36,31,44
6	+	-	+	-	5,34,47
7	-	+	+	-	39,14,38
8	+	+	+	-	17,33,51
9	-	-	-	+	19,13,37
10	+	-	-	+	46,23,40
11	-	+	-	+	25,15,9
12	+	+	-	+	26,49,24
13	-	-	+	+	7,45,16
14	+	-	+	+	18,10,8
15	-	+	+	+	30,41,29
16	+	+	+	+	32,11,21
17	c	c	c	c	50,42,6

where $C_{measured}$, C_0, and C_w were the conductivities of the eluate at any time t, initial conductivity of the MBL in the bed, and conductivity of the wash liquor respectively. Dimensionless exit conductivity (C) was plotted against eluate ratio (ER) to produce breakthrough curves at the exit of the bed. Eluate ratio (ER) was defined as the ratio of volume of wash liquor injected into the cell up to any time "t" to the initial volume of MBL in the bed. Eluate ratio (ER) at time t is defined as

$$\text{Eluate ratio (ER)} = \frac{tQ}{\varepsilon AL} \qquad 4.4$$

where Q was the volumetric flow rate of the wash liquor, A was the area of bed normal to flow, L was the length of the bed, and ε was the porosity of the bed before the commencement of displacement. The breakthrough curves were corrected for the dead time incurred by the presence of dead volume (7 mL) of liquid held in the line between the exit of the cell and the conductivity sensor. The dead time was calculated as the ratio of dead volume of liquid to the volumetric flow rate of wash liquor injected into the cell.

Figure 4.12 demonstrates the effect of the presence of probes on breakthrough curves in a homogeneous bed during washing with water. Washing efficiencies, discussed in detail in section 4.3.2, for washing with water in homogeneous beds in presence and absence of probes were within ± 3% of each other. Since the highest 95% confidence interval about the mean of

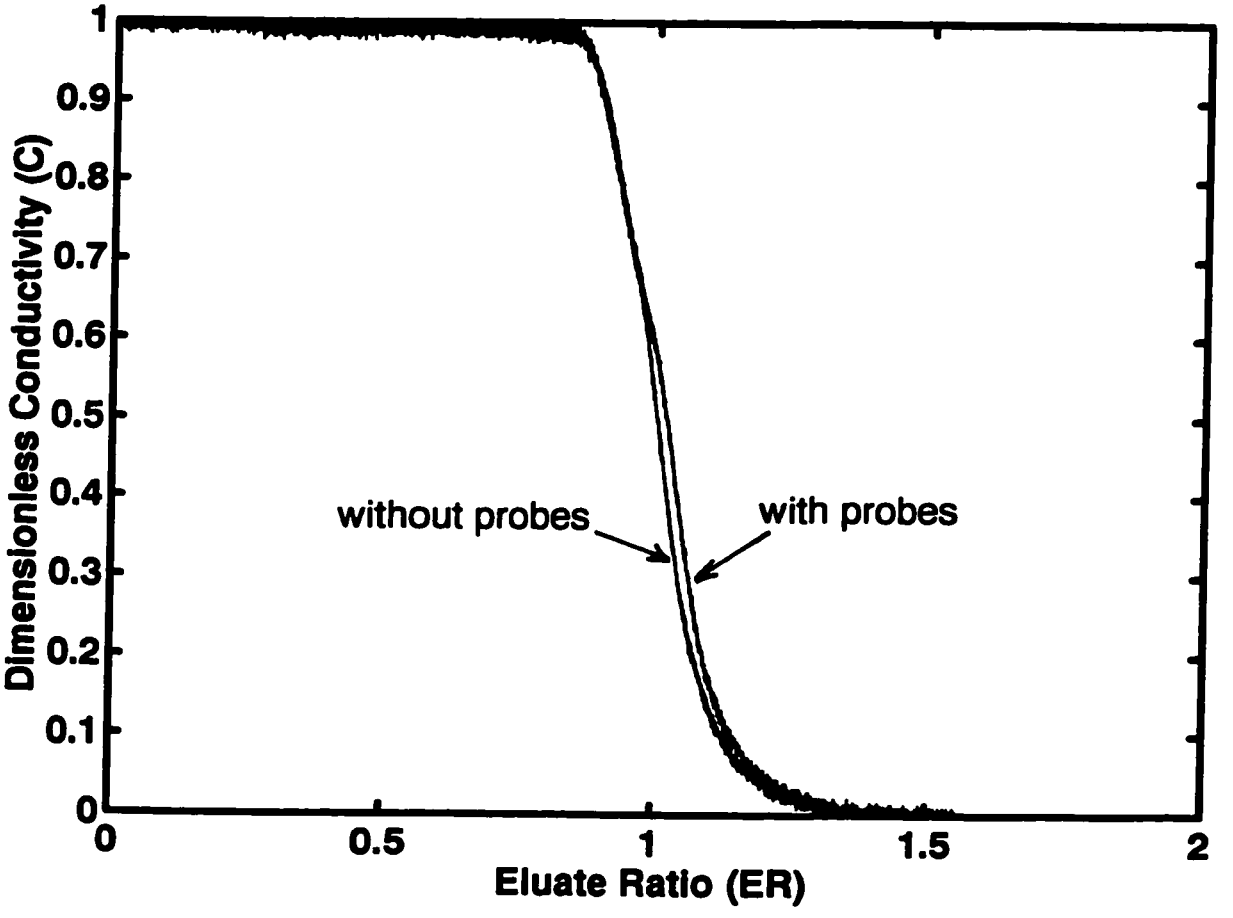

Figure 4.12 Breakthrough curves at the exit of homogeneous bed in the presence and absence of probes inside the bed. Concentration of lignin in MBL was 2.5 g/L and flow rate was 30 mL/min.

washing efficiencies measured in replicate runs in a homogeneous bed was around 3%, it was concluded that presence of probes inside a model bed had little effect on the displacement flow profile during washing experiments.

Figure 4.13 shows the breakthrough curves at the exit of model beds during various displacement washing experiments. The variation of conductivity of the

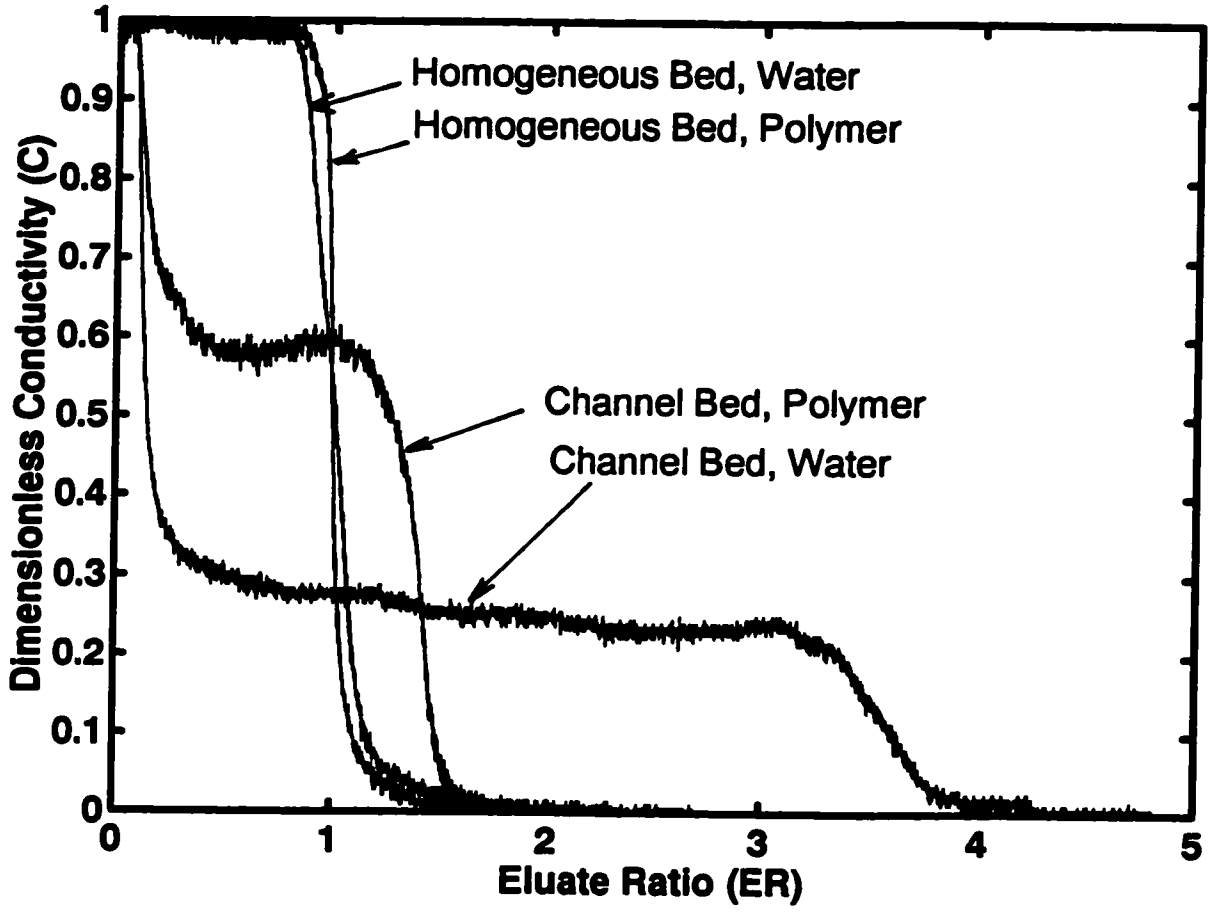

Figure 4.13 Breakthrough curves at the exit of beds for various displacement washing experiments. Concentration of lignin in MBL was 25 g/L and flow rate was 230 mL/min.

MBL solution during dilution with either water or the polymer solution was established to vary linearly with the concentration of lignin in the MBL solution in section A.3 in Appendix A. Consequently, breakthrough curves in Figure 4.13 represent the variation of concentration of lignin in the eluate with eluate ratio during a displacement washing run. Figure 4.13 demonstrates that the volume of wash liquor needed to wash a channel bed completely was more than that in a homogeneous bed. The volume of wash liquor needed to wash a channel bed completely was highest when it was washed with water. However, when a channel bed was washed with the polymer solution, the volume of wash liquor needed to wash the bed completely was reduced to almost half of the volume of wash liquor needed when the channel bed was washed with water. Also, the concentration of lignin in the eluate was higher in a channel bed during washing with polymer solution than when the channel bed was washed with water. Figure 4.13 also demonstrates that the breakthrough curve for a homogeneous bed during washing with the polymer solution was steeper than that when a homogeneous bed was washed with water.

Figure 4.14 shows the typical profiles of pressure drop against eluate ratio during displacement washing in model beds for various displacement washing conditions. Figure 4.14 demonstrates that steady state pressure drop was highest in a homogeneous bed washed with the polymer solution, followed by those in a homogeneous bed washed with water, in a channel bed washed with

polymer solution, and in a channel bed washed with water. The cyclic oscillations in pressure drops in Figure 4.14 was due to the presence of pulses in the displacing fluid imparted by the squeezing action of motor heads on a flexible tube in the peristaltic pump that was used to pump the displacing phase into the model beds.

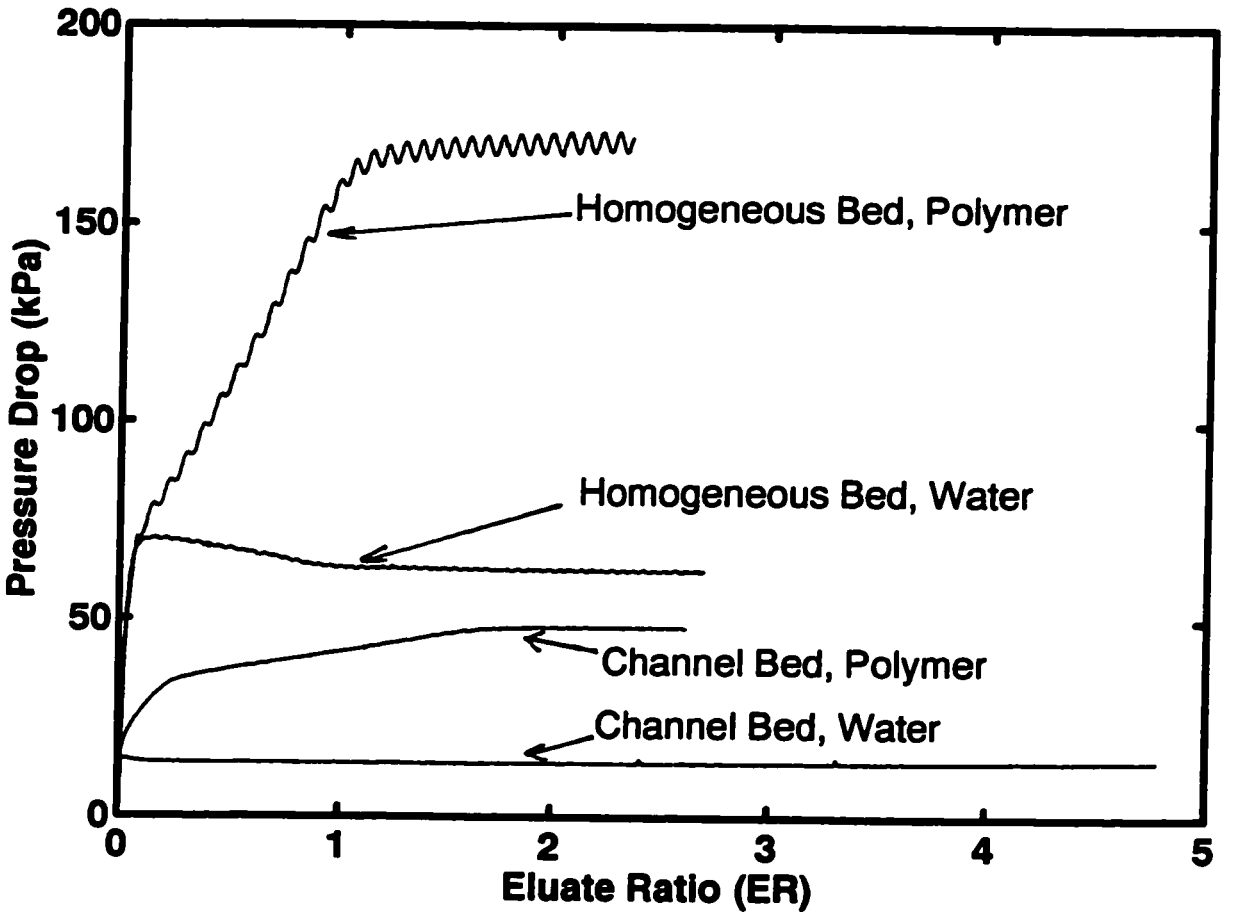

Figure 4.14 Plot of pressure drop against eluate ratio for various displacement washing experiments. Concentration of lignin in MBL was 25 g/L and flow rate was 230 mL/min.

4.3.2 Evaluation of Responses

The responses computed from the breakthrough curve at the exit of the bed and from the pressure drop profile obtained in an experiment in the experimental design were, (a) washing efficiency (WE), and (b) permeability of the bed (K_S) after washing was completed and pressure drop reached a steady state. The following section describes the methodology for evaluating the responses.

(a) Washing Efficiency (WE)

The breakthrough curve at the exit of the bed in Figure 4.13 represents the variation of concentration of lignin with eluate ratio (ER) during a displacement washing process. The total area under a breakthrough curve in Figure 4.13 represents the total amount of lignin removed during a washing run. The total area must be equal to 1 to obey the law of mass conservation. The area under the breakthrough curve up to a certain eluate ratio (ER) represents the amount of lignin that was washed out of the bed up to the time that corresponds to that eluate ratio. Traditionally, the washing efficiency (WE) of a displacement run is defined using a reference eluate ratio (ER) of 1 using the relation

$$WE = \frac{\int_0^1 Cd(ER)}{\int_0^\infty Cd(ER)} \qquad 4.5$$

(Trinh et al., 1989). The numerator in Equation (4.5) represents the amount of lignin that was removed from the bed when the volume of wash liquor injected into the washing cell was equal to one displacement volume of the bed. The denominator represents the total amount of lignin that was removed from the bed when washing was completed, i.e., the conductivity in the breakthrough curve reached the value for water. In an ideal plug flow displacement washing without any interfacial mixing, washing efficiency defined in Equation (4.5) must be 1. Washing efficiencies computed from the breakthrough curves obtained at the exit of beds in the experiments in the experimental design are listed in Table 4.3.

(b) Permeability of Bed after Complete Washing (K_S)

Permeability (K_S) of a bed after complete washing was computed from Darcy's law of fluid permeation in a porous bed.

$$K_S = \frac{Q\mu L}{A(\Delta P)_S} \qquad 4.6$$

where $(\Delta P)_S$ was the corrected pressure drop when washing was completed and pressure drop reached a steady state. The pressure drop was corrected by subtracting the pressure drop measured without any glass beads in the cell from

Table 4.3 Responses evaluated for the 2^4 factorial experimental design. Numbers in the parenthesis indicate the order in which runs were carried out.

Experiment no:	Response 1 (WE) Washing efficiency	Response 2 (K_S) Permeability $X10^{-8}$ (cm^2) after washing
1	$0.940^{(12)}$,$0.917^{(3)}$,$0.924^{(35)}$	$10.2^{(12)}$,$9.1^{(3)}$,$8.41^{(35)}$
2	$0.927^{(48)}$,$0.917^{(20)}$,$0.923^{(27)}$	$6.28^{(48)}$,$8.96^{(20)}$,$8.76^{(27)}$
3	$0.925^{(43)}$,$0.945^{(2)}$,$0.939^{(28)}$	$6.66^{(43)}$,$8.54^{(2)}$,$7.14^{(28)}$
4	$0.941^{(1)}$,$0.930^{(4)}$,$0.939^{(22)}$	$8.28^{(1)}$,$8.23^{(4)}$,$8.28^{(22)}$
5	$0.853^{(36)}$,$0.860^{(31)}$,$0.811^{(44)}$	$7.47^{(36)}$,$7.63^{(31)}$,$6.51^{(44)}$
6	$0.849^{(5)}$,$0.850^{(34)}$,$0.819^{(47)}$	$8.72^{(5)}$,$8.25^{(34)}$,$7.02^{(47)}$
7	$0.760^{(39)}$,$0.810^{(14)}$,$0.777^{(38)}$	$6.38^{(39)}$,$6.82^{(14)}$,$6.47^{(38)}$
8	$0.794^{(17)}$,$0.786^{(33)}$,$0.790^{(51)}$	$7.6^{(17)}$,$8.2^{(33)}$,$7.64^{(51)}$
9	$0.332^{(19)}$,$0.334^{(13)}$,$0.312^{(37)}$	$35.8^{(19)}$,$36.5^{(13)}$,$35.7^{(37)}$
10	$0.318^{(46)}$,$0.31^{(23)}$,$0.312^{(40)}$	$34.7^{(46)}$,$35^{(23)}$,$35.2^{(40)}$
11	$0.541^{(25)}$,$0.631^{(15)}$,$0.565^{(9)}$	$33.6^{(25)}$,$34.7^{(15)}$,$32.6^{(9)}$
12	$0.642^{(26)}$,$0.632^{(49)}$,$0.637^{(24)}$	$23.5^{(26)}$,$20.7^{(49)}$,$23.9^{(24)}$
13	$0.336^{(7)}$,$0.333^{(45)}$,$0.318^{(16)}$	$33.8^{(7)}$,$33.7^{(45)}$,$34.4^{(16)}$
14	$0.31^{(18)}$,$0.337^{(10)}$,$0.312^{(8)}$	$32.2^{(18)}$,$31.6^{(10)}$,$29.1^{(8)}$
15	$0.528^{(30)}$,$0.511^{(41)}$,$0.514^{(29)}$	$31.6^{(30)}$,$25.4^{(41)}$,$31.7^{(29)}$
16	$0.574^{(32)}$,$0.580^{(11)}$,$0.574^{(21)}$	$20.2^{(32)}$,$28.9^{(11)}$,$25.6^{(21)}$
17	$0.873^{(50)}$,$0.86^{(42)}$,$0.84^{(6)}$	$5.06^{(50)}$,$5.44^{(42)}$,$4.61^{(6)}$

the actual pressure drop measured during a washing run. Permeabilties (K_S) of the beds in the runs in the experimental design are given in Table 4.3.

Software was developed in MATLAB® to calculate the corrected breakthrough curves, pressure drop profiles, and the two responses from the raw data obtained in a displacement washing run. The code of the software is given in the Appendix B.

4.3.3 Statistical Analysis of Responses

Multiple regression analysis was performed on the data of two responses listed in Table 4.3 to evaluate the effects of the four variables listed in Table 4.1 and their interactions on the responses washing efficiency (WE) and permeability of the bed (K_S) after washing was completed. The regression equation used for both responses was

Response=

$$a_0 + \sum_{i=1}^{4} b_i X_i + \sum_{i=1}^{4} c_i X_i^2 + \sum_{j=1}^{4}\sum_{i=j+1}^{4} d_{ij} X_i X_j + \sum_{k=1}^{4}\sum_{j=k+1}^{4}\sum_{i=j+1}^{4} f_{ijk} X_i X_j X_k + g_{1234} X_1 X_2 X_3 X_4 \qquad 4.7$$

where X_1, X_2, X_3, and X_4 were the coded values of concentration of lignin in MBL solutions, concentration of polymer in the polymer solution, flow rate, and

diameter of glass bead in the center channel in a model bed respectively. a_0, b_i, c_i, d_{ij}, f_{ijk}, and g_{1234} were the regression coefficients.

Table 4.4 Subsets of predictors identified by stepwise regression on the responses.

Response 1 (WE) Washing Efficiency			Response 2 (K_S) Permeability X 10^{-8} (cm^2) of bed after washing		
Significant predictors	Coefficient	Successive t-ratio	Significant predictors	Coefficient	Successive t-ratio
Constant	0.8577	-	Constant	5.037	-
D	-0.2111	-85.38	D	11.51	44.21
[P]*D	0.0691	27.96	D^2	14.3	13.31
[P]	0.0586	23.68	[P]	-1.72	-6.59
$[L]^2$	-0.1969	-19.31	[P]*D	-1.42	-5.46
F	-0.0364	-14.72	[L]*D	-1.33	-5.10
F*D	0.0223	9.01	[L]	-1.13	-4.32
[P]*F	-0.0165	-6.66	[L]*[P]*D	-0.88	-3.38
[L]*[P]	0.0096	3.87	F	-0.7	-2.71
[L]*[P]*D	0.0077	3.13	[L]*[P]*F*D	0.61	2.36
[L]	0.006	2.42	-	-	-
R^2 = 99.58%, s = 0.0171 s = estimated standard deviation about regression			R^2 = 98.23%, s = 1.8 s = estimated standard deviation about regression		

The nomenclature of the variables adopted in multiple regression analysis is given in Table 4.1. The full Equation (4.7) was initially fitted to the experimentally obtained responses listed in Table 4.3 and a significant subset of predictors was determined by the procedure of stepwise regression (Minitab 9.2, 1993). Stepwise regression identifies significant predictors at each step by calculating their t-ratios and, based on 95% confidence intervals of the coefficient of a predictor, either it accepts or rejects the predictor into the model at each step. The procedure continues till no more predictors can be included or

Table 4.5 Results of multiple regression on the response, washing efficiency (WE).

Response 1 Washing Efficiency (WE)				
Predictors	Coefficient	Standard deviation	t-ratio	p
Constant	0.857667	0.00989	86.72	0.000
D	-0.211104	0.002473	-85.38	0.000
[P]*D	0.069146	0.002473	27.96	0.000
[P]	0.058563	0.002473	23.68	0.000
$[L]^2$	-0.19685	0.01019	-19.31	0.000
F	-0.036396	0.002473	-14.72	0.000
F*D	0.022271	0.002473	9.01	0.000
[P]*F	-0.016479	0.002473	-6.66	0.000
[L]*[P]	0.009563	0.002473	3.87	0.000
[L]*[P]*D	0.007729	0.002473	3.13	0.003
[L]	0.005979	0.002473	2.42	0.020
R^2 = 99.6%, R^2 (adj) = 99.5%, s = 0.01713 s = estimated standard deviation about regression				

removed from the model. The subset of predictors identified by stepwise regression on the data of two responses at 95% confidence intervals of their coefficients and their respective t-ratios are given in Table 4.4. Multiple regressions (Minitab 9.2, 1993) on the data of two responses listed in Table 4.3 were carried out using the subsets of predictors identified by stepwise regression. The coefficients of regression for the predictors, their standard deviations, the t-ratio for testing whether the coefficients were zero at 95% confidence intervals, and p values for this test are listed in Tables 4.5 and 4.6 respectively for the two responses. The results of analysis of variance for the

Table 4.6 Results of multiple regression on the response, permeability of model bed (K_S) after complete washing.

Response 2 Permeability $X10^{-8}$ (cm^2) (K_S)				
Predictors	Coefficient	Standard deviation	t-ratio	p
Constant	5.037	1.042	4.84	0.000
D	11.5115	0.2604	44.21	0.000
D^2	14.289	1.074	13.31	0.000
[P]	-1.716	0.2604	-6.59	0.000
[P]*D	-1.4215	0.2604	-5.46	0.000
[L]*D	-1.329	0.2604	-5.1	0.000
[L]	-1.1252	0.2604	-4.32	0.000
[L]*[P]*D	-0.8802	0.2604	-3.38	0.002
F	-0.7048	0.2604	-2.71	0.01
[L]*[P]*F*D	0.6140	0.2604	2.36	0.023
R^2 = 98.2%, R^2 (adj) = 97.8%, s = 1.804 s = estimated standard deviation about regression				

regressions are given in Tables 4.7 and 4.8.

Table 4.7 Results of analysis of variance of multiple regression analysis on response, washing efficiency (WE).

Response 1 Washing Efficiency (WE)					
Source	Degrees of freedom	Sum of Squares	Mean Squares	F	P
Regression	10	2.75205	0.2752	937.79	0.000
Error	40	0.01174	0.00029	-	-
Total	50	2.76379		-	-

Source	Degrees of freedom	Sequential sum of squares
D	1	2.13912
[P]*D	1	0.2295
[P]	1	0.16462
$[L]^2$	1	0.10942
F	1	0.06358
F*D	1	0.02381
[P]*F	1	0.01304
[L]*[P]	1	0.00439
[L]*[P]*D	1	0.00287
[L]	1	0.00172

Table 4.8 Results of analysis of variance of multiple regression analysis on response, permeability (K_S) of bed after complete washing.

Response 2 Permeability $X10^{-8}$ (cm^2) (K_S)					
Source	Degrees of freedom	Sum of Squares	Mean Squares	F	P
Regression	9	7400.19	822.24	252.63	0.000
Error	41	133.45	3.25	-	
Total	50	7533.64	-	-	

Source	Degrees of freedom	Sequential sum of squares
D	1	6360.66
D^2	1	576.53
[P]	1	141.35
[P]*D	1	96.99
[L]*D	1	84.77
[L]	1	60.77
[L]*[P]*D	1	37.19
F		23.84
[L]*[P]*F*D	1	18.09

The adequacies of the regressed models were tested by diagnostic checks of residuals of regressions against order of runs and each variable. Figures 4.15 and 4.16 demonstrate that residuals for regressions for both the responses were distributed randomly about a mean of zero when plotted against run number and one of the variables such as concentration of polymer. Also, the models were accepted at 95% confidence limit through lack of fit tests. As a result, there was no adequate evidence to reject the models.

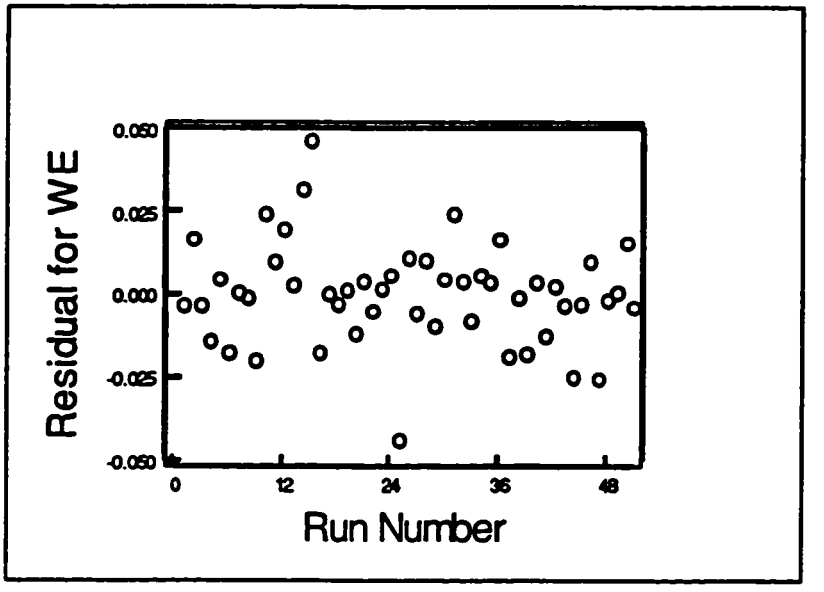

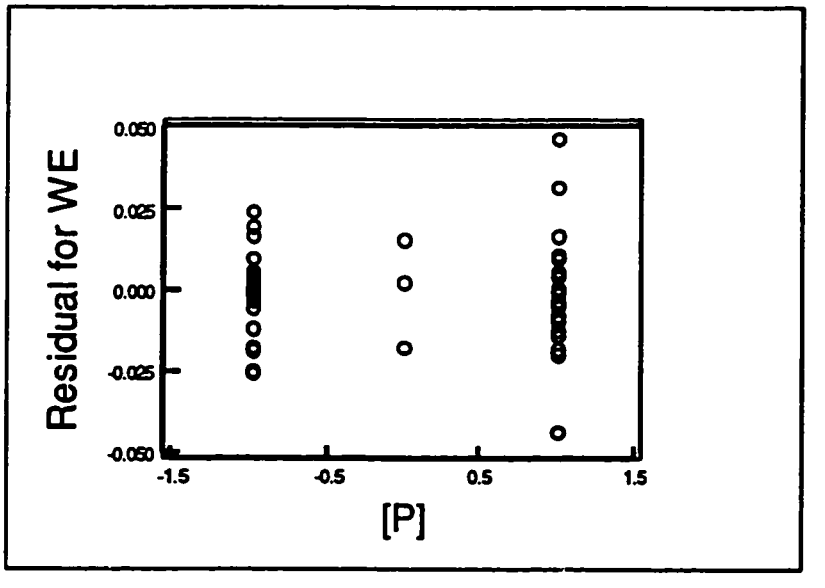

Figure 4.15 Diagnostic checks of residuals for regression on response, washing efficiency (WE)

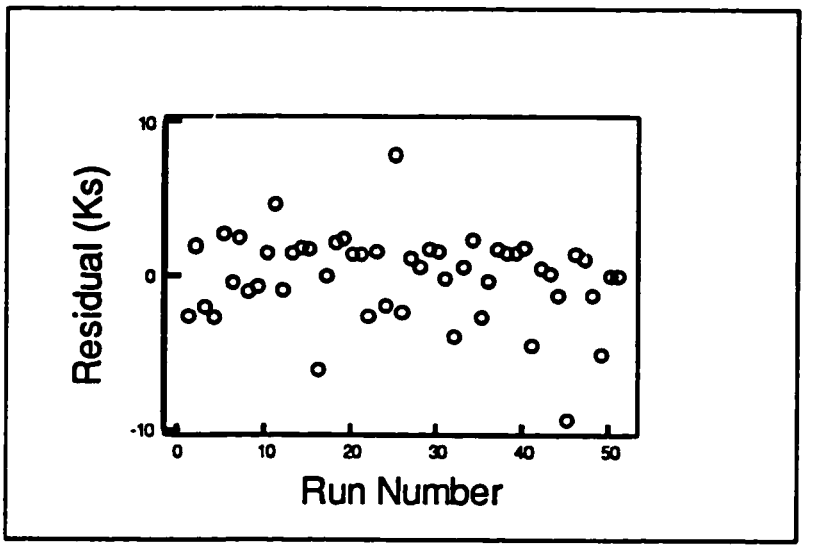

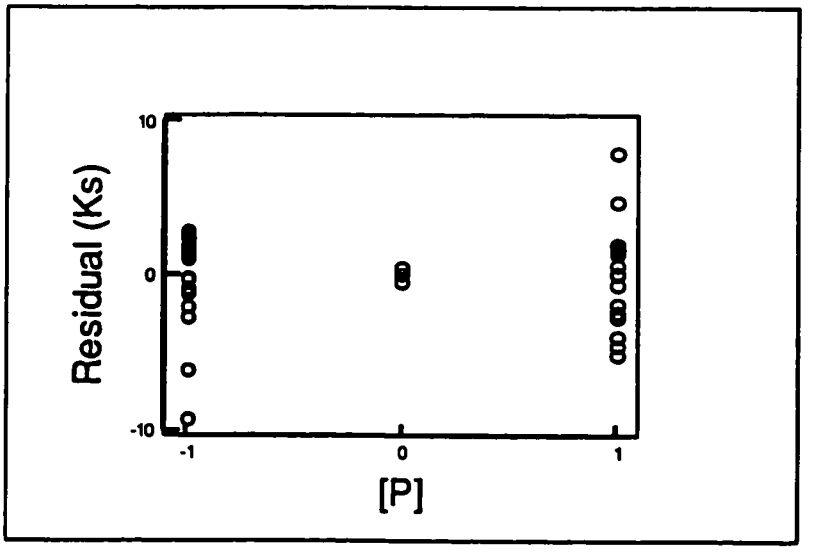

Figure 4.16 Diagnostic checks of residuals for regression on response, steady state permeability (K_s).

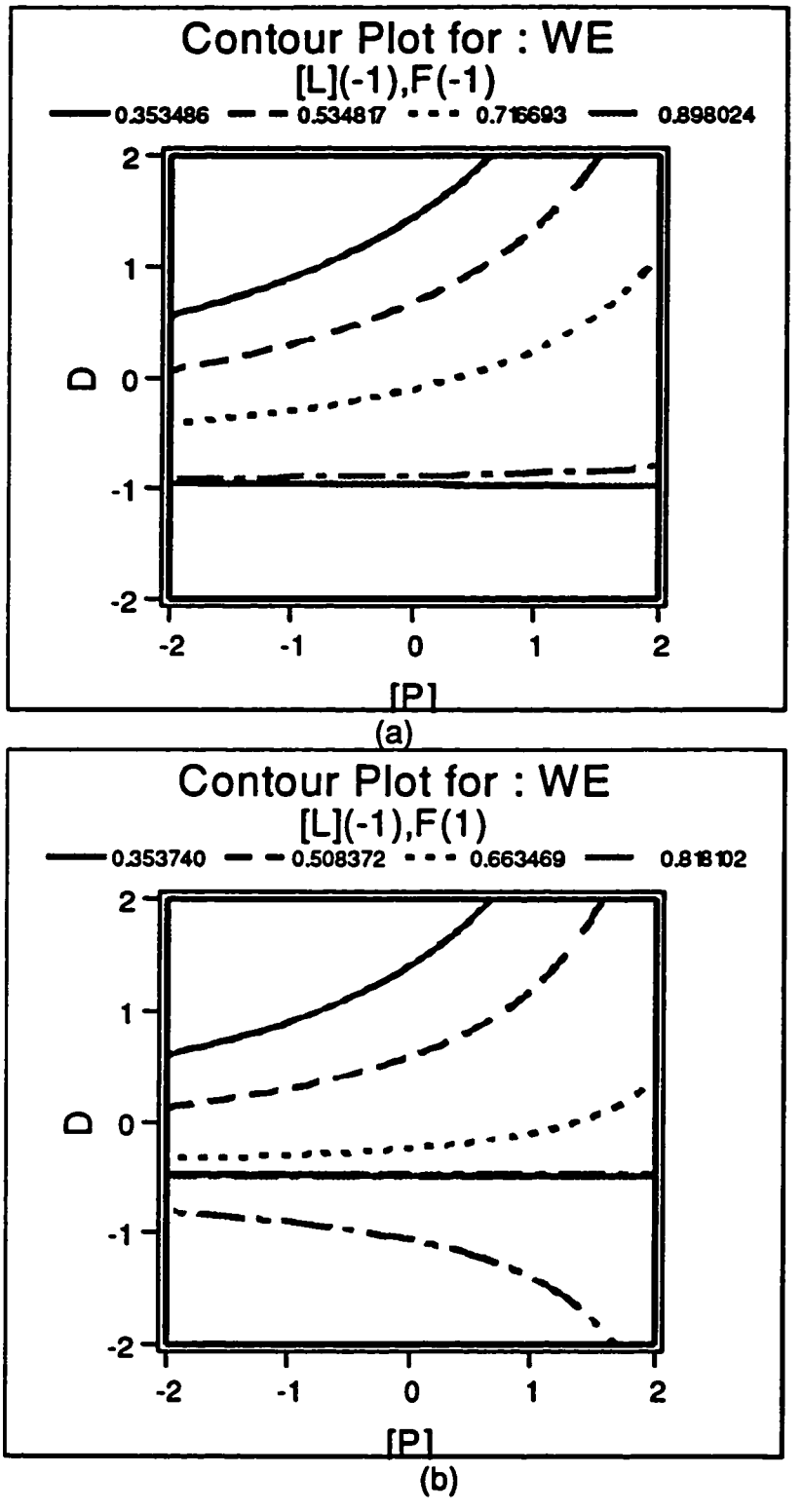

Figure 4.17-1 Contour plots of washing efficiency (WE). Contours represent lines of constant washing efficiencies.

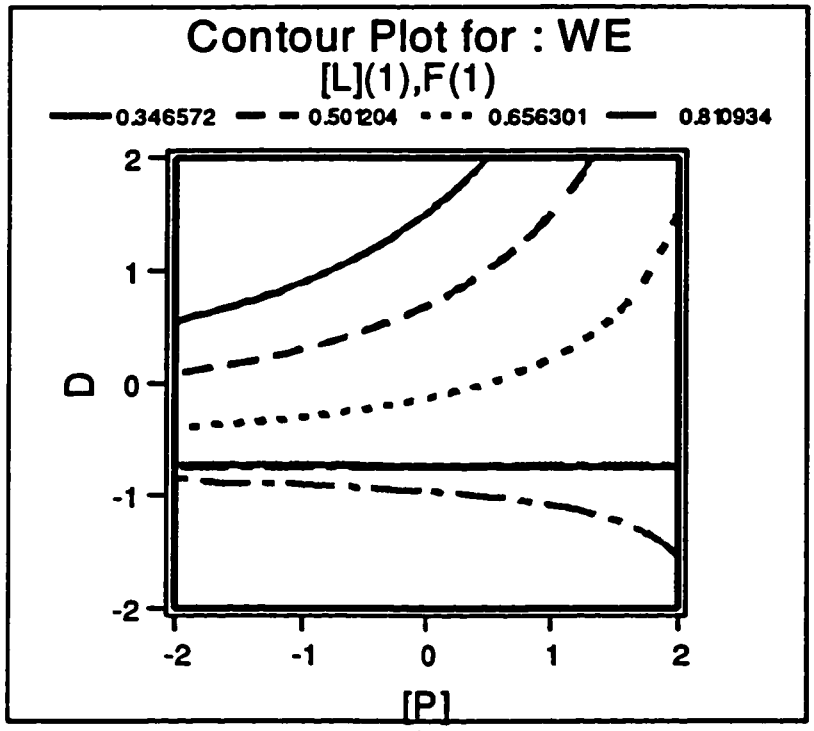

(a)

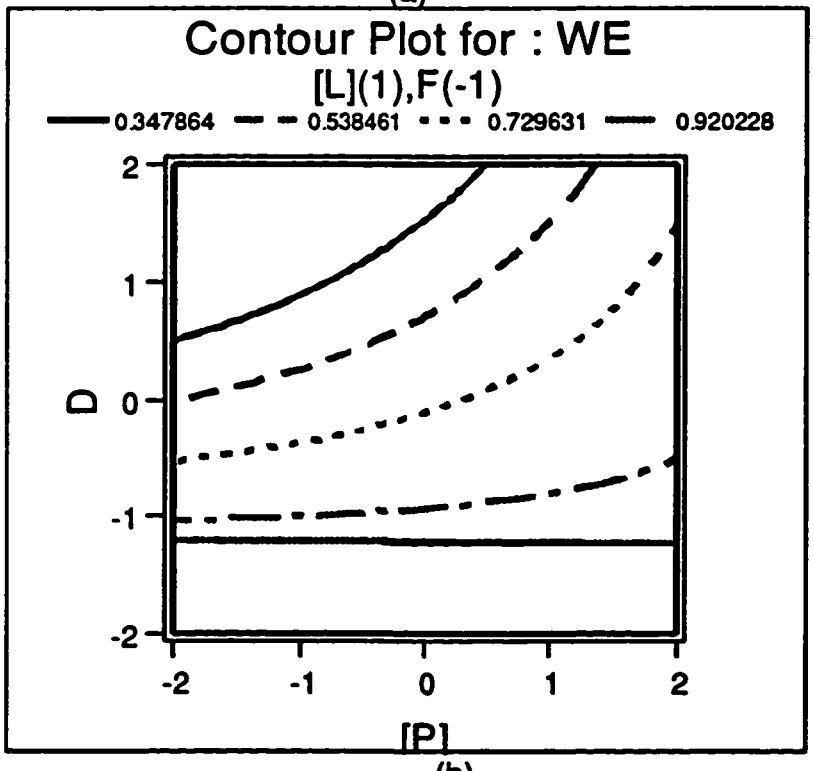

(b)

Figure 4.17-2 Contour plots of washing efficiency (WE). Contours represent lines of constant washing efficiencies.

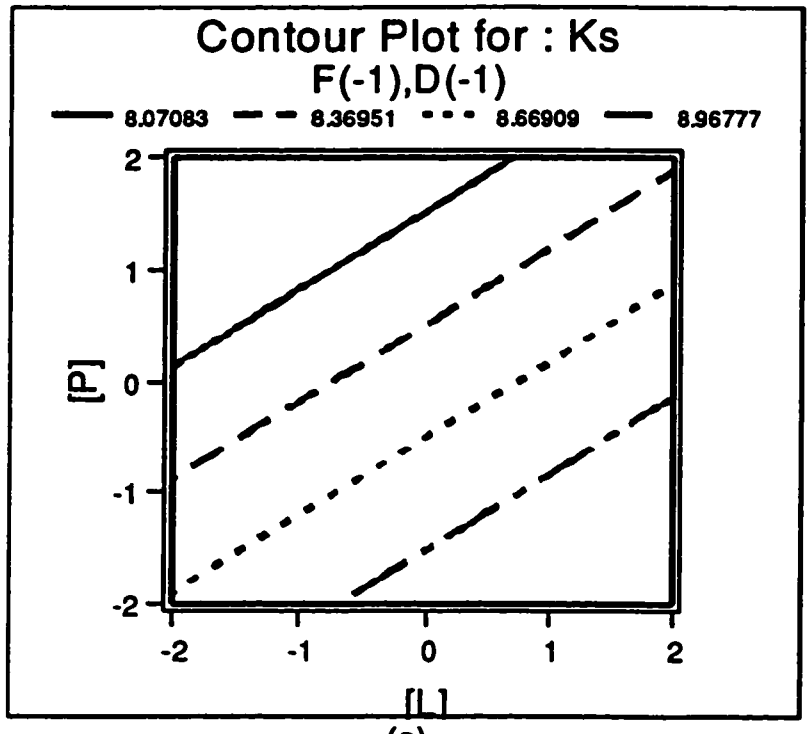

(a)

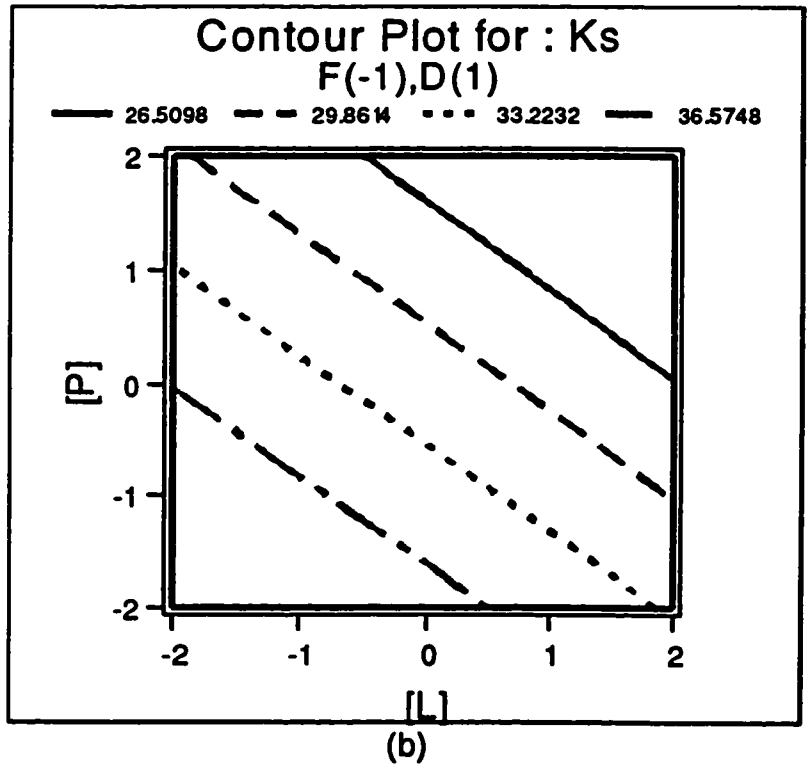

(b)

Figure 4.18-1 Contour plots of steady state permeability (K_S). Contours represent lines of constant steady state permeabilities.

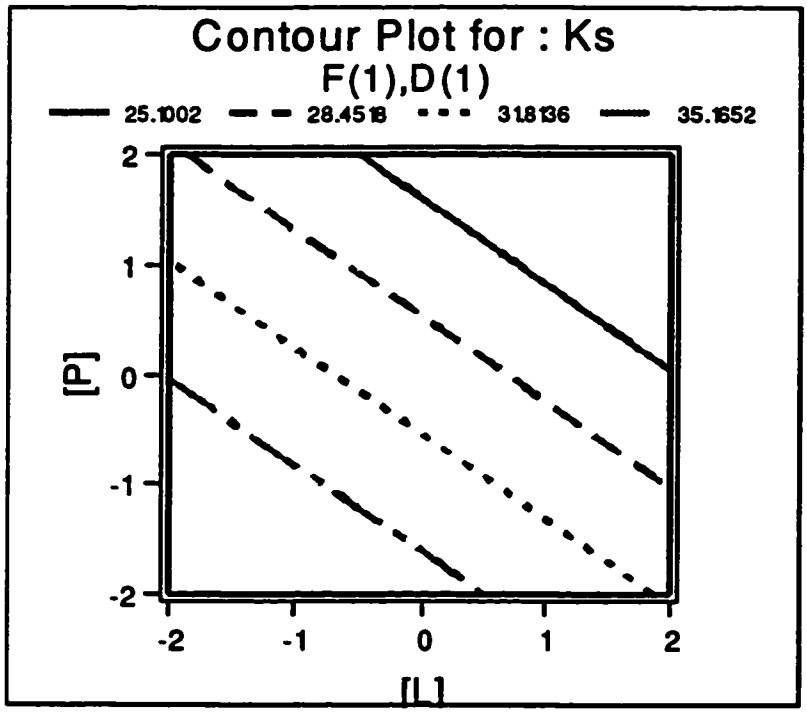

(a)

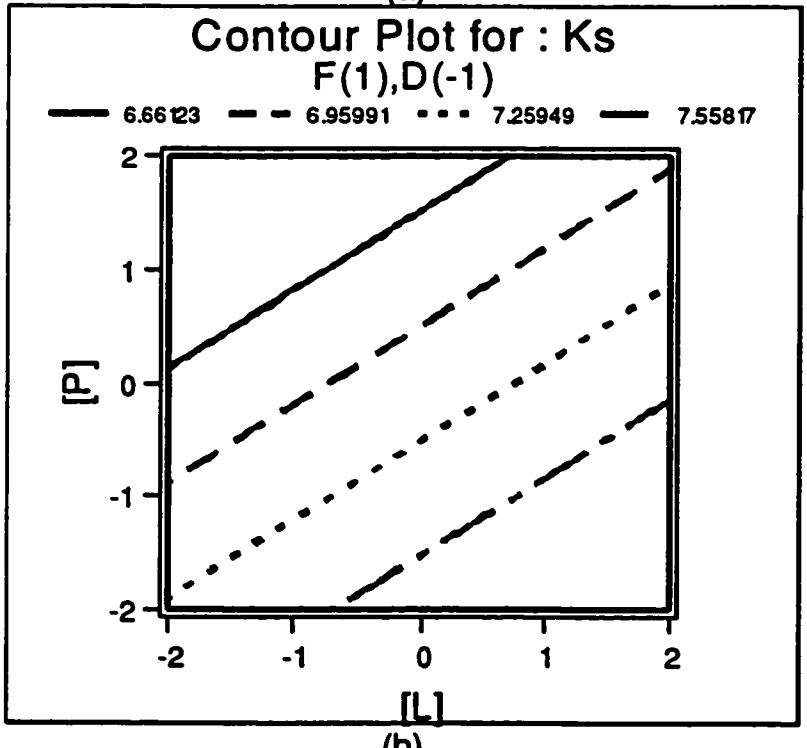

(b)

Figure 4.18-2 Contour plots of steady state permeability (K_S). Contours represent lines of constant steady state permeabilities.

4.4 Discussion

Tables 4.5 and 4.6 demonstrate the complex dependence of the two responses, washing efficiency (WE) and steady state permeability (K_S) on the four variables and their interactions. Regressed models obtained in Tables 4.5 and 4.6 were used to examine the intricate dependence of the responses on the four variables and their interactions through contour diagrams, shown in Figures 4.17-1, 4.17-2, 4.18-1, and 4.18-2. A contour diagram consists of contours of responses with constant values when any two of the four key variables listed in Table 4.1 are varied together over their ranges while keeping the other two variables fixed either at high or low level. The range of the variables studied in this work spanned from -1 to 1 in Figures 4.17-1, 4.17-2, 4.18-1, and 4.18-2. For the sake of clarity of the contours, the ranges of variables in Figures 4.17-1, 4.17-2, 4.18-1, and 4.18-2 were extended from -2 to 2. However, the levels of variables that were kept fixed were either at -1 or 1. The coded levels of the variables that were kept fixed are listed at the top of each figure in Figures 4.17 - 1, 4.17-2, 4.18-1, and 4.18-2. In the following sections, absolute values of the responses at a given set of levels of the four variables were computed from the regressed models obtained in Tables 4.5 and 4.6.

4.4.1 Washing Efficiency (WE)

Figure 4.17-1(a) demonstrates that at the low level of concentration of lignin in the MBL solution and at the low level of flow rate, washing efficiency decreased from around 92% in a homogeneous bed to around 33% in a channel bed when they were washed with water. When the channel bed was washed with the polymer solution instead of water, the washing efficiency increased from around 33% to 58%. In a homogeneous bed that was washed with polymer solution instead of water, washing efficiency increased slightly by around 2%.

At the high level of flow rate and at the low level of lignin concentration in the MBL solution, Figure 4.17-1(b) shows that washing efficiency decreased from around 84% in a homogeneous bed to around 33% in a channel bed when they were washed with water. When a channel bed was washed with the polymer solution instead of water, washing efficiency increased from around 33% to 52%. Figure 4.17-1(b) also shows that washing efficiency in a homogeneous bed was around 4% lower when it was washed with the polymer solution than the washing efficiency when water was used. A comparison of Figure 4.17-1(a) and Figure 4.17-1(b) reveals that with an increase in flow rate, washing efficiency decreased by around 8 and 14% in a homogeneous bed when washed with water and the polymer solution respectively. However, with an increase in flow rate, washing efficiency in a channel bed that was washed with

water remained almost constant whereas washing efficiency in the channel bed decreased by around 6% when washed with the polymer solution.

Figure 4.17-2(b) shows that at the high level of lignin in the MBL solution and at the low level of flow rate, washing efficiency in a homogeneous bed decreased from around 93% to around 31% in a channel bed when washed with water. When a homogeneous bed was washed with the polymer solution instead of water, washing efficiency increased by around 2%. In a channel bed that was washed with the polymer solution instead of water, washing efficiency increased from around 31% to 63%.

Figure 4.17-2(a) shows that washing efficiency decreased from around 84% in a homogeneous bed to around 31% in a channel bed when washed with water. In a channel bed washing efficiency increased from around 31% to 57% when washed with the polymer solution instead of water. In a homogeneous bed that was washed with the polymer solution instead of water, washing efficiency went down by around 4%. A comparison of Figure 4.17-2(a) and Figure 4.17-2(b) demonstrates that at the high level of concentration of lignin in the MBL and with an increase in the level of flow rate from low to high, washing efficiency in a homogeneous bed decreased by around 9 and 15% when washed with water and the polymer solution respectively. Washing efficiency in the channel bed remained constant with flow rate, whereas in a channel bed washed with the polymer solution, washing efficiency decreased by around 6%.

At both high and low levels of concentration of lignin in the MBL and at both high and low levels of flow rate of wash liquors, washing efficiency in a channel bed was less than that in a homogeneous bed when washed with either water or the polymer solution due to channeling of the wash liquor through the more permeable channel at the center of a model channel bed. Washing efficiency in a channel bed increased by 1.7 to 2 times when washed with the polymer solution instead of water due to selective plugging of the center channel with precipitate formed from reaction of the anionic lignin in the MBL and the cationic polymer in the polymer solution, discussed in detail in Chapter 3. Selective plugging reduced the permeability of the center channel. Consequently, channeling through the center channel decreased, resulting in higher washing efficiency. In Figure 4.13, the early breakthrough of either water or the polymer solution in a channel bed was due to channeling of the wash liquor. During washing with the polymer solution and with plugging of center channel, breakthrough curves shifted towards those characteristic to a homogeneous bed. As a result, less volume of wash liquor was needed for complete washing with the polymer solution than with water in a channel bed.

At both high and low levels of flow rate in a channel bed that was washed with the polymer solution, increase in the concentration of lignin in the MBL resulted in a 5% increase in washing efficiency. This increase in washing efficiency was probably due to the higher amount of precipitate that was formed

in the center channel as the concentration of lignin in the MBL at the high level of lignin concentration and that of the cationic polymer in the polymer solution were at an optimum ratio reported by Lappan et al. (1996). At the optimum ratio of concentration of lignin in the MBL at 25 g/L to concentration of polymer in the polymer solution at 29.4 g/L, the highest amount of precipitate could be formed. Deviation from the optimum ratio led to formation of less precipitate (Lappan et al., 1996). At both high and low levels of lignin concentration in the MBL, around 6% decrease in washing efficiency with an increase in the level of flow rate in a channel bed washed with the polymer solution was probably due to dislodging and removal of some of the precipitate from the center channel.

In a homogeneous bed that was washed with either water or the polymer solution, the 9-15% decrease in washing efficiency with an increase in flow rate from low to high was probably due to more interfacial mixing between the MBL and either water or the polymer solution at both high and low levels of concentration of lignin. Increased interfacial mixing due to the increase in hydrodynamic dispersion (Lake, 1989; Bear, 1972) of lignin between the wash liquor and the MBL solution reduced washing efficiency by 9-15% when the flow rate was changed from 30 mL/min to 230 mL/min. However, in a channel bed that was washed with water, washing efficiency remained constant with the increase in flow rate. At a given overall flow rate, channeling in a channel bed caused the displacement front in the annulus to move more slowly than that in a

homogeneous bed. With an increase in overall flow rate, the increase in absolute value of Darcy interstitial velocity in a homogeneous bed was higher than that in the annulus of a channel bed. Since the dispersion becomes more prominent at higher interstitial velocity of fluid (Bear, 1972), the relative increase in dispersion with increase in overall flow rate in a homogeneous bed could be expected to be more pronounced than that in the annulus in a channel bed. The effect of hydrodynamic dispersion on washing efficiency in a channel bed was probably controlled by hydrodynamic dispersion in the annulus since the cross sectional area of the annulus was approximately eight times higher than that of the channel. As a result, washing efficiency in the channel bed remained unchanged since dispersion in the annulus in a channel bed did not increase significantly with the increase in flow rate.

At the low flow rate and the high level of concentration of lignin, washing efficiency in a homogeneous bed tended to increase by 2-3% when washed with the polymer solution instead of water. This was probably due to retardation in interfacial mixing caused by the presence of a highly viscous soluble layer of lignin/polyDADMAC complex that separated the MBL and the polymer solution during washing. At the low concentration of lignin, the layer of soluble precipitate was probably weak and retardation of interfacial mixing was probably insignificant explaining almost no change in washing efficiency. With an increase in flow rate, washing efficiency in a homogeneous bed washed with

polymer solution decreased, probably due to breaking away of the soluble layer of precipitate, resulting into more dispersion.

4.4.2 Permeability of Bed after Complete Washing (K_s)

Figure 4.18-1 and Figure 4.18-2 demonstrate that at low levels of lignin concentration, steady state permeability (K_s) varied from around 10 $x10^{-8}$ cm^2 in a homogeneous bed to 35.6 $x10^{-8}$ cm^2 in a channel bed at the low flow rate and from around 7.4 $x10^{-8}$ cm^2 in a homogeneous bed to 35.4 x 10^{-8} cm^2 in a channel bed at the high flow rate when they were washed with water. At the low level of concentration of lignin in the MBL and in a channel bed that was washed with the polymer solution instead of water, steady state permeability decreased slightly from around 35.6 $x10^{-8}$ cm^2 to 31$x10^{-8}$ cm^2 at low flow and 35.4 $x10^{-8}$ cm^2 to 29.7 $x10^{-8}$ cm^2 at high flow. Decrease in permeability of a homogeneous bed with the increase in flow rate was probably due to compaction of a homogeneous bed at high flow rate. However, when channeling was present, the channel bed probably remained at the same level of compaction at both high and low flow rate and the permeability of a channel bed probably remained relatively constant with change in flow rate.

Figures 4.18-1 and 4.18-2 also demonstrate that at the high level of lignin concentration, steady state permeability increased from around 7.5 $x10^{-8}$ cm^2 in a homogeneous bed to around 33.7 $x10^{-8}$ cm^2 in a channel bed at the low level of

flow and from 7.3 $x10^{-8}$ cm^2 in a homogeneous bed to 31.1 $x10^{-8}$ cm^2 in a channel bed at the high level of flow after washing with water. However, when the channel bed was washed with the polymer solution, steady state permeability decreased from around 33.7 $x10^{-8}$ cm^2 to 24.4 $x10^{-8}$ cm^2 at the low level of flow and 31.1 $x10^{-8}$ cm^2 to 24.2 $x10^{-8}$ cm^2 at the high level of flow approximately.

Figures 4.18-1 through 4.18-2 also show that with an increase in flow rate at both low and high levels of concentration of lignin in MBL, steady state permeability in a homogeneous bed either washed with water or the polymer solution decreased slightly due to probable compaction of the bed at high flow rate. However, permeability of a channel bed washed with water remained relatively constant with change in flow rate.

The presence of a more permeable channel in a channel bed increased its permeability to 3.6 to 4.7 times that of a homogeneous bed when washed with water. However, when a channel bed was washed with the polymer solution, due to selective precipitate formation and plugging of center channel, permeability of the center channel decreased. As a result, overall permeability of a channel bed decreased when it was washed with a polymer solution instead of water. In the following section, percentage reduction in the permeability of the center channel at the end of washing with the polymer solution is calculated.

A channel bed can be modeled as a combination of a higher permeable bed of coarse beads and lower permeable bed of fine beads held in parallel. The

flow rates in each bed and the overall flow rate through the channel bed can be described by Darcy's law of fluid permeation as

$$\frac{Q_c}{A_c} = \frac{K_c}{\mu}\frac{\Delta P}{L} \qquad 4.8$$

$$\frac{Q_f}{A_f} = \frac{K_f}{\mu}\frac{\Delta P}{L} \qquad 4.9$$

$$\frac{Q}{A} = \frac{K}{\mu}\frac{\Delta P}{L} \qquad 4.10$$

where K and ΔP are permeability of the channel bed and pressure drop across the channel bed respectively. The subscripts "c" and "f" represent the beds of coarse beads and fine beads respectively in the channel bed. The total flow rate Q and cross sectional area of the channel bed A can be expressed as

$$Q = Q_c + Q_f \qquad 4.11$$

and

$$A = A_c + A_f \qquad 4.12$$

Assuming the pressure drops across the higher permeable bed of coarse beads and lower permeable bed of fine beads are equal to each other, Equations (4.8) through (4.12) can be manipulated to obtain Equation (4.13).

$$KA = K_c A_c + K_f A_f \qquad 4.13$$

Figures 4.18-1 through 4.18-2 demonstrate that the permeability of a homogeneous bed of fine glass beads remained constant after washing with the polymer solution. Flow visualization experiments in Chapter 3 revealed that precipitates were only retained in the center channel in a channel bed after washing with the polymer solution. Consequently, it can be assumed that after washing a channel bed with the polymer solution, only the permeability of the center channel changed due to selective precipitate retention in the channel. As a result, using Equation (4.13), percentage reduction of the permeability of the center channel can be expressed as

$$\%\text{Reduction in } K_c = \frac{(K_C)_w - (K_C)_p}{(K_C)_w} \times 100 = \frac{A\left[(K)_w - (K)_p\right]}{\left[(K)_w A - K_f A_f\right]} \times 100 \qquad \textbf{4.14}$$

where subscripts "w" and "p" refer to the values of respective permeabilities when water and the polymer solution were used as wash liquors respectively.

In a channel bed, a 1.7 cm diameter central channel of coarse glass beads was surrounded by an annulus of fine beads in the washing cell of 5.2 cm internal diameter. In Chapter 3, it is established that the permeability of coarse glass beads in channel was around 28 times higher than that of fine glass beads in the annulus of the channel bed. Using Equation (4.13), it can be shown that the permeability of a channel bed should be 4.35 times higher than that of a

homogeneous bed of fine glass beads. The permeabilities of channel beds calculated from experiments shown in Figure 4.18-1 through Figure 4.18-2 were 3.6 to 4.7 times higher than that of homogeneous bed after washing with water.

Using Equation (4.14), percentage reduction in the permeability of the center channel after washing with the polymer solution was calculated from the overall permeability data of channel bed that was washed with either water or the polymer solution. At the low level of concentration of lignin and the low flow rate, reduction of the permeability of the central channel was 17.3%, whereas at the high flow rate it was 19.8%. At the high lignin concentration and at the low flow rate, reduction in center channel permeability was 34.5%, whereas at the low flow rate it was 28.1%. Due to a lack of the optimum ratio of lignin concentration and concentration of the polymer in the polymer solution at the low level of lignin concentration, less precipitate was formed in the center channel both at both low and high levels of flow. As a result, both at high and low flow rate, center channel permeability was reduced less than that when the level of concentration of lignin was high.

With an increase in flow rate, percentage reduction in permeability of the center channel decreased by around 6% at the high level of concentration of lignin. As the flow rate was increased, precipitates were probably dislodged and carried away from the center channel due to higher shear forces. At the high level of lignin concentration and at the high flow rate, more precipitates were

formed in the channel and as a result, chances of dislodging and removal of precipitates were probably higher resulting in a 6% decrease in reduction in permeability of the center channel at the high level of flow. Since less precipitate was formed in the center channel at the low level of concentration of lignin, percentage reduction in the center channel permeability remained relatively insensitive to flow rate. Percentage reduction in permeability of the center channel was calculated from the data of permeability of beds after washing was completed. During washing with the polymer solution, precipitates were formed and plugged the center channel, and with the advancement of washing, they might have been dislodged and carried away from the bed. As a result, actual reduction in permeability of the center channel during washing might be even higher than that after washing had been completed.

4.5 Conclusions

(a) The intrusive way of measuring conductivity inside the model beds by conductivity probes had little effect on the displacement flow profile since washing efficiency in the presence and absence of probes in a homogeneous bed washed with water varied within ± 3%.

(b) Due to channeling of wash water through the more permeable channel in a channel bed, washing efficiency (31 to 33%) was substantially lower than those (93-84%) in a homogeneous bed. Presence of the more permeable channel at the center of a channel bed increased permeability of the channel bed by 3.6 to 4.7 times that of a homogeneous bed.

(c) The presence of a cationic polymer in the wash liquor increased the washing efficiency in a channel bed by 1.7 to 2 times that in a channel bed that was washed with water. Selective plugging of the center channel of a channel bed with precipitate reduced channeling, resulting in an increase in washing efficiency. Permeability of the center channel was reduced by 34.5 to 28.1% at the high lignin concentration of 25 g/L and by 17.3 to 19.8% at a lignin concentration of 2.5 g/L.

(d) With an increase in flow rate from 30 mL/min to 230 mL/min, washing efficiency in a homogeneous bed was reduced by 9-15% due to more interfacial mixing of the MBL solution and the wash liquors. In a channel bed that was washed with the polymer solution, an increase in flow rate from 30 mL/min to 230 mL/min reduced washing efficiency by 6%, probably due to dislodging and removal of precipitates from the center channel.

(e) An increase in concentration of lignin from 2.5 g/L to 25 g/L resulted in a 5% increase in washing efficiency in a channel bed that was washed with the polymer solution. The probable cause for this increase in washing efficiency was the optimum ratio of concentration of lignin (25 g/L) and concentration of polymer (29.4 g/L), which produced a maximum amount of precipitate in the center channel in a channel bed.

List of Variables

a_0	Constant in Eqn (4.7), dimensionless.
A	Cross sectional area of bed, m^2.
b_i	Regression coefficient in Eqn (4.7), dimensionless.
c_i	Regression coefficient in Eqn (4.7), dimensionless.
d_{ij}	Regression coefficient in Eqn (4.7), dimensionless.
f_{ijk}	Regression coefficient in Eqn (4.7), dimensionless.
g_{1234}	Regression coefficient in Eqn (4.7), dimensionless.
C	Conductivity defined in Eqn (4.3), dimensionless.
$C_{measured}$	Conductivity of eluate at any time t in Eqn (4.3), $ohm^{-1}m^{-1}$.
C_o	Initial conductivity of MBL in bed in Eqn (4.3), $ohm^{-1}m^{-1}$.
C_w	Conductivity of wash liquor in Eqn (4.3), $ohm^{-1}m^{-1}$.
D_p	Diameter of particle, m.
ER	Eluate ratio, dimensionless.
K	Permeability, m^2.
Ks	Steady state permeability defined in Eqn (4.6), m^2.
L	Length of the bed, m.
ΔP	Pressure drop, Pa.
ΔP_s	Steady state pressure drop, Pa.
Q	Superficial flow rate, m^3/s.
Re_p	Particle Reynolds number, dimensionless.
t	Time for displacement, s.
V	Average Darcy superficial velocity, m/s.
V_{bed}	Volume of bed in washing cell in Equation 4.1, m^3.
V_f	Volume of upto final level of liquid in cell in Equation 4.1,m^3.
V_i	Initial volume of liquid in washing cell in Equation 4.1, m^3.
WE	Washing efficiency defined in Eqn (4.5), dimensionless.

X_i	Coded value of variable in Eqn (4.7), dimensionless.
X_j	Coded value of variable in Eqn (4.7), dimensionless.
X_1	Coded value of concentration of lignin, dimensionless.
X_2	Coded value of concentration of polymer, dimensionless.
X_3	Coded value of flow rate, dimensionless.
X_4	Coded value of diameter of beads, dimensionless.

Subscripts

c	Coarse beads.
f	Fine beads.
m	Medium beads.
p	Polymer
w	Water

Greek Letters

ε	Porosity of bed, dimensionless.
μ	Viscosity of fluid, Pa.s.
ρ	Density of fluid, Kg/m^3.

Abbreviations

I/O	Input / Output.
MBL	Model black liquor.
MW	Molecular weight.
VDC	Voltage, direct current.

References

Bear, J., Dynamics of Fluids in Porous Media, Elsevier, New York (1972).

Blackwell, R. J., J. R. Rayne, and W. M. Terry, Trans AIME, **216**, 1 (1959).

Crotogino, R. H., N. A. Poirier, and D. T. Trinh, "The Principles of Pulp Washing," Tappi, **70**, 95(1987).

Hofman, J. A. M. H., and H. N. Stein, " Permeability Reduction of Porous Media on Transport of Emulsions through them," Colloid and Surfaces, **61**, 317 (1991).

Lake, L.W., Enhanced Oil Recovery, Prentice Hall, New Jersey (1989).

Lappan, R., R. H. Pelton, and A. H. Hrymak, unpublished work, McMaster University, Hamilton, Ontario, Canada (1996).

Lee, P. F., "Channeling and Displacement Washing of Wood Pulp Fiber Pads," Tappi, **67(11)**, 100 (1984).

Li, P., and R. H. Pelton, "Wood pulp washing: 2. Displacement Washing of Aqueous Lignin from Model Beds with Cationic Polymer Solutions," Colloids and Surfaces, **64**, 223 (1992).

Mathews, J. L., Emanuel, A. S., and Edwards, K. A., "A Modeling Study of the Mitsue Stage 1 Miscible Flood using Fractal Geometries," SPE 18327, 63rd Annual Technical Conference of SPE, Houston, 661 (1988).

McCool, C. S., D. W. Green, and G. P. Willhite, "Permeability Reduction Mechanisms involved in *in-situ* Gelation of a Polyacrylamide/Chromium (VI)/ Thiourea system," SPERE, 77-83, Trans AIME, **291**, February (1991).

Miller, M. J., and H. S. Fogler., "A Mechanistic Investigation of Waterflood Diversion using Foamed Gels," SPE Production & Facilities, **63**, February (1995).

Minitab Inc, Release 9.2, State College, PA, USA (1993).

Tang, R. W., Behrens, R. A., and Emanuel, A. S.,"Reservoir Studies using Geostatistics to Forecast Performance," SPE 18432, SPE symposium on Reservoir Simulation, Houston, 321(1989).

Todd, B. J., G. P. White, and D. W. Green, "A Mathematical Model of *in-situ* Gelation of Polyacrylamide by a Redox Process," SPE Reservoir Engineering, **51**, February (1993).

Trinh D. T., N. A. Poirier, R. H. Crotogino, and W. J. M. Douglas, "Displacement Washing of Wood Pulp - An Experimental Study," JPPS, **15(1)**, J28, January (1989).

Chapter 5

A Direct Experimental Method to Study the Modification of Flow Profile using Conductivity Probes during Reactive Polymer Enhanced Miscible Displacement of Model Black Liquor in Model Beds of Glass Beads

Abstract

Conductivity probes were installed inside model black liquor (MBL)-saturated model beds of glass beads to monitor the displacement front during displacement washing with either water or a polymer solution. Analysis of the velocity of the displacement front during displacement washing in a homogeneous bed of 121 μm beads confirmed the ability of the probes to monitor the displacement front in model beds. In a channel bed that consisted of a central channel of 638 μm beads surrounded by an annulus of 121 μm beads, lower velocity of front in the annulus and higher velocity of front in the channel than those in a homogeneous bed indicated poor displacement washing resulting from the channeling of the displacing phase through the center channel compared to that in a homogeneous bed. However, when a channel bed was displaced with the polymer solution instead of water, direct evidence of the

modification of the flow profile by selective precipitation in the center channel, and thus reduction in channeling and improvement in the performance of displacement in the channel bed, was observed from the data obtained by conductivity probes for the first time. Data obtained by the probes confirmed the lowering of flow rate in the center channel, increase in flow rate in the annulus, and reduction in the mixing lengths in both center channel and annulus in the model channel bed when polymer was used as the displacing phase instead of water. During washing with the polymer solution in a homogeneous bed, mixing lengths were observed to be slightly lower than those when the bed was washed with water. The reason for this has been attributed to the possible retardation of interfacial mixing between the MBL and the polymer solution by the presence of a soluble, viscous layer of lignin/polyDADMAC complex at the interface between MBL and polymer solution. Data obtained by the probes also confirmed no anomalous behavior of the model beds when they were washed with water.

5.1 Introduction

Poor displacement washing due to bypassing or channeling of the displacing phase through more permeable channels in porous media is encountered in many fields of chemical engineering including the brownstock washing stage in Kraft pulping process, tertiary oil recovery in petroleum

engineering, and ground water flow in hydrology (Blackwell et al., 1959; Crotogino et al., 1987; Lee, 1984; Lake, 1989; Tang et al., 1989). Researchers (Lee, 1984; Li and Pelton, 1992; Lake, 1989) have described the use of polymeric additives in the displacing phase to improve the performance of displacement washing by suppressing channeling through both compressible and incompressible porous beds during the displacement process.

Lee (1984) conducted displacement washing experiments of wood pulp fibers in laboratory scale using aqueous nonionic polymer solutions as the displacing phase. He reported that due to reduction of mobility of an aqueous solution of a high molecular weight nonionic polymer, displacement washing efficiency was improved by suppression of channeling in the pad of pulp fibers. He ascribed the reduction of mobility of the aqueous solution of the high molecular weight nonionic polymer to an increased resistance to flow of the swollen microgels of the polymer through pores of the pulp pad.

Li and Pelton (1992) used a cationic polymer in water to improve displacement washing in black liquor saturated model beds of glass beads. They postulated that channeling was suppressed by precipitate formation in the more permeable channels in a porous bed from the reaction of the cationic polymer with the anionic lignin present in the black liquor, leading to improved displacement washing. De and Pelton (Chapter 4) have confirmed the results of Li and Pelton (1992) by measuring quantitatively the displacement washing

performance in model beds using an aqueous solution of a cationic polymer as the displacing phase. However, none of these studies reported any details of the displacement front properties within the bed.

The major objective of this work was to evaluate the performance of displacement washing by monitoring such properties as velocity and mixing length of the displacement front with conductivity probes inserted into the bed during displacement washing of black liquor either with water or a polymer solution in packed beds of glass beads.

5.2 Experimental

5.2.1 Materials

Glass beads no:3 and no: 10, model black liquor solutions (MBL), and polymer solutions, described in detail in section 3.2.1 in Chapter 3, were used in the displacement experiments. No: 3 (average diameter 638 μm) and no: 10 (average diameter 121 μm) glass beads are denoted as coarse (subscript "c") and fine (subscript "f") beads respectively in the rest of this chapter.

5.2.2 Apparatus

The computerized displacement washing apparatus, described in detail in section 4.2.2 in Chapter 4, was employed to perform displacement washing

experiments in model beds of glass beads using either water or the polymer solution as wash liquors.

5.2.3 Locations of Probes inside the Cell

Conductivity probes were used to monitor the properties of the displacement front as a function of time. The location of twelve conductivity probes inside the porous bed is depicted in Figure 5.1. At each of the four axial

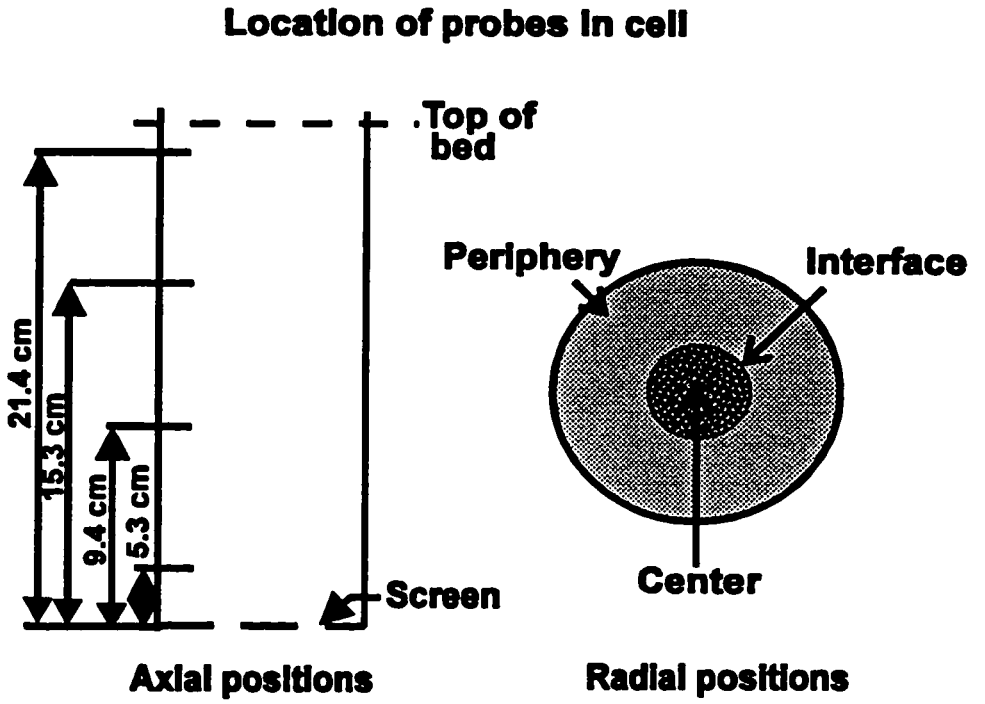

Figure 5.1 Axial and radial positions of probes employed to monitor displacement front inside a porous bed during miscible displacement. Three probes were placed at each axial position.

positions, three probes were inserted near the periphery (0.7 cm from inner wall of cell), near the interface of fine and coarse beads (2.2 cm from inner wall of cell), and at the center of channel of coarse beads (2.5 cm from inner wall of cell). Details of the probes and associated electronics are described in detail in sections A.1 and A.2 in Appendix A.

5.2.4 Procedure

Conductivity probes were placed inside the model beds of glass beads during the displacement washing experiments, described in detail in Chapter 4. MBL-saturated model beds of glass beads were formed in the displacement washing cell following the order of experiments in Table 4.2. The procedure for preparing a MBL-saturated model bed has been described in detail in section 4.2.3 in Chapter 4. Conductivity probes were inserted into the desired positions inside the bed through the side ports of the washing cell, shown in Figure 4.1. The probes were connected to the channels of multichannel conductivity apparatus. The data acquisition software listed in Appendix B was started to ensure that each probe registered the correct conductivity value for the MBL. The bed was conditioned and a displacement washing experiment was initiated following the procedure described in section 4.2.3 in Chapter 4. During a displacement washing experiment, voltages measured by each probe were stored as functions of time.

The effect of the presence of probes inside the bed on displacement performance during a displacement washing experiment was tested by carrying out displacement washing experiments without the probes inside the bed. The presence of probes inside the bed had little effect on washing performance since the displacement washing efficiency of the experiments in the presence and absence of probes was found to vary within ± 3% of each other, as discussed in section 4.3.1 in Chapter 4.

5.3 Results

5.3.1 Treatment of Data

The conductivity values measured by a probe at any time t was computed from the three voltages V_1, V_2, and V_3 recorded by the probe using Equation (A.1), as described in section A.2 in Appendix A. The sampling time for experiments with flow rate 230 mL/min was 0.05 seconds and that for experiments with flow rate 30 mL/min was 0.1 seconds. The time "t" was taken as the average of the three consecutive sampling times against which the three voltages were recorded by the probe. Conductivity results were made dimensionless following the relation

$$\text{Dimensionless conductivity} = \frac{C_{measured} - C_w}{C_0 - C_w} \qquad 5.1$$

where $C_{measured}$, C_0, and C_w were the conductivity measured by a probe at any time t, initial conductivity measured by the probe, and final conductivity measured by the probe after the displacement front passed across it. The breakthrough curve for each probe was produced by plotting the dimensionless conductivity (C) measured by the probe against the eluate ratio (ER). Eluate ratio (ER) was defined as the ratio of volume of wash liquor injected into the cell to the void volume of the bed before the commencement of a displacement washing experiment. Eluate ratio also represented the dimensionless time (t_d) that was the time required by the displacement front to pass across a probe from the onset of the displacement washing experiment. Eluate ratio (ER) or dimensionless time (t_d) was expressed as

$$\text{Eluate Ratio (ER)} = \text{Dimensionless time } (t_d) = \frac{tQ}{\varepsilon AL} \qquad 5.2$$

where t was the real time for measuring conductivity, Q was the volumetric flow rate of wash liquor, A was the area normal to flow, L was the length of bed, and ε was the porosity of the bed. Figure 5.2 shows a set of typical breakthrough curves for the twelve probes during a displacement washing experiment.

In section A.3 in Appendix A, it was established that conductivity of MBL varied linearly with concentration of lignin in MBL solution during dilution of MBL

either with water or polymer solution. As a result, the breakthrough curves for each probe represented the variation of concentration of lignin in MBL solution with eluate ratio during the passage of displacement front across the probe.

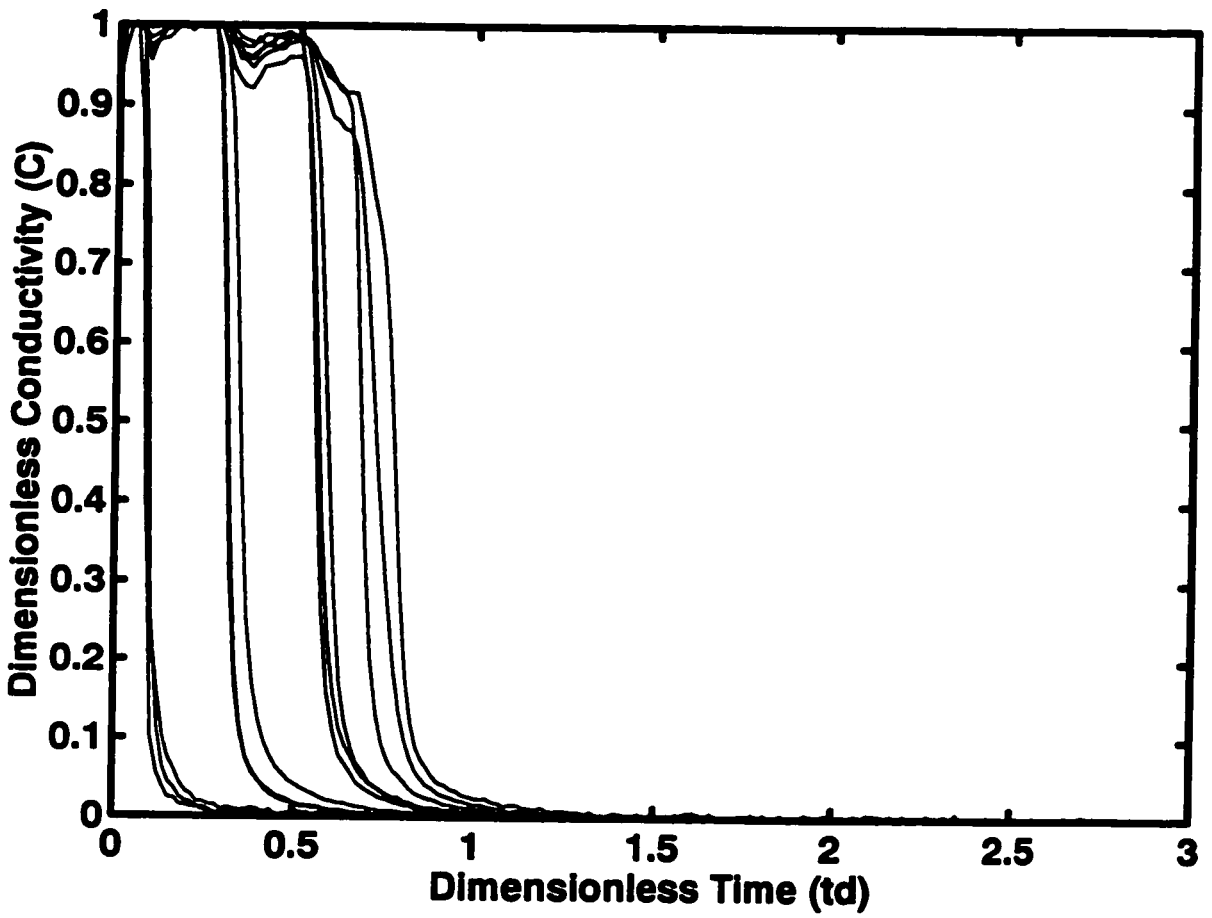

Figure 5.2 Typical breakthrough curves of twelve conductivity probes during a miscible displacement experiment in a homogeneous bed (flow rate, 230 mL/min; concentration of Indulin C, 2.5 g/L).

5.3.2 Analysis of Data

To characterize the performance of displacement washing, the velocities and mixing lengths of fronts were calculated from the breakthrough curves of probes obtained during displacement washing of MBL from a model bed. Mixing parameters D'_L calculated from the data of mixing lengths of fronts were compared to those calculated from a correlation proposed by Harleman et al., (1963).

5.3.2.1 Velocity of Displacement Front during Displacement Washing

The velocities of displacement fronts down the bed during displacement washing were calculated from the probe breakthrough curves. Figure 5.3 illustrates the method of constructing the dimensionless time (t_d) versus dimensionless

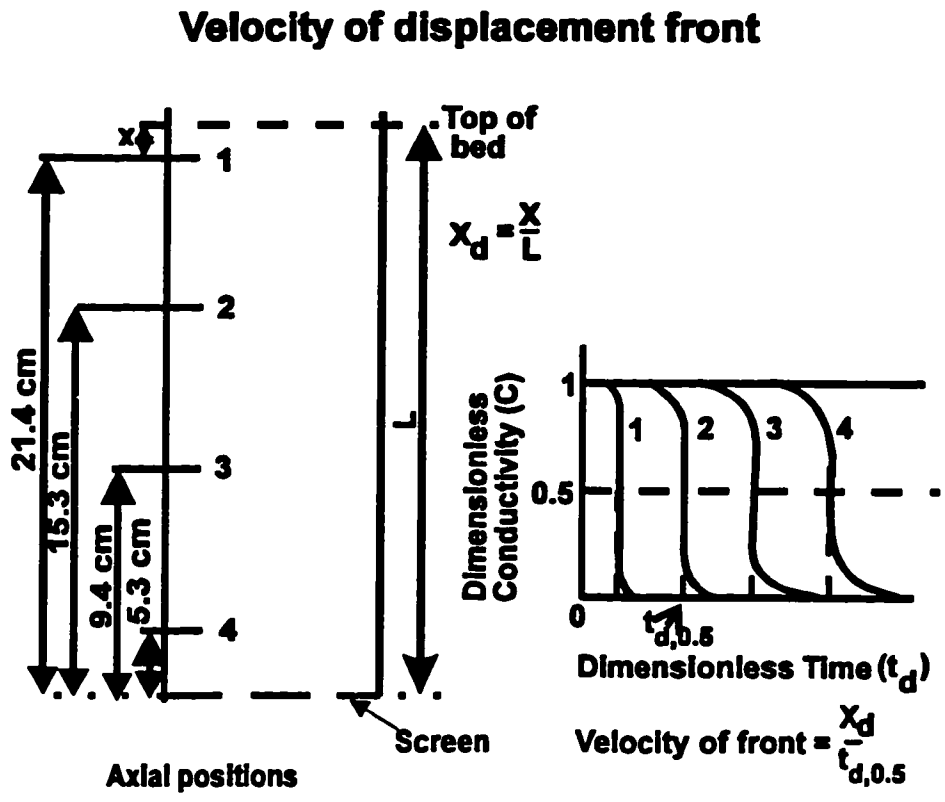

Figure 5.3 Method of construction of plots of dimensionless time versus probe location.

distance (x_d) plots. At a fixed radial position, e.g., at the periphery, the breakthrough curves of four probes at four axial positions were compared. A reference point of 50% change in the dimensionless conductivity (C) was arbitrarily chosen to evaluate the velocity of the displacement front that passed across the probes placed successively along the length of the bed during a displacement experiment. The dimensionless times ($t_{d,50\%}$), called hereafter breakthrough times, required to achieve 50% change in the conductivity (C)

were determined from the breakthrough curves of the probes. The dimensionless distance(x_d) of a probe was calculated according to the relation

$$\text{Dimensionless distance } (x_d) = \frac{X}{L} \qquad 5.3$$

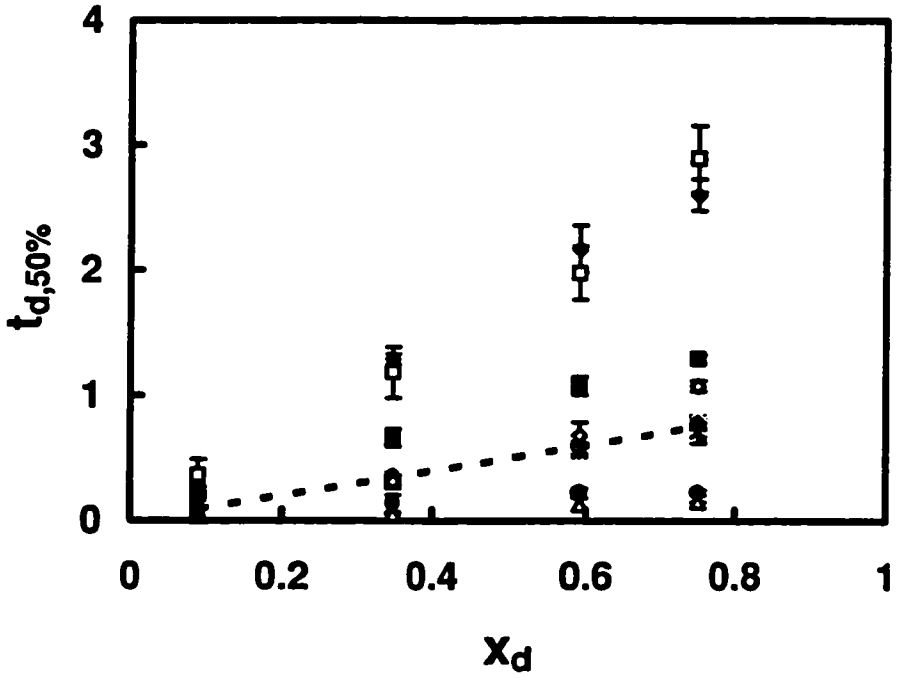

Figure 5.4 Plot of dimensionless time versus dimensionless distance of probes (flow rate 230 mL/min, concentration of Indulin C 25 g/L). Legends for probes in homogeneous bed washed with water, (×) periphery, (*) interface, (-) center; in homogeneous bed washed with polymer, (+) periphery, (o) interface, (–) center; in channel bed washed with water, (□) periphery, (•) interface, (Δ) center; in channel bed washed with polymer, (▪) periphery, (◊) interface, (•) center.(—) line represents average Darcy interstitial velocity. Error bars represent 95% confidence intervals of the mean of three replicated runs.

where X was the axial distance of the probe from the top of the bed and L was the length of the bed.

Figure 5.4 and Figure 5.5 show the dimensionless time ($t_{d,50\%}$) versus dimensionless distance (x_d) plots of probes under various displacement washing conditions.

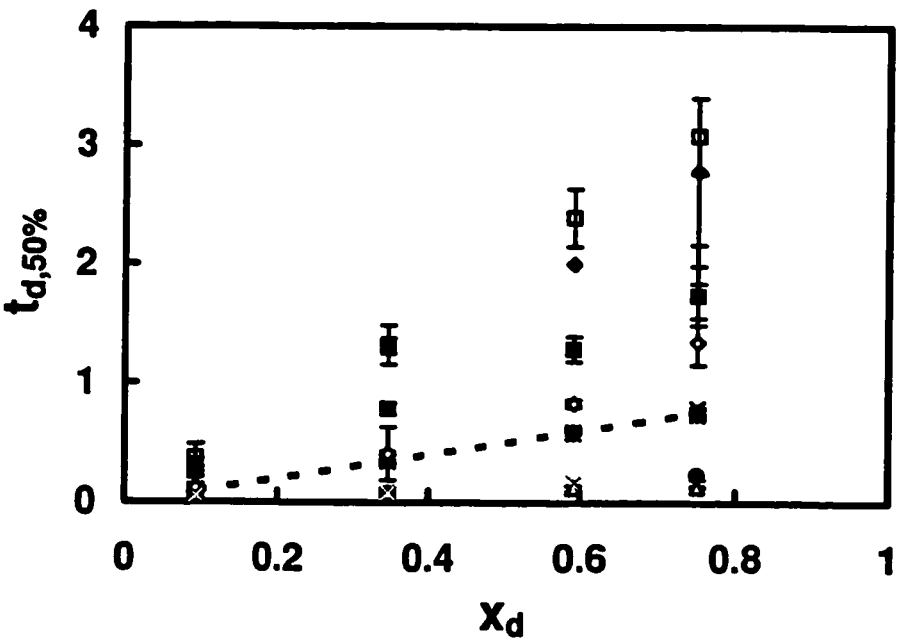

Figure 5.5 Plot of dimensionless time versus dimensionless distance of probes (flow rate 230 mL/min, concentration of Indulin C 2.5 g/L). Legends for probes in homogeneous bed washed with water, (×) periphery, (*) interface, (-) center; in homogeneous bed washed with polymer, (+) periphery, (o) interface, (–) center; in channel bed washed with water, (□) periphery, (♦) interface, (Δ) center; in channel bed washed with polymer, (▪) periphery, (◊) interface, (•) center.(—) line represents average Darcy interstitial velocity. Error bars represent 95% confidence intervals of the mean of three replicated runs.

Figure 5.4 and Figure 5.5 demonstrate that during washing with either water or polymer solution in a homogeneous bed, breakthrough times for all three probes at any axial position were close to the respective breakthrough times for probes if the front had moved with average Darcy interstitial velocity. However, during washing with either water or polymer solution in a channel bed, breakthrough times for the probes at periphery and interface at any axial position were longer than those in a homogeneous bed. Breakthrough times for the probes in the center of a channel bed were shorter than those in homogeneous bed during washing with either water or polymer solution. A comparison of the breakthrough times for probes in a channel bed reveals that at any axial position, the breakthrough times for probes at periphery and interface were less during washing with polymer solution than those during washing with water.

The slope of the straight line passing through the breakthrough times ($t_{d,50\%}$) of probes placed at a fixed radial position represented the reciprocal of normalized interstitial velocity (u_d) of the displacement front that passed across the probes during a displacement experiment.

$$\text{Slope} = \frac{t_{d,50\%}}{x_d} = \frac{1}{\frac{x_d}{t_{d,50\%}}} = \frac{1}{\frac{(X/t_{50\%})}{(Q/A\varepsilon)}} = \frac{1}{\frac{u}{V}} = \frac{1}{u_d} \qquad 5.4$$

where u was the measured interstitial velocity (referenced to the 50% change in the dimensionless conductivity, C) of the front that passed locally across a probe. V was the average interstitial velocity of the front that was computed from Darcy's law of fluid permeation in the bed. For a homogeneous bed, the inverse of the slope must be 1 to agree to Darcy's law of fluid permeation. A slope of greater than 1 indicated slower movement of the front than that expected from Darcy's law of fluid permeation and vice versa. Linear regression was performed through the breakthrough times of probes placed at a radial position in four axial positions inside the bed to compare the velocities of the displacement front inside the bed during different displacement washing conditions.

Tables 5.1 and 5.2 show the slopes, the reciprocal of the slopes, and the correlation coefficients (R^2) of the regressed lines passing through the breakthrough times for probes placed at different radial positions for various displacement washing conditions. Tables 5.1 and 5.2 also demonstrate that the interstitial velocity measured by the probes at any radial position inside a homogeneous bed during washing with either water or the polymer solution was close to the average Darcy interstitial velocity since the slopes of regressed lines were close to 1.

Table 5.1 Slopes, reciprocal of slopes and correlation coefficients (R^2) of regressed lines through breakthrough times for probes during miscible displacements in model beds of glass beads. Flow rate of wash liquor was 230 mL/min and concentration of Indulin C in black liquor was 25 g/L.

	slope	(1 / slope)	R^2
Homogeneous, water			
periphery	1.0247	0.9759	0.9976
interface	0.9417	1.062	0.9989
center	0.8654	1.155	0.9982
Homogeneous , polymer			
periphery	1.0389	0.9626	0.9994
interface	1.0134	0.9868	0.9989
center	0.9943	1.006	0.9979
Channel bed, water			
periphery	3.6286	0.2756	0.9821
interface	3.545	0.2820	0.9894
center	0.2016	4.96	0.9126
Channel bed, polymer			
periphery	1.7815	0.5613	0.9853
interface	1.2729	0.7856	0.934
center	0.338	2.9585	0.7062

Tables 5.1 and 5.2 demonstrate that during the washing of a channel bed with either water or the polymer solution, the slopes of regressed lines near the periphery and the interface were higher than 1, implying less interstitial velocity at the periphery and the interface than those in a homogeneous bed. At the center in a channel bed, the interstitial velocity of front was higher than that in a homogeneous bed since the slope of the regressed line was less than 1. A

comparison of the slopes of the regressed lines during washing of a channel bed with water and the polymer solution reveals that the interstitial velocities of fronts at the periphery and interface were almost two times higher in a channel bed during washing with the polymer solution than those during washing with water. Tables 5.1 and 5.2 also demonstrate that during washing in a channel bed with the polymer solution, the interstitial velocity at the center of the bed was almost

Table 5.2 Slopes, reciprocal of slopes and correlation coefficients (R^2) of regressed lines through breakthrough times for probes during miscible displacements in model beds of glass beads. Flow rate of wash liquor was 230 mL/min and concentration of Indulin C in black liquor was 2.5 g/L.

	slope	(1 / slope)	R^2
Homogeneous, water			
periphery	1.0368	0.9645	0.9968
interface	0.9843	1.0159	0.9992
center	0.9514	1.051	0.998
Homogeneous , polymer			
periphery	1.0111	0.989	0.998
interface	0.9961	1.004	0.9993
center	0.9997	1.0003	0.9996
Channel bed, water			
periphery	4.0488	0.247	0.9979
interface	3.6004	0.2777	0.9891
center	0.2036	4.9116	0.903
Channel bed, polymer			
periphery	2.2602	0.4424	0.9948
interface	1.5867	0.6302	0.9314
center	0.2914	3.4317	0.8775

reduced by half of that obtained when washing with water. The results in Tables 5.1 and 5.2 further reveal that the increase in the interstitial velocity at the periphery and interface in the annulus and the decrease in the interstitial velocity in the center with the use of the polymer solution as a displacing phase instead of water was more pronounced at higher concentration of lignin (25 g/L) in the MBL solution.

5.3.2.2 Mixing Length of Displacement Front

The mixing length of the displacement front that passed across a probe during a displacement washing experiment could be directly related to the quality of displacement washing in a model bed. In absence of any interfacial mixing in an ideal plug flow displacement, the mixing length in the displacement front should be zero (Lake, 1989). More deviation of mixing length in the front from zero indicates larger interfacial mixing of a component, resulting into poorer displacement washing.

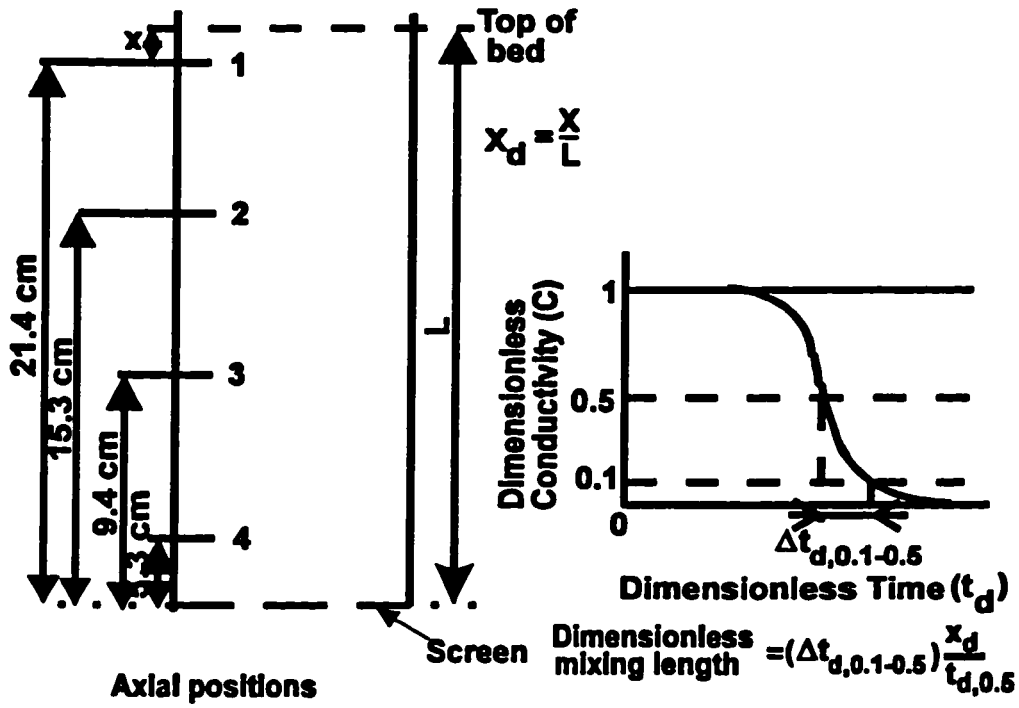

Figure 5.6 Method of calculation of mixing length from breakthrough curves.

Figure 5.6 demonstrates the method of calculation of mixing length in a front from the breakthrough curve of a probe. The difference in the dimensionless time ($\Delta t_{d,10\%-50\%}$) in the breakthrough curve of a probe required to achieve a change in the dimensionless conductivity (C) from 50% to 10% was arbitrarily chosen and the dimensionless mixing length ($\Delta l_{d,mix}$) was defined as

$$\Delta l_{d,mix} = \frac{\Delta l_{50\%-10\%}}{L} = \left(t_{d,10\%} - t_{d,50\%}\right)\left(\frac{x_d}{t_{d,50\%}}\right) \qquad 5.5$$

where $\Delta l_{50\%-10\%}$ was the axial distance between the positions in the front that

Table 5.3 Dimensionless mixing lengths calculated from breakthrough curves of probes. Flow rate = 230 mL/min, Concentration of lignin = 25 g/L. CI represents confidence interval calculated from three replicates.

Radial location	Axial location	Homogeneous bed, water		Homogeneous bed, polymer		Channel bed, water		Channel bed, polymer	
	x_d	$\Delta l_{d,mix}$ Mean	95% CI	$\Delta l_{d,mix}$ Mean	95% CI	$\Delta l_{d,mix}$ Mean	95% CI	$\Delta l_{d,mix}$ Mean	95% CI
Periphery	0.092	0.077	0.01	0.338	0.236	0.043	0.013	0.037	0.02
Periphery	0.346	0.067	0.029	0.077	0.05	0.056	0.008	0.045	0.034
Periphery	0.592	0.086	0.028	0.075	0.006	0.068	0.019	0.083	0.015
Periphery	0.75	0.081	0.045	0.067	0.008	0.0660	0.016	0.085	0.01
Interface	0.092	0.055	0.006	0.097	0.055	0.036	0.013	0.026	0.002
Interface	0.346	0.071	0.006	0.076	0.034	0.043	0.004	0.126	0.038
Interface	0.592	0.088	0.001	0.074	0.004	0.057	0.009	0.152	0.036
Interface	0.75	0.108	0.008	0.061	0.005	0.088	0.017	0.148	0.036
Center	0.092	0.04	0.014	0.13	0.06	0.113	0.039	0.098	0.004
Center	0.346	0.069	0.012	0.06	0.006	0.525	0.066	0.263	0.007
Center	0.592	0.093	0.017	0.067	0.002	0.655	0.035	0.402	0.109
Center	0.75	0.103	0.014	0.067	0.003	0.843	0.026	0.534	0.103

Table 5.4 Dimensionless mixing lengths calculated from breakthrough curves of probes. Flow rate = 230 mL/min, Concentration of lignin = 2.5 g/L. CI represents confidence interval calculated from three replicates.

Radial location	Axial location	Homogeneous bed, water		Homogeneous bed, polymer		Channel bed, water		Channel bed, polymer	
	x_d	$\Delta l_{d,mix}$ Mean	95% CI	$\Delta l_{d,mix}$ Mean	95% CI	$\Delta l_{d,mix}$ Mean	95% CI	$\Delta l_{d,mix}$ Mean	95% CI
Periphery	0.092	0.06	0.006	0.199	0.034	0.035	0.011	0.048	0.028
Periphery	0.346	0.077	0.015	0.078	0.006	0.056	0.008	0.059	0.007
Periphery	0.592	0.076	0.027	0.096	0.016	0.055	0.009	0.066	0.026
Periphery	0.75	0.079	0.016	0.07	0.024	0.058	0.004	0.069	0.014
Interface	0.092	0.036	0.009	0.083	0.031	0.044	0.003	0.034	0.006
Interface	0.346	0.051	0.004	0.066	0.023	0.036	0.008	0.126	0.085
Interface	0.592	0.07	0.013	0.074	0.023	0.067	-	0.143	-
Interface	0.75	0.103	0.016	0.068	0.022	0.084	0.067	0.158	0.02
Center	0.092	0.027	0.008	0.085	0.052	0.103	0.048	0.029	0.009
Center	0.346	0.044	0.006	0.065	0.026	0.307	0.086	0.364	0.042
Center	0.592	0.076	0.026	0.073	0.011	0.543	0.058	0.409	-
Center	0.75	0.082	0.016	0.058	0.021	0.703	0.05	0.424	0.097

represented 50% and 10% change in the conductivity respectively. In Equation (5.5) the average velocity of the front between the interval 50% and 10% change in conductivity was taken to be the mean velocity of the front, which

corresponded to the 50% change in conductivity. The calculation of approximated mixing lengths being based on the mean velocity of 50% concentration level in the front has also been reported by Blackwell, 1962 and Blackwell et al., 1959.

Tables 5.3 and 5.4 show the means and 95% confidence intervals of dimensionless mixing lengths calculated using Equation (5.5) from the

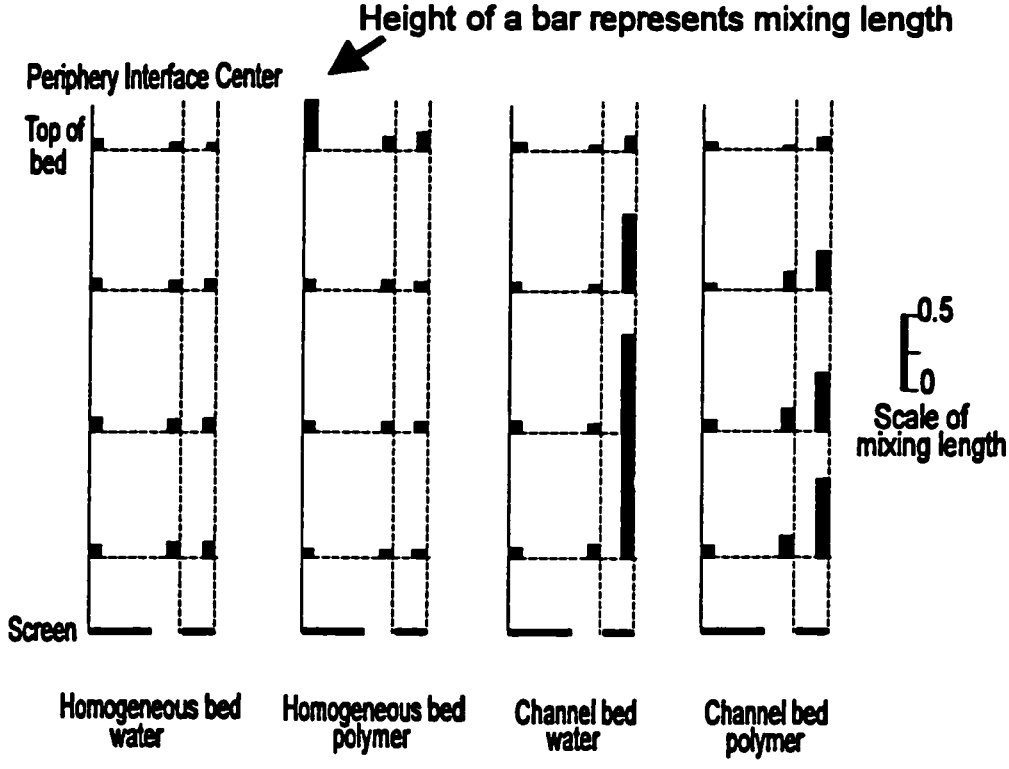

Figure 5.7 Pictorial representation of mixing zones of fronts around probes in a model bed during miscible displacement experiments. Height of bars proportional to the scale given on the picture represent mixing zones of fronts around probes during a displacement experiment. Flow rate of wash liquor was 230 mL/min and concentration of Indulin C in black liquor was 25 g/L.

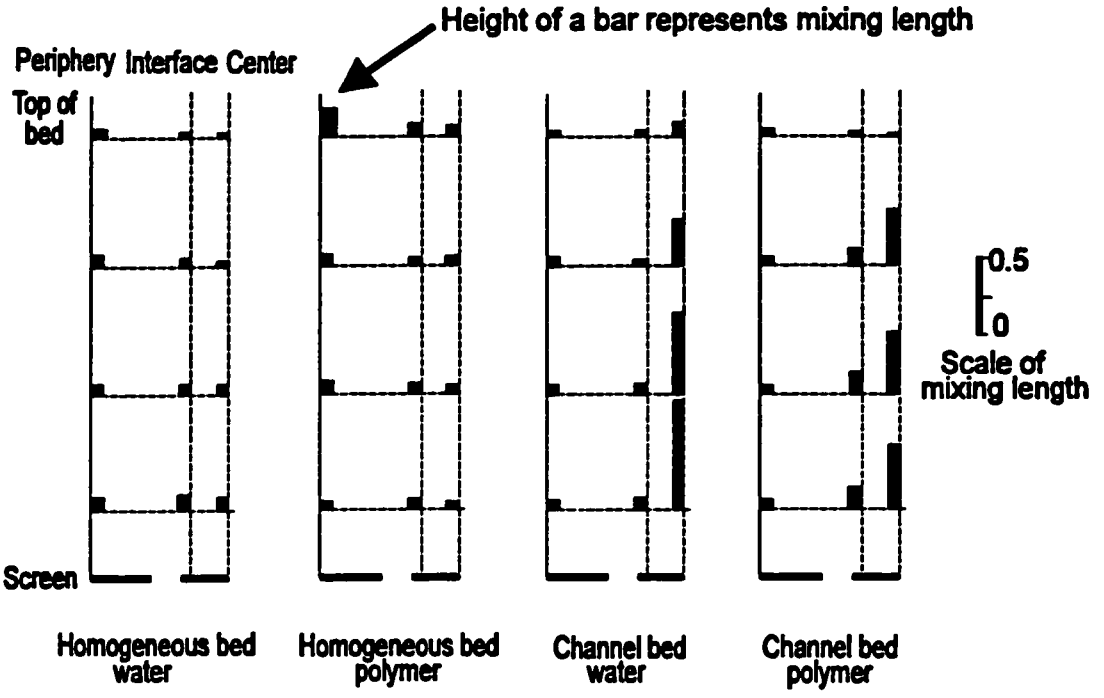

Figure 5.8 Pictorial representation of mixing zones of fronts around probes in a model bed during miscible displacement experiments. Height of bars proportional to the scale given on the picture represent mixing zones of fronts around probes during a displacement experiment. Flow rate of wash liquor was 230 mL/min and concentration of Indulin C in black liquor was 2.5 g/L.

breakthrough curves of probes inserted at various axial and radial locations inside the bed for different displacement washing conditions. Figure 5.7 and Figure 5.8 demonstrate the pictorial representations of the dimensionless mixing lengths of fronts at different axial and radial positions in the model bed under various washing conditions. A comparison of the mixing lengths depicted in

Figures 5.7 and 5.8 indicates that at a given axial position, mixing lengths of fronts at the three radial positions were similar except at the entrance in a homogeneous bed during washing with either water or the polymer solution.

Values of mixing lengths for the comparison of different cases of displacement can be seen in Tables 5.3 and 5.4. Along the length of either a channel bed or a homogeneous bed, mixing lengths of fronts grew. Near the exit in a homogeneous bed, the mixing length at any position was shorter when washing with the polymer than when washing with water. During washing in a channel bed either with water or the polymer solution, mixing lengths of fronts in the center were notably higher than those at any position in a homogeneous bed and at the interface and periphery of the channel beds. Figures 5.7 and 5.8 also demonstrate that in a channel bed, mixing lengths of fronts in the center were lowered when the polymer was used as the displacing phase instead of water. Also, in a channel bed that was washed with the polymer solution, mixing lengths of fronts at the interface were higher than those at the interface and periphery during washing with water and at the periphery during washing with polymer solution. The mixing lengths of fronts at the periphery at any axial position in the channel bed were more or less equal to each other during washing with water and the polymer solution.

5.3.2.4 Calculation of Mixing Parameter (D'_L)

Values of the mixing parameter D'_L were computed from the data of mixing lengths and were compared to those calculated from the correlation of Harleman et al. (1963).

Harleman et al. (1963) proposed a correlation that predicts the longitudinal dispersion coefficient (D_L) in uniform porous media consisting either of spheres or sand grains. For uniform spheres, the correlation proposed by them was

$$\left(\frac{D_L}{\nu}\right) = 0.66\left(\frac{|u|d_{50}}{\nu}\right)^{1.2} \qquad 5.6$$

where $|u|$ was the absolute value of average Darcy interstitial velocity in cm/s, ν was the kinematic viscosity in cm^2/s, and d_{50} was the 50% particle size in cm from a standard gravimetric sieve analysis. Equation (5.6) can be rearranged as

$$D'_L = \left(\frac{D_L}{|u|^{1.2}}\right) = 0.66\left(\frac{d_{50}^{1.2}}{\nu^{0.2}}\right) \qquad 5.7$$

Kinematic viscosity, ν in Equation (5.7) was calculated as the ratio of averages of viscosities to densities of displacing and resident phases reported in Chapter 3. The parameter D'_L in Equation (5.7) is called the mixing parameter. Several researchers (Sherman, 1964; Aris et al., 1957; Klinkenberg et al.,1956) have

predicted that the mixing parameter D'_L should be constant for a given bed. Sherman (1964) reported that the mixing parameter D'_L is a measure of fluid particle dispersion and is dependent on pore size distributions in beds of packed solids. In the presence of a distribution of pore sizes, larger variation in velocity in the pores will result in a higher D'_L (Sherman, 1964).

For one-dimensional flow in a homogeneous and isotropic porous medium and with the step input of an ideal tracer at the entrance of a semi-infinite column as a sharp interface, in the absence of any adsorption the longitudinal dispersion coefficient (D_L) can be expressed from the analytical solution of exit concentration of tracer as

$$D_L = 0.5\sigma^2 Lu \qquad 5.8$$

where σ^2 is the spread of the breakthrough curve at the bed exit (Bear, 1972). The spread σ^2 in Equation (5.8) is dimensionless since dimensionless concentration is plotted against dimensionless time in the breakthrough curve, shown in Figure 5.3. Since model channel beds were not homogeneous, model beds were treated as black boxes to calculate D_L using Equation (5.8) from the data of mixing lengths of fronts measured by the probes. In Equation (5.8), L and u were replaced by the axial distance X of a probe from the top of the bed and the interstitial velocity corresponding to the 50% position in the breakthrough

curve of a probe respectively. The spread between 50% and 10% positions in the breakthrough curve of a probe was expressed from normal distribution as

$$\sigma^2 = \left(\frac{t_{d,10\%} - t_{d,50\%}}{1.28 \times t_{d,50\%}} \right)^2 \qquad 5.9$$

The values of longitudinal dispersion coefficients (D_L) calculated using Equation (5.8) reflect the effects of variation in the interstitial velocity, particle size and shape, and the distribution of particle sizes at different positions inside the model bed on the longitudinal dispersion coefficients. Longitudinal dispersion coefficient (D_L) calculated in Equation (5.8) was corrected for the different interstitial velocities of fronts around the probes in the model channel bed, resulting in the mixing parameter D'_L represented as

$$D'_L = \frac{D_L}{\left(\frac{x_d}{t_{d,50\%}} \right)^{1.2}} \qquad 5.10$$

Figures 5.9 through 5.16 show the plots of mixing parameter D'_L calculated by using Equations (5.8) through (5.10) against dimensionless axial positions of the probes (x_d) for different cases of displacement washing experiments. Figures 5.9 through 5.16 show that the mixing parameters calculated from data of mixing lengths were consistently higher than those calculated from the correlation of Harleman et al. (1963). The probable reason

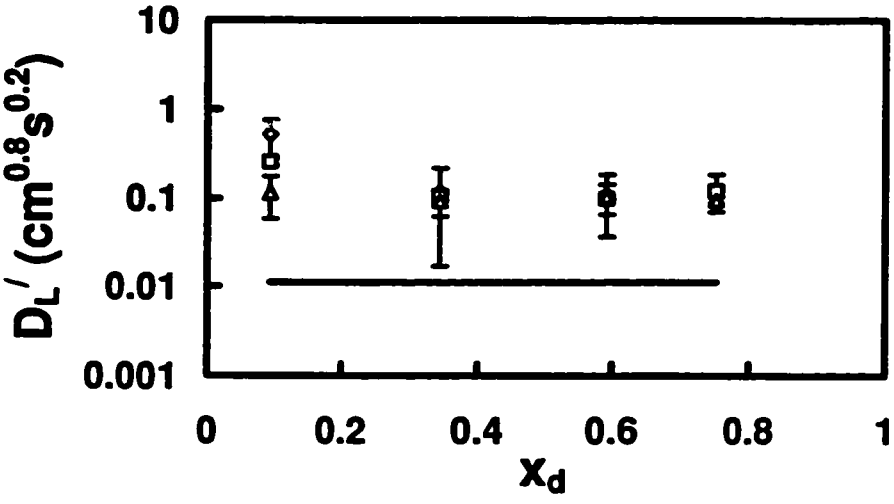

Figure 5.9 Plot of mixing parameter D_L' against axial positions of probes (x_d) in a homogeneous bed washed with water. Legends for probes: (◊) periphery, (□) interface, (Δ) center, and (—) correlation. Error bars represent 95% confidence intervals based on three replicate runs. Flow rate 230 mL/min and concentration of Indulin C 25 g/L.

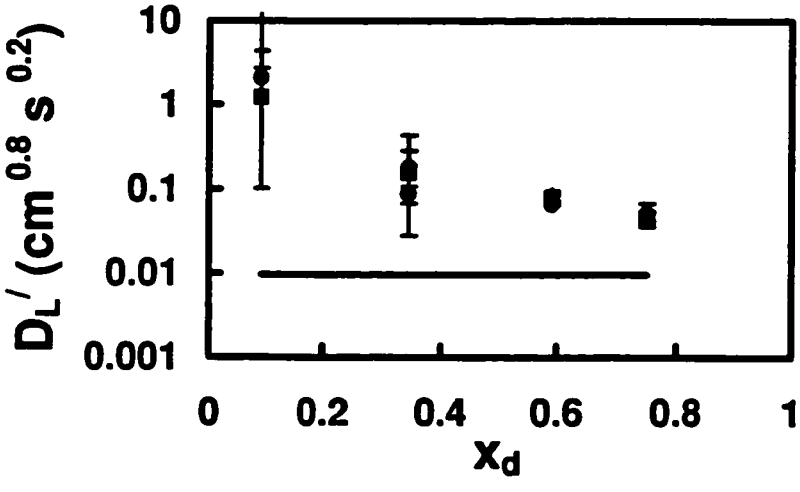

Figure 5.10 Plot of mixing parameter D_L' against axial positions of probes (x_d) in a homogeneous bed washed with polymer. Legends for probes: (♦) periphery, (▪) interface, (●) center, and (—) correlation. Error bars represent 95% confidence intervals based on three replicate runs. Flow rate 230 mL/min, concentration of Indulin C 25 g/L.

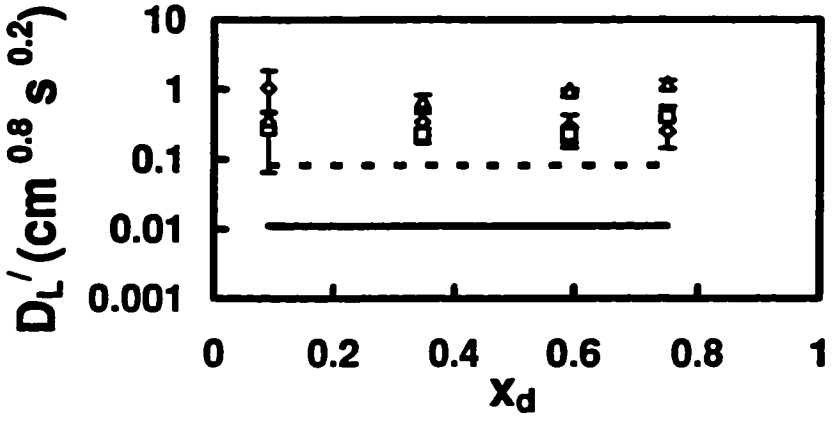

Figure 5.11 Plot of mixing parameter D_L' against axial positions of probes (x_d) in a channel bed washed with water. Legends for probes: (◊) periphery, (□) interface, (Δ) center, and (—, ---) correlation. Error bars represent 95% confidence intervals based on three replicate runs. Flow rate 230 mL/min and concentration of Indulin C 25 g/L.

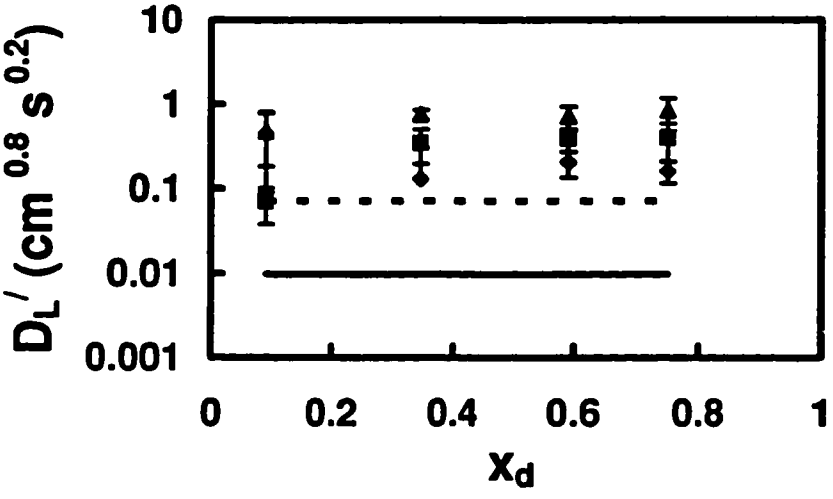

Figure 5.12 Plot of mixing parameter D_L' against axial positions of probes (x_d) in a channel bed washed with polymer. Legends for probes: (•) periphery, (▪) interface, (•) center, and (—, ---) correlation. Error bars represent 95% confidence intervals based on three replicate runs. Flow rate 230 mL/min, concentration of Indulin C 25 g/L.

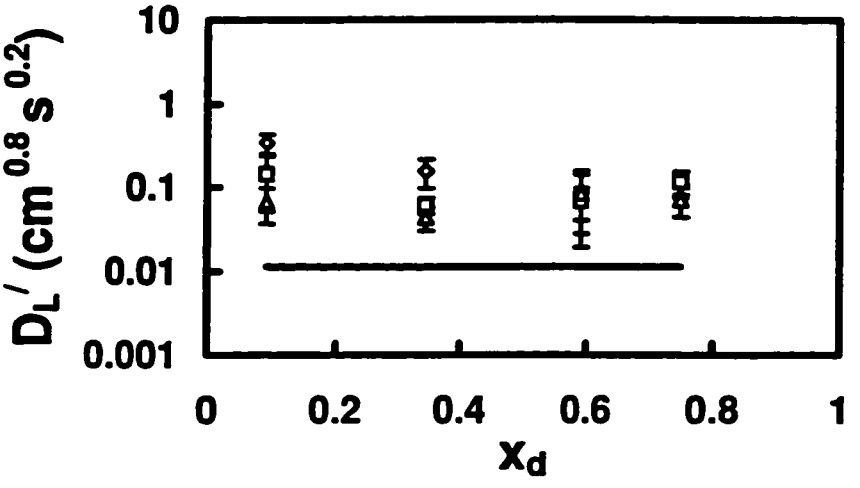

Figure 5.13 Plot of mixing parameter D_L' against axial positions of probes (x_d) in a homogeneous bed washed with water. Legends for probes: (◊) periphery, (□) interface, (Δ) center, and (—) correlation. Error bars represent 95% confidence intervals based on three replicate runs. Flow rate 230 mL/min and concentration of Indulin C 2.5 g/L.

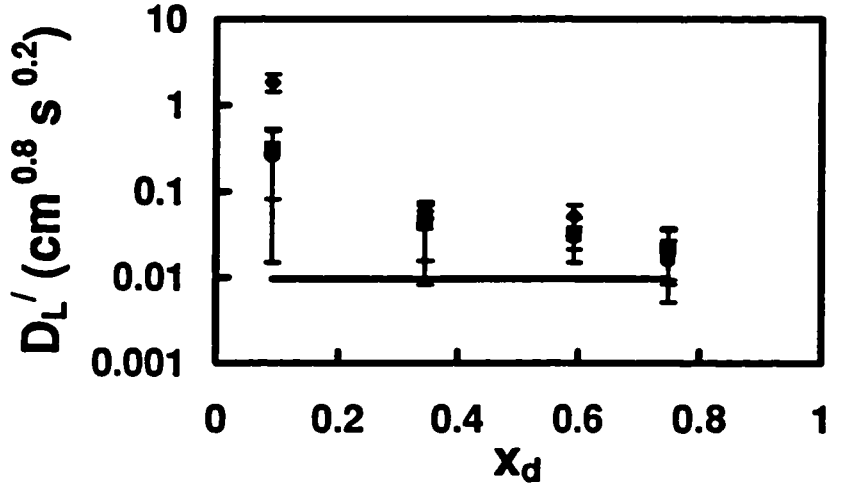

Figure 5.14 Plot of mixing parameter D_L' against axial positions of probes (x_d) in a homogeneous bed washed with polymer. Legends for probes: (♦) periphery, (▪) interface, (•) center, and (—) correlation. Error bars represent 95% confidence intervals based on three replicate runs. Flow rate 230 mL/min, concentration of Indulin C 2.5 g/L.

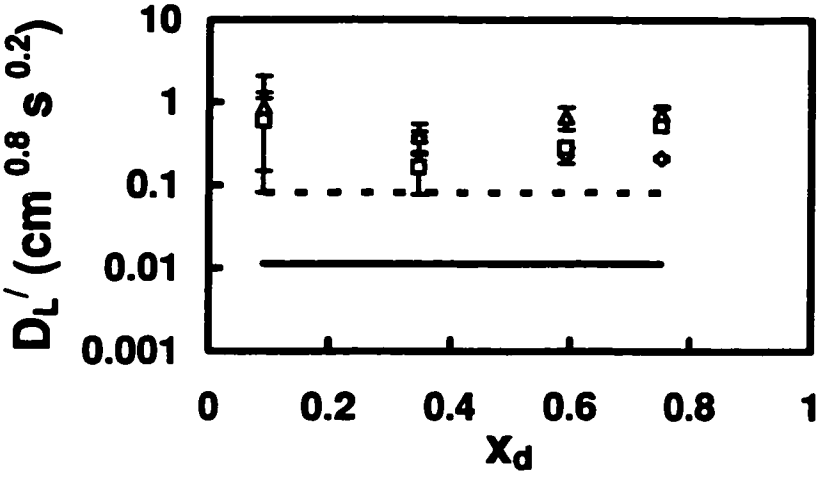

Figure 5.15 Plot of mixing parameter D_L' against axial positions of probes (x_d) in a channel bed washed with water. Legends for probes: (◊) periphery, (□) interface, (Δ) center, and (—, ---) correlation. Error bars represent 95% confidence intervals based on three replicate runs. Flow rate 230 mL/min and concentration of Indulin C 2.5 g/L.

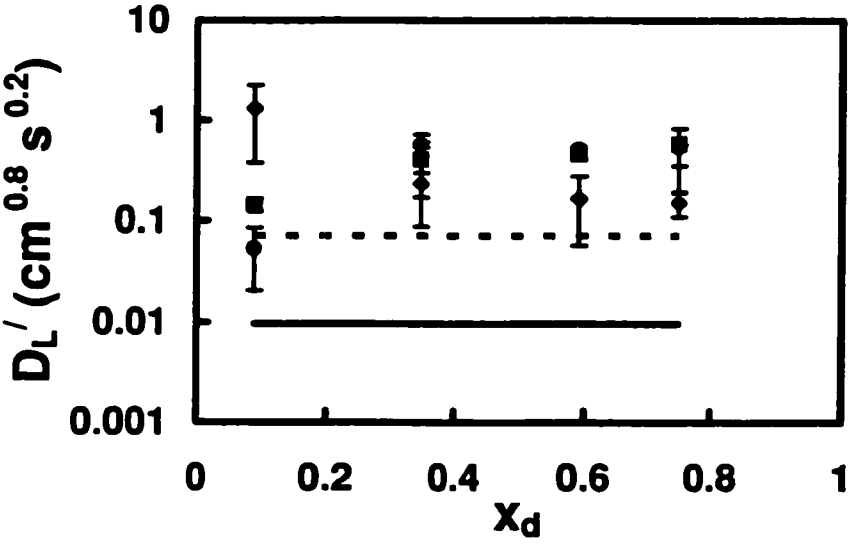

Figure 5.16 Plot of mixing parameter D_L' against axial positions of probes (x_d) in a channel bed washed with polymer. Legends for probes: (♦) periphery, (▪) interface, (●) center, and (—, ---) correlation. Error bars represent 95% confidence intervals based on three replicate runs. Flow rate 230 mL/min, concentration of Indulin C 2.5 g/L.

for the higher values of D'_L computed from the data of mixing lengths than those computed from the correlation of Harleman et al. (1963) was a distribution of particle sizes reported in Chapter 3. Han et al. (1985), Niemann (1969), Eidsath et al. (1983), and Carbonell (1979) observed strong dependence of longitudinal dispersion coefficients, and thus the mixing parameters, on the spread of size distribution of particles. Raimondi et al. (1959) have also reported that due to the presence of a wide size distribution of pores in sandstone, the mixing parameter for it was 200 times higher than that in packing of uniform size granular particles having the same permeability of sandstone. Han et al. (1985) argued that an increased distribution of particle sizes resulted into increased distribution of pore sizes leading to large scale nonuniformity in flow field in the bed and thus larger values of D'_L.

Figures 5.9, 5.10, 5.13, and 5.14 demonstrate that D'_L reached a steady state near the exit of a homogeneous bed that was washed with water, whereas a steady decrease in D'_L was observed along the length of a homogeneous bed that was washed with the polymer solution. Figures 5.11, 5.12, 5.15, and 5.16 demonstrate that D'_L for fronts at the interface were higher than those at the periphery near the exit of a channel bed that was washed with either water or the polymer solution.

The large scatter in mixing lengths reported in Tables 5.3 and 5.4 and in D'_L in Figures 5.9 through 5.16 at the entrance of either a homogeneous bed or a channel bed during displacement with either water or the polymer solution was probably due to the poor injection condition of either water or polymer solution at the entrance of the bed. Poor injection condition of the displacing phase resulted in the lack of a sharp interface between the displacing phase and the MBL solution at the entrance of the bed. Maldistribution of the displacing phase and any presence of dead volume at the inlet of the bed might have caused poor injection of the displacing phase at the inlet of bed. However, results in Tables 5.3 and 5.4 and Figures 5.9 through 5.16 show that along the length of the beds, the scatter in mixing lengths and D'_L decreased.

At any position in the model beds, the errors in breakthrough times ($t_{d,50\%}$) in Figures 5.4 and 5.5, in mixing lengths in Tables 5.3 and 5.4, and in D'_L in Figures 5.9 through 5.16 were probably due to the difference in the microscopic heterogeneities in permeability along the cross section of the beds. This was a result of the variation in the packing in the replicated experiments, nonidentical injection of the displacing phase in the replicated experiments due to the poor injection at the entrance of the beds, and irreproducible packing at any position due to the nonuniform shape and presence of a size distribution in the particles inside the bed. In addition, nonideality of MBL as a tracer due to the difference in its viscosity (1.17 mPa.s for 25 g/L and 1.05 mPa.s for 2.5 g/L) to

that of the displacing phase (1 mPa.s for water and 3.2 mPa.s for polymer) might be another contributing factor to the error.

The weak growth of mixing lengths along the length of either a homogeneous bed or a channel bed was due to the attainment of a steady dispersion along the length of the beds as discussed by Han et al. (1985).

5.4 Discussion

5.4.1 Displacement Washing Experiments in Homogeneous Beds

In the absence of channeling at the center of a homogeneous bed during washing with either water or the polymer solution, the displacement front moved uniformly across any cross section of the bed with an average interstitial Darcy velocity. As a result, at any axial position (x_d) inside the homogeneous bed during washing with either water or the polymer solution, velocities of the front at the three radial positions were close to the average Darcy interstitial velocity as demonstrated in Figures 5.4 and 5.5 and Tables 5.1 and 5.2. On the other hand, it was also confirmed that probes were capable of monitoring the movement of the displacement front in model beds during the displacement washing experiments. Since the displacement front moved uniformly across the cross

section of a homogeneous bed with average Darcy interstitial velocity, mixing lengths of fronts depicted in Figure 5.7 and 5.8 were close to each other at the three radial positions in a given axial position in a homogeneous bed that was either washed with water or the polymer solution.

A surprising result was the steady decreasing trend of D'_L along the length of a homogeneous bed during washing with the polymer solution shown in Figure 5.10 and Figure 5.14. This effect was probably due to the retardation of interfacial mixing of the MBL and lignin by the presence of a soluble viscous layer of lignin/polyDADMAC complex at the interface between the MBL and the polymer solution.

5.4.2 Displacement Washing Experiments in Channel Beds

Due to the presence of channeling of the displacing phase through the central more permeable zone of a channel bed, the velocity of the front was higher at the center and lower in the periphery and interface of a channel bed than the average Darcy interstitial velocity in a homogeneous bed shown in Figures 5.4 and 5.5. When a channel bed was washed with the polymer solution, selective retention of the precipitates only in the center channel reduced the permeability of the center channel and hence lowered the channeling in a channel bed, as discussed in detail in Chapter 3 and Chapter 4. Due to the

reduction in channeling in a channel bed during washing with the polymer solution, the velocity of the front in the periphery and interface almost doubled and that at the center decreased approximately by half of that during washing with water shown in Figures 5.4 and 5.5 and Tables 5.1 and 5.2.

At the high concentration of lignin (25 g/L) in the MBL solution, the increase in the velocity at the periphery and interface and the decrease in the velocity in the center in a channel bed during washing with the polymer solution was more pronounced than that at the low concentration of lignin (2.5 g/L) demonstrated in Tables 5.1 and 5.2 and Figures 5.4 and 5.5. The probable reason for this was the formation of a maximum amount of precipitate in the center channel at the high concentration of lignin due to the attainment of an optimum ratio of concentration of lignin (25 g/L) to concentration of polymer (29.4 g/L), as reported by Lappan et al. 1996.

The mixing lengths reported in Figures 5.7 and 5.8 reflect the effects of different interstitial velocities of the front at three radial positions in a given axial location in a channel bed, particle size and distribution, and the physical properties of the displacing and resident phases. Higher mixing lengths in the channel than those at the periphery and interface during washing with either water or the polymer solution was due to higher particle diameter (638 μm) and higher interstitial velocity of the front in the channel than those in the annulus in the channel bed as reported in Figures 5.4 and 5.5. However, when the polymer

solution was used as the displacing phase instead of water, mixing length in the channel was reduced due to the reduction in velocity in the channel and modification of the channel by the retention of the precipitate. Mixing lengths at the periphery in a channel bed during washing with either water or the polymer solution and those in the homogeneous beds were similar. Tables 5.3 and 5.4 show that the front velocity at the periphery and interface in a channel bed during washing with water was almost half of that obtained when washing with the polymer solution and was almost one-fifth of that in a homogeneous bed. If the same level of velocity is considered, mixing lengths at the periphery and interface for washing with the polymer can be expected to be lower than those for washing with water and higher than that obtained in a homogeneous bed for washing with either water or the polymer solution. The implication of the mixing lengths towards changing of the properties of channel bed during displacement washing experiments was examined through the analysis of mixing parameters D'_L in the following section.

In Figures 5.11, 5.12, 5.15, and 5.16, higher values of D'_L at the interface than those at the periphery of a channel bed were probably due to a broader distribution of sizes of pores at interface than in the annulus. Broader distribution of the pore sizes at the interface was probably due to the mixing and rearrangement of two kinds of beads at the interface during the displacement experiment reported in detail in Chapter 3. At the center in a channel bed, values

of D'_L were larger than those at the periphery and interface since the particle diameter of coarse beads in the channel was around five times higher than that of fine beads in the annulus. In Figures 5.9 through 5.16, values of mixing parameters at the interface and periphery in a channel bed were higher than those in a homogeneous bed. This was probably the result of more compact packing and thus relatively less spread in the distribution of pore sizes in a homogeneous bed than that in a channel bed obtained during the conditioning of the beds described in detail in Chapter 3. During the conditioning of beds before a displacement experiment was started, channeling of liquid through the more permeable channel in a channel bed probably left the annulus of the channel bed more loosely packed than in a homogeneous bed.

5.5 Conclusions

(a) For the first time, direct observation with conductivity probes inside model channel beds confirmed that during washing with the polymer solution instead of water, precipitates formed in the channel lowered the flow rate in the channel, increased the flow rate in the annulus, and lowered the mixing lengths in both the center channel and the annulus in the channel bed.

(b) Mixing lengths in the homogeneous beds were slightly lower during washing with the polymer solution than those during washing with water. A probable reason for this was the retardation of interfacial mixing of the MBL and the polymer by the presence of a viscous, soluble layer of lignin/polyDADMAC complex at the interface between them.

(c) Data obtained by the probes confirmed no anomalous behavior in either homogeneous or channel beds during washing with water.

List of Variables

A	Cross sectional area of bed, m^2.
C	Conductivity in Equation (5.1), dimensionless.
C_o	Final conductivity in Equation (5.1), $ohm^{-1}\ m^{-1}$.
C_w	Initial conductivity in Equation (5.1), $ohm^{-1}\ m^{-1}$.
$C_{measured}$	Measured conductivity in Equation (5.1), $ohm^{-1}\ m^{-1}$.
d_p	Diameter of particle, m.
d_{50}	Particle diameter in 50% cut in Equation(5.7), m.
D_L	Coefficient of longitudinal dispersion, m^2/s.
D'_L	Mixing parameter defined in Equation (5.10), $m^{0.8}\ s^{0.2}$.
$\Delta l_{50\%-10\%}$	Mixing length in Equation (5.5), m.
$\Delta l_{d,mix}$	Mixing length in Equation (5.5), dimensionless.
L	Length of the bed, m.
Q	Superficial flow rate, m^3/s.
R^2	Correlation coefficient of regression, dimensionless.
t	Time for displacement, s.
t_d	Time defined in Equation (5.2), dimensionless.
$t_{d,50\%}$	Breakthrough time defined in Figure 5.3, dimensionless.
$\Delta t_{d,10\%-50\%}$	Time defined in Figure 5.6 for mixing length, dimensionless

$t_{50\%}$	Breakthrough time in Equation (5.4), s.
u	Interstitial velocity, m/s.
u_d	Interstitial velocity defined in Equation (5.4), dimensionless.
V	Average Darcy interstitial velocity, m/s.
V_1	Voltage across reference conductance in Figure A.3, volt.
V_2	Voltage across load conductance in Figure A.3, volt.
V_3	Voltage across ground in Figure A.3, volt.
X	Axial distance of probe from top of bed, m
x_d	Axial distance of probe from top of bed, dimensionless

Subscripts

c	Coarse beads.
f	Fine beads.

Greek Letters

ε	Porosity of bed, dimensionless.
ν	Kinematic viscosity, m^2/s
σ^2	Spread in Equation (5.8), dimensionless.

Abbreviations

MBL	Model black liquor.
ER	Eluate ratio.

References

Aris, R., and N. R. Amundson, A.I.ChE.J., **3**, 280 (1957).

Bear, J., Dynamics of Fluids in Porous Media, Elsevier, New York (1972).

Blackwell, R. J., "Laboratory Studies of Microscopic Dispersion Phenomena," SPEJ., March ,1 (1962).

Blackwell, R. J., J. R. Rayne, and W. M. Terry, Trans AIME, **216**, 1 (1959).

Carbonell, R. G., "Effect of Pore Size Distribution and Flow Segregation on Dispersion in Porous Media," Chem. Eng. Sci., **34**, 1031 (1979).

Crotogino, R. H., N. A. Poirier, and D. T. Trinh, "The Principles of Pulp Washing," Tappi, **70**, 95 (1987).

De, D., "Reactive polymer enhanced miscible displacement in porous media," Ph. D. thesis, Chapter 4, Chem. Eng. Dept., McMaster University, Hamilton, Canada (1996).

Eidsath, A., et al., "Dispersion in Pulsed Systems. Part III: Comparison Between Theory and Experiments in Packed Beds," Chem. Eng. Sci., **38**, 1803 (1983)

Han, N. W., J. Bhakta, and R. G. Carbonell, "Longitudinal and Lateral Dispersion in Packed Beds: Effect of column length and particle size distribution," AIChE Journal, **31(2)**, 277 (1985).

Harleman D. R. F., P. F. Mehlhorn, and R. R. Rumer, "Dispersion-Permeability Correlation in Porous Media," Proc. ASCE J. Hydr. Div., **67**, 67 (1963).

Klinkenberg, A. and F. Sjenitzer, Chem. Eng. Sci., **5**, 258 (1956).

Lake, L.W., Enhanced Oil Recovery, Prentice Hall, New Jersey (1989).

Lappan, R., A. H. Hrymak, and R. H. Pelton, unpublished work, McMaster University, Hamilton, Canada (1996).

Lee, P. F., "Channeling and Displacement Washing of Wood Pulp Fiber Pads," Tappi, **67(11)**, 100 (1984).

Li, P., and R. H. Pelton, "Wood Pulp Washing: 2. Displacement Washing of Aqueous Lignin from Model Beds with Cationic Polymer Solutions," Colloids and Surfaces, **64**, 223 (1992).

Niemann, E. H., "Dispersion during Flow in Non-uniform Heterogeneous Porous Media," MS Thesis, Chem. Eng. Dept., Purdue University, Lafayette, IN, USA (1969).

Raimondi, P., G. H. F. Gardner, and C. B. Petrick, Paper presented at Fifty-second Annual meeting of the A.I.ChE. (Dec. 6-9, 1959).

Sherman, R. W., "The Movement of a Soluble Material during the Washing of a Bed of Packed Solids," A.I.ChE.J., **10(6)**, 855 (1964).

Tang, R. W., Behrens, R. A., and Emanuel, A. S.,"Reservoir Studies using Geostatistics to Forecast Performance," SPE 18432, SPE symposium on Reservoir Simulation, Houston, 321(1989).

Chapter 6

A Mechanistic Model for Reactive Polymer Enhanced Miscible Displacement of Model Black Liquor in Model Beds of Glass Beads

Abstract

A mechanistic communicating channel bed model was developed to describe the miscible displacement of a model black liquor (MBL) with either water or a polymer solution from a model channel bed that consists of a 1.7 cm diameter central channel of coarse beads (638 μm) surrounded by an annulus of fine beads (121 μm) contained in a 5.2 cm diameter cylindrical column. The communicating channel bed model accounted for the communication between the channel and annulus in the model channel bed using a technique called network of zones originally proposed by Van de Vusse (1962). Two adjustable parameters were needed in the communicating channel bed model to describe the miscible displacement of the MBL in the channel bed with water. However, the model needed three adjustable parameters to describe the reduction of channeling and the enhancement of miscible displacement of the MBL in the channel bed when the polymer solution was used as the displacing phase

instead of water. The communicating channel bed model successfully predicted the breakthrough curve and profiles of interstitial velocities in the annulus and in the channel during displacement of the MBL with either water or the polymer solution in the channel bed. Though the model predicted pressure drop profiles during displacement of the MBL with water, pressure drop predicted by the model was higher than that obtained experimentally during displacement of the MBL with the polymer solution. The mismatch between the predicted and experimental pressure drops during displacement of the MBL with the polymer was explained in terms of the limitations of the model. When the polymer solution was used as the displacing phase instead of water in the channel bed, the communicating channel bed model predicted the enhancement of displacement of MBL in terms of the plugging of pore throats with precipitate formed from the reaction of lignin and the polymer and the reduction in the permeability of the center channel resulting in the suppression of channeling in the channel bed. The communicating channel bed model also predicted approximately double the interstitial velocity of the front in the annulus during displacement of the MBL with the polymer solution in the model channel bed than that when water was used as the displacing phase.

In the absence of communication between the channel and annulus, the non-communicating channel bed model predicted the breakthrough curve, pressure drop profile, and profile of interstitial velocity inside the homogeneous

beds of fine beads during the displacement of the MBL with either water or the polymer solution. However, the non-communicating channel bed model was unable to predict the breakthrough curve during the displacement of the MBL with water in the channel bed and the deviation was attributed to the presence of communication between the channel and the annulus that was reported as cross flow in Chapter 3.

6.1 Introduction

The process of displacement of a fluid from a porous medium by another fluid that is miscible with the first fluid is called miscible displacement. Miscible displacement in porous media plays a pre-eminent role in many branches of engineering such as recovery of oil in petroleum engineering, contamination of ground water by seepage of salt water or waste products disposed underground, recovery of spent liquors in brownstock washing stage in a Kraft pulping process, and so on.

Performance of miscible displacement in a heterogeneous porous bed that consists of higher permeable channels surrounded by lower permeable regions in the bed is severely limited by channeling (Lake, 1989). Channeling refers to bypassing of resident fluid by displacing fluid that preferentially passes through the channels in a heterogeneous porous medium (Lake, 1989; Tang et

al., 1989; Blackwell et al., 1959, Crotogino et al., 1987, Lee, 1984). In tertiary oil recovery, profile modification techniques have been developed to suppress channeling of the displacing fluid by reduction of its mobility in channels during miscible displacement in heterogeneous porous media. Profile modification can be achieved by polymer floods, gel placement in channel, flow of emulsion, and placement of foamed gels in the heterogeneous porous medium (Miller et al., 1995; McCool et al., 1991; Hofman et al., 1991; Lake, 1989).

Li and Pelton (1992) have exploited the formation of a macroscopic precipitate from the reaction between an anionic polymer in the resident phase and a cationic polymer in the displacing phase to suppress channeling in a heterogeneous porous bed. They carried out displacement experiments in a model channel bed that consisted of a central, more permeable channel surrounded by a less permeable annulus. They saturated the model bed with a model black liquor solution (MBL) containing anionic lignin and reported that miscible displacement of the MBL in the model channel bed was improved by using an aqueous solution of a cationic polymer, polyDADMAC, as a displacing phase instead of water. The reason for the improvement in performance of miscible displacement was speculated by them to be selective plugging of channels by precipitates formed by the reaction of anionic and cationic polymers. Pelton and Grosse (1994) have provided direct experimental evidence of selective plugging of a channel by precipitates during displacement of the

MBL by an aqueous solution of a cationic polymer in a model channel bed similar to that which was used by Li and Pelton (1992). Pelton and Grosse (1994) hypothesized that selective formation of precipitate in the channel was due to the mixing of the cationic polymer in the channel with lignin that was driven from annulus to channel by a transverse pressure gradient developed due to difference in the velocity of the fluid in the channel and in the annulus in the model channel bed.

De and Pelton (Chapter 3) have carried out flow visualization experiments to confirm the hypothesis of Pelton and Grosse (1994). They concluded that selective formation of the precipitate in the channel was due to higher dispersion and hence better interfacial mixing of the two polymers at the interface between the two phases in the channel than that in the annulus, lateral transfer of lignin from the annulus to the channel caused by sharp gradient in concentration of lignin in the channel and in the annulus after breakthrough in the channel, and cross flow of lignin from the annulus to the channel due to a screen-bead interaction proposed by Lappan et al. (1996). De and Pelton (Chapter 4) also measured the improvement of displacement performance and the reduction of permeability of the channel quantitatively during displacement of the MBL from the model channel bed by an aqueous solution of a cationic polymer as the displacing phase instead of water. However, none of these studies have proposed a mechanistic model to predict the improvement of displacement

performance of an anionic polymer in a heterogeneous porous bed when an aqueous solution of a cationic polymer was used as the displacing phase instead of water.

The overall objective of this chapter is to develop a mechanistic model to predict the improvement in displacement performance of an anionic polymer in a heterogeneous porous bed when an aqueous solution of cationic polymer was used as the displacing phase instead of water. However, the specific objectives are to predict the breakthrough and pressure drop profiles obtained during displacement of the MBL from the model channel beds, described in detail in Chapter 4, using either water or an aqueous solution of a cationic polymer as the displacing phase.

6.2 Mathematical Formulation

The model channel bed consisting of 1.7 cm diameter central channel of 638 μm coarse beads surrounded by an annulus of 121 μm fine beads, described in detail in Chapter 3, is considered to be a combination of two separate homogeneous beds connected in parallel, shown in Figure 6.1. Cross sectional area (A_c) and permeability (k_c) of the column of coarse beads that represents the central channel in the channel bed in Figure 6.1 are equal to the cross sectional area and permeability of the channel in the channel bed

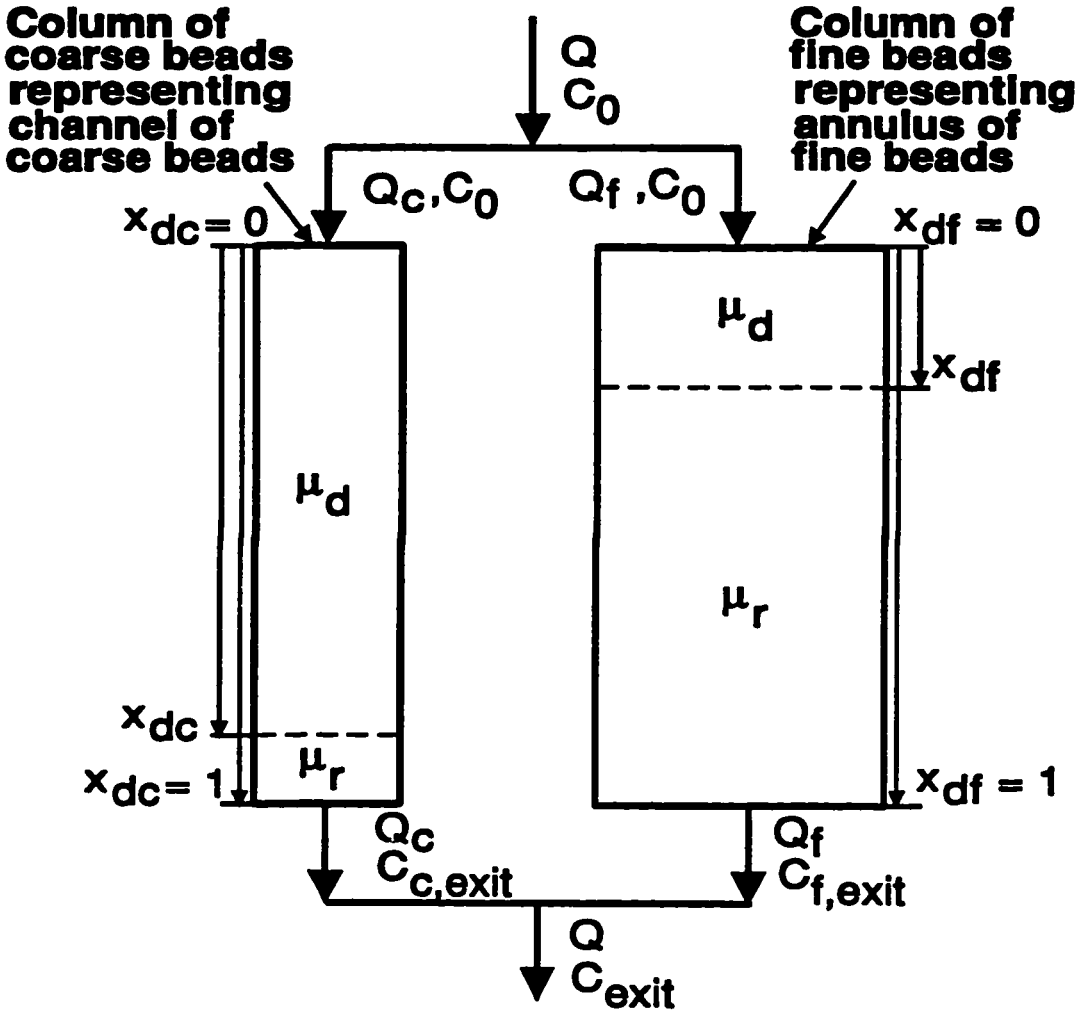

Figure 6.1 Representation of model channel bed as combination of two separate non-communicating homogeneous beds connected in parallel.

respectively. Similarly, the cross sectional area (A_f) and permeability (k_f) of the annulus of fine beads in model channel bed are equal to those of the column of fine beads that represents the annulus of fine beads in model channel bed

respectively. The cross sectional area (A) of the model channel bed is expressed as sum of the area of channel, A_c, and of the annulus, A_f.

$$A = A_c + A_f \qquad 6.1$$

Each of the separate beds in Figure 6.1 is considered to be homogeneous with uniform permeability throughout them. The permeability of the channel was twenty-eight times higher than that of fine annulus (Chapter 3) and the ratio of permeability of the column of coarse beads to that of the column of fine beads, r_k, is expressed as

$$r_k = \frac{k_c}{k_f} \qquad 6.2$$

6.2.1 Two Separate Non-Communicating Parallel Homogeneous Beds

This formulation of the non-communicating channel bed model is adapted from the non-communication displacement model for displacement in a two-layer horizontal reservoir with no vertical communication first proposed by Dykstra and Parsons (1950) and then modified by Lake (1989). The assumptions made in the formulation are, (a) there is no horizontal communication between the two parallel beds, shown in Figure 6.1; (b) both of the beds are saturated with MBL solutions initially; (c) the displacement of the MBL from both beds is plug flow; (d) the displacement front that separates the MBL solution and displacing phase

in each bed during displacement represents 50% change in concentration of a species at the interface of the MBL and either water or the polymer solution; (e) the flow is unidirectional along the length of each bed; (f) the flow is incompressible; and (g) the total volumetric flow rate of displacement phase at the inlet of channel bed remains constant during displacement.

In the rest of this chapter, the columns (see Figure 6.1) are named in relation to the channel bed. That is, the column of coarse beads is called either the channel or the central channel. Similarly, the fine bead column is called the annulus or the annulus of fine beads.

The frontal position, x, in either of the beds in Figure 6.1 at any time t after the start of displacement in the model channel bed is made dimensionless as

$$x_d = \frac{x}{L} \qquad 6.3$$

where L is the length of each bed. At the onset of displacement in the model channel bed, i.e., at time t= 0, frontal positions both in channel, x_{dc} , and that in the annulus of fine beads, x_{df}, are zero. At the end of displacement in the channel and in the annulus in the model channel bed, dimensionless frontal positions in the channel and in the annulus reach unity respectively as shown in Figure 6.1. In the rest of this chapter, subscripts "c" and "f" will refer to the

channel of coarse beads and the annulus of fine beads in Figure 6.1 respectively.

Frontal position, x, in each bed in Figure 6.1 is determined from Darcy's law of fluid permeation in a homogeneous porous bed as

$$\frac{dx}{dt} = v = \frac{k\Delta P}{\varepsilon \mu L} \qquad 6.4$$

where v is the interstitial velocity of fluid, k and ε are the permeability and porosity of the bed, μ is the viscosity of the flowing fluid, and ΔP is the pressure drop across the bed. Since permeability of the channel was twenty-eight times higher (Chapter 3) than that of annulus in a model channel bed, the front in channel is expected to move faster than that in the annulus of fine beads in Figure 6.1.

6.2.1.1 Calculation of Frontal Positions, x_{df} and x_{dc}:

Depending on the position of the front in the channel during displacement in the model channel bed, two cases are considered.

(a) Before Breakthrough in Channel when $x_{dc} < 1$ and $x_{df} < 1$:

Before breakthrough in the channel in the model channel bed, both the displacing and the resident phases are present in both the channel and the

annulus in the channel bed. The dimensionless frontal position in the channel, x_{dc}, and that in the annulus, x_{df}, are determined by modifying Equation (6.4) as

$$L\frac{dx_{dc}}{dt} = v_c = \frac{k_c}{\varepsilon_c\left[x_{dc}\mu_d + (1-x_{dc})\mu_r\right]}\frac{\Delta P_c}{L} \qquad 6.5$$

$$L\frac{dx_{df}}{dt} = v_f = \frac{k_f}{\varepsilon_f\left[x_{df}\mu_d + (1-x_{df})\mu_r\right]}\frac{\Delta P_f}{L} \qquad 6.6$$

where μ_d and μ_r are the viscosities of the displacing phase and the MBL solution respectively. Assuming equal pressure drops across the beds representing channel and annulus of the model channel bed in Figure 6.1, i.e. $\Delta P = \Delta P_c = \Delta P_f$, and dividing Equation (6.5) by Equation (6.6), one gets

$$\frac{dx_{dc}}{dx_{df}} = \frac{\left(\frac{k_c}{\varepsilon_c}\right)\left[x_{df}\mu_d + (1-x_{df})\mu_r\right]}{\left(\frac{k_f}{\varepsilon_f}\right)\left[x_{dc}\mu_d + (1-x_{dc})\mu_r\right]} \qquad 6.7$$

Equation (6.7) is rewritten as

$$\frac{dx_{dc}}{dx_{df}} = r_{cf}\frac{\left[x_{df} + M(1-x_{df})\right]}{\left[x_{dc} + M(1-x_{dc})\right]} \qquad 6.8$$

where

$$r_{cf} = \frac{\left(\frac{k_c}{\varepsilon_c}\right)}{\left(\frac{k_f}{\varepsilon_f}\right)} \qquad 6.9$$

and

$$M = \left(\frac{\mu_r}{\mu_d}\right) \qquad 6.10$$

Equation (6.8) is integrated with the boundary condition that at the onset of displacement in model channel bed, frontal position in both channel and annulus are zero i.e. when $x_{dc} = 0$, $x_{df} = 0$, resulting in

$$\left(\frac{1-M}{2}\right)x_{dc}^2 + Mx_{dc} = r_{cf}\left[\left(\frac{1-M}{2}\right)x_{df}^2 + Mx_{df}\right] \qquad 6.11$$

Equation (6.11) is used to determine the frontal position in one bed when that in the other bed is known before breakthrough in the center channel in the model channel bed.

At breakthrough in the center channel, i.e., at $x_{dc} = 1$, the position of the front in the annulus (x^o_{df}) is found with Equation (6.11) by substituting 1 for x_{dc}:

$$x_{df}\Big|_{x_{dc}=1} = x^o_{df} = \frac{\left[M^2 + \left(\frac{1-M^2}{r_{cf}}\right)\right]^{\frac{1}{2}} - M}{(1-M)} \qquad 6.12$$

(b) After Breakthrough in Channel when $x_{dc} > 1$ and $x_{df} < 1$:

After breakthrough in the center channel in the model channel bed, i.e., when x_{dc} is greater than 1, only the displacing phase is present throughout the channel whereas both the displacing and the resident phases are present in the annulus. Consequently, Equation (6.4) can be modified to determine the frontal positions x_{dc} and x_{df} as

$$L\frac{dx_{dc}}{dt} = v_c = \frac{k_c}{\varepsilon_c \mu_d}\frac{\Delta P_c}{L} \qquad 6.13$$

$$L\frac{dx_{df}}{dt} = v_f = \frac{k_f}{\varepsilon_f\left[x_{df}\mu_d + (1-x_{df})\mu_r\right]}\frac{\Delta P_f}{L} \qquad 6.14$$

Assuming equal pressure drops across the beds in Figure 6.1, i,e., $\Delta P = \Delta P_c = \Delta P_f$, and dividing Equation (6.13) by Equation (6.14) results in

$$\frac{dx_{dc}}{dx_{df}} = r_{cf}\left[x_{df} + M(1-x_{df})\right] \qquad 6.15$$

Equation (6.15) can be integrated with the boundary condition that at breakthrough in center channel, i.e., when $x_{dc} = 1$, position of the front in the annulus is $x_{df} = x^{o}_{df}$, as determined in Equation (6.12). Integration of Equation (6.15) results in

$$x_{dc} = 1 + r_{cf}\left[\left(\frac{1-M}{2}\right)\left\{x_{df}^2 - \left(x_{df}^{o}\right)^2\right\} + M\left(x_{df} - x_{df}^{o}\right)\right] \qquad 6.16$$

Equation (6.16) can be used to calculate the frontal position in one bed when that in the other bed is known after breakthrough in the center channel in the model channel bed.

6.2.1.2 Calculation of Pressure Drops, ΔP_f and ΔP_c:

Before breakthrough both in the channel and in the annulus in the model channel bed, i.e. when both x_{dc} and x_{df} are less than 1, Equations (6.5) and (6.6) can be rearranged to calculate pressure drops across the annulus (ΔP_f) and the channel (ΔP_c) respectively as

$$\Delta P_f = \left(\frac{v_f \varepsilon_f L}{k_f}\right)\left[x_{df}\mu_d + (1-x_{df})\mu_r\right] \qquad \textbf{6. 17}$$

$$\Delta P_c = \left(\frac{v_c \varepsilon_c L}{k_c}\right)\left[x_{dc}\mu_d + (1-x_{dc})\mu_r\right] \qquad \textbf{6. 18}$$

At and after breakthrough in the channel in the model channel bed, pressure drop across the channel is calculated by rearranging Equation (6.13) as

$$\Delta P_c = \left(\frac{v_c \varepsilon_c L \mu_d}{k_c}\right) \qquad \textbf{6. 19}$$

At and after breakthrough in the annulus when x_{df} is greater than or equal to 1 and only the displacing phase flows in the annulus after displacement is completed in the channel bed, pressure drop across the annulus is calculated by modifying Equation (6.17) as

$$\Delta P_f = \left(\frac{v_f \varepsilon_f L \mu_d}{k_f} \right) \qquad \textbf{6. 20}$$

6.2.1.3 Calculation of Superficial Flow Rates, Q_c and Q_f :

Total superficial flow rate (Q) of displacing liquid entering the model channel bed consists of two parts, as shown in Figure 6.1. A part (Q_c) of the total flow rate flows through the center channel and the other part (Q_f) flows through the annulus. The total superficial flow rate (Q) can be expressed as

$$Q = Q_c + Q_f \qquad \textbf{6. 21}$$

Equation (6.5) and (6.6) are rewritten to determine the flow rates Q_c and Q_f respectively as

$$\frac{Q_c}{A_c} = u_c = v_c \varepsilon_c = \frac{k_c}{\left[x_{dc} \mu_d + (1 - x_{dc}) \mu_r \right]} \frac{\Delta P_c}{L} \qquad \textbf{6. 22}$$

$$\frac{Q_f}{A_f} = u_f = v_f \varepsilon_f = \frac{k_f}{\left[x_{df} \mu_d + (1 - x_{df}) \mu_r \right]} \frac{\Delta P_f}{L} \qquad \textbf{6. 23}$$

where u_c and u_f are the superficial velocities of fluid in the channel and in the annulus in the model channel bed respectively. Dividing Equation (6.22) by Equation (6.23), rearranging and using Equations (6.21) and (6.10) results in

$$\frac{Q_c}{Q_c+Q_f}=\frac{Q_c}{Q}=\frac{1}{1+\left[\left(\frac{k_f A_f}{k_c A_c}\right)\left[\frac{M+(1-M)x_{dc}}{M+(1-M)x_{df}}\right]\right]} \qquad \textbf{6. 24}$$

Equation (6.24) can be used to calculate the superficial flow rates in the channel (Q_c) and in the annulus (Q_f) from the total superficial flow rate (Q) during displacement in the channel bed.

6.2.1.4 Calculation of Dimensionless Times, t_d, t_{dc}, and t_{df} :

During displacement in the model channel bed, time t measured since the onset of displacement is made dimensionless as

$$t_d=\frac{tQ}{\varepsilon AL}=\frac{t\left(Q_c+Q_f\right)}{\varepsilon AL}=\frac{\varepsilon_c A_c x_{dc}}{\varepsilon A}+\frac{\varepsilon_f A_f x_{df}}{\varepsilon A} \qquad \textbf{6. 25}$$

where ε is the overall porosity of the model channel bed. Dimensionless time, t_d, represents the ratio of total fluid injected into the model channel bed up to time, t, to the void volume of the model channel bed. The contributions to the overall dimensionless time t_d from the fluids flowing through the channel and the annulus in the channel bed are shown in Equation (6.25). Dimensionless times,

t_{dc} and $t_{df,}$ corresponding to flows in the homogeneous beds of channel of coarse beads and annulus of fine beads in Figure 6.1 are also expressed as

$$t_{dc} = \frac{\varepsilon_c A_c x_{dc}}{\varepsilon_c A_c} = x_{dc} \qquad 6.26$$

$$t_{df} = \frac{\varepsilon_f A_f x_{df}}{\varepsilon_f A_f} = x_{df} \qquad 6.27$$

6.2.1.5 Calculation of Exit Concentrations, $C_{c,exit}$ and $C_{f,exit}$:

The extent of mixing between solvent and solute phases in the miscible displacement of an initially homogeneous solute from a homogeneous porous medium of finite length by the introduction of solvent can be characterized by a convective-diffusion type equation (Brenner, 1962) as

$$\frac{\partial c}{\partial t} + v\frac{\partial c}{\partial x} = D_L \frac{\partial^2 c}{\partial x^2} \qquad 6.28$$

where c = c(x,t) is the concentration of solute and D_L is the longitudinal dispersion coefficient.

Brenner(1962) proposed the boundary and initial conditions required to solve Equation (6.28) as;

(1) at the inlet of bed, i.e. at x = 0, with a step input of the displacing phase, the boundary condition is

$$vc - D_L \frac{\partial c}{\partial x} = vc_f \qquad \text{for all } t > 0 \qquad \textbf{6. 29}$$

where c_f is the concentration of solute in the incoming displacing fluid. c_f is assumed constant throughout the experiment. The above boundary condition imposes the condition that there is no loss of solute from the bed through the plane at which the displacing fluid is introduced. It also implies that $c(0, t) \neq c_f$ (Brenner, 1962).

(2) At the exit of bed, i.e., at x=L, another boundary condition is

$$\frac{\partial c}{\partial x} = 0 \qquad \text{at } x=L \qquad \text{for all } t > 0 \qquad \textbf{6. 30}$$

The above boundary condition avoids the unacceptable solution that solute concentration passes through a maximum or minimum inside the bed, discussed by Danckwerts (1953). The boundary condition at the bed exit implies that $c_e = c(L,t)$ (Brenner, 1962).

(3) The initial condition is

$$c(x,0) = c_0 = \text{constant} \qquad \text{for all } x \qquad \textbf{6. 31}$$

where c_0 is the initial concentration of solute in the bed. c_0 is assumed constant throughout the bed at time t = 0.

Brenner (1962) made Equation (6.28) dimensionless by manipulating the variable c as

$$C = \frac{c - c_f}{c_0 - c_f} \qquad 6.32$$

and variables x and t to x_d and t_d using Equations (6.3) and (6.25) respectively. The dimensionless form of Equation (6.28) was expressed by Brenner (1962) as

$$\frac{\partial C}{\partial t_d} + \frac{\partial C}{\partial x_d} = \frac{1}{4P}\frac{\partial^2 C}{\partial x_d^2} \qquad 6.33$$

where

$$P = \frac{vL}{4D_L} = \frac{Pe_L}{4} \qquad 6.34$$

and Pe_L is the Peclet number based on bed length L. An asymptotic solution of Equation (6.33) was given by Brenner (1962) as:

$$C(x_d,t_d) = 1 - 0.5\ \mathrm{erfc}[(P / t_d)^{0.5}(x_d - t_d)] - (4P\ t_d / \pi)^{0.5} \exp[-P(x_d - t_d)^2 / t_d] + 0.5\ [1 + 4P\ (x_d + t_d)] \exp(4P\ x_d) \times \mathrm{erfc}[(P / t_d)^{0.5}(x_d + t_d)] - 2(4P\ t_d / \pi)^{0.5}\ [1 + P(2 - x_d + t_d)] \times \exp(4P - \{[P\ (2 - x_d + t_d)^2] / t_d\}) + 2P[2(2 - x_d + t_d) + t_d + 2P(2 - x_d - t_d)^2] \times \exp(4P)\ \mathrm{erfc}[(P / t_d)^{0.5}(2 - x_d + t_d)] \qquad 6.35$$

where the complementary error function erfc(z) is defined as

$$\mathrm{erfc}(z) = 1 - \mathrm{erf}(z) = \frac{2}{\sqrt{\pi}} \int_z^\infty \exp(-y^2)\,dy \qquad 6.36$$

The exit concentrations of lignin, $C_{c,exit}$ and $C_{f,exit}$, in Figure 6.1 are obtained from Equation (6.35) by setting x_{df} and x_{dc} to 1 respectively and using corresponding values of P in the beds concerned.

An initial estimate of the longitudinal dispersion coefficient, D_L, based on the length of the bed is obtained from the correlation of Harleman et al. (1963) that predicts longitudinal dispersion coefficient, D_p, based on the particle diameter, d_p in uniform porous media consisting of spheres as

$$\left(\frac{D_p}{\nu}\right) = 0.66\left(\frac{|v|d_{p,50}}{\nu}\right)^{1.2} \qquad 6.37$$

where $|v|$ is the absolute value of average Darcy interstitial velocity, ν is the kinematic viscosity, and $d_{p,50}$ is the 50% particle size from a standard gravimetric sieve analysis. Kinematic viscosity (ν) is calculated as the ratio of averages of viscosities and densities of displacing and resident phases. Longitudinal dispersion coefficients (D_L) for different cases of displacement experiments are calculated using

$$D_L = \delta D_p \qquad 6.38$$

The constant δ in Equation (6.38) is adjusted so that the tails of computed and experimental breakthrough curves fit best to each other.

Overall exit concentration of lignin, C_{exit} at the exit of channel bed can be calculated using the mixing-cup model at the exits of the beds in Figure 6.1 as

$$C_{exit} = \frac{C_{c,exit}Q_c + C_{f,exit}Q_f}{Q} \qquad 6.39$$

6.2.1.6 Method of Computation for Displacement with Water

The algorithm and a brief description of the steps involved for the computation of exit concentration (C_{exit}), pressure drop (ΔP), and position of the front, x_{dc} in the channel and x_{df} in the annulus, against dimensionless time, t_d, during the displacement of MBL in a model channel bed is given in Figure B.1 in the Appendix B. The code of the computer program is given in the Appendix B.

6.2.1.7 Results of Non-Communicating Channel Bed Model

Figure 6.1 implies that when the permeability (k_c) and particle diameter (d_{pc}) in the channel are equal to the permeability (k_f) and particle diameter (d_{pf}) in the annulus respectively, displacement in the model channel bed that is considered as a combination of two separate non-communicating homogeneous beds connected in parallel becomes displacement in a homogeneous bed in the column. The computer code was validated by predicting results for the homogeneous beds.

Table 6.1 shows the model parameters used to compute the exit concentration (C_{exit}), pressure drop (ΔP), and positions of front, x_{dc} in the channel and x_{df} in the annulus, against dimensionless time t_d during the

Table 6.1 Values of parameters used in the models

Input variables	Non-communicating channel bed model			Communicating channel bed model	
	Homo bed water	Homo bed polymer	Channel bed water	Channel bed water	Channel bed polymer
Length of bed, L (cm)	24	24	24	24	24
Dia. of column, d (cm)	5.2	5.2	5.2	5.2	5.2
Total flow rate, Q (mL/min)	230	230	230	230	230
Viscosity of displacing phase, μ_d (poise)	0.01	0.032	0.01	0.01	0.032
Viscosity of resident phase, μ_r (poise)	0.0117	0.0117	0.0117	0.0117	0.0117
Density of displacing phase, ρ_d (gm/cm^3)	1.0	0.996	1.0	1.0	0.996
Density of resident phase, ρ_r (gm/cm^3)	1.0	1.0	1.0	1.0	1.0
Initial porosity of channel bed, ε	0.4	0.4	0.4	0.4	0.4
Initial porosity of column of coarse beads, ε_c	-	-	0.4	0.4	0.4
Initial porosity of column of fine beads, ε_f	0.4	0.4	0.4	0.4	0.4
Diameter of coarse beads, d_{pc} (cm)	-	-	0.0638	0.0638	0.0638
Diameter of fine beads, d_{pf} (cm)	0.0121	0.0121	0.0121	0.0121	0.0121
Initial ratio of permeability, r_k	1.0	1.0	28	28	28
Permeability of column of fine beads, k_f (cm^2)	7.2×10^{-8}	7.7×10^{-8}	9.0×10^{-8}	9.0×10^{-8}	9.0×10^{-8}
Number of cells, n	-	-	-	10	10

displacement of MBL in a model channel bed using the non-communicating channel bed model. In Table 6.1, permeability of the column of fine beads in both channel beds and homogeneous beds were adjusted to match the pressure drop profiles obtained across the respective beds. Table 4.3 in Chapter 4 shows that in a homogeneous bed, the experimentally measured permeability of fine beads varied from 6.38 X 10^{-8} cm^2 to 10 x 10^{-8} cm^2. The permeability of the column of fine beads either in a channel bed or in a homogeneous bed in the models was within the measured values reported in Table 4.3.

Figure 6.2 demonstrates that experimental and computed breakthrough curves agree well with each other during displacement of MBL in homogeneous beds of fine beads with either water or the polymer solution. Peclet numbers for the breakthrough curves at the exit of homogeneous beds of fine beads during displacement with water and the polymer solution are 164 and 381 respectively. However, the computed and experimental breakthrough curves do not match to each other during displacement of MBL in the model channel bed with water. Figure 6.2 also shows that after breakthrough in the center channel, concentration of lignin in the experimental breakthrough curve is higher than that

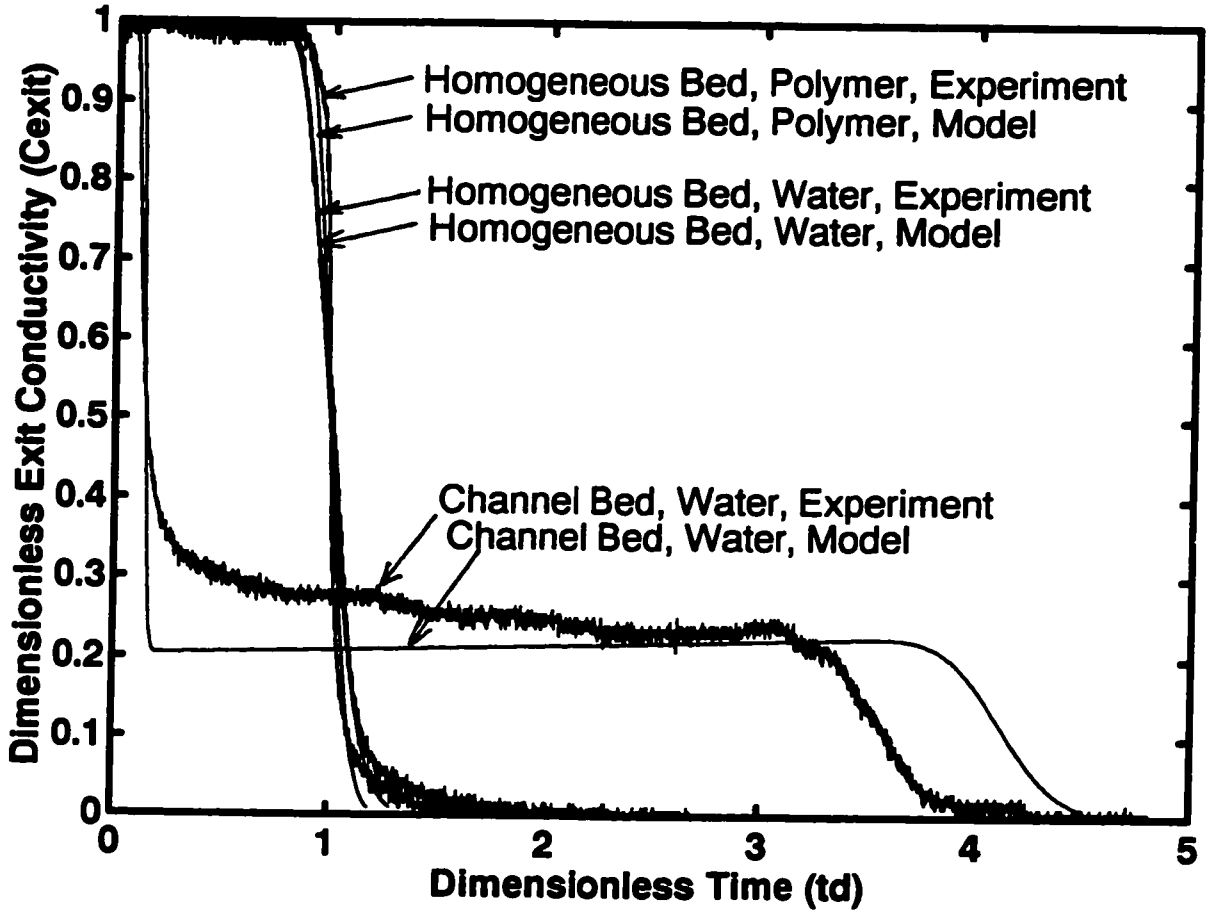

Figure 6.2 Comparison of experimental breakthrough curves with those predicted by model that considers the model channel bed a combination of two separate non-communicating homogeneous beds connected in parallel.

in the computed breakthrough curve during displacement of MBL with water in the model channel bed.

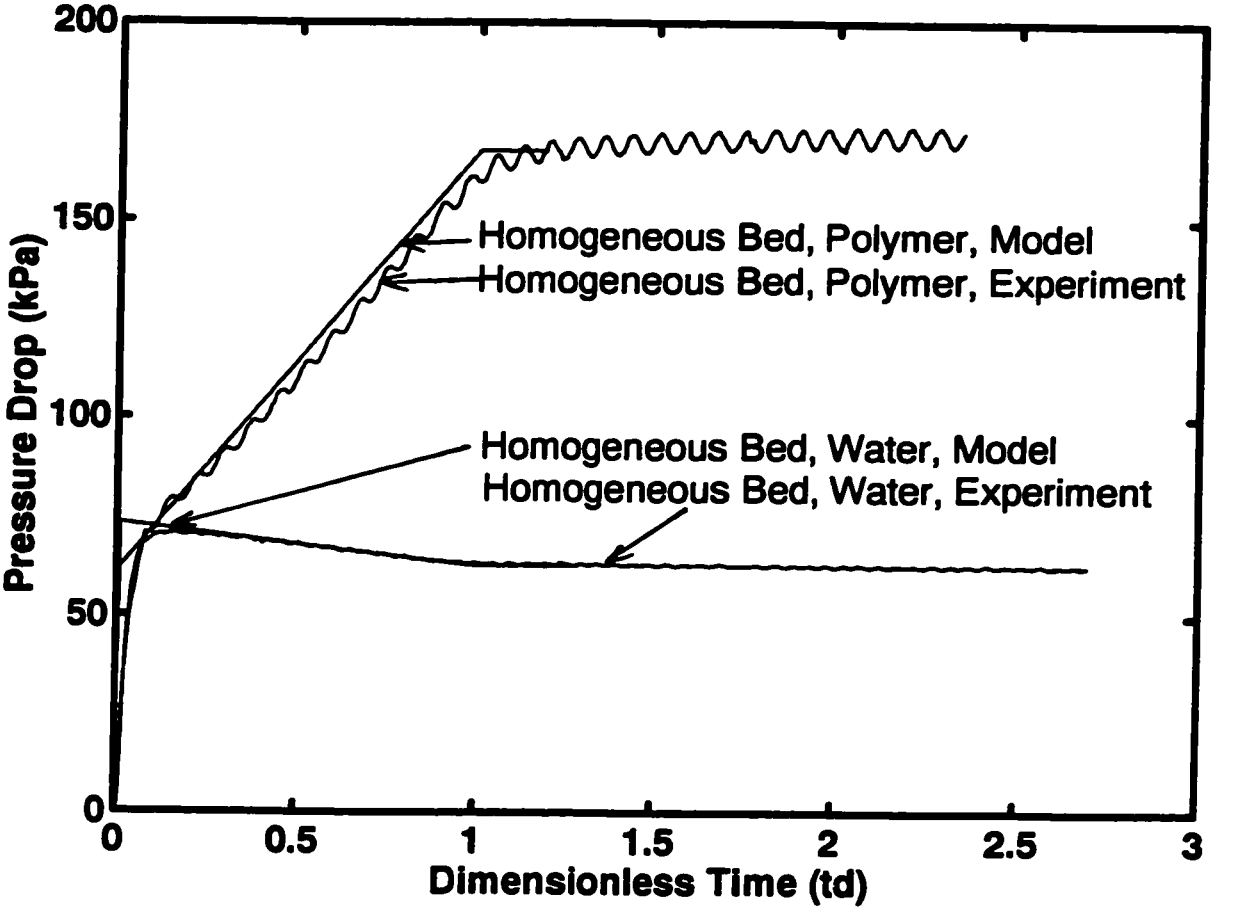

Figure 6.3 Comparison of experimental pressure drop profiles with those predicted by model that considers the model channel bed a combination of two separate non-communicating homogeneous beds connected in parallel.

Figure 6.3 demonstrates that during displacement of MBL in the homogeneous beds of fine beads with either water or polymer solution, the computed and experimental profiles of pressure drop agree well to each other.

The cyclic oscillations in the pressure drop profiles in Figure 6.3 were due to the presence of pulses in the displacing fluid imparted by the squeezing action of motor heads on a flexible tube in the peristaltic pump that was used to pump the displacing fluid into the bed. Figure 6.3 reveals that pressure drop across the homogeneous bed decreases steadily till it reaches the steady state during displacement with water whereas during displacement with the polymer solution, pressure drop across the homogeneous bed increases steadily till it reaches the steady state.

Figure 6.4 shows the comparison of computed positions of fronts in the annulus, x_{df} , and in the channel, $x_{dc,}$ in the channel bed against dimensionless time, $t_{d,}$ with those measured by the probes, described in detail in Chapter 5. The positions of fronts in the annulus, $x_{df,}$ and in the channel, $x_{dc,}$ are equal to each other during displacement in homogeneous beds of fine beads with either water or the polymer solution. Figure 6.4 demonstrates that the computed positions of fronts against dimensionless time agree well to those measured by the probes during displacement with either water or the polymer solution in the homogeneous beds of fine beads. However, time, $t_{d,}$ required by the front in the annulus in the channel bed is higher than those measured by the probes at the periphery and interface at any axial position in the channel bed during washing with water. The positions of fronts, $x_{dc,}$ in the channel against dimensionless

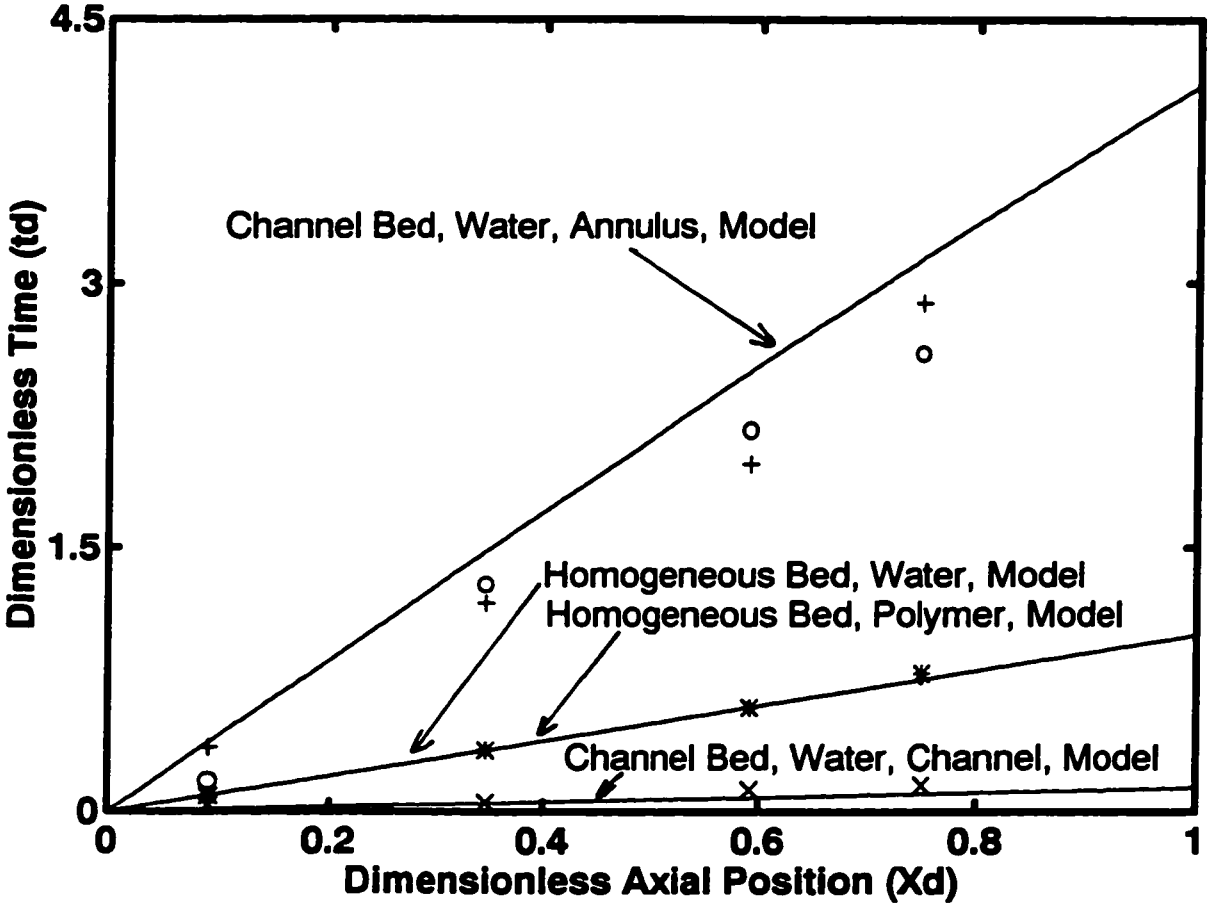

Figure 6.4 Comparison of time required by front to reach an axial position in bed as measured by probes with those predicted by non-communicating channel bed model. Locations of probes are, channel bed, water, (+) periphery, (o) interface, (x) center; homogeneous bed, water, (*) center; and homogeneous bed, polymer, (.) center.

time, t_d, match well with those measured by the probes in the channel in the channel bed during displacement with water.

6.2.1.8 Discussions

Figure 6.2 demonstrates that the computed and experimental breakthrough curves agree for the displacement of the MBL in the homogeneous beds of fine beads using either water or the polymer solution as the displacing phase. The higher Peclet number (Pe_L = 381) of the computed breakthrough curve for displacement with the polymer solution than that (Pe_L = 164) with water implies less interfacial mixing in the front during displacement with the polymer solution than that with water. Probable reasons for the less interfacial mixing in the front during displacement of the MBL in the homogeneous bed of fine beads with the polymer solution than that with water were (a) less viscous fingering due to stable displacement (Lake, 1989) with the polymer solution as the viscosity of the polymer solution (3.2 mPa.s) was higher than that of the MBL solution (1.17 mPa.s), and (b) formation of a soluble, viscous layer of lignin/polyDADMAC complex at the interface between the MBL and the polymer solution that might have retarded interfacial mixing of the MBL and the polymer solution during the displacement.

Figure 6.2 demonstrates the mismatch between the computed and experimental breakthrough curves in the model channel bed during displacement of the MBL with water. It can be observed in Figure 6.2 that during the entire displacement process after breakthrough in the center channel, concentration of lignin in the experimental breakthrough curve is higher than that

in the computed breakthrough curve. The difference between them is the highest just after the breakthrough in the center channel and gradually the difference smears out as displacement proceeds. The mismatch between computed and experimental breakthrough curves clearly points toward communication between the center channel and annulus during displacement of the MBL in a model channel bed with water. The communication between the channel and annulus in a model channel bed had also been observed experimentally and reported in Chapter 3 in terms of cross flow that described the lateral movement of tracer particles from the annulus towards the center channel in a model channel bed.

Figure 6.3 shows that the computed pressure drop profile matches well with respective experimental pressure drop profiles during displacement of the MBL in homogeneous beds of fine beads using either water or the polymer solution as the displacing phase. The initial steady decrease in the pressure drop before it reaches a steady state during displacement with water was due to the introduction of the less viscous water into the bed, displacing the more viscous MBL solution from the bed. On the other hand, the initial steady increase in the pressure drop before it reaches a steady state during displacement with the polymer solution was due to the introduction of the more viscous polymer solution into the bed that displaced the less viscous MBL solution from the bed.

Figure 6.4 demonstrates that during displacement in the homogeneous beds of fine beads with either water or the polymer solution, computed positions

of the front against dimensionless time match well with those measured experimentally by probes at any axial position in the bed, described in detail in Chapter 5. Since the rate of advancement of the front at any axial position inside the bed represents the interstitial velocity of the fluid at that position inside the bed, the model predicts well the profiles of interstitial velocities inside the homogeneous beds during the displacement of the MBL with either water or the polymer solution. However, Figure 6.4 also demonstrates that in a model channel bed, the computed time required by the front in the annulus to pass a fixed position in the annulus is higher than that measured by probes at the respective positions in the annulus during displacement with water. This implies faster movement of the front in the annulus as measured experimentally than that predicted by the model and was probably due to the communication between the annulus and the channel resulting in the loss of black liquor from the annulus to the channel during displacement with water in the model channel bed.

In the following section, the previous model developed that considered the model channel bed as a combination of two separate non-communicating homogeneous beds connected in parallel is modified to incorporate communication between the two beds during the course of displacement.

6.2.2 Two Communicating Homogeneous Parallel Beds

The communication between channel and annulus in a model channel bed during the displacement of MBL with either water or the polymer solution is modeled using a technique called the network of zones. Van de Vusse (1962) pioneered the use of the network of zones through assemblages of perfectly back-mixed interconnected zones to describe the internal mixing rates in a stirred tank reactor where the pumping action of the stirrer caused turbulence that induced both axial and radial dispersion of a tracer injected at one point in the tank. Khang and Levenspiel (1976) advanced the network of zones analysis to obtain approximate analytical results for dispersion of an inert tracer using loops of back-mixed zones within an open flow vessel configuration. Mann and Mavros (1982) have modeled the mixing of a tracer injected at a point in a closed mixing tank using a network of ideally mixed tanks with lateral exchange of flows between the tanks. Several researchers (Brown and Halstea, 1979; Sasakura et al., 1980; Mann et al., 1981; Mann et al., 1992; Knysh and Mann, 1984; Wang and Mann, 1992; Brucato et al, 1990) have advanced the network of zones approach originally proposed by Van de Vusse (1962) in various tanks and configurations.

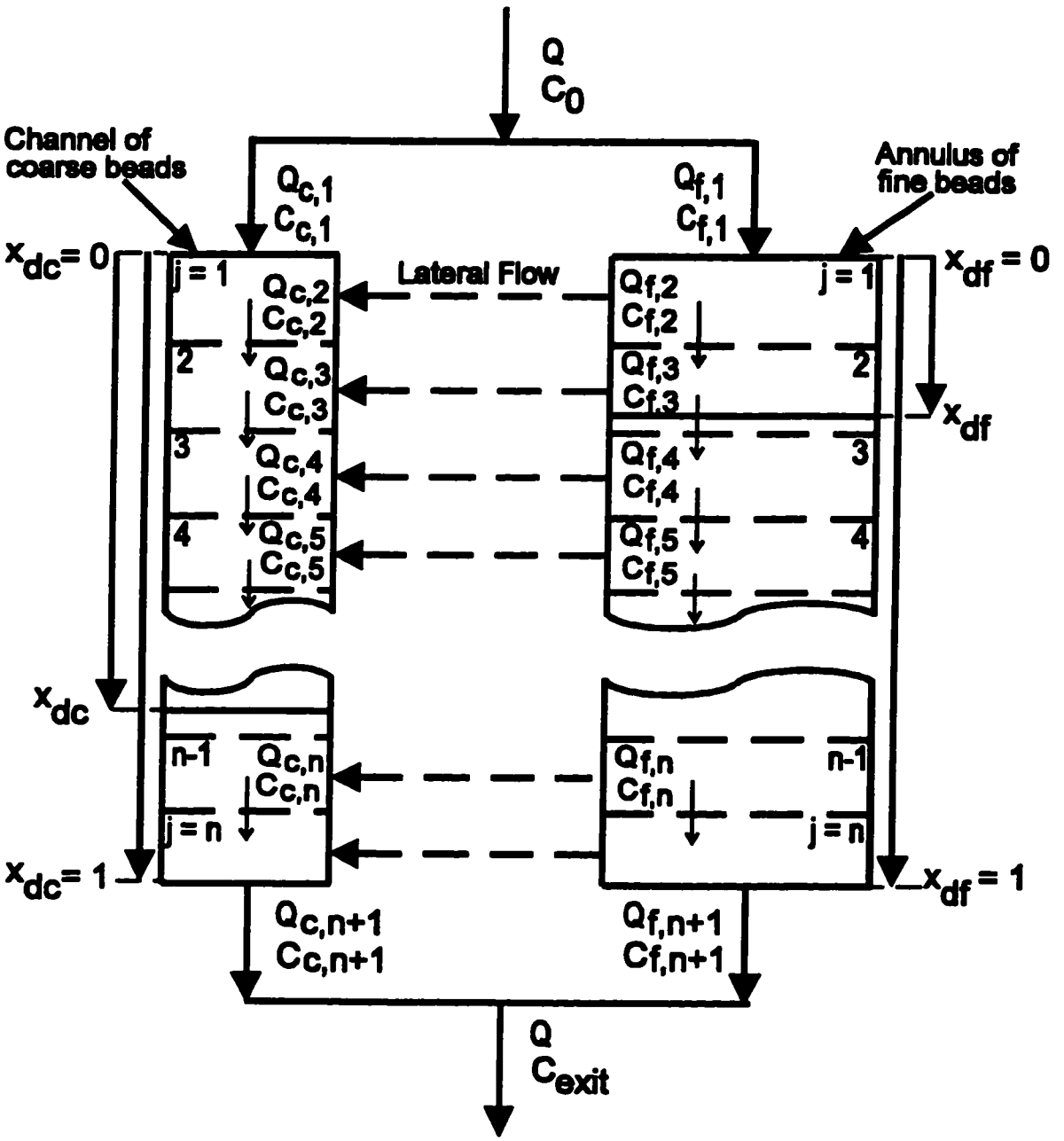

Figure 6.5 Representation of model channel bed as combination of two separate communicating homogeneous beds connected in parallel.

Figure 6.5 depicts a model channel bed that is divided into number of interconnected cells. Cells either in the channel or in the annulus are separated by imaginary boundaries. It is assumed that the heights of the cells either in the channel or in the annulus are equal to each other and mainflow is only along the length of the bed. In addition to all assumptions made in section 6.2.1 for two

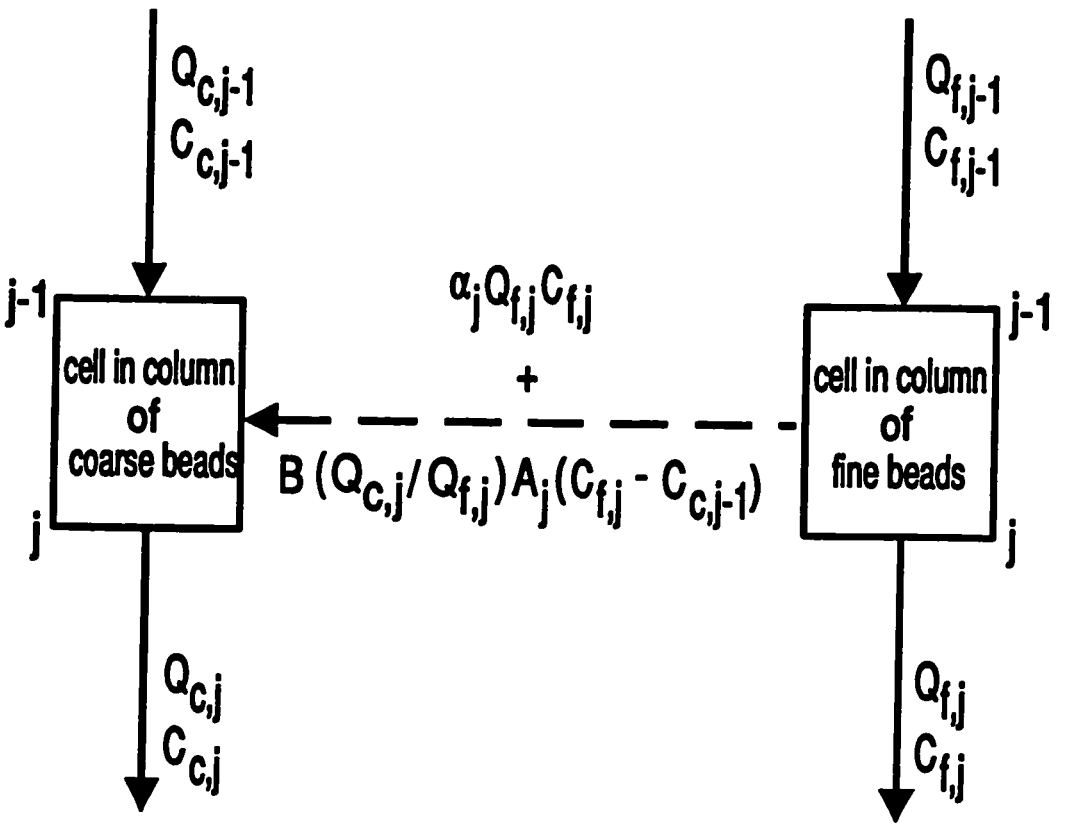

Figure 6.6 Lateral transfer of mass between two communicating adjacent cells in channel and in annulus.

non-communicating homogeneous beds connected in parallel, lateral transfer of mass caused by both convective and diffusional flow between adjacent cells in the annulus and in the channel is permitted. Figure 6.6 depicts a cell in the channel with its adjacent cell in the annulus. The cell either in the channel or in the annulus is separated from its nearest cells either in the channel or in the annulus respectively by boundaries, boundary (j-1) and boundary (j). Figure 6.6 also delineates the mainstreams of flow, the lateral transfer of mass between the adjacent cells in the annulus and in the channel, and the concentration of lignin in each stream. The following section describes the material balance and balance of flow rates in cells in the channel and annulus separately during displacement of MBL in the model channel bed with either water or the polymer solution.

6.2.2.1 Lateral Transfer of Lignin during Displacement with Water

6.2.2.1.1 Cells in Channel:

The assumptions made for material balance around a cell in the channel are (a) displacement of MBL by a displacing phase in the direction of main flow, i.e. along the length of bed, is like plug flow, and (b) lignin that is transferred into the cell in channel from the adjacent cell in the annulus by either convective or

diffusive flow is mixed instantaneously throughout the cell volume in the channel, resulting in a uniform concentration of lignin in the cell in channel.

Two modes of lateral transfer of lignin from a cell in the annulus to an adjacent cell in the channel are considered: (a) lateral transfer of lignin due to lateral convective flow or bulk flow of the MBL solution from the cell in the annulus to the adjacent cell in the channel and (b) diffusive flow of lignin from the cell in annulus to the adjacent cell in the channel caused by the sharp difference in the concentration of lignin between the adjacent cells. The lateral convective flow of the MBL solution is due to the cross flow of fluid elements from the annulus to the channel in the channel bed due to screen-bead interaction, discussed in detail in Chapter 3. On the other hand, during displacement in the model channel bed when the front in the channel passes the lower boundary, boundary (j) of the cell in the channel in Figure 6.6 and the front in the annulus has yet to pass the upper boundary, boundary (j-1) of the adjacent cell in the annulus, the concentration of lignin in the cell in the channel becomes zero whereas that in the cell in the annulus remains at the concentration of lignin in the MBL solution. This sharp difference in the concentration of lignin in adjacent cells in the channel and annulus causes lateral diffusive flow of lignin from the cell in the annulus to the adjacent cell in the channel.

Figure 6.6 demonstrates that the only direction of lateral transfer of lignin is from the cell in the annulus to the adjacent cell in the channel and no transfer of mass is permitted in the opposite direction. It is further assumed that the loss of lignin from the MBL solution in the annulus due to lateral transfer is accounted for only by the decrease in the level of MBL in the annulus, described in detail in section 6.2.2.1.2. As a result, dimensionless concentration of lignin in the MBL solution in the annulus remains always at unity during lateral transfer of lignin from the annulus to the channel.

In Figure 6.6, if α_j, an adjustable parameter that represents the fraction of flow rate, $Q_{f,j}$ that goes into the cell in the channel from the adjacent cell in the annulus caused by convective cross flow of the MBL solution, flow rate, $Q_{c,j}$, of fluid that goes out of the cell in the channel in Figure 6.6 can be determined from a balance of the flow rates around the cell in the channel as

$$Q_{c,j} = Q_{c,j-1} + \alpha_j Q_{f,j} \qquad \textbf{6. 40}$$

The rate of lateral transfer of mass of lignin with cross convective flow of MBL solution shown in Figure 6.6 can be expressed as:

$$\text{rate of lateral convective transfer of mass of lignin} = \alpha_j\, p\, Q_{f,j}\, C_{f,j} \qquad \textbf{6. 41}$$

where p is a factor that converts the dimensionless concentration of lignin to its actual value. The dimension of the factor p is mass per volume. The rate of

transfer of mass of lignin due to lateral diffusional transfer of lignin can be expressed as:

rate of diffusive transfer of mass of lignin = B p ($Q_{c,j}$ / $Q_{f,j}$) A_j ($C_{f,j}$ - $C_{c,j-1}$) **6. 42**

where B is a constant and A_j is the interfacial area normal to the direction of mass transfer between the two adjacent cells. In Equation (6.42), the assemblage of terms B ($Q_{c,j}$ / $Q_{f,j}$) is like a mass transfer coefficient that depends on the ratio of flow rates in the cells in the channel and in the annulus and have a dimension of length per time. The definition of the assemblage of terms in Equation (6.42) that represents the mass transfer coefficient is arbitrary.

A material balance around the cell in channel in Figure 6.6 results in

$$V_{c,j,j-1}\left(\frac{dC_{c,j}}{dt}\right) = Q_{c,j-1}C_{c,j-1} + \alpha_j Q_{f,j}C_{f,j} + \beta_j\left(\frac{Q_{c,j}}{Q_{f,j}}\right)\left(C_{f,j} - C_{c,j-1}\right) - Q_{c,j}C_{c,j} \qquad \textbf{6. 43}$$

where $V_{c,j,j-1}$ is the volume of the cell in the channel having boundaries, boundary (j-1) and boundary (j), and β_j is an adjustable parameter defined as

$$\beta_j = BA_j \qquad \textbf{6. 44}$$

It is assumed that during a small change in time, Δt, concentration, $C_{c,j}$, in the cell in the channel remains unchanged and as a result Equation (6.43) can be rewritten as

$$C_{c,j} = \left[\frac{Q_{c,j-1}C_{c,j-1} + \alpha_j Q_{f,j}C_{f,j} + \beta_j \left(\frac{Q_{c,j}}{Q_{f,j}} \right) \left(C_{f,j} - C_{c,j-1} \right)}{Q_{c,j}} \right] \qquad 6.45$$

The plug flow displacement of the MBL with water in the cell in channel in Figure 6.6 results the following conditions:

(a) when the position of the front, x_{dc}, in the cell in the channel is less than or equal to the upper boundary, boundary (j-1) of the cell, the cell in the channel contains undisplaced MBL solution. As a result,

$$C_{c,j} = 1, \text{ if } x_{dc} \leq \text{boundary}(j-1) \qquad 6.46$$

(b) when the position of front, x_{dc}, in the cell in the channel is greater than or equal to the lower boundary, boundary (j) of the cell, displacement in the cell is completed and concentration of lignin in the cell becomes zero in the absence of any lateral transfer of lignin into the cell. However, due to lateral transfer of lignin from the cell in the annulus to the adjacent cell in the channel, the

resulting concentration of lignin in any cell in the channel can be calculated from Equation (6.45) and hence

$$C_{c,j} = C_{c,j}, \quad \text{if } x_{dc} \geq \text{boundary}(j-1) \qquad 6.47$$

During computation of the breakthrough curves, the frontal position, x_{dc}, in the channel is increased from boundary to boundary of the cells in channel. As a result, the conditions expressed in Equations (6.46) and (6.47) are sufficient to describe the concentration of lignin in any cell in the channel during displacement with water in the model channel bed.

At the inlet of the bed, the flow rate and concentration of lignin in the lignin-free displacing fluid that is injected into the channel are $Q_{c,1}$ and $C_{c,1} = C_0 = 0$ respectively.

6.2.2.1.2 Cells in Annulus

The assumptions made to perform material balance around a cell in the annulus are (a) displacement of the MBL by water in the direction of the length of bed is plug flow and (b) the diffusion of lignin from the annulus to the center channel does not influence lignin concentration in the annulus. The second condition implies that dimensionless concentration of lignin in the MBL solution in the annulus is always unity during the lateral transfer of lignin from the annulus to the channel in the model channel bed.

A balance of flow rates around the cell in the annulus having boundaries, boundary (j-1) and boundary (j) in Figure 6.6 results in

$$Q_{f,j} = \frac{Q_{f,j-1}}{\left(1+\alpha_j\right)} \qquad 6.48$$

This section describes the calculation of decrease in the level of MBL in the annulus due to the loss of lignin by lateral transfer from the annulus to the channel. The total mass of lignin that is transferred during a small step in time, Δt, by both cross convective flow and diffusive flow from all cells in the annulus to the adjacent cells in the channel, shown in Figure 6.5, is calculated using Equations (6.41), (6.42), and (6.44) as:

total mass of lignin transferred by lateral flow from all cells in annulus during Δt

$$= \sum_{\text{cells}} \left[\alpha_j Q_{f,j} C_{f,j} + \beta_j \left(\frac{Q_{c,j}}{Q_{f,j}} \right) \left(C_{f,j} - C_{c,j-1} \right) \right] p \Delta t \qquad 6.49$$

The total mass of lignin transferred up to time, t, from all cells in the annulus to the cells in the center channel due to lateral convective and diffusive flows is called total loss of lignin from the annulus. Total loss of lignin can be

calculated as the cumulative sum of the total mass of lignin transferred during the small time interval, Δt, up to time t, resulting in Equation (6.50):

total loss of mass of lignin from annulus up to time, t

$$= \sum_{t=0}^{t} \left\{ \sum_{cells} \left[\alpha_j Q_{f,j} C_{f,j} + \beta_j \left(\frac{Q_{c,j}}{Q_{f,j}} \right) \left(C_{f,j} - C_{c,j-1} \right) \right] p \Delta t \right\} \qquad 6.50$$

The total loss of mass of lignin from the annulus to the center channel can be accounted for by the decrease in the level of MBL in the annulus or by the increase in the frontal position in the annulus, x_{df}, resulting in a corrected frontal position, nx_{df}, in the annulus:

$$nx_{df} = x_{df} + \left(\frac{\text{Total loss of mass of lignin upto time t from annulus in Eqn(7.50)}}{pLA_f \varepsilon_f} \right) \qquad 6.51$$

where x_{df} is the frontal position in the annulus that is calculated using Equations (6.11), (6.12), and (6.16) assuming no lateral exchange of lignin between the channel and annulus during displacement in a model channel bed. In Equation (6.51), the ratio of total loss of mass of lignin from the annulus to the factor p results in the volume of MBL that is associated with the total transfer of lignin from the annulus to the channel.

The plug flow displacement of the MBL solution in the annulus with water imposes the following conditions in the cell in the annulus in Figure 6.6;

(a) when the corrected frontal position, nx_{df} is either less than or equal to the upper boundary, boundary (j-1) of the cell, the cell contains undisplaced MBL solution, resulting in

$$C_{f,j} = 1, \text{ when } nx_{df} \leq \text{boundary}(j-1) \qquad \textbf{6. 52}$$

(b) when the corrected frontal position, $nx_{df,}$ is either greater than or equal to the lower boundary, boundary (j) of the cell in the annulus, the cell is free of lignin as displacement is already completed in it, resulting in

$$C_{f,j} = 0, \text{ when } nx_{df} \geq \text{boundary}(j) \qquad \textbf{6. 53}$$

and, (c) when the corrected position of the front, $nx_{df,}$ is intermediate between the upper and lower boundary of the cell in the annulus, concentration of lignin in the cell is interpolated linearly as

$$C_{f,j} = \frac{\text{boundary}(j) - nx_{df}}{\text{boundary}(j) - \text{boundary}(j-1)}, \text{ when boundary}(j-1) < nx_{df} < \text{boundary}(j) \qquad \textbf{6. 54}$$

In condition (c), concentration of lignin, $C_{f,j}$, in the upper part of the cell that is limited by boundary (j-1) and nx_{df} is zero, and that in lower part of the cell that is limited by boundary (j) and nx_{df} is unity.

Since during the lateral transfer of lignin from the annulus to the channel, the dimensionless concentration of lignin in the MBL in the annulus is assumed to be unity, the concentration of lignin at the exit of the annulus, $C_{f,n+1}$ can be calculated using Equation (6.35), implying $C_{f,n+1} = C_{f,exit}$.

At the inlet of the bed, the flow rate and concentration of lignin in the lignin-free displacing phase are $Q_{f,1}$ and $C_{f,1} = C_0 = 0$ respectively.

6.2.2.2 Lateral Transfer of Lignin during Displacement with Polymer

During displacement of MBL with the polymer solution in the model channel bed, lignin transferred from the annulus to the channel by both convective cross flow and diffusive flow formed precipitate by reaction with the polymer solution that was flowing down the center channel. Consequently, with the deposition and/ or filtration of the precipitate in the channel (Chapter 3), the porosity (ε_c) and permeability (k_c) of the center channel, the ratio of permeability (r_k) of the center channel to that of the annulus, and the overall porosity (ε) of the channel bed changed continuously with the advancement of displacement with the polymer solution. The following section describes the modeling of the

changes in properties (ε_c, k_c, ε, and r_k) of the model channel bed during displacement with the polymer solution.

6.2.2.2.1 Cells in the Channel

The reaction of lignin with the polymer to form a precipitate is assumed to be an elementary reaction described as

$$\text{Lignin} + \text{Polymer} \rightarrow \text{Precipitate} \qquad \textbf{6. 55}$$

It is further assumed that the above reaction is irreversible and first order in the concentration of both lignin and polymer. Consequently, the rate of the reaction forming precipitate can be expressed as

$$\frac{d[\text{Precipitate}]}{dt} = K[\text{Lignin}][\text{Polymer}] \qquad \textbf{6. 56}$$

where K is the rate constant of the reaction. After breakthrough in any cell in the channel, lignin transferred from the annulus by both convective and diffusional flow meets fresh polymer solution in the cell in the channel. Assuming that the polymer is in excess in a cell in the channel after breakthrough in it, the concentration of polymer in that cell in the channel is assumed to be constant. As a result, the rate equation in Equation (6.56) is modified as

$$\frac{d[\text{Precipitate}]}{dt} = K'[\text{Lignin}] \qquad \textbf{6. 57}$$

where K' is the new rate constant. It is further assumed that the total mass of lignin that is transferred from the annulus to the channel by lateral exchange over small time, Δt, given in Equation (6.49) is completely and instantaneously converted into precipitate in the center channel. Consequently, Equation (6.57) can be written as

$$\frac{d[\text{Precipitate}]}{dt} = K'\left(\frac{\text{loss of mass of lignin from all cells given in Equation (6.49)}}{LA_c\varepsilon_c}\right) \qquad 6.58$$

The total volume of precipitate that is formed in the center channel over time, Δt, is determined from Equation (6.58) as

$$\text{Total volume of precipitate over } \Delta t = K'\left(\frac{\text{loss from all cells in Equation (6.49)}}{\rho_{precipitate}}\right)\Delta t \qquad 6.59$$

where $\rho_{precipitate}$ is the density of the precipitate that is assumed to be unity.

All precipitate that formed in the center channel over small time, Δt, is assumed to be distributed uniformly throughout the center channel in the model channel bed. As a result, the reduction in the porosity of the center channel is assumed to be uniform throughout the center channel. Precipitate formed in the channel is assumed to constrict or plug the pore throats in the center channel. As a result, the new porosity of the center channel, $\varepsilon_{c,app}$, after plugging of pore

throats with precipitates formed over time, Δt, is computed following the relation proposed by McCune et al., 1973 as

$$\varepsilon_{c,app} = \varepsilon_{c,old} \exp\left[-\tau\left(\frac{\text{total volume of precipitate over } \Delta t \text{ in Eqn. (6.59)}}{A_c L}\right)\right]$$

$$= \varepsilon_{c,old} \exp\left[-\lambda\left(\frac{\text{total loss of lignin from all cells over } \Delta t \text{ in Equation (6.49)}}{\rho_{precipitate} A_c L}\right)\Delta t\right] \qquad \textbf{6. 60}$$

where $\lambda = K'\tau$ and $\varepsilon_{c,old}$ is the porosity of the center channel before time, Δt. The term λ in Equation (6.60) is an adjustable parameter.

The new permeability of the center channel, $k_{c,app}$, that is a result of the plugging of pore throats in the center channel over time, Δt, is calculated using the relationship between permeability and porosity in the Ergun equation (McCabe et al., 1985) as

$$k_{c,app} = \left(\frac{d_{pc,e}^2 \, \varepsilon_{c,app}^3}{150\left(1-\varepsilon_{c,app}\right)^2}\right) \qquad \textbf{6. 61}$$

where $d_{pc,e}$ is the equivalent particle diameter of the coarse bead in the center channel. The value of $d_{pc,e}$ is calculated using Equation (6.61) from the initial conditions before the start of displacement in a channel bed when $k_{c,app} = k_c$ and

$\varepsilon_{c,app} = \varepsilon_c$. Also, the values of k_c and ε_c are known and remain unchanged during displacement with water in a channel bed.

Plugging of the pore throats in the center channel with precipitate causes reduction in the porosity of the center channel, as described in Equation (6.60). Consequently, the reduction in the porosity of the center channel also causes a decrease in the overall porosity (ε) of the channel bed. New overall porosity, ε_{app}, of the model channel bed after time, Δt, is calculated from the balance of void volumes in the model channel bed as

$$\varepsilon_{app} = \frac{\left(\varepsilon_{c,app} A_c\right) + \left(\varepsilon_f A_f\right)}{A} \qquad \textbf{6. 62}$$

The balances in the flow rates and material, plug flow conditions, and conditions at the inlet of bed, given in Equations (6.40) through (6.46) in section 6.2.2.1.1, remain valid for the cells in the channel during displacement with the polymer solution. However, the condition of plug flow during displacement with water in the cell in the channel, described in Equation (6.47), is no longer valid during displacement with the polymer solution since all lignin transferred from the annulus to the channel is converted into precipitate resulting in the concentration of lignin in the cell in the channel, $C_{c,j} = 0$. Hence, Equation (6.47) is modified as

$$C_{c,j} = 0, \quad \text{if } x_{dc} \geq \text{boundary}(j-1) \qquad \textbf{6. 63}$$

Consequently, the concentration of lignin, $C_{c,n+1}$ at the exit of channel is calculated using Equation (6.35) implying $C_{c,n+1} = C_{c,exit}$ during displacement with the polymer solution.

6.2.2.2.2 Cells in the Annulus

The balances in the flow rates and materials, correction in the frontal position in the annulus due to lateral exchange of lignin between the annulus and the channel, the conditions of plug flow displacement of the MBL in the cells in the annulus, and the conditions at the inlet of the bed, given in Equations (6.48) through (6.54) in section 6.2.2.1.2, remain valid in the cells in the annulus during displacement with the polymer solution.

6.2.2.3 Adjustable Parameters α_j and γ_j :

The adjustable parameters α_j and β_j introduced respectively in Equation (6.40) and (6.43) are expressed as

$$\alpha_j = \psi \times \text{boundary(j)} \times \left(\frac{\left(r_k\right)_{\text{at any time, t}}^{-1}}{\left(r_k\right)_{\text{at time, t = 0}}^{-1}} \right) \qquad \textbf{6. 64}$$

and $$\gamma_j = \beta_j \left(\frac{\left(r_k\right)_{\text{at any time, t}}^{-1}}{\left(r_k\right)_{\text{at time, t = 0}}^{-1}} \right) = B\ A_j \left(\frac{\left(r_k\right)_{\text{at any time, t}}^{-1}}{\left(r_k\right)_{\text{at time, t = 0}}^{-1}} \right) \qquad \textbf{6. 65}$$

where ψ is a constant and γ_j is an adjustable parameter. Since during displacement with polymer solution, the permeability of the center channel changes with time due to the plugging of pore throats in the channel, both convective cross flow and diffusive flow of lignin from the annulus to the channel become time-dependent, as discussed below. Equation (6.64) and (6.65) are introduced to make both the convective cross flow and diffusive flow of lignin time dependent and the parameter β_j in Equations (6.43), (6.45), (6.49), and (6.50) is replaced by the adjustable parameter γ_j.

In the absence of any precipitate formation in the channel during displacement of the MBL solution in a model channel bed with water, r_k, the ratio of permeability of the channel to that of the annulus remains constant with time. Consequently, Equations (6.64) and (6.65) reveal that the parameter α_j is only dependent on the axial position of the cell and the parameter γ_j is independent of both the axial position of the cell and time. The increase in α_j along the length of the bed is justified since the extent of the convective cross flow of lignin from the annulus to the center channel increased towards the bottom of the bed, because the back pressure that developed due to screen-bead interaction was higher near the bottom of the bed than at the top of the bed, as discussed in detail in Chapter 3.

Equations (6.64) and (6.65) also imply that during displacement with the polymer solution, as r_k decreases with time due to the plugging of pore throats in the center channel, α_j becomes dependent on both the axial position of the cell and time whereas γ_j remains dependent only on time. Since the value of r_k is highest at the beginning of displacement with the polymer solution when the channel remains free of precipitate, both α_j at any given axial position and γ_j at all axial positions in the bed are largest at the beginning of the displacement and both of them decrease as displacement with the polymer solution proceeds.

6.2.2.4 Method of Computation in Communicating Channel Bed Model

To satisfy the conditions of plug flow displacement in the channel described in Equations (6.46), (6.47), and (6.63) during the displacement with either water or the polymer solution, the step length in x_{dc} was chosen as

$$\Delta x_{dc} = \frac{1}{\text{number of cells}} = \frac{1}{n} \qquad \textbf{6. 66}$$

The overall exit concentration, C_{exit}, from the channel bed in Figure 6.5 was calculated using a mixing-cup model at the exit of channel bed. For displacement with water, C_{exit} was calculated as

$$C_{exit} = \frac{C_{c,n+1}Q_{c,n+1} + C_{f,n+1}Q_{f,n+1}}{Q} \qquad \textbf{6. 67}$$

Since the total mass of lignin transferred to the channel due to the presence of lateral exchange of lignin is assumed to be converted into precipitate during displacement with the polymer solution, no lignin that is transferred by lateral exchange comes out at the exit of channel in Figure 6.5. As a result, during displacement with the polymer solution, the exit concentration from channel $C_{c,n+1}$ becomes equal to $C_{c,exit}$ and was predicted by Equation (6.35). The overall exit concentration during displacement with the polymer solution was calculated as

$$C_{exit} = \frac{C_{c,exit}Q_{c,n+1} + C_{f,n+1}Q_{f,n+1}}{Q} \qquad 6.68$$

The algorithms for the computation of exit concentration, C_{exit}, from the model channel bed, pressure drop, ΔP across the channel bed, and positions of the fronts in the annulus and in the channel against dimensionless time during displacement with water and the polymer solution are given in Figures B.2 and B.3 respectively in the the Appendix B. A brief discussion of the steps involved in the algorithm and the code of computer program are given in the Appendix B.

6.2.2.5 Results

Table 6.1 shows the values of the model parameters that were used to compute the results for displacement in a model channel bed with either water or the polymer solution using the communicating channel bed model. Table 6.2

shows the values of the adjustable parameters used in the communicating channel bed model for displacement in the channel bed with water and the polymer solution.

Table 6.2 Adjustable parameters in communicating channel bed model

Adjustable Parameter	Communicating Channel Bed Model	
	Channel Bed, Water	Channel Bed, Polymer
β_i (cm^3/s)	0.53	0.53
ψ	0.005	0.005
λ (s^{-1})	-	253

In the absence of any lateral exchange between the channel and the annulus, i.e., when both α_j and γ_j are zero, and when the exit concentration in the channel was calculated by Equation (6.35), the communicating channel bed model successfully predicted the results for the displacement with water in a channel bed that was predicted by the non-communicating channel bed model. The results of displacement in the homogeneous bed either with water or the polymer solution predicted by the non-communicating channel bed model were also predicted by the communicating channel bed model when permeability (k_c) and particle diameter (d_{pc}) in the channel are equal to permeability (k_f) and particle diameter (d_{pf}) in the annulus respectively, lateral exchange of lignin was

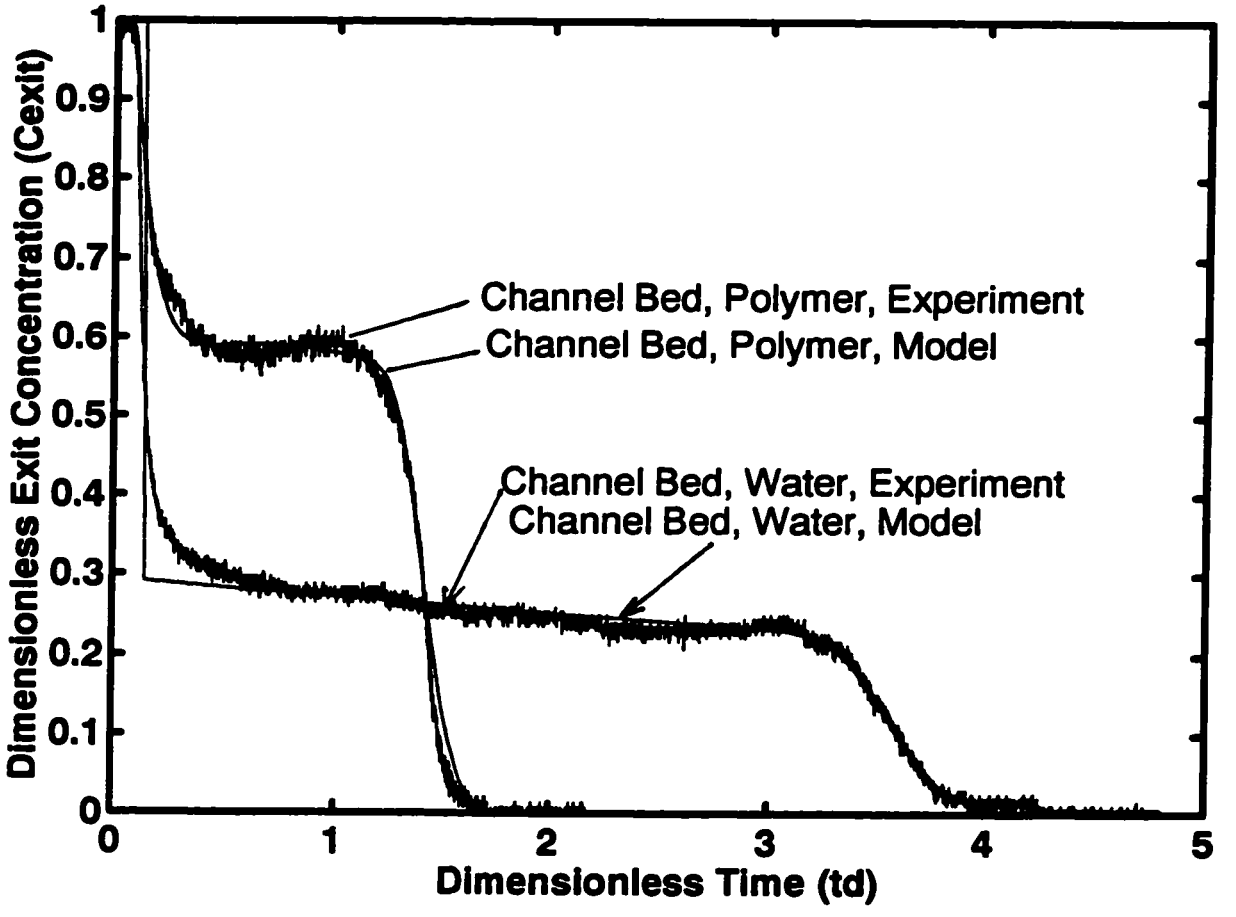

Figure 6.7 Comparison of experimental breakthrough curves with those predicted by model that considers the model channel bed a combination of two communicating homogeneous beds connected in parallel.

absent, i.e. both α_j and γ_j were zero, and the exit concentration in the channel was calculated by Equation (6.35).

Figure 6.7 shows the comparison of experimental and computed breakthrough curves for the displacement of MBL with either water or the polymer solution in

the model channel bed. Both the channel and the annulus in the model channel bed were divided into ten identical cells. The values of ψ and β_j for the calculation of parameters α_j and γ_j in Equations (6.64) and (6.65) respectively during displacement with water were 0.005 and 0.53 respectively. For displacement with water, Peclet number of the front in the annulus was 690 and displacement in the channel was assumed to be plug flow. The values ψ and β_j for calculation of parameters α_j and γ_j in Equations (6.64) and (6.65) respectively and that of λ in Equation (6.60) were 0.005, 0.53, and 253 respectively during displacement with the polymer solution. The Peclet numbers of the front in the annulus and in the channel were 5.14 and 435 respectively for displacement with the polymer solution. Initially, only the parameter α_j was included in the communicating channel bed model, neglecting diffusive flow of lignin, i.e., $\gamma_j = 0$. However, the communicating channel bed model could not predict the breakthrough curves in Figure 6.7. In the absence of diffusive flow of lignin, i.e. when γ_j=0, an increase in the parameter α_j resulted in a steady lowering of the exit concentration of lignin in the channel bed due to excessive dilution of the resulting mixture at the bed exit by excessive flow of fresh water into the channel from the annulus due to the presence of high cross flow.

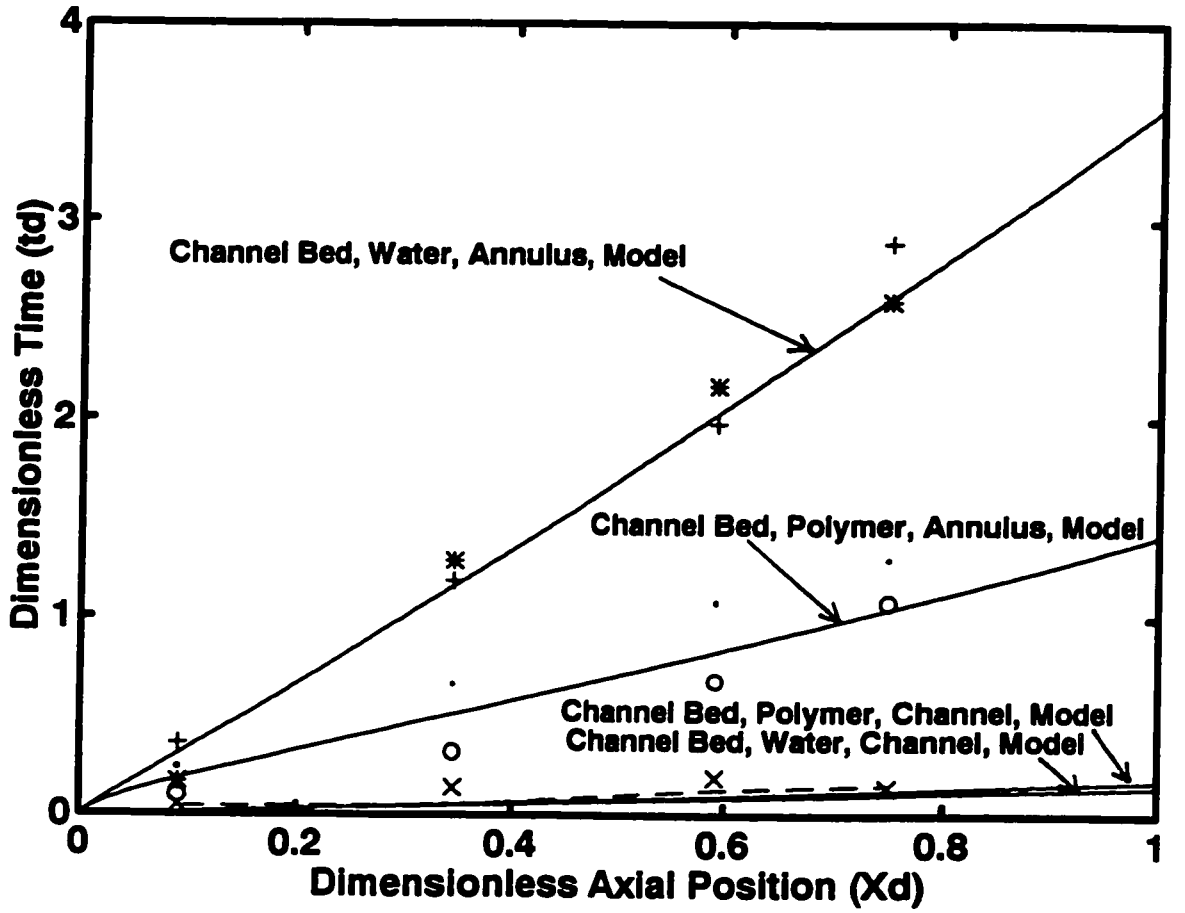

Figure 6.8 Comparison of time required by front to reach an axial position in bed as measured by probes with those predicted by communicating channel bed model. Location of probes are, channel bed, water, (+) periphery, (*) interface, (x) center; channel bed, polymer, (.) periphery; (o) interface, (---) center.

Figure 6.8 shows the comparison of computed positions of front in the annulus, nx_{df}, and that in channel, x_{dc}, against dimensionless time, t_d, with those measured by probes placed at different axial and radial locations inside the bed,

as described in Chapter 5, during displacement with water and the polymer solution. Figure 6.8 demonstrates that the time required by the front in the annulus to reach any axial position inside the channel bed is intermediate between those measured by probes at the periphery and interface. During displacement with either water or the polymer solution, the time required by the front in the channel as predicted by the model in Figure 6.8 agree well with those measured by the probes at the center of the channel bed. Figure 6.8 also demonstrates that dimensionless time, t_d, required by the front in the annulus to pass a fixed axial position in the annulus during displacement with the polymer solution is nearly half of that required by the front during displacement with water in the model channel bed.

Figure 6.9 and Figure 6.10 demonstrate the computed profiles of instantaneous and cumulative volumes of the MBL solution that was transferred laterally expressed as the fraction of void volume of the annulus against dimensionless time, t_d, during displacement with either water or the polymer solution. Figure 6.9 also demonstrates that volume of the MBL that was transferred laterally reaches a maximum approximately corresponding to the breakthrough time in the center channel in both cases. After reaching the maximum, the volume of MBL transferred laterally decreases steadily to zero during displacement with water, whereas during displacement with the polymer solution, it decreases rapidly after breakthrough in the center channel and then

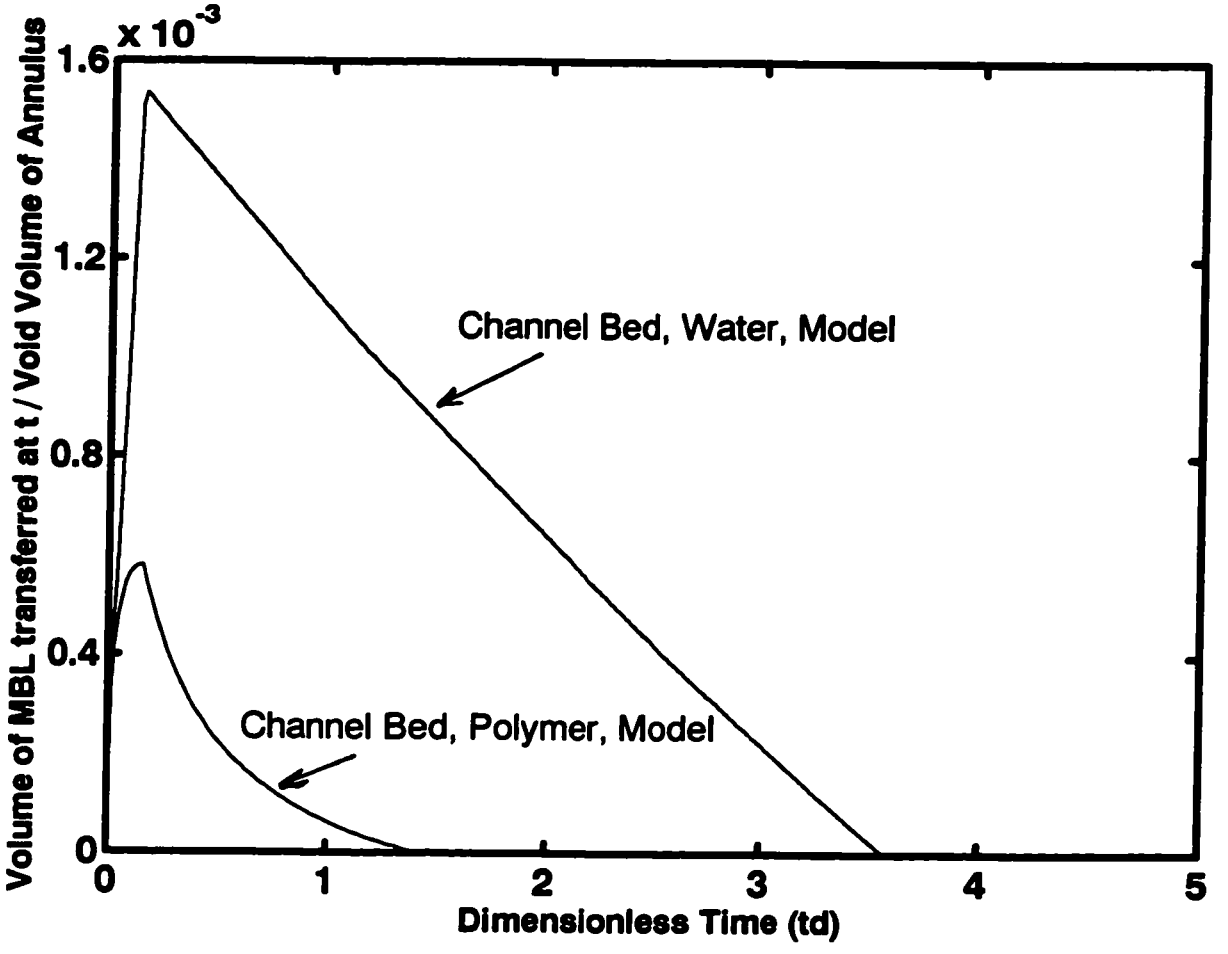

Figure 6.9 Variation of instantaneous lateral flow of volume of MBL expressed as fraction of void volume of annulus against dimensionless time predicted by communicating channel bed model.

slowly near the end of displacement. Figure 6.10 demonstrates that the cumulative volume of MBL transferred laterally increases steadily during the displacement for both cases.

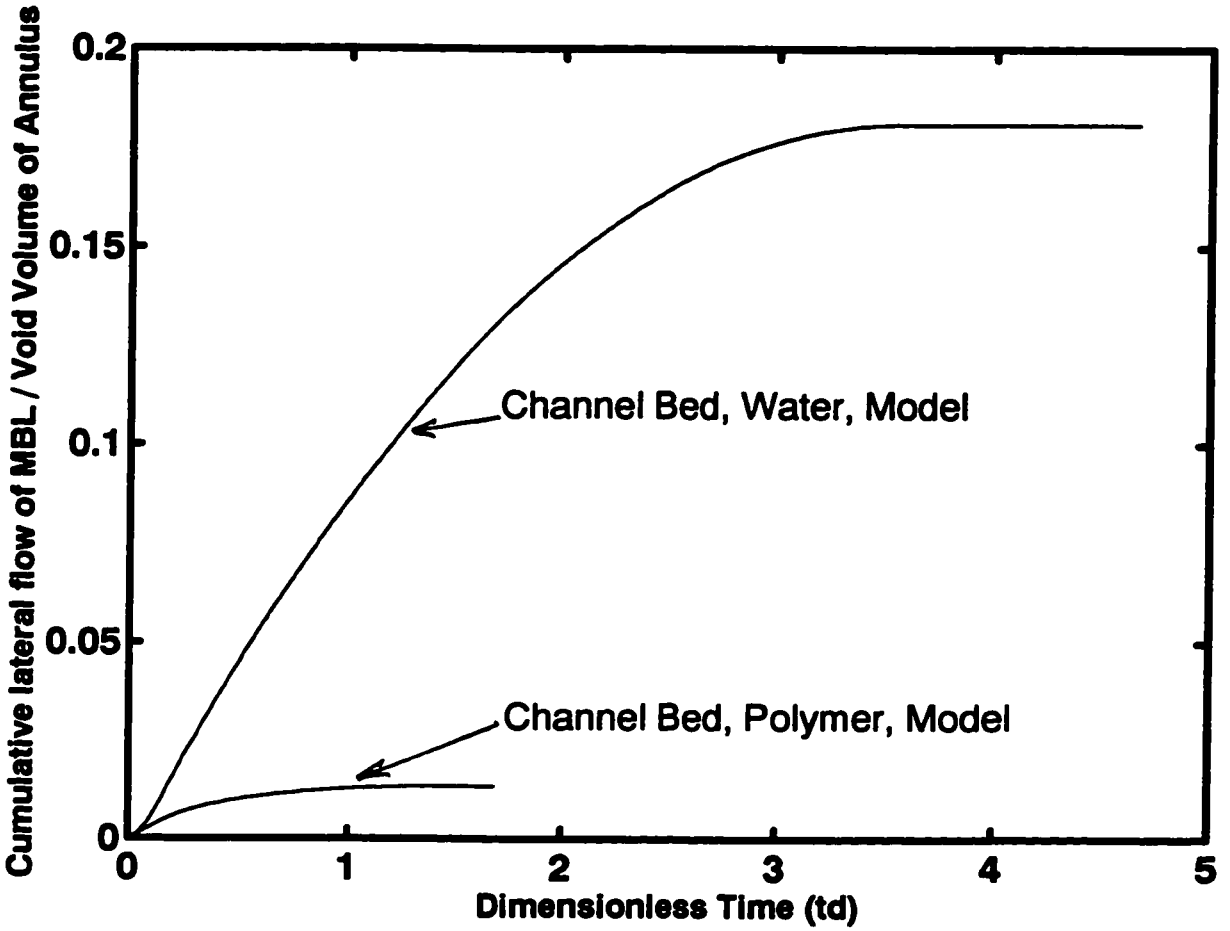

Figure 6.10 Variation of cumulative lateral flow of volume of MBL expressed as fraction of void volume of annulus against dimensionless time predicted by communicating channel bed model.

However, Figure 6.10 shows that at the end of displacement, the cumulative volume of MBL that is transferred laterally is higher for displacement with water than that with polymer solution. The possible reasons for the above observations are discussed in section 6.2.2.6.

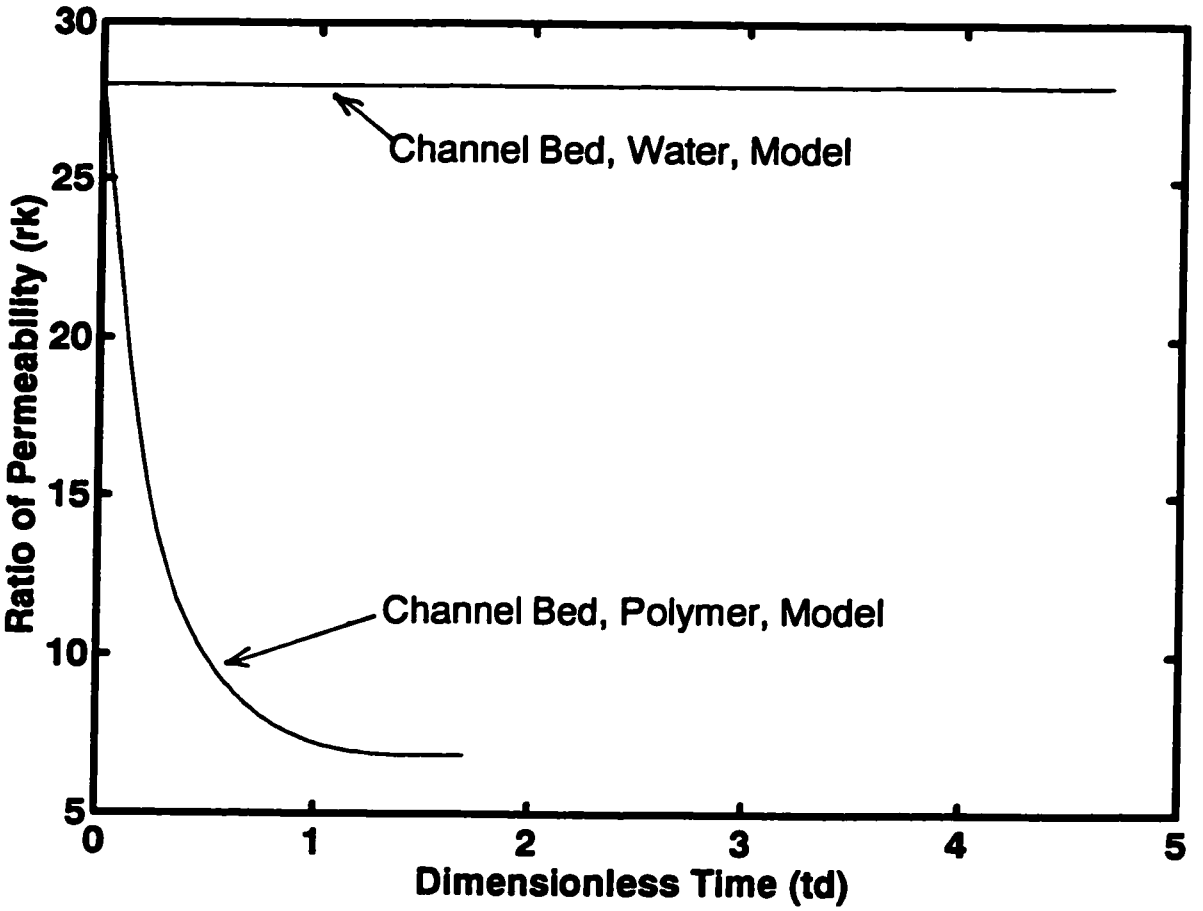

Figure 6.11 Variation of ratio of permeability, r_k, against dimensionless time predicted by communicating channel bed model.

The variations of the ratio of permeability of the center channel to that of the annulus, r_k, with dimensionless time, t_d, during displacement with either water or the polymer solution are shown in Figure 6.11. Since no precipitate formed in the channel during displacement with water, r_k remains unchanged in

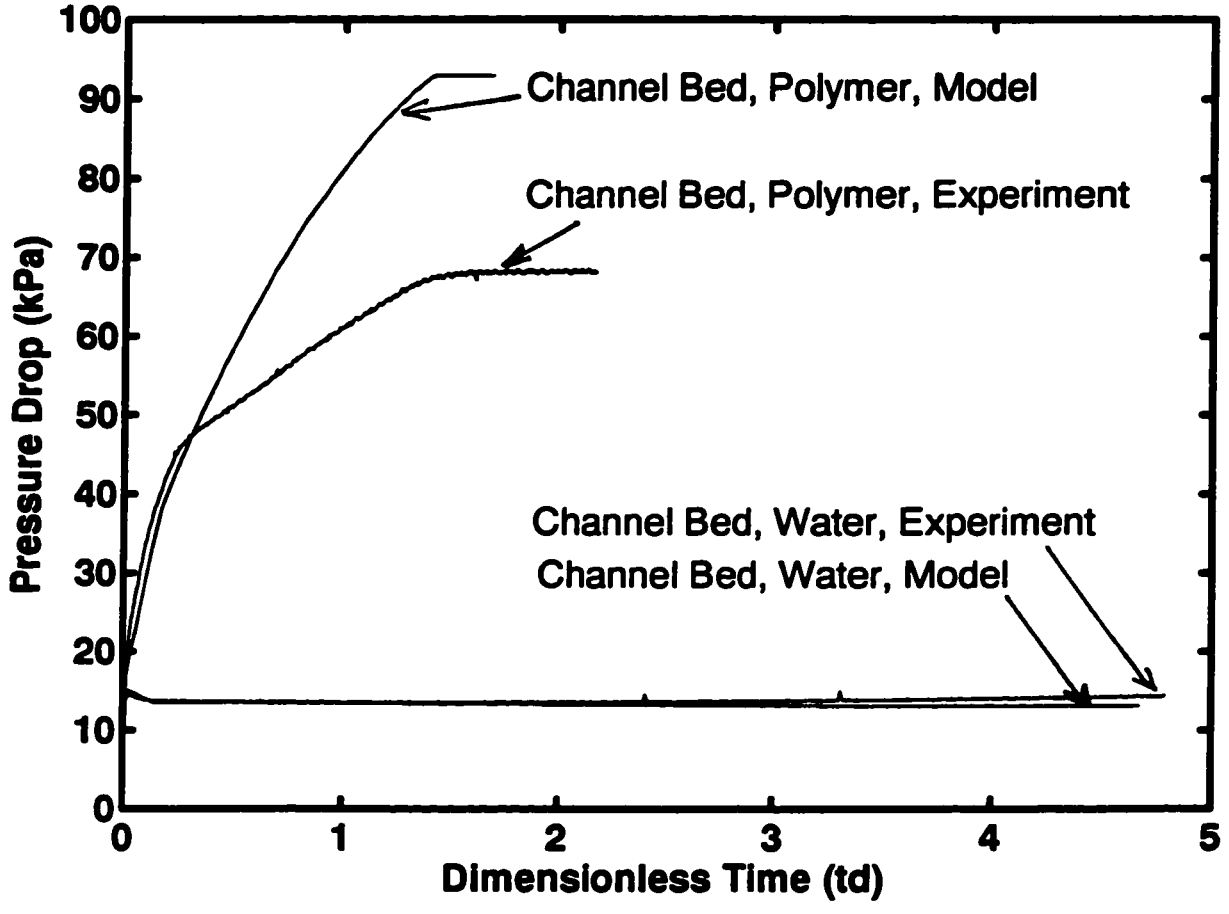

Figure 6.12 Comparison of experimental pressure drop profiles with those predicted by communicating channel bed model.

Figure 6.11 during displacement with water. However, during displacement with the polymer solution, r_k decreases rapidly at the start of displacement and gradually levels off near the end of displacement.

Figure 6.12 shows the comparison of the computed and experimental pressure drop profiles across the channel bed against dimensionless time, t_d,

during displacement with either water or the polymer solution. Figure 6.12 demonstrates that with the advancement of the displacement with water, experimental pressure drop was around 10% greater than that predicted by the model. However, during displacement with the polymer solution, Figure 6.12 demonstrates that at the end of displacement, computed pressure drop is around 30% higher than that obtained experimentally.

6.2.2.6 Discussion

Figure 6.7 demonstrates that the computed and experimental breakthrough curves agree well except in the region of breakthrough in the center channel during displacement with water. The deviation is probably due to the assumption of plug flow displacement of the MBL with water in the channel that does not include interfacial mixing in the front in the channel. A comparison of computed breakthrough curves in the non-communicating and communicating channel beds in Figure 6.2 and Figure 6.7 respectively reveals that lateral flow of lignin in the communicating channel bed causes higher concentration of lignin in the effluent than that in the non-communicating channel bed during displacement with water. As a result, displacement in the channel bed with communication between the channel and the annulus was faster than that in the non-communicating channel bed.

The computed and experimental breakthrough curves show good agreement during displacement with the polymer solution in the model channel bed as shown in Figure 6.7. When the polymer solution was used instead of water as the displacing phase, lignin transferred from the annulus to the channel by both convective cross flow and diffusive flow reacted with the fresh polymer in the channel and pore throats in the center channel were plugged with precipitate, resulting in the reduction of the ratio of permeability of the channel to the annulus r_k as demonstrated in Figure 6.11. With the reduction of the ratio of permeability, $r_{k,}$ in the channel bed during the course of displacement with the polymer solution, the channel bed was modified towards a homogeneous bed and channeling of fluid through the center channel was reduced, resulting in enhanced displacement of MBL from the channel bed. Initially, the reduction in the porosity of the center channel was calculated from the volume of precipitate that formed in the channel and the corresponding decrease in the permeability of the center channel was calculated using Equation (6.61). However, the reduction of the porosity of center channel calculated from the volume of precipitate formed in the channel was not sufficient to predict the nature of the breakthrough curve during displacement in the channel bed with the polymer solution. Consequently, the pore plugging model of McCune et al., 1973 was employed to account for the reduction in the permeability of the center channel with the precipitate.

The decrease in the rate of reduction of the ratio of permeability, r_k, during displacement with the polymer solution as shown in Figure 6.11, was due to the decreasing rate of lateral transfer of lignin into the channel, shown in Figure 6.9. At the beginning of displacement with the polymer solution, the channel was relatively free of precipitate and a greater mass of lignin was transferred to the channel, causing more formation of precipitate and hence more reduction in the porosity of the channel, ε_c, and the permeability ratio, r_k. With the advancement of displacement with the polymer solution, the channel bed behaved more like a homogeneous bed, since the ratio of permeability, r_k, decreased with time. Consequently, the rate of lateral exchange of lignin decreased, resulting in the decrease in the rate of reduction of porosity of the channel, ε_c, and the permeability ratio, r_k. Since the instantaneous rate of transfer of lignin into the channel decreased as the displacement in the channel bed proceeded with the polymer solution, the cumulative amount of transferred lignin also decreased with time, explaining the lower cumulative amount of lignin transferred at the end of displacement with the polymer solution than that with water, as shown in Figure 6.10.

Since the front both in the annulus and in the channel in the channel bed is assumed to be flat and represents 50% change in the concentration of a species in the interface between the MBL and the displacing phase, computed

dimensionless times, t_d, required by the front to pass any axial position in the annulus can be expected to be intermediate between those measured by the probes at the periphery and interface at that axial position as shown in Figure 6.8. However, at any axial position inside the channel bed, the model successfully predicts the values of dimensionless time required by the front in the annulus during displacement with water to be approximately two times higher than those required by the front when the polymer solution is used as the displacing phase. Figure 6.8 also demonstrates that the model is able to predict successfully the position of the front in the channel against dimensionless time during displacement of the MBL with either water or the polymer solution. A comparison of Figure 6.4 and Figure 6.8 further reveals that the front in the annulus moves faster in a communicating channel bed than that in a non-communicating channel bed during displacement with water. This also implies that presence of communication between the more permeable channel and less permeable annulus caused faster displacement in a communicating channel bed than that in a non-communicating channel bed during displacement with water.

Figure 6.12 demonstrates that the computed and experimental pressure drop profiles agree well with each other during displacement of the MBL with water in the channel bed. The initial decrease in the pressure drop during displacement with water was the result of displacement of the more viscous MBL solution by the less viscous water from the model channel bed. Higher (around

10%) experimental pressure drop than that computed from the model near the end of displacement with water was probably due to the drift in the pressure transducer as the measured pressure was near the lower extreme of the range (0 to 172 kPa) of the transducer. Another potential reason for the higher experimental pressure drop was the migration of fine beads from the annulus to the channel during displacement with water as observed in flow visualization experiments, described in detail in Chapter 3. Migration and rearrangement of beads at the interface between the channel and annulus might have created a mixed region that extended into both the channel and the annulus, resulting in the reduction of permeability of the channel bed.

Figure 6.12 also shows that during displacement with the polymer solution, the computed and experimental pressure drops agree well with each other during breakthrough in the center channel. However, at the end of breakthrough in the center channel, the experimental pressure drop was higher than that predicted by the model. This was probably due to the entrainment of additional precipitate into the channel bed from the entrance of bed, where mixing of lignin and polymer was difficult to avoid. The higher (around 30% at the end of displacement) computed pressure drop after breakthrough in the center channel till it reached a steady state than that obtained experimentally was probably due to several reasons, which are discussed in the following section.

(a) The model assumes that the interface between the MBL and the polymer solution is sharp and that the change in viscosity from the viscosity of the polymer solution to that of the MBL across the interface is abrupt. However, in reality, due to the presence of interfacial mixing of the MBL and the polymer solution across the interface, there would be a gradient in viscosity across the interface that would not be sharp. The presence of a gradient in viscosity across the interface might have reduced the pressure drop across the model bed compared to that predicted by the model.

(b) It is assumed in the model that lignin transferred into the center channel due to lateral exchange forms precipitate and reduces the porosity and permeability of the center channel uniformly throughout its volume. However, in flow visualization experiments described in Chapter 3, it was observed that more and more area at the bottom of center channel retained precipitate, leaving a precipitate-free conical shaped zone in the center channel with its apex at the center of the bottom of the center channel. Nonuniform distribution of precipitate both along the length and radius of the center channel might have caused the mismatch between the experimental and computed values of pressure drop.

(c) Continuous loss of precipitate from the channel bed was observed during displacement of MBL with the polymer solution. However, the model assumes that all of the precipitate is distributed uniformly throughout the center channel. Continuous loss of precipitate from the model channel bed and a different mechanism of pore plugging might have caused lower experimental pressure drop than that computed by the model.

6.3 Conclusions

(1) The non-communicating channel bed model that considers the model channel bed a combination of two separate homogeneous non-communicating beds connected in parallel can predict successfully the breakthrough curve, pressure drop profile, and profile of interstitial velocity along the length of bed during displacement of MBL from a homogeneous bed of fine beads using either water or the polymer solution.

(2) The non-communicating channel bed model cannot predict the breakthrough curve and profile of interstitial velocity in the annulus during displacement of MBL in a channel bed with water. The mismatch between the computed and experimental breakthrough curves during displacement in a channel bed with

water is ascribed to the communication between the channel and the annulus that was observed in flow visualization experiments described in Chapter 3.

(3) The non-communicating channel bed model is modified to a communicating channel bed model using a network of interconnected communicating zones originally proposed by Van de Vusse (1962). The model allows convective flow of MBL and diffusive flow of lignin from a zone in the annulus to an adjacent zone in the channel. Two adjustable parameters are needed in the model to describe the displacement of MBL with water in a channel bed. The model needs three adjustable parameters to describe the process of displacement in a channel bed with the polymer solution when pore throats in the center channel were plugged with precipitate formed by the reaction of lignin and polymer.

(4) The communicating channel bed model can successfully predict the breakthrough curve, pressure drop profile, and profiles of interstitial velocities in the annulus and in the channel during displacement of MBL in a channel bed with water.

(5) The communicating channel bed model can also predict successfully breakthrough curve and profiles of interstitial velocities in the annulus and in the channel during displacement of MBL in a channel bed with the polymer solution.

However, after breakthrough in the center channel during displacement with the polymer solution in a channel bed, pressure drop predicted by the model is higher than that obtained experimentally. The deviation between the computed and experimental pressure drops has been attributed to the limitations of the model.

(6) The communicating channel bed model successfully demonstrates the enhancement of displacement of MBL in a model channel bed when the polymer solution was used as the displacing phase instead of water. The model predicts interstitial velocity of the front in the annulus in a channel bed during displacement with the polymer solution to be approximately two times higher than that when water was used as the displacing phase.

List of Variables

A	Cross sectional area of bed, m^2.
A_c	Cross sectional area of column of coarse beads, m^2.
A_f	Cross sectional area of column of fine beads, m^2.
A_j	Interfacial area in Equation (6.42), m^2.
boundary(j-1)	Upper boundary of a cell in Figure 6.6, dimensionless.
boundary(j)	Lower boundary of a cell in Figure 6.6, dimensionless.
B	Constant in Equation (6.42), m/s.
c	Concentration of solute in Equation (6.28), Kg/m^3.
c_e	Concentration of solute in fluid at exit of bed, Kg/m^3.
c_f	Concentration of solute in incoming fluid, Kg/m^3.
c_o	Initial concentration of solute in bed, Kg/m^3.
C_0	Concentration of lignin in displacing phase, dimensionless.
C	Concentration of solute in Equation (6.32), dimensionless.
C_{exit}	Exit concentration of lignin in the bed, dimensionless.
$C_{c,\,exit}$	Exit concentration of lignin in column of coarse beads, dimensionless.
$C_{c,j}$	Concentration of lignin in the stream coming out of a cell in column of coarse beads, dimensionless.
$C_{f,\,exit}$	Exit concentration of lignin in column of fine beads, dimensionless.
$C_{f,j}$	Concentration of lignin in the stream coming out of a cell in column of fine beads, dimensionless.
d	Diameter of cylindrical column, m.
d_p	Diameter of particle, m.
d_{pc}	Diameter of coarse particle, m.
$d_{pc,e}$	Equivalent diameter of coarse particle, m.
d_{pf}	Diameter of fine particle, m.
$d_{p,50}$	Particle diameter in 50% cut in Equation (6.37), m.
D_L	Longitudinal dispersion coefficient based on length of bed, L, m^2/s.
D_p	Longitudinal dispersion coefficient based on particle dia.,d_p, m^2/s.
j	Index in Figure 6.5, dimensionless.
k	Permeability of bed, m^2.
k_c	Initial permeability of column of coarse beads, m^2.
$k_{c,app}$	New apparent permeability of column of coarse beads, m^2.
k_f	Permeability of column of fine beads, m^2.

K	Rate constant in Equation (6.56), $m^3/(Kg.s)$.
K'	Rate constant in Equation (6.57), s^{-1}.
L	Length of bed, m.
[Lignin]	Concentration of lignin in Equation (6.56), Kg/m^3.
M	Mobility ratio defined in Equation (6.10).
n	Number of cells in Figure 6.5, dimensionless.
p	A factor in Equation (6.41), Kg/m^3.
P	Factor defined in Equation (6.34).
Pe_L	Peclet number based on length of bed, dimensionless.
[Polymer]	Concentration of polymer in Equation (6.56), Kg/m^3.
[Precipitate]	Concentration of precipitate in Equation (6.56), Kg/m^3.
ΔP	Pressure drop across bed, Pa.
ΔP_c	Pressure drop across column of coarse beads, Pa.
ΔP_f	Pressure drop across column of fine beads, Pa.
Q	Superficial flow rate of displacing phase, m^3/s.
Q_c	Superficial flow rate in column of coarse beads, m^3/s.
$Q_{c,j}$	Superficial flow rate out of a cell in column of coarse beads, m^3/s.
Q_f	Superficial flow rate in column of fine beads, m^3/s.
$Q_{f,j}$	Superficial flow rate out of a cell in column of fine beads, m^3/s.
r_{cf}	Heterogeneity contrast in Equation (6.9), dimensionless.
r_k	Initial permeability ratio in Equation (6.2), dimensionless.
t	Time, s.
Δt	Small change in time, s.
t_d	Time defined in Equation (6.25), dimensionless.
$t_{d,50\%}$	Breakthrough time in Figure 5.3 (Chapter 5), dimensionless.
t_{dc}	Time defined in Equation (6.26), dimensionless.
t_{df}	Time defined in Equation (6.27), dimensionless.
u_c	Superficial velocity in column of coarse beads, m/s.
u_f	Superficial velocity in column of fine beads, m/s.
v	Interstitial velocity, m/s.
v_c	Interstitial velocity in column of coarse beads, m/s.
v_f	Interstitial velocity in column of fine beads, m/s.
$V_{c,j,j-1}$	Volume of cell in column of coarse beads in Figure 6.6, m^3.
x	Position of front from top of bed, m
x_d	Dimensionless position of front, dimensionless.
x_{dc}	Position of front in column of coarse beads, dimensionless.
Δx_{dc}	Small increment in x_{dc}, dimensionless.

x_{df}	Position of front in column of fine beads, dimensionless.
x^0_{df}	Position of front in column of fine beads at breakthrough in column of coarse beads in Equation (6.12), dimensionless.
nx_{df}	Corrected position of front in column of fine beads, dimensionless.
y	A term in Equation (6.36), dimensionless.
z	A term in Equation (6.36), dimensionless.

Subscripts

c	Column of coarse beads.
f	Column of fine beads.

Greek Letters

α_j	Adjustable parameter in Equation (6.40), dimensionless.
β_j	Adjustable parameter defined in Equation (6.44), m^3/s.
δ	Constant in Equation (6.38), dimensionless.
ε	Initial porosity of bed, dimensionless.
ε_{app}	New apparent porosity of channel bed, dimensionless.
ε_c	Initial porosity of column of coarse beads, dimensionless.
$\varepsilon_{c,app}$	New apparent porosity of column of coarse beads, dimensionless.
$\varepsilon_{c,old}$	Old porosity of column of coarse beads, dimensionless.
ε_f	Initial porosity of column of fine beads, dimensionless.
γ_j	Adjustable parameter defined in Equation (6.65), m^3/s.
λ	Adjustable parameter in Equation (6.60), s^{-1}.
μ	Dynamic viscosity of fluid, Pa.s.
μ_d	Dynamic viscosity of displacing phase, Pa.s.
μ_r	Dynamic viscosity of resident phase, Pa.s.
ν	Kinematic viscosity, m^2/s.
ρ_d	Density of displacing phase, Kg/m^3.
$\rho_{Precipitate}$	Density of precipitate, Kg/m^3.
ρ_r	Density of resident phase, Kg/m^3.
τ	Constant in Equation (6.60), dimensionless.
ψ	Adjustable parameter in Equation (6.64), dimensionless.

Abbreviations

MBL	Model black liquor.

References:

Blackwell, R. J., J. R. Rayne, and W. M. Terry, Trans AIME, **216**, 1 (1959).

Brenner, H., "The Diffusion Model of Longitudinal Mixing in Beds of Finite Length. Numerical Values," Chem. Eng. Sci., **17**, 229 (1962).

Brucato, A., F. Magelli, M. Nocentini, and L. Rizzuti, "An Application of the Network-of-Zones Model to Solids Suspension in Multiple Impeller Mixers," Trans IChemE, **69(A)**, 43 (1990).

Brown, D. E. and D. J. Halstea, "Liquid Phase Mixing Model for Stirred Gas-Liquid Contactor," Chem. Eng. Sci., **34**, 853 (1979).

Crotogino, R. H., N. A. Poirier, and D. T. Trinh, "The Principles of Pulp Washing," Tappi, **70**, 95(1987).

Danckwerts, P. V., Chem. Eng. Sci., **6**, 227 (1957).

De, D., "Reactive Polymer Enhanced Miscible Displacement in Porous Media," Chapter 4 in this thesis, Chem. Eng. Dept., McMaster University, Hamilton, Canada (1996).

De, D., "Reactive Polymer Enhanced Miscible Displacement in Porous Media," Chapter 5 in this thesis, Chem. Eng. Dept., McMaster University, Hamilton, Canada (1996).

Dykstra, H. and R. L. Parsons, " The Prediction of Oil Recovery by Waterflood," Secondary Recovery of Oil in the United States, Principles and Practice, 2nd ed., American Petroleum Institute, 160-174 (1950).

Harleman D. R. F., P. F. Mehlhorn, and R. R. Rumer, "Dispersion-Permeability Correlation in Porous Media," Proc. ASCE J. Hydr. Div., **67**, 67 (1963).

Hofman, J. A. M. H., and H. N. Stein, " Permeability Reduction of Porous Media on Transport of Emulsions through them," Colloid and Surfaces, **61**, 317 (1991).

Khang, S., J. and O. Levenspiel, "New Scale-up and Design Method for Stirrer Agitated Batch Mixing Vessels," Chem. Eng. Sci., **31**, 569 (1976)

Knysh, P. and R. Mann, "Utility of Networks of Interconnected Backmixed Zones to represent Mixing in a Closed Stirred Vessel," IChemE Symp Ser, **No. 89**, 127 (1984).

Lake, L.W., Enhanced Oil Recovery, Prentice Hall, New Jersey (1989).

Lappan, R., A. Hrymak, and R. H. Pelton, Unpublished Work, Dept. of Chem. Eng., McMaster University, Hamilton, Canada (1996).

Lee, P. F., "Channeling and Displacement Washing of Wood Pulp Fiber Pads," Tappi, **67(11)**, 100 (1984).

Li, P., and R. H. Pelton, "Wood pulp washing: 2. Displacement Washing of Aqueous Lignin from Model Beds with Cationic Polymer solutions," Colloids and Surfaces, **64**, 223 (1992).

Mann, R. and P. Mavros, "Analysis of Unsteady Tracer Dispersion and Mixing in a Stirred Vessel using Interconnected Networks of Ideal Flow Zones," Proc 4th Europ Conf Mix, Apr 27-29, **B3**, 35 (1982).

Mann, R., P. Ying, K. Baker, and R. Edwards, "Mixing of Inert and Reactive Tracers in a Twin-Impeller Stirred Vessel," AIChE Annual Meeting, Miami Beach, Florida, Paper No. 109a, October (1992).

McCabe, W. L., J. C. Smith, and P. Harriot, Unit Operations of Chemical Engineering, 4 th ed., McGraw-Hill, New York (1985).

McCool, C. S., D. W. Green, and G. P. Willhite, "Permeability Reduction Mechanisms Involved in *in-situ* Gelation of a Polyacrylamide/Chromium (VI)/ Thiourea system," SPERE, 77-83, Trans AIME, **291**, February (1991).

McCune, C. C., and H. S. Fogler, 74th National Meeting of AIChE, New Orleans, March 11-15 (1973).

Miller, M. J., and H. S. Fogler., "A Mechanistic Investigation of Waterflood Diversion using Foamed Gels," SPE Production & Facilities, **63**, February (1995).

Pelton, R. H., and B. Grosse, "Polymer Enhanced Displacement of Lignin Solution from Model Packed Beds," JPPS, **20(3)**, March (1994).

Sasakura, T., Y. Kato, S. Yamamuro, and N. Ohi, "Mixing Process in a Stirred Vessel," Int. Chem. Eng., **20**, 251 (1980).

Tang, R. W., Behrens, R. A., and Emanuel, A. S.,"Reservoir Studies using Geostatistics to Forecast Performance," SPE 18432, SPE symposium on Reservoir Simulation, Houston, 321 (1989).

Van de Vusse, J. G., "A New Model for the Stirred Tank Reactor," Chem. Eng. Sci., **17**, 507 (1962).

Wang, Y. and R. Mann, "Partial Segregation in Stirred Batch Reactors," Trans IChemE, **70**, 282 (1992).

Appendix A

A.1 Conductivity Probes

Twelve conductivity probes were fabricated for measuring the instantaneous conductivity of fluid flowing through a porous bed. The photograph and schematic of a probe are given in Figure A. 1.

A probe consisted of a stainless steel wire of diameter 0.04 cm inserted into a stainless steel tube of outer and inner diameters of 0.165 and 0.117 cm respectively, shown in Figure A. 1. The wire and the tube were insulated from each other by wrapping Scotch® electrical tape on the surface of the wire. The outer surface of the tube was also wrapped with insulating tape to minimize electrical contact between the tube and surrounding fluid. The part of wire that protruded out of the tube and the sharpened end of the tube were kept uninsulated to facilitate electrical contact between them and the flowing fluid. A nylon Swagelock® and a rubber gasket inside the Swagelock® held the wire and tube together and prevented leakage of fluid through the probes during experiments. Electrical wires soldered to the tube connected the probes to the channels of multichannel conductivity apparatus.

(a) Photograph of a conductivity probe

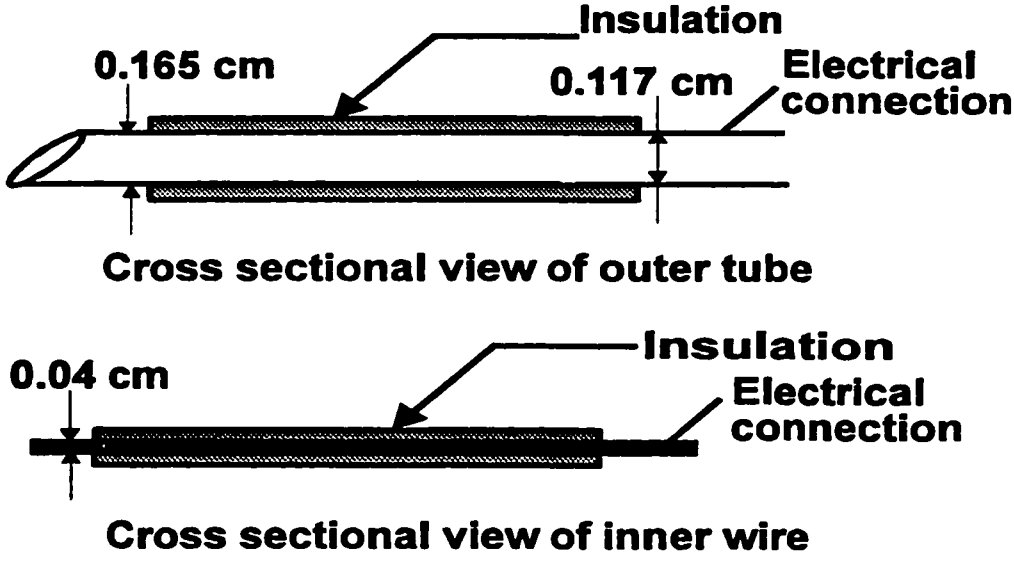

(b) Schematic of a conductivity probe

Figure A. 1 Photograph and schematic of a conductivity probe.

A.2 Multichannel Conductivity Apparatus

The multichannel conductivity apparatus built by S.E.E.S (Science and Engineering Electronics Shop), McMaster University was an assembly of twelve conductivity measurement units. Aluminum boxes denoted as amplifier banks A and B encased six of these units each. Figure A. 2 shows the photograph of one of these amplifier banks. Conductivity probes, as described in section A.1, were connected to these units stacked inside the amplifier banks through circular slots called channels.

The principle of measuring conductivity of each unit is depicted in Figure A. 3. An AC signal source of frequency 10 kHz excited the load conductance (G_{cell}) connected in series with a known reference conductance (G_{ref}). Voltage V_1 across reference conductance (G_{ref}) and load conductance (G_{cell}) and voltage V_2 across the load conductance (G_{cell}) were then measured by the A/D converter and stored in a computer. Another voltage, V_3, that corresponded to zero volt or a ground signal and compensated for DC shifts due to the use of amplifiers was measured by the A/D converter and stored in the computer. The conductance of the load was then calculated using the following equation:

$$G_{cell} = \frac{V_1 - V_2}{V_2 - V_3} G_{ref} \qquad \text{A. 1}$$

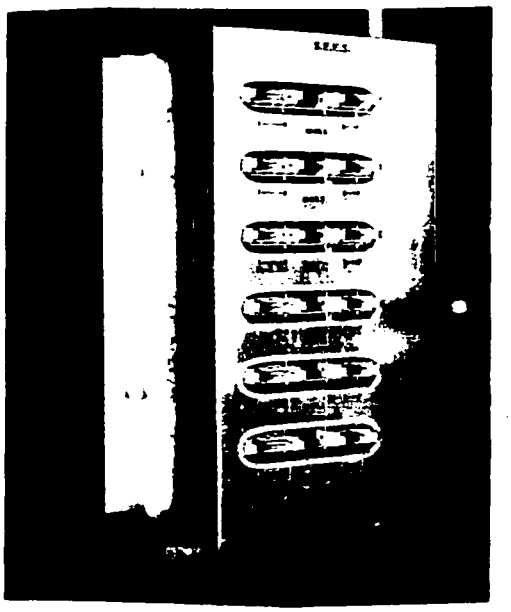

Figure A. 2 Photograph of an amplifier bank.

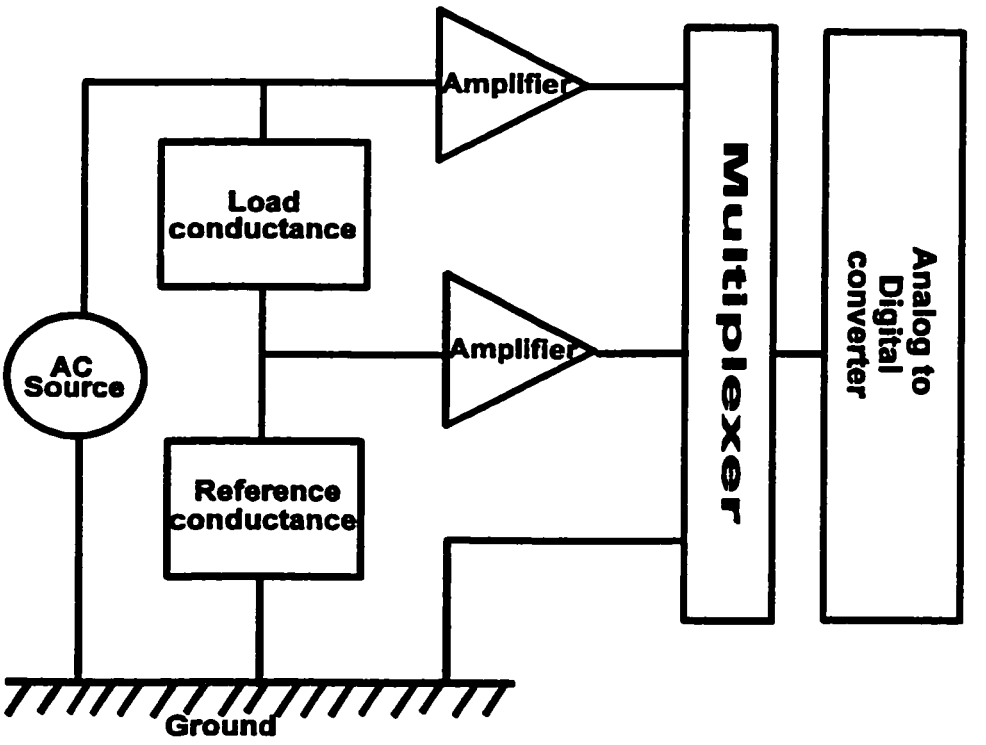

Figure A. 3 Schematic of principle of measuring conductivity in multichannel conductivity apparatus.

If $V_3 \approx 0$, Equation (A.1) can be simplified to give

$$G_{cell} = \frac{V_1 - V_2}{V_2} G_{ref} \qquad \text{A. 2}$$

Specifications of the range and reference conductance (G_{ref}) in each unit are given in Table A.1.

Table A.1 Specifications of a conductivity unit in Multichannel Conductivity Apparatus.

	Range 1	Range 2	Range 3	Range 4	Range 5	Range 6	Range 7	Range 8
G_{ref} (μS)	1000	200	100	20	10	5	2	1
Range (μS)	50 -10^4	10 -100	9 - 90	4 - 70	1 - 10	1 - 10	1 - 10	1 - 10

A.3 Calibration of Flow through Conductivity Cell

A.3.1 Batch Experiments

A stock MBL solution was diluted with water to produce ten diluted solutions. The percent concentration of MBL in these solutions decreased from 100 to 0 by a step of 10 and conductivity values were recorded. The concentration of lignin

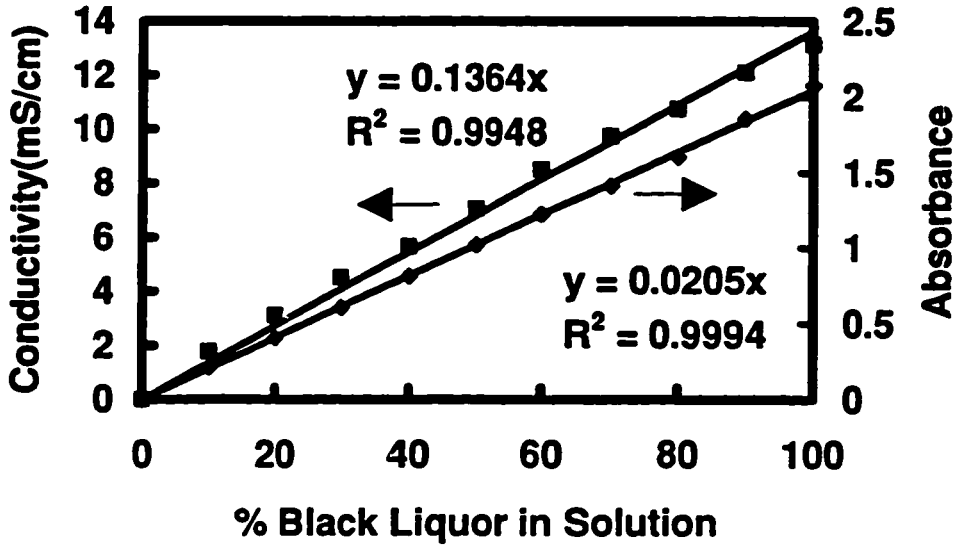

Figure A.4 Variation of conductivity and absorbance of lignin with dilution with water. Error bars (too small to be distinguished) represent 95% confidence intervals based on three replicate measurements.

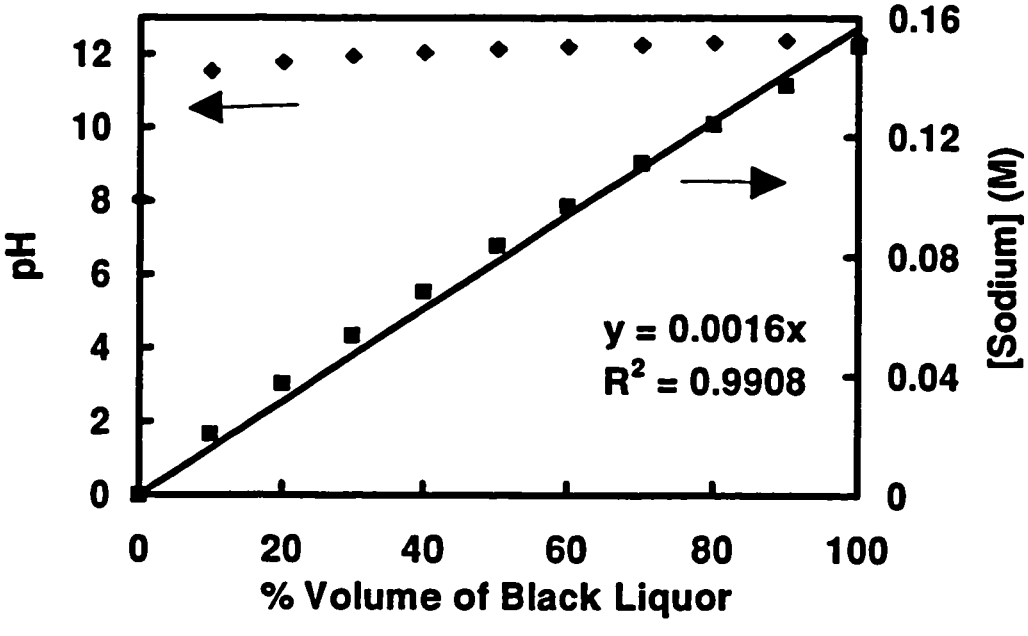

Figure A.5 Variation of pH and sodium ion concentration against dilution with water. Error bars (too small to be distinguished) represent 95% confidence intervals based on three replicate measurements.

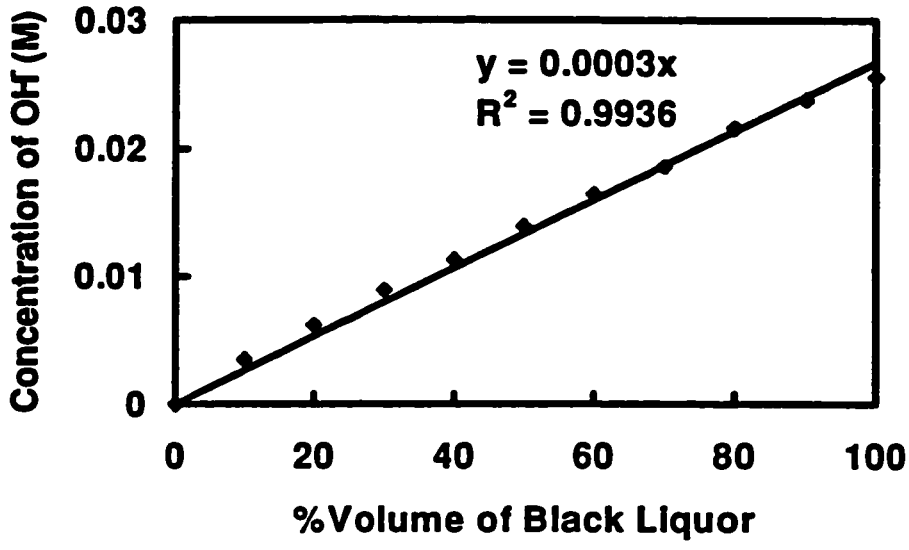

Figure A. 6 Hydroxyl ion concentration as a function of extent of dilution with water. Error bars (too small to be distinguished) represent 95% confidence intervals based on three replicate measurements.

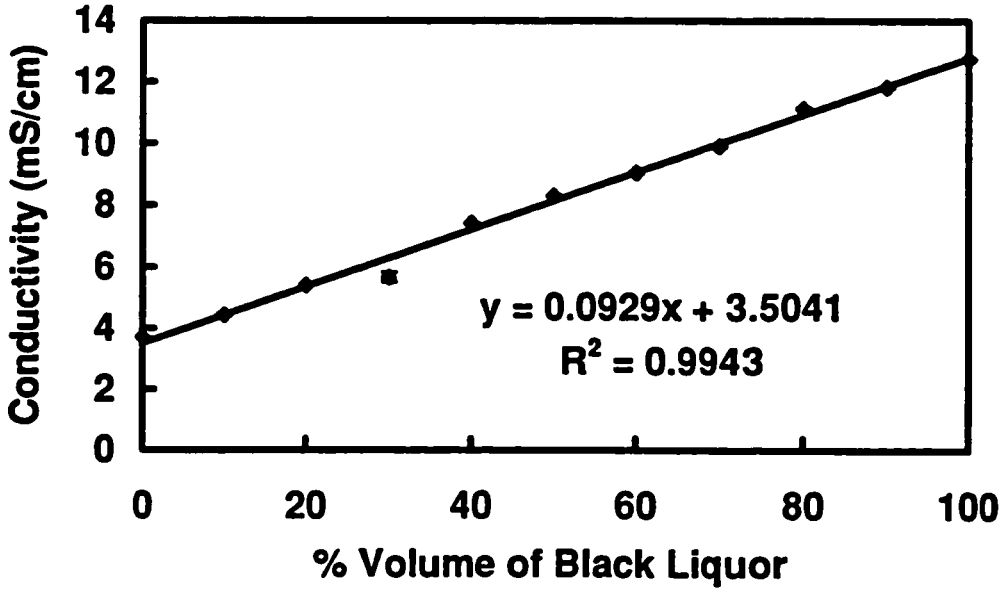

Figure A. 7 Conductivity of MBL as a function of extent of dilution with polymer. Error bars (too small to be distinguished) represent 95% confidence intervals based on three replicate measurements.

in each solution was measured by UV spectrophotoscopy at 280 nm. The pH of the diluted solutions was also measured. Sodium ion concentrations in the diluted solutions were measured with a Corning sodium combination electrode, catalogue no: 476138. Plots of conductivities and absorbances of lignin in the resultant diluted solutions against the extent of dilution produced linear calibration curves as shown in Figure A.4. Variation of pH and sodium ion concentrations of diluted solutions against degrees of dilution are shown in Figure A.5. Figure A. 6 shows the variation of hydroxyl ion concentration against dilution of MBL with water. It was observed that concentrations of sodium and hydroxyl ions varied linearly with dilution of MBL with water. Figure A. 7 shows the linear mode of variation of conductivity of the MBL solution when it was mixed with the polymer solution.

A.3.2 Semi-Batch Experiments

The mode of variation of conductivity of a MBL solution with continuous addition of either water or the polymer solution was tested in semi-batch experiments. The schematic of an experimental setup is shown in Figure A. 8. A known volume (V_0) of MBL was added to a beaker and water was added continuously at a constant flow rate (Q) to the beaker by a peristaltic pump. Conductivity of the diluted solution was recorded continuously against time (t) by

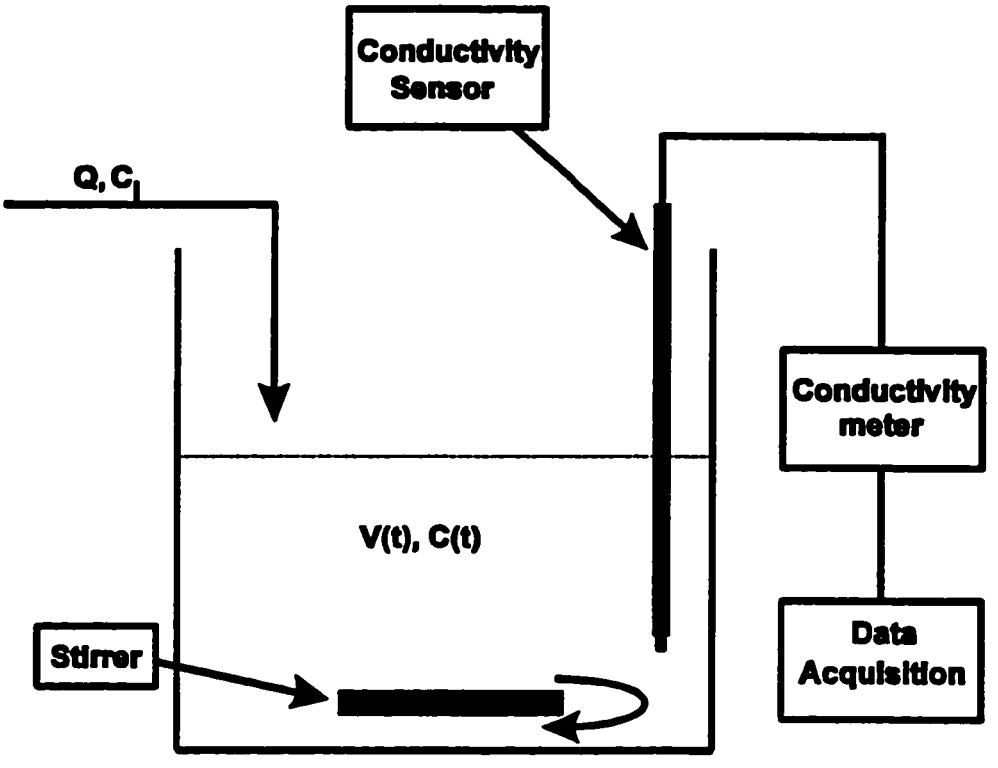

Figure A. 8 Schematic of the semi-batch dilution experiment.

the data acquisition system. A known volume (V_0) of the diluted solution produced at the end of the previous experiment was kept inside the beaker and the experiment was repeated with continuous addition of water. Five experiments were performed to span a broad range of dilution. Figure A. 9 shows the variation of conductivity of the solution during dilution with water against dilution ratio. Dilution ratio was the ratio of volume of water added (Qt) to the initial volume of MBL (V_0) and is expressed as

$$\text{Dilution ratio} = \frac{Qt}{V_0} \qquad \text{A. 3}$$

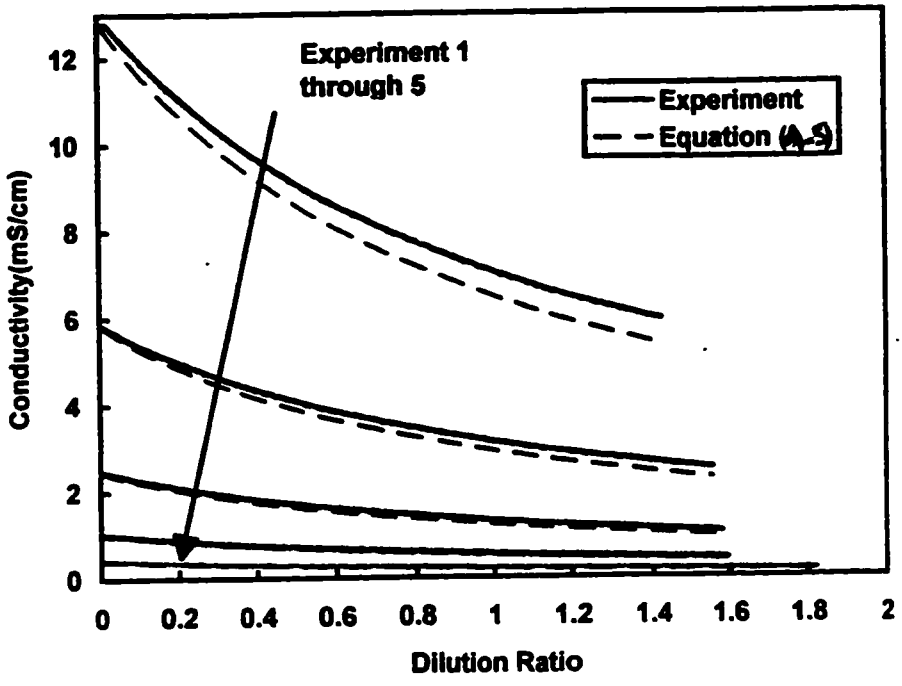

Figure A. 9 Variation of conductivity in the semi-batch experiment during dilution with water.

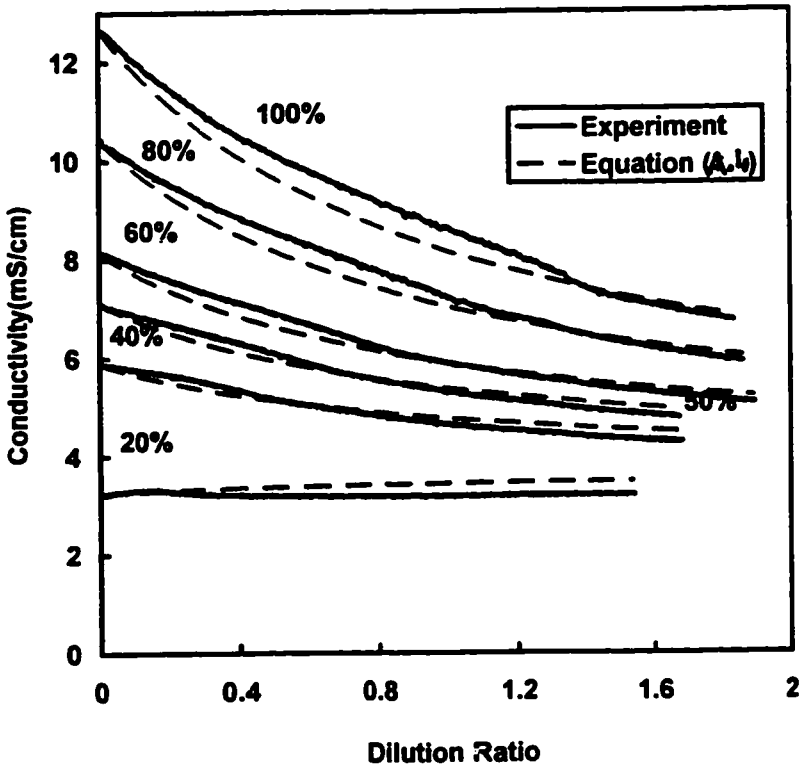

Figure A.10 Variation of conductivity in the semi-batch experiment during dilution with polymer solution.

Semi-batch experiments similar to those done with water were performed with continuous addition of the polymer solution to a known volume (V_0) of MBL in the beaker. Figure A.10 shows the variation of conductivity of the solution against dilution ratio for different initial stock solutions of MBL.

A mass balance on an species at any time (t) in the beaker shown in Figure A. 8 results

$$C = \left(\frac{C_0 - C_i}{1 + \frac{Qt}{V_0}} \right) + C_i \qquad \text{A. 4}$$

where C and V are the concentration of that species and the volume of the mixture at any time (t). C_i is the concentration of the species in the input stream and C_0 is the initial concentration of the species in solution in the beaker. Q is the volumetric flow rate of the incoming stream and V_0 is the initial volume of liquid in the beaker. For dilution with water, $C_i = 0$ and Equation (A.4) simplifies to be

$$C = \left(\frac{C_0}{1 + \frac{Qt}{V_0}} \right) \qquad \text{A. 5}$$

Figure A. 9 demonstrates that the change of conductivity of MBL solutions against dilution ratio was in tandem with that predicted by Equation

(A.5), spanning the entire range of dilution. During dilution with the polymer solution, negatively charged lignin macromolecules and positively charged polyDADMAC macromolecules formed precipitates by electrostatic interaction according to Equation (A.4).

$$ArCOO^{-}Na^{+} + ArN^{+}Cl^{-} \rightarrow \text{Precipitate} + NaCl \qquad \text{A. 6}$$

The change in overall conductivity of the diluted solution during dilution of MBL with the polymer solution was compensated by the release of free counter ions in the solution. An analysis similar to the case of the dilution of MBL with water produced Figure A.10, which shows the change in overall conductivity of the solution during dilution with the polymer solution. The measured conductivity in Figure A.10 levelled off to a lower value than that predicted from mass balance in Equation (A.6). This was ascribed to the absorption of some of the free ions into the precipitates.

Both batch and semibatch experiments involving dilution of MBL either with water or the polymer solution demonstrated that the variation of conductivity of the MBL during dilution was linear to the variation of concentration of lignin, sodium and hydroxyl ions in solution.

A.4 Testing of Displacement Washing Apparatus

The accuracy of the displacement washing apparatus was tested by carrying out experiments of permeation of water in homogeneous beds of no:10

glass beads. The procedure for preparing a water-saturated homogeneous bed of no:10 glass beads in the washing cell is described in section 4.2.2.7.1 in Chapter 4. The adjustable plunger was then placed on the top of the bed. The tube inside the plunger was then filled with water and connected to the line leading to the peristaltic pump. It was ensured that all connections were sealed properly to prevent any leakage of fluid through them. Water was pumped into the washing cell at a constant flow rate. A permeation experiment was continued until the pressure drop across the washing cell reached a steady state. Pressure drop measured across the washing cell was the summation of pressure drop across the bed of glass beads and that across the washing cell without any bed of glass beads in the washing cell. Pressure drop was measured for the blank run consisting of no beds of glass beads inside the washing cell. Corrected pressure drop across the bed of glass beads was obtained by subtracting the pressure drop measured across the cell without glass beads from that measured across the washing cell during a permeation experiment. The cumulative mass flow rate of the eluate was measured by the electronic Mettler PM 16 balance. In a permeation experiment, the flow rate set in the peristaltic pump and that calculated for the eluate agreed to each other within ± 3%. Permeation experiments of beds of No: 10 glass beads were performed at four different flow rates of 30, 100, 160, and 230 mL/min. At each flow rate, beds of four different heights, i.e., 4.8, 10.6, 17.2, and 22.5 cm, were used.

An experimentally derived form of Darcy's law for flow of a homogeneous incompressible fluid through a homogeneous porous medium can be described as

$$\frac{Q}{A} \propto \frac{\Delta P}{L} \qquad \text{A. 7}$$

where Q is the volumetric flow rate of the fluid coming out of the bed, A is the cross sectional area of the bed normal to the direction of flow, ΔP is the pressure drop across the bed, and L is the length of the bed. Equation (A.7) can be expressed mathematically as

$$\frac{\Delta P}{L} = \frac{\mu Q}{KA} \qquad \text{A. 8}$$

where K is the permeability of the porous medium. According to Darcy's law, a plot of $\Delta P/L$ versus Q/A should give a straight line passing through the origin and the slope of the line should represent the ratio of viscosity of fluid to permeability of the porous bed. Figure A. 11 shows the plot of experimentally measured values of $\Delta P/L$ versus different specific discharges or superficial velocities, Q/A. The data fell on a straight line going through the origin, demonstrating a close agreement with Darcy's law. From the slope of the regressed line, the permeability (K) of the porous bed was calculated to be 6.895×10^{-8} cm^2. In the

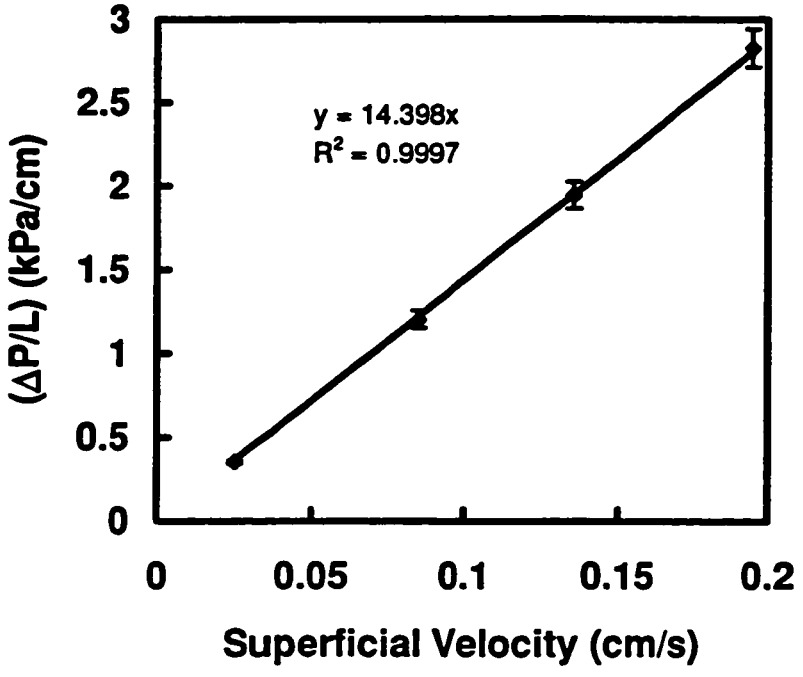

Figure A. 11 Testing of apparatus in Darcy flow regime; error bars represent 95% confidence intervals based on three replicate runs.

Darcy flow regime where viscous forces are dominant over inertial forces, the Kozeny-Carman equation states that

$$\frac{\Delta P D_p^2 \varepsilon^3}{UL\mu(1-\varepsilon)^2} = 150 \qquad \text{A. 9}$$

Equation (A.9) can be expressed in the form of Darcy's law as

$$U = \frac{Q}{A} = \frac{D_p^2 \varepsilon^3 \Delta P}{150\mu(1-\varepsilon)^2 L} \qquad \text{A. 10}$$

A comparison of Equations (A.8) and (A.10) is made to express K in terms of D_p and ε as

$$K = \frac{D_p^2 \varepsilon^3}{150(1-\varepsilon)^2} \qquad \text{A. 11}$$

The value of K (6.895×10^{-8} cm^2) calculated from the slope of the regressed line in Figure A. 11 is used to determine the representative average particle diameter from Equation (A.11). The representative average particle diameter is calculated to be 113.6 μm, which agrees closely with the measured average diameter of 121 μm.

In flow through porous media, the commonly used dimensionless number Fanning friction factor, f, and the particle Reynolds number, $N_{Re,p}$ were defined as

$$f = \frac{D_p \Delta P}{2L\rho U^2} \qquad \text{A. 12}$$

$$N_{Re,p} = \frac{\rho U D_p}{\mu} \qquad \text{A. 13}$$

(Bear, 1972). Various investigators, based on their experimental results, suggested that for $N_{Re,p}$ values below 10, Darcy's law is valid and the relationship between Fanning friction factor, f and $N_{Re,p}$ was expressed as

$$f = \frac{1000}{N_{Re,p}} \qquad \text{A. 14}$$

(Bear, 1972). The results of the permeation experiments were plotted as a relationship between Fanning friction factor, f and particle Reynolds number, $N_{Re,p}$ resulting in Figure A. 12.

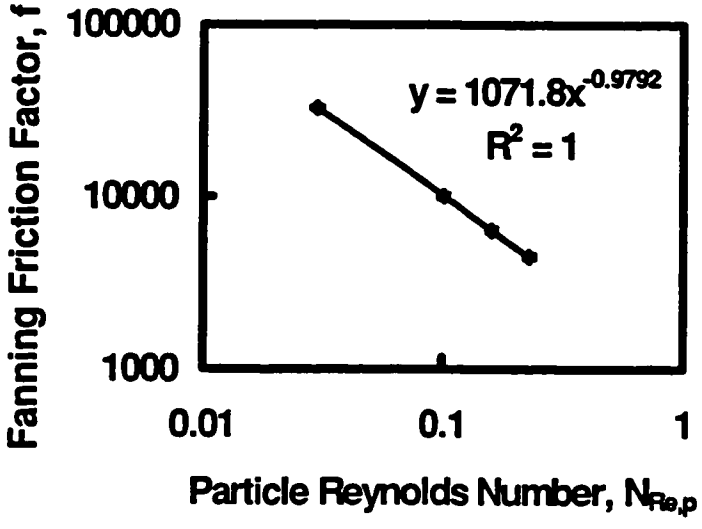

Figure A. 12 Plot of f versus $N_{Re,p}$; error bars (too small to be distinguished) represent 95% confidence intervals based on three replicate measurements.

A regression of experimental data in Figure A. 12 yielded the following relation, which is in close agreement with the relation given in Equation (A.14).

$$f = \frac{1071}{N_{Re,p}^{0.9792}} \qquad \text{A. 15}$$

A.5 Conclusions

Close agreement of experimental results with Darcy's law, Kozeny-Karman equation and the correlation given in Equation (A.14) confirms the accuracy of the constant flow washing apparatus. It is verified that the domain of flow in the experiments conducted in the apparatus will remain in Darcy's flow regime as long as the superficial flow rate does not exceed 230 mL/min.

List of Variables

A	Cross sectional area of bed, m^2.
C	Concentration of a species in Equation (A.4), Kg/m^3.
C_i	Concentration of species in input stream, Kg/m^3.
C_o	Concentration of species in output stream, Kg/m^3.
D_p	Diameter of particle, m.
f	Fanning friction factor, dimensionless.
G_{cell}	Conductance of load in Figure A.3, ohm^{-1}.
G_{ref}	Conductance of reference load in Figure A.3, ohm^{-1}.
K	Permeability of bed, m^2.
L	Length of the bed, m.
ΔP	Pressure drop across the bed, Pa.
Q	Superficial flow rate, m^3/s.
	Volumetric flow rate in Figure A.8, m^3/s.
$N_{Re,p}$	Particle Reynolds number, dimensionless.
t	Time, s.
U	Superficial velocity, m/s.
V_0	Initial volume of MBL in the beaker in Figure A.8, m^3.
V_1	Voltage across reference conductance in Figure A.3, volt.
V_2	Voltage across load conductance in Figure A.3, volt.
V_3	Voltage across ground in Figure A.3, volt.

Greek Letters

ε	Porosity of bed, dimensionless.
μ	Viscosity of fluid, Pa.s.
ρ	Density of fluid, Kg/m^3.

Abbreviations

AC	Alternating current.
A/D	Analog to digital.
DC	Direct current.
I/O	Input / output.
MBL	Model black liquor.
MW	Molecular weight.
r.p.m	Revolutions per minute.
VDC	Voltage, direct current.

Reference:

Bear, J., Dynamics of Fluids in Porous Media, Elsevier, New York, 1972.

Appendix B

The description of the variables in the following sections is already given in Chapter 6. The algorithm for the computation of C_{exit}, ΔP, and the profile of frontal positions against dimensionless time in the non-communicating channel bed model is given in Figure B.1. Figures B.2 and B.3 describe the algorithms of computation of C_{exit}, ΔP, and the profile of frontal positions in the communicating channel bed model during displacement with water and the polymer solution respectively. A brief discussion of the steps involved in the algorithms are given below.

B.1 Method of Computation in Non-Communicating Channel Bed Model:

Step 1: All variables that were known initially were specified. Variables specified were L, length of bed; d, diameter of column; Q, total superficial flow rate of displacing phase; μ_d and μ_r, viscosities of displacing and resident phases respectively; ρ_d and ρ_r, densities of displacing and resident phases respectively; ε, ε_c, and ε_f, initial porosities of overall channel bed and columns of coarse and

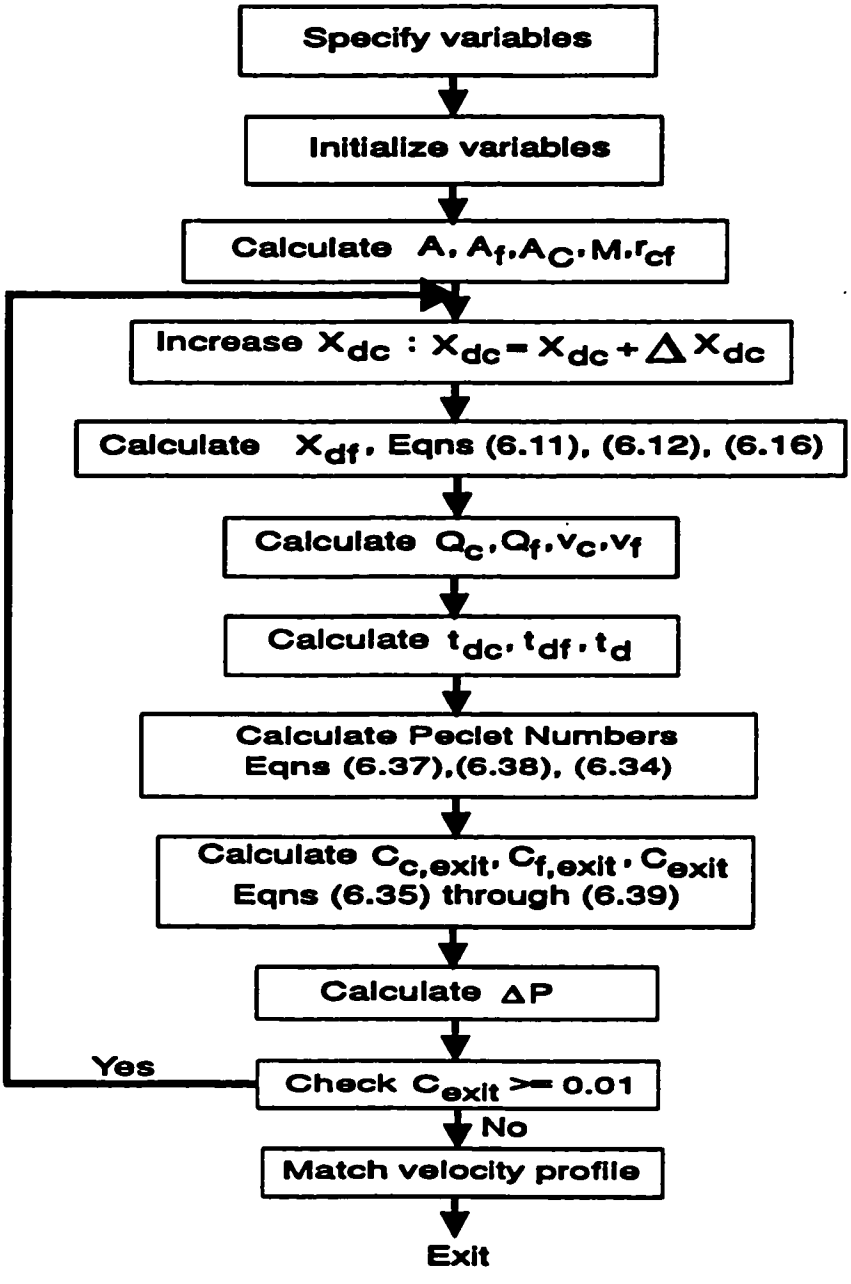

Figure B.1 Algorithm for computation of C_{exit}, ΔP, and profile of interstitial velocity in a non-communicating channel bed model.

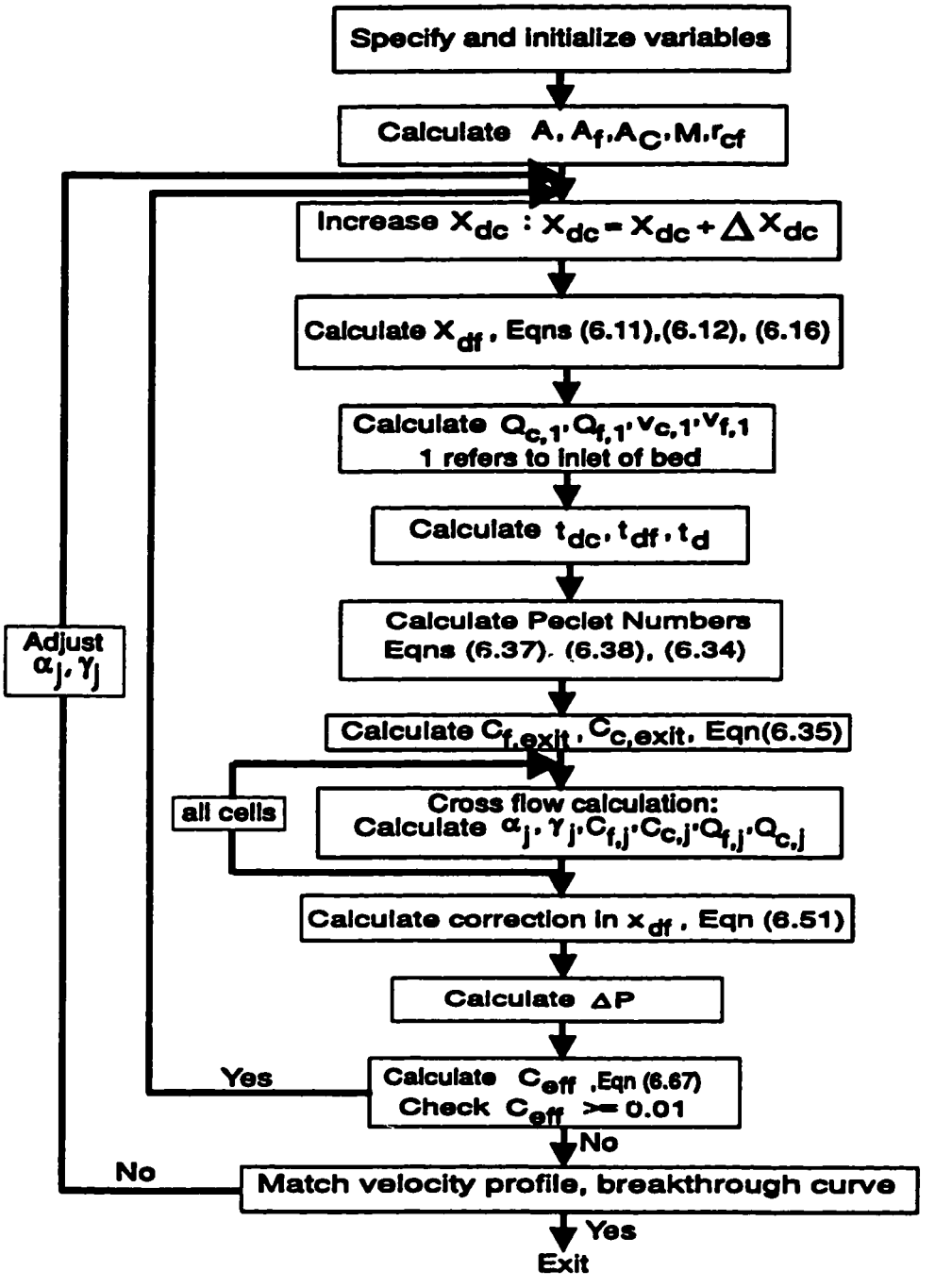

Figure B.2 Algorithm for computation of C_{exit}, ΔP, and profile of interstitial velocity in a communicating channel bed model during washing with water.

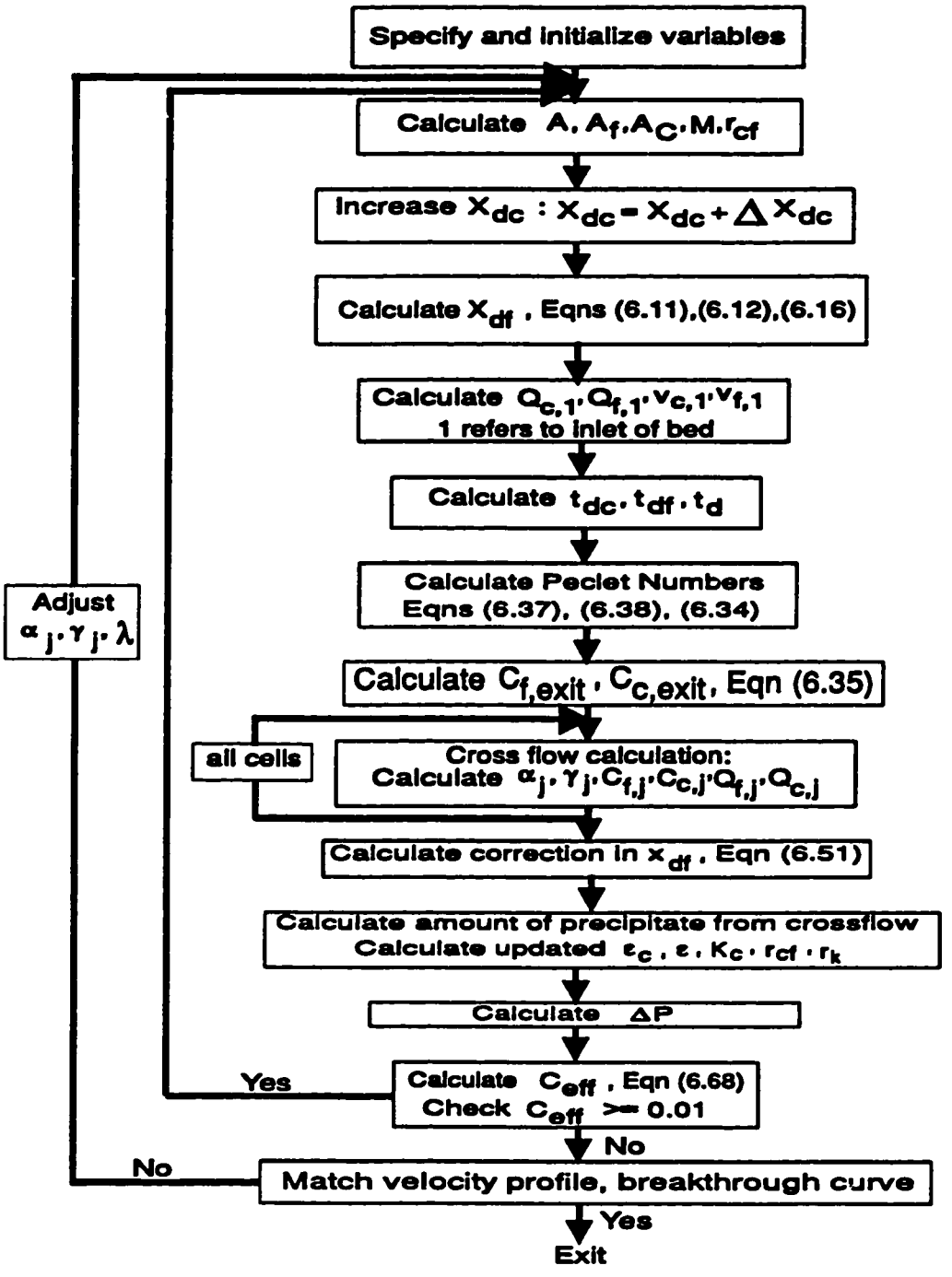

Figure B.3 Algorithm for computation of C_{exit}, ΔP, and profile of interstitial velocity in a communicating channel bed model during washing with polymer solution.

fine beads respectively; d_{pc} and d_{pf}, particle diameters of coarse beads and fine beads respectively; and r_k and k_f, initial ratio of permeability of the column of coarse beads to the column of fine beads and permeability of the column of fine beads.

Step 2: The variables A, A_c, and A_f were calculated from the diameter of column, diameter of column of coarse beads, and Equation (6.1) respectively. Variables M and r_{cf} were calculated using Equations (6.10) and (6.9) respectively. The variables ε, ε_c, r_k, k_c, and r_{cf} remained unchanged during displacement with water in a channel bed since there was no precipitate formation and reduction of permeability of the column of coarse beads.

Step 3: The frontal position in the column of coarse beads, x_{dc}, that was zero at the inception of displacement was increased by a small step, Δx_{dc}.

Step 4: The frontal position in column of fine beads, x_{df}, that was zero at the inception of displacement was calculated using either Equation (6.11) before breakthrough in the column of coarse beads or Equations (6.12) and (6.16) at and after breakthrough in column of coarse beads in the model channel bed.

Step 5: In columns of coarse and fine beads, superficial flow rates Q_c and Q_f and interstitial velocities v_c and v_f were then calculated using Equations (6.24), (6.21), (6.22), and (6.23) respectively.

Step 6: Total dimensionless time, t_d, dimensionless time corresponding to flow in column of coarse beads, t_{dc}, and that in column of fine beads, t_{df} were then calculated using Equations (6.25) through (6.27) respectively.

Step 7: Initial estimates of longitudinal dispersion coefficients (D_L) based on bed length, L in both columns of coarse and fine beads and corresponding Peclet numbers, Pe_L were obtained from Equations (6.37), (6.38) and (6.34) respectively.

Step 8: Exit concentration in the column of coarse beads, $C_{c,exit}$, and that in the column of fine beads, $C_{f,exit}$, were calculated using Equation (6.35). Overall exit concentration, C_{exit}, at the exit of the channel bed was calculated using Equation (6.39). The overall exit concentration, C_{exit}, was checked to be less than 1% or not. If it was more than 1%, calculation was continued from step 3. If it was less than 1%, the next step was followed.

Step 9: Pressure drops ΔP_c and ΔP_f across the columns of coarse and fine beads respectively were calculated using Equations (6.17) through (6.20).

Step 10: Once the overall exit concentration, C_{exit}, was less than 1%, the computed breakthrough curve obtained by plotting C_{exit} against t_d was compared with the experimental breakthrough curve. If the fit of the computed and experimental curves was unsatisfactory, the parameter δ in Equation (6.38) was

changed and the entire computation was restarted from step 1. In the case of satisfactory fit, the position of fronts in column of coarse beads x_{dc}, and that in column of fine beads x_{df} were plotted against dimensionless time t_d and compared with the plots of $t_{d,50\%}$ versus x_d obtained experimentally using probes in model channel bed, discussed in detail in Chapter 5.

B.2 Method of Computation in Communicating Channel Bed Model:

Step 1: In addition to Step 1 in the non-communicating channel bed model, n, the number of cells in the columns of coarse and fine beads was included.

Step 2: Since there was no precipitate formation during displacement with water in a channel bed, the variables ε, ε_c, r_k, k_c, r_{cf} remained unchanged with time. However, during displacement with the polymer solution, each of the variables, ε, ε_c, r_k, k_c, and r_{cf} changed with displacement. In addition to Step 2 in the non-communicating channel bed model, updated values of ε, ε_c, r_k, k_c, and r_{cf} were calculated in the following steps.

Step 3: The frontal position in column of coarse beads x_{dc} that was zero at the inception of displacement was increased by a small step Δx_{dc}. To satisfy the conditions of plug flow like displacement in the column of coarse beads given in

Equations (6.46), (6.47), and (6.63) during displacement with either water or polymer solution, the step length was chosen as

$$\Delta x_{dc} = \frac{1}{\text{number of cells}} = \frac{1}{n}$$

Step 4: The frontal position in column of fine beads x_{df} was calculated using either Equation (6.11) before breakthrough in the column of coarse beads or Equations (6.12) and (6.16) at and after breakthrough in column of coarse beads. x_{df} was calculated with the assumption that there was no lateral exchange of lignin between the columns of coarse and fine beads during displacement with either water or the polymer solution.

Step 5: Step 5 was identical to that in the non-communicating channel bed model.

Step 6: Step 6 was identical to that in the non-communicating channel bed model except that the calculation was based on, nx_{df} in Equations (6.25) through (6.27)

Step 7: Step 7 was identical to that in non-communicating channel bed model.

Step 8: Exit concentrations of lignin $C_{f,exit}$ and $C_{c,exit}$ in the columns of fine and coarse beads respectively were calculated using Equation (6.35). It can be noted that concentration of lignin at the exit of the column of fine beads $C_{f,n+1}$ was equal to $C_{f,exit}$ during displacement with either water or the polymer solution.

Concentration of lignin at the exit of column of coarse beads $C_{c,n+1}$ was equal to $C_{c,exit}$ during displacement with the polymer solution.

Step 9: Lateral transfer of lignin between each couple of adjacent cells in the columns of coarse and fine beads and total loss of lignin due to lateral transfer were calculated using Equations (6.40) through (6.54) and Equations (6.63) through (6.65). Exit concentration of lignin at the outlet of the column of coarse beads $C_{c,n+1}$ was calculated from Equation (6.45) during displacement with water.

Step 10: Correction in x_{df} due to lateral transfer of lignin from column of fine beads to column of coarse beads was calculated using Equation (6.51).

Step 11: This step was only executed for displacement with the polymer solution. The volume of precipitate formed in the column of coarse beads from total lateral transfer of lignin from all cells in column of fine beads over a small time, Δt, that corresponded to the step length, Δx_{dc}, was calculated using Equation (6.59). Due to the formation and retention of precipitate in the column of coarse beads during displacement with the polymer solution, updated values of variables, ε_c, k_c, ε, r_{cf}, and r_k, were calculated using Equations (6.60) through (6.62), (6.9), and (6.2) respectively. During displacement with water, all of these variables remained unchanged with time.

Step 12: Calculation of pressure drop profiles was identical to that in the non-communicating channel bed model. Updated values of variables, ε_c, k_c, ε, r_{cf}, and r_k were used during displacement with the polymer solution in a channel bed.

Step 13: Overall exit concentration, C_{exit}, from the channel bed was calculated using a mixing-cup model at the exit of bed. For displacement with water and the polymer solution, C_{exit} was calculated using Equations (6.67) and (6.68). The overall exit concentration, C_{exit} was checked to be less than 1% or not. If it was more than 1%, calculation was continued from step 2. If it was less than 1%, next step was followed.

Step 14: Once the overall exit concentration, C_{exit}, was less than 1%, the computed breakthrough curve, i.e., C_{exit} versus t_d, was plotted against the experimental breakthrough curve. If the fit of the computed and experimental curves was unsatisfactory, the parameters ψ, β_j, and λ in Equations (6.64), (6.65), and (6.60) respectively were changed and the entire computation was restarted from step 1. The tail of the computed breakthrough curve was fitted closely to the experimental breakthrough curve by adjusting δ in Equation (6.38).

Computation was first performed for displacement with water. In the case of a satisfactory fit, the plots of computed positions of the front x_{dc} and nx_{df} in the

columns of coarse and fine beads respectively against dimensionless time t_d were compared to the plots of $t_{d,50\%}$ versus x_d obtained using probes in the model channel bed, discussed in detail in Chapter 5. A similar procedure was followed for displacement with the polymer solution keeping the same set of ψ and β_j used for computation of the breakthrough curve for displacement with water. The parameter λ in Equation (6.60) was adjusted to fit the computed breakthrough curve to the experimental breakthrough curve obtained during displacement with the polymer solution. After a satisfactory fit, plots of the positions of the front x_{dc} and nx_{df} against dimensionless time were compared with those obtained experimentally using probes inside the model channel bed.

B3. Codes of Computer Programs

Codes of the computer programs are available either from the author or from Professor Robert H. Pelton, Department of Chemical Engineering, McMaster University, Hamilton, Canada in printed form or on formatted diskettes.

IMAGE EVALUATION TEST TARGET (QA-3)

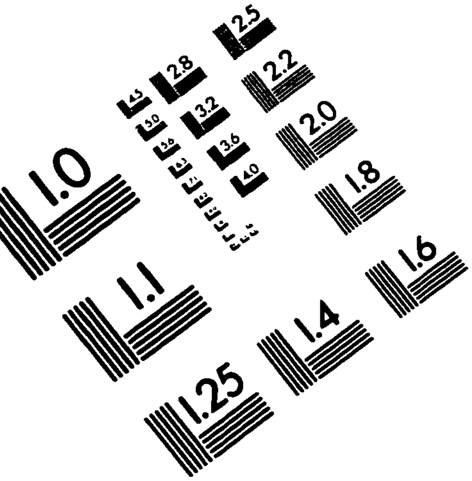

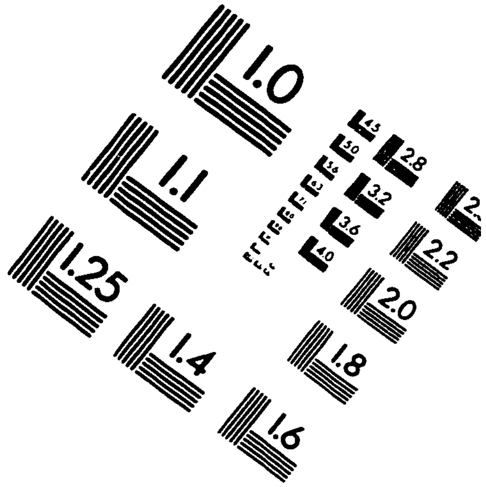

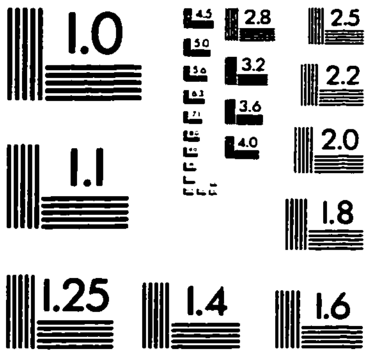

150mm

6"

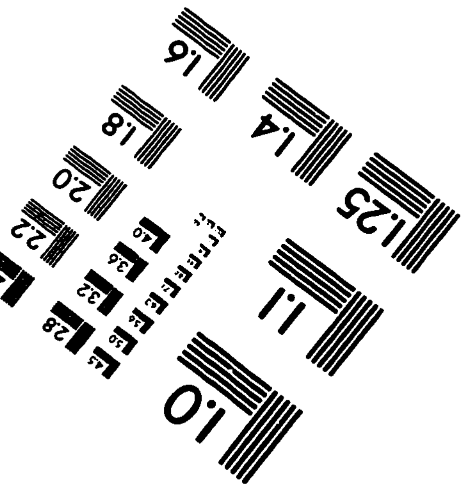

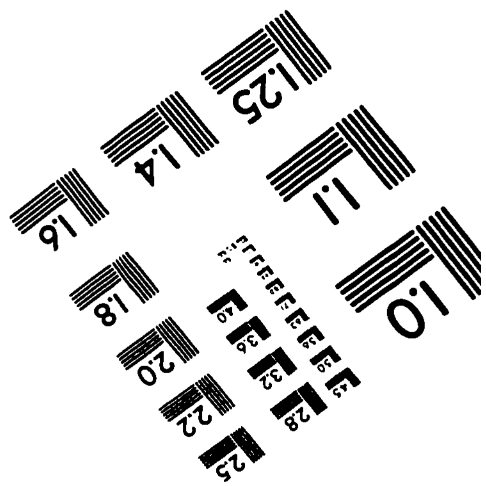

APPLIED IMAGE . Inc
1653 East Main Street
Rochester, NY 14609 USA
Phone: 716/482-0300
Fax: 716/288-5989